Energetic responses to transient high temperature stress in cyanobacteria. A dynamic system examined *in vivo*

Duncan Fitzpatrick

A thesis submitted for the degree of Doctor of Philosophy

Australian National University

December 2016

© Duncan Fitzpatrick 2016

All rights reserved

Declaration

I hereby certify that the work in this thesis is wholly my own, except where otherwise acknowledged.

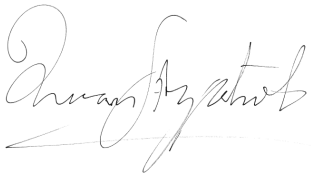

Duncan Fitzpatrick

December 2016

Word count:78,326

Acknowledgments

There are more people to whom I owe my thanks, than there are pages in this document. I want to thank everybody who has been a part of my life during the completion of this arduous project. Like all PhDs to some extent, this one has been well punctuated by the good and the bad. But I was privileged to have the support of a caring, intelligent, and broad range of people to keep me going, and interested.

The amazing community at RSB, and across ANU more broadly, have been wonderfully supportive. My friends around Canberra, those with whom I have lived in various sharehouses over the years, those who kept me going from overseas, and back in Melbourne. Thank you so much. You are the reasons that I can say I would do it all again.

Thank you to my patient supervisory panel. Dean Price and Murray Badger, for being there from the start. Fred Chow, your addition was the silver lining to our misfortune.

To everyone in the workshops: without you, ANU is just administration. Thanks for enabling me to look for knowledge, through sharing your amazing expertise.

To everyone who has helped me into the world of biology, from Honours through to here, I would literally not have made it.

To Michael and Alonso. It was a privilege to have spent these years with you both in the lab. You have both taught me so much, and really helped me cope with the changes.

Mum and Pierre, you have never questioned my madness, and have always given me so much love, support and confidence to do anything I want.

Dad, your brain is amazing and your way of thinking outside the square is enviable. I hope it has rubbed off. Thank you for teaching me so much.

To my siblings: blood, marriage, other: you guys are all amazing people. How are we such a diverse bunch? I find it easy to stay confident in what I'm doing, with the knowledge that I have such capable people ready to support me in pretty much anything I need.

Katie: thank you for being such a wonderful support on a daily basis, throughout my stress and madness. You and Tags have given me so much to enjoy, and pushed me to enjoy it!

Sari, Henry and Stella. Thank you. Hanging out with you all made it much easier than it would have otherwise been. Your strength and resilience gave me mine.

In Memory

Warwick Hillier

8 October 1967 – 10 January 2014

A man always two steps ahead of all others. Nobody wants to see this photograph, because he was very ill. Behind him, is he and Sari's first home. It is brimming with solar collectors, paid for by the sale of his telescopes and camera gear. Henri and Stella were playing inside. This photo exemplifies his selflessness in the face of a cruel reality. Warwick was brilliant and kind, his research career was short, but I am very grateful for the many things he taught me, and the time I was lucky to share with him.

Jan Anderson

13 May 1932 – 28 August 2015

Jan is often cited as being an inspirational scientists for women. This sells her a long way short, she remains an inspiration to many young scientists, including me. She made sure to support me as Warwick became ill, and entertained me with some incredible stories about her life a scientist, working in Calvin's lab and living as foreigner during McCarthyism. Thank you Jan.

Abstract

This thesis investigated the energetic response of a moderately thermophillic cyanobacterium, *Thermosynechococcus elongatus* BP.1 (BP.1), to high-temperature damage.

Previous published work has investigated the physiological impacts of high-temperature stress on BP.1, and has focused primarily on understanding the absolute functional stability of discrete cellular components, exposed to high temperatures. The majority of this work was conducted *in vitro,* on isolated components, or through the addition of artificial electron donors and acceptors to cells. The results have clearly shown that photosystem two (PSII) is the thermally weakest cellular component of BP.1. Furthermore, the temperatures that inhibit PSII are very close to the optimal temperature for growth in this species. Strong evidence suggests that thylakoid components downstream of PSII, specifically photosystem one (PSI), and primary components of the electron transport chain, exhibit significantly greater tolerance to high temperatures than PSII. There has been no published work investigating the possible physiological significance of this. Furthermore, no data has been published on the tolerance to high temperatures of crucial cellular processes, carbon fixation and respiration.

A key aim of the research was to identify whether any cellular functions, such as respiration, still operated in cells after high temperatures had inhibited PSII. To undertake this work, an *in vivo* methodology was developed to measure functionality of key cellular components, following high-temperature exposure. The method involved the integration of membrane inlet mass spectrometry (MIMS), including simultaneous gas flux measurements of CO_2 and stable isotope differentiation of concurrent oxygen evolution and consumption fluxes, with pulse/probe spectroscopy of P700, the reaction-centre chlorophyll of PSI.

Gas fluxes and P700 redox dynamics were measured from samples under steady state conditions of photosynthesis, following ten minutes of dark incubation across a range of damaging temperatures. The results showed clearly that respiratory systems, and probably CO_2 fixation, were more stable than PSII. Furthermore, as PSII function declined to < 95 % of maximal rates, respiration was no longer inhibited by illumination.

The P700 data indicated that PSI activity was maintained at a level that could not be supported solely by the remaining function of PSII, following high-temperature incubations. This suggested that published *in vitro* data, demonstrating greater thermal tolerance for PSI than PSII, may be functionally significant. Evidence that reductant sourced from respiration was driving PSI photochemistry, after PSII inhibition, was obtained. A hypothesis is proposed that the cyanobacterium utilises stored reductant to poise the thylakoid membrane for cyclic electron flux (CEF), once PSII is inhibited. The mechanism proposed in this thesis enables cells to maximise the utilisation of their stored energy, by enabling PSI to continue harnessing light energy if PSII is inhibited. A thylakoid proton gradient is maintained through PSI function, instead of standard *chlororespiratory* pathways that utilise a terminal oxidase. A new term, "*delayed* cyclic electron flux", (CEF_d) is proposed to describe this mechanism. It differentiates CEF around PSI, driven by PSII, from that supported by alternative sources of reductant, such as the respiratory complex succinate dehydrogenase (SDH). *Delayed* implies that the reductant has been stored in the cell.

Abbreviations

µE – photon flux density (µmol(photons).$m^{-2}s.^{-1}$

6803 – Synechocystis sp. PCC 6803

ATP – Adenosine triphosphate

BP-1 – *Thermosynechococcus elongatus* BP.1

CEF – Cyclic electron flux around PSI

CEF_d – proposed term: *delayed* cyclic electron flux around PSI

Ci – Inorganic carbon

[Chl] – Concentration of Chlorophyll *a,* (µg.ml^{-1})

CCM – CO_2 concentrating mechanism

Cox – Cytochrome c oxidase

Cyd – Quinol oxidase

Cyt – cytochrome

ETR1 – Electron transport estimated through PSI

ΔFlux – difference between ETR and $LEFO_2$, defined as CEF through PSI

f_i – Fraction of absorbed light partitioned to PSI

fixCO_2up – CO_2 uptake/fixation rate, derived value

$FNR_{(S/L)}$ – Ferredoxin:$NADP^+$ oxidoreductase (short/long form)

GrO_2ev – Gross rate of O_2 evolution

GrO_2up – Gross rate of O_2 uptake

$LEFO_2$ – Electron transport flux estimated through PSII

NetCO_2up – Net rate of CO_2 uptake

regO_2up – Regulatory O_2 uptake, function of Mehler type O_2 uptake, derived value

rspCO_2ev – Respiratory O_2 evolution, derived value

rspO_2up – Respiratory O_2 consumption, derived value

M55 – NDH-1 deficient mutant of cells did no

MIMS – Membrane Inlet Mass Spectrometry

MSP – Manganese Stabilising Protein (extrinsic subunit of PSII)

NADH – nicotinamide adenine dinucleotide (reduced)

NADPH- nicotinamide adenine dinucleotide phosphate (reduced)

NDH-1 – $NADH_{1,2}$ dehydrogenase

OD_{750} – Optical density at 750 nm

OPPP – Oxidative Pentose Phosphate Pathway

P680 – Reaction centre chlorophyll of PSII

P700/$P700^{+}$- Reaction centre chlorophyll of PSI, reduced/oxidised

Pm – maximum oxidisable level of P700

P – level of $P700^{+}$ in actinic light

Pm'- Maximum level of $P700^{+}$in actinic light

PSI – Photosystem one

PSII – photosystem two

PQ – Plastoquinone

Rubisco – Ribulose bisphosphate carboxylase/oxygenase

SDH – Succinate dehydrogenase

TCA – Tricarboxylic acid cycle

TCi – Total Inorganic carbon

WT – Wild Type

Y(I) – Photochemical Yield of PSI

Y(NA) – Acceptor side limitation of PSI

Y(ND) – Donor side limitation of PSI

Table of Contents

Declaration i

Acknowledgments iii

In Memory v

Abstract vii

Abbreviations ix

Table of Contents xi

Table of Figures xvii

List of Tables xxi

Chapter 1. Photosynthetic thermal stress Organism responses & how to measure them 23

1.1 Photosynthesis: the big picture 25

1.2 Cyanobacteria 25

1.2.1 The thylakoid membrane and photosynthesis 26

1.2.2 Alternative electron pathways and respiration 27

1.2.3 Pseudo CEF and chlororespiration 28

1.2.4 Carbon fixation 29

1.3 The impacts of high temperatures on photosynthesis 30

1.3.1 Measuring and interpreting thermal damage in a phototroph 31

1.3.2 A summary of thermal damage in mesophiles 32

1.4 Understanding thermal damage in thermophiles 35

1.4.1 What is the thermal tolerance of inter-chain ET complexes? 38

1.4.2 Novel methodological approach 39

1.5 Hypothesis formulation, thesis aims and structure overview 41

Chapter 2. Materials and Methods summary of the main techniques used 45

2.1 Cell culturing 47

2.1.1 Growth Media 47
2.1.2 Growth conditions 48
2.1.3 Agar Plates 49
2.1.4 Contamination checks 49
2.1.5 Cryostorage 49
2.1.6 Optical density 49
2.1.7 Measuring Chlorophyll a Concentrations [Chl] 50
2.1.8 Dry cell mass 50
2.2 Cell counting 50
2.3 Producing Cyano-discs. 51
2.4 Main MIMS methods 52
2.4.1 Membrane Consumption 53
2.4.2 Signal calibration: [Gas]/mV 54
2.5 Spectroradiometer/ cyano-leaf absorptance measurements 58
2.6 P700 measurements 60
Chapter 3. Technique Development and Optimisation New methods for unique measurements 61
3.1 Cell Culturing 64
3.1.1 Selecting a Standard Cultivation Temperature and [CO_2] 64
3.1.2 Comparing Orbital Platform vs Bubble Lift Cultivation 65
3.1.3 Growth Medium: comparing the options 67
3.1.4 Growth Measurements: Confirming their Accuracy 68
3.2 Membrane Inlet Mass Spectrometry (MIMS) 69
3.2.1 MIMS Flux Measurements at High Temperatures 70
3.2.2 Cuvette Problems: developing a new system 72
3.2.3 MIMS vs O_2 Electrode: Validating the Data Analysis Spreadsheet 75
3.2.4 Temperature and Cultivation Method vs Cell Performance 75

3.3 Integrating MIMS with P700 measurements 76

3.3.1 P700 with MIMS, Proof of Concept with Spinach 77

3.3.2 Initial Set up and Measurements; Creating a "Leaf" with Cyanobacteria 78

3.3.3 Cyanodiscs – Good for P700 AND absorptance measurements! 82

3.3.4 Do Cyano-discs in gas phase perform like a liquid culture? 84

3.3.5 Chlorophyll extraction and quantification comparison 85

3.4 Carboxysome isolation for *in vitro* ^{14}C assays in 4.1.4 87

3.5 Key Points and Ideas from Chapter 3 90

Chapter 4. Deconvoluting cyanobacterial gas fluxes: *determining activity* of specific components *in vivo* 93

4.1 Measuring continuous thermal stress and acclimation in BP.1 96

4.1.1 Method summary 97

4.1.2 Results of gas fluxes under continuous thermal stress 99

4.1.3 Fluorescence data supports interpretation of Gross O_2 evolution 105

4.1.4 In vitro check of Rubisco's thermal stability 107

4.1.5 Summarising results of gas fluxes at the temperature of interest 110

4.2 Post incubation measurements of transient thermal stress 112

4.2.1 Method summary for transient stress analysis on cyano-discs 114

4.2.2 Data from cyano-disc gas fluxes, post incubations 116

4.3 Analysing the physiology behind steady state gas fluxes 118

4.3.1 Using a mass balance approach to investigate gas fluxes 119

4.3.2 Explaining the mass balance estimation 120

4.4 Applying the mass balance to thermally damaged cells 125

4.4.1 What happened when PSII failed due to heat stress? 127

4.4.2 Testing scenario one: Zero CO_2 fixation. 128

4.4.3 Testing scenario two: CO_2 fixation = 100 % PSII activity. 129

4.4.4 Selecting which scenario matches the data 129

4.4.5 Can dark rates of respiration occur during illumination? 130

4.4.6 Drawing out nuances in the raw gas flux data 132

4.4.7 Incubation temperatures > 65 ˚C: severe damage and signal noise 136

4.4.8 Testing the two scenarios with mass balance estimations in highly damaged cells 139

4.4.9 Selecting and interpreting the more probable scenario 140

4.4.10 Conclusions of the gas fluxes due to transient heat stress 143

4.5 Final summary and conclusions of Chapter Four 145

Chapter 5. PSI's potential support role in cellular respiration Once PSII is severely inhibited by high temperatures 147

5.1 The response of PSI to transient thermal damage 150

5.2 Monitoring the activity of PSI post thermal incubations 152

5.2.1 Determining the maximum level of oxidisable P700 ($\boldsymbol{Pm}$) 154

5.2.2 The Yield of PSI and its Donor & Acceptor side Limitations 155

5.3 Impacts of thermal incubations on Yield of PSI ($\boldsymbol{Y(I)}$) 158

5.3.1 Dynamics of acceptor side limitation ($\boldsymbol{Y(NA)}$) 159

5.3.2 Dynamics of donor side limitation ($\boldsymbol{Y(ND)}$) 160

5.4 As PSII failed, PSI activity maintained relatively more activity 160

5.5 Unlocking hidden data in the raw $\boldsymbol{P700max}$ and $\boldsymbol{Y(I)}$ curves 164

5.5.1 Loss of PSII Kinetic area consistent with gas flux data 166

5.5.2 Higher respiration correlated to lower PSI oxidation 168

5.5.3 Respiratory electrons altered rates of dark $\boldsymbol{Y(I)}$ re-reduction 169

5.5.4 Alternative electrons depressed value determined for $\boldsymbol{Pm}$ 176

5.6 Conductivity measurements of electrolyte leakage & cell lysis 178

5.7 Chapter 5 conclusions: oxidation of stored carbohydrates seemed to reduce $P700^{+}$ as PSII failed due to high temperature 180

Chapter 6. Cyclic Electron flux around PSI Recycling respiratory reductant?.....183

6.1 Reproducing reported CEF values in Spinach leaf discs.....188

6.1.1 Determining $\boldsymbol{fi}$ and $\boldsymbol{\Delta Flux}$ in AA^+ & AA^- spinach discs.....189

6.1.2 CEF in AA^- Spinach discs.....191

6.1.3 Comparing $\boldsymbol{Y(I)}$, $\boldsymbol{Y(NA)}$ & $\boldsymbol{Y(ND)}$ in AA^+ and AA^- Discs.....192

6.2 Cyanobacterial cyclic measurements.....195

6.2.1 Using 6803 and the M55 mutant – growth considerations.....197

6.2.2 Measuring Absorptance of cyanobacterial cells on disc.....198

6.2.3 Determining $\boldsymbol{fi}$ and Measuring the Rate of CEF as a Function of irradiance in Synechocystis 6803, and the NDH-1 mutant M55.....199

6.2.4 Validation of the steady state CEF measurement in cyanobacteria: results and comparison between the WT and Mutant.....202

6.2.5 $\boldsymbol{ETR1}$, $\boldsymbol{LEFO2}$ and $\boldsymbol{\Delta Flux}$, post thermal incubations at 500 µE.....208

6.2.6 $\boldsymbol{ETR1}$, $\boldsymbol{LEFO2}$ and $\boldsymbol{\Delta Flux}$ at 100 µE, post thermal incubations.....210

6.2.7 Can literature data support 'recycling' of respiratory reductant?.....215

6.3 Comparing $\boldsymbol{Y(I)}$, $\boldsymbol{Y(NA)}$ & $\boldsymbol{Y(ND)}$ at 100µE from incubated samples of M55 and 6803.....216

6.4 Key Findings from Chapter 6.....220

Chapter 7. Results discussion & conclusions Summarising the data & extending the findings 223

7.1 Integrated MIMS/P700 measurements provided sufficient information, and resolving power for the *in vivo* deconvolution of complex cellular physiology.....227

7.1.1 The future for MIMS measurements.....230

7.2 Hypothesis: PSII exhibits lower thermal tolerance than other key metabolic components of the moderate thermophile BP.1.....231

7.2.1 Examining cellular activity, once PSII had failed.....233

7.2.2 Discussion of results, PSII failed before other components.....234

7.2.3 Key cellular components were more tolerant than PSII to transiently high temperatures 236

7.3 Hypothesis: At temperatures that inhibit PSII, reductant sourced from respiration can drive the activity of PSI. - PSI became a component of the respiratory chain 237

7.3.1 Literature examples of alternative $P700^+$ reduction 238

7.3.2 Thesis data supports $P700^+$ was reduced by respiration 240

7.3.3 Anoxygenic, aerobic respiration? The competition for O_2 242

7.4 Hypothesis: Reductant sourced through respiration may poise the redox balance of the thylakoid membrane, enabling the cycling of electrons around PSI if PSII is inhibited 243

7.4.1 Thesis data supporting recycling of respiratory reductant 245

7.4.2 Potential issues with the result, and how they manifest in the literature 247

7.4.3 How to address this problem? 248

7.5 Extending the findings of this thesis 249

7.5.1 The illumination of chlororespiration"The energy leveraging hypothesis" 250

7.5.2 'Linear' energy leveraging, rationale and evidence 251

7.5.3 Cyclic energy leveraging of respiratory products - Recycling reductant to generate ATP & PMF 256

7.5.4 Evidence it could apply to a broad range of phototrophs 257

7.5.5 Eco-physiological relevance of proposed 'energy leveraging' ideas: evolutionary advantage of minimising energy use 258

7.5.6 Providing a name to clarify the difference between chlororespiration, and illuminated chlororespiration. 259

7.5.7 Concluding remarks on 'illuminated chlororespiration' 261

7.6 Thesis Novelty 262

7.7 Future Directions 262

Literature Cited 265

Table of Figures

Fig. 1-1: Illustrative definition of mesophiles, thermophiles and hyperthermophiles as they are approximately categorised by temperature. 33

Fig. 1-2: Basic Z scheme of photosynthetic electron transfer from H_2O to $NADP^+$ in upper panel, with values of thermal stability after 5 minute incubations across a range of elevated temperatures for the primary components in the electron transport chain of *Thermosynechococcus elongatus* BP.1 (BP.1) in lower panel. 36

Fig. 2-1: Summary of cyano disc generation, and absorptance measurements.....59

Fig. 3-1: Comparison of growth of BP1 under varying conditions of temperature and [CO_2] on an orbital platform at 120 rpm, illuminated at 80 µE in BG-11 medium at pH 8.0. 65

Fig. 3-2: Comparison of BP.1 cell growth when cultivated in bubble lift or orbital incubators. 66

Fig. 3-3: A comparison of growth of *BP.1* cells when cultured in BG-11 and JDM media - bubbled with air containing ambient [CO_2] or 2% CO_2 enriched air at 55 °C and 85 µE. 68

Fig. 3-4: Quantifying the relationship between OD_{750} vs Dry Cell Weight, Cell number and [Chl] in cultures of BP.1 69

Fig. 3-5: The MIMS and P700 equipment as set up after the building move from the Robertson to the Linnaeus Building. 70

Fig. 3-6: Data illustrating the thermal effects on fundamental measurement parameters. 71

Fig. 3-7: A new stainless steel cuvette: 73

Fig. 3-8: Comparison of the rates of gas flux vs time, in the liquid phase, generated at two different cuvette temperatures in the original brass cuvette. 74

Fig. 3-9: Impact of cultivation method on rates of Net O_2 evolution measured in MIMS, with cuvette set to each of the indicated temperatures: note different [Chl] between samples. 76

Fig. 3-10: Integrated set up of P700 system and MIMS cuvette, focus on the P700 system. 77

Fig. 3-11: P700 signals measured in liquid samples of BP.1 cells in the MIMS cuvette. 79

Fig. 3-12: The effect of corn starch additions on the rates of net O_2 evolution from BP.1 cells at 20 $\mu g.mL^{-1}$ [Chl] at 55 °C. 80

Fig. 3-13: measurement of transmitted light through BP.1 sample culture at 20 $\mu g.ml^{-1}$ [Chl], with and without starch..... 81

Fig. 3-14: P700 signals and gas fluxes measured from BP.1 cells fixed into a glass fibre filter disc..... 82

Fig. 3-15: Comparison of the Porra *et al's.* (1989), with Meeks and Castenholz (1971) methods for Chlorophyll a determination in MeOh, and test of capacity for glass fibre discs to hold cells. 86

Fig. 3-16: comparison of attempts to purify carboxysome samples with sucrose gradients, prepared with the β-method left, and α-method right. 87

Fig. 3-17: A comparison of the protein content obtained from the pellet vs the supernatant of the initial spin of cbx isolation. 89

Fig. 4-1: Yamaoka *et al's.*, original figure (1978) comparing net O_2 evolution rates in BP.1 at a range of temperatures..... 97

Fig. 4-2: Comparison of total gas fluxes at varied measurement temperatures from cells cultivated at 45°C and 57°C. 100

Fig. 4-3: The efficiency of photosynthesis, determined via Fv/Fm fluorescence data of BP.1. 106

Fig. 4-4: *In vitro* measurements Rubisco function after 10 minute incubations, determined through measured through ^{14}C fixation of carboxysome enriched fractions of Tris Percholl (TP) pellets isolated from BP.1 cells. 108

Fig. 4-5: Post incubation steady state gas fluxes of thermosynechococcus elongatus BP.1 'cyano discs' in the light (Panel A) and dark (Panel B). 116

Fig.4-6: Photosynthetic irradiance curve of a BP.1 cyano-disc illustrating the concept of 'regulatory' oxygen uptake. 123

Fig. 4-7: Accuracy of assumptions behind Mass Balance equation: 126

Fig. 4-8: Comparison of gas flux versus time data, used to generate Fig. 4-5 (gas flux vs incubation temperature) illustrating change in fluxes with incubation temperatures at 62 °C, 65 °C, 67 °C and 70 °C. 135

Fig. 4-9: Blank run, an example of data generated each day to validate the 'instrument consumption offset' 136

Fig. 5-1: Schematic ilustration of the P700 measurement protocol. 153

Fig. 5-2: The photochemical Yield of PSI (Y(I)) as a function of incubation temperature, compared to its complimentary yields of Donor (Y(ND)) and Acceptor (Y(NA)) side limitations. 158

Fig. 5-3: Comparison of normalised activity of PSII, PSI, respiration rates and 1-(normalised to maximal rate of Y(ND)) (donor side limitation of PSI). 161

Fig. 5-4: Integrated PSII Kinetic Area as a function of incubation temperature. 166

Fig. 5-5: Comparison of $\mathbf{P700max}$ and $\mathbf{Y(I)}$ raw signals at increasing incubation temperatures. 171

Fig. 5-6 : Support for the hypothesis that respiratory reductant was reducing $P700^+$ at temperatures where PSII had been inhibited, found through a further comparison of raw $P700_{max}$ and Y(I) data. In the upper panel the proportion of P700 oxidised by weak FR light as a proportion of the total oxidisbale P700 (P_m) is plotted against the incubation temperature. That this is declining, given the conditions between samples

during measurments were kept unchanged, suggests something was reducing the $P700^+$ as it was generated by the weak FR light. 173

Fig. 5-7 : Conductivity measurements versus incubation temperature: a proxy for membrane rupture and cell lysis, measured after five minute dark incubations of liquid samples at the temperatures stated. 178

Fig. 6-1: Measuring $\mathbf{fi}$ and determining Δflux in cyclic electron flux inhibited spinach discs. 190

Fig. 6-2: $\mathbf{ETR1, LEFO2}$ and $\mathbf{\Delta Flux}$ as a function of irradiance measured in non-infiltrated spinach discs. 192

Fig. 6-3: $\mathbf{Y(I)}$, $\mathbf{Y(NA)}$ and $\mathbf{Y(ND)}$ of infilitrated vs non infiltrated spinach discs vs Irradience. 193

Fig. 6-4: Total absorptance of cyano discs as a function of [Chl]. 198

Fig. 6-5: $\mathbf{ETR1,\ LEFO2}$ and $\mathbf{\Delta Flux}$ as a function of irradiance in M55 mutant and 6803 WT (top two panels). 203

Fig. 6-6: Comparison of $\mathbf{ETR1,\ LEFO2}$ and $\mathbf{\Delta Flux}$ as in WT and M55 at 500 µE irradiance after 10 minute dark incubations across a range of temperatures. 209

Fig. 6-7: $\mathbf{fi}$ determined in the M55 mutant and $\mathbf{ETR1,\ LEFO2}$ and $\mathbf{\Delta Flux}$ determined in both M55 and the 6803 WT as a function of incubation temperature. 213

Fig. 6-8: $\mathbf{Y(ND)}$, $\mathbf{Y(I)}$, $\mathbf{Y(NA)}$ vs Incubation Temperature at 100 µE. Comparison of WT cells on the left and M55 on the right. 217

Fig. 7-1: Schematic of electron transport routes through thylakoid membranes of cyanobacterial cells: Comparison of undamaged cells in light and darkness, with illuminated samples suffering PSII inhibition (ie. incubations ≥ 65 °C in this thesis work with BP.1 cells) 254

List of Tables

Table 1. Quick summary of the broad processes measured for by monitoring each gas 40

Table 2: Nutrient composition of JDM Medium 47

Table 3: data points extracted from Fig.4-6 used as an example for a mass balance analysis of gas fluxes. 124

Table 4: 'Baseline values' for gas fluxes from non-damaged cells, generating by combing fluxes after incubations at 50 °C, 55 °C and 60 °C. 125

Table 5: Gas flux data averaged from cells incubated at 65°C. 127

Table 6: gas flux data averaged from cells incubated at 67°C and 70 °C. 137

Chapter 1.

Photosynthetic thermal stress

Organism responses & how to measure them

1.1 Photosynthesis: the big picture

Life on Earth exists as we know it, because of the oxygenic photosynthetic pathway. By harnessing the energy of photons to drive chemical reactions, leading ultimately to the formation of energy rich organic compounds, it provides the energy necessary for nearly all life on earth (Barber, 2008). The O_2 by-product of water oxidation initially led to the world's first mass extinction event by switching the planet's redox state from a reductive, to an oxidative environment (Hohmann-Marriott and Blankenship, 2011). However, molecular O_2 provided an abundant oxidant capable of driving highly energetic biochemical reactions, leading to the evolution of aerobic glycolysis (Barber, 2008), and provided the Earth with protection from UV radiation, through the generation of an ozone layer (Sessions *et al.*, 2009). These developments, combined with the plentiful supply of energy rich organic compounds, allowed for the evolution of large, multicellular organisms.

The first oxygenic phototroph was likely to be a cyanobacterium, which evolved the capacity to split water enzymatically with the manganese, calcium cluster, at least 2.5 Billion Years ago(Blankenship, 2010). This event was never evolutionarily repeated, and the two photosystem model of photosynthesis developed by cyanobacteria, has been modified but largely conserved, through the evolution of phototrophs to algae, and then plants (Allen and Williams, 1998). The processes that underpin oxygenic photosynthesis are broadly understood. However, there is still a lot to be learned about the details. From the precise mechanism of water oxidation (Williamson *et al.*, 2011), to the management of energy sources and sinks in a fluctuating light environment (Allahverdiyeva *et al.*, 2013), phototrophs hold many secrets to be revealed. This is significant, because photosynthesis provides us, humanity, with the food we eat. Although not an applied project, understanding how cyanobacteria may be dynamically adjusting their energetic systems in response to thermal damage, could provide some information to improve our understanding of how significant crop plants may deal with similar stresses.

1.2 Cyanobacteria

Cyanobacteria represent a distinctive subsection of prokaryotes, capable of performing oxygenic photosynthesis. They are gram negative bacteria, with a simple structure that consists of an outer membrane and a plasma membrane, separated by a peptoglycan layer.

A carbohydrate sheath, the glycocalyx protects, the cells from stresses such as desiccation, and predation (Hoiczyk and Hansel, 2000, Liberton *et al.*, 2013) surrounding the outer membrane. Within the cells a system of thylakoid membranes, functionally distinct from the plasma membrane, are the site for oxygenic photosynthesis and some respiration. Whilst the plasma membrane hosts a number of other functions including involvement in the CO_2 concentrating mechanism (Badger and Price, 2003)and respiration (Mullineaux, 2014a).

1.2.1 *The thylakoid membrane and photosynthesis*

The thylakoid membrane is a continuous loop, forming intact compartments that physically distinguish areas termed the cytosol, on the outside, with the lumen contained within (Bryant, 1995). The thylakoid membrane in cyanobacteria is functionally very similar to plant chloroplasts. However, in the prokaryotic system lacking discrete functional compartments such as mitochondria, key components of the electron transport chain of the thylakoid membrane is shared between photosynthetic and respiratory processes (Mullineaux, 2014a). This provides the cells with great metabolic flexibility, but also makes studying the cells *in vivo* quite complex.

The primary electron transport activities along the thylakoid are traditionally defined by whether they occur primarily in light, or in darkness. Photosynthetic processes are obviously light driven, and presented schematically in the 'z-scheme' in Fig 1-2, or with the relevant protein structures in panel A of Fig 7-1. Electrons released through the oxidation of H_2O by the catalytic activity of PSII reduces an internal-membrane pool of plastoquinone (PQ), able to diffuse throughout the thylakoid membrane (Hohmann-Marriott and Blankenship, 2011). The protons released by this step accumulate within the membrane's lumen. During photosynthesis under 'standard' conditions, the reduced PQ delivers electrons to the cytochrome-b_6f (cyt-b_6f) (Hervás *et al.*, 1996). This complex pumps further protons across the membrane through the 'Q cycle' before reducing a luminal charge carrier, plastocyanin or cytochrome-c_6 (cyt-c_6) (Hirano *et al.*, 1980). This charge carrier donates directly to photosystem one (PSI), reducing the oxidised reaction centre chlorophyll of this complex, $P700^+$, to P700 (Fan *et al.*, 2016). The following light driven turnover of the photosystem re-elevates the energy potential of this electron, and allows it to reduce a stromal charge carrier, ferredoxin (Fd). During linear electron transport, being described here, Fd reduces $NADP^+$ via the ferredoxin:$NADP^+$ oxidoreductase (FNR), which catalyses the production of NADPH on the acceptor side of PSI. In cyanobacteria, a short and a long

isoform of FNR is present in the genome, FNR_s and FNR_L. (Thomas *et al.*, 2006). The former is required for linear electron transport, driving the reduction of $NADP^+$, the latter will be discussed below. The protons accumulated during this process within the lumen are used to drive ATP synthase. The final energetic products, ATP and NADPH are used by the cells for anabolic processes, such as carbon fixation and general cellular maintenance. However they can also be diverted to perform a myriad of functions, such as Na^+ pumping, CO_2 concentrating (Badger and Price, 2003), and the reduction of NO_3^- (Flores *et al.*, 2005).

1.2.2 *Alternative electron pathways and respiration*

The electron transport chain is very complex and branched, a result of the fact that multiple processes must occur within the same physical space. This provides the cells with a large degree of metabolic flexibility, and an ability to fine tune the redox state of the system (Beck *et al.*, 2012). For example, once Fd has been reduced, it can be utilised directly by the NADH dehydrogenase-like complex (NDH-1), to reduce the PQ pool, termed cyclic electron flux around PSI (CEF) (Shikanai, 2014), as the electron can once again travel through the cyt-b6f to re-reduce $P700^+$. This allows the cells to fine tune the ratio of ATP to NADPH being generated to match the cell's requirements(Peltier *et al.*, 2016), and can also ensure a sufficient electron donor is maintained for PSI, to avoid this system suffering photodamage (Shimakawa *et al.*, 2016).

Respiration in cyanobacteria occurs along both the cytoplasmic and thylakoid membranes , and makes use of components along both the plasma and thylakoid membranes (Vermaas, 2001).Cells are able to operate a multitude of respiratory pathways, to extract reductant through the oxidation of stored carbohydrates, generated during photosynthesis. Glycogen is the main storage molecule in the cells, and this can be broken down through glycolytic pathways feeding into a modified tricarboxylic acid cycle (TCA) cycle (Zhang and Bryant, 2011), and through the oxidative pentose phosphate pathway (OPPP) . The cells attempt to maximise the generation of NADPH through their respiration (Spaans *et al.*, 2015), as the anabolic systems rely on this reductant (Spaans *et al.*, 2015). There is such a reliance on NADPH that the inhibition of a transhydrogenase protein that catalyses the reduction of $NADP^+$ with NADH, in *Synechocystis* sp SPP 6803 (6803) resulted in severely impaired heterotrophic growth (Kämäräinen *et al.*, 2016). The succinate dehydrogenase complex (SDH) is a thylakoid membrane bound component of the TCA cycle, oxidising succinate to produce fumarate and reduce the PQ pool (Cooley *et al.*, 2000).

This step translocates a proton across the membrane, generates an NADH equivalent and can reduce the PQ pool directly, if the thylakoid is sufficiently oxidised (Cooley and Vermaas, 2001). The NDH-1 complex, already mentioned with relation to its role in CEF, can also be a component of respiration. It is possible for NADPH generated through a respiratory step, to be oxidised by the FNR_s complex, to reduce Fd. Once again, the Fd can reduce the NDH-1 complex, which mediates the reduction of the PQ pool and the translocation of a proton (Peltier *et al.*, 2016). However in contrast to the previous description of this step, this processes can occur in the dark. Obviously, darkness discounts the 'cyclic' component of the NDH-1's role described above. So, what happens to the electrons that reduce the PQ pool in darkness?

The final component of the respiratory process, following the liberation of electrons and generation of a proton gradient, is to find a sink to safely reduce. Aerobic respiration tends to utilise terminal oxidases, able to catalyse the reduction of O_2 directly to H_2O. The thylakoid membrane provides two 'respiratory terminal oxidases' for this to occur. The Cytochrome c oxidase, (Cox), and the cytochrome bd quinol oxidase (Cyd) (Ermakova *et al.*, 2016). Their function is generally defined as 'chlororespiration' (Peltier and Cournac, 2002). These components complete the set of respiratory complexes that make use of the thylakoid membrane's capacity to generate a proton gradient for ATP generation through respiration.

1.2.3 *Pseudo CEF and chlororespiration*

With respect to energetic balancing of the thylakoid membrane, two significant ideas have already been covered, (1) the capacity to cycle electrons around PSI to rebalance the NADPH to ATP ratio and ensure sufficient acceptors do not allow for the 'over-reduction' of PSI. (2) the shared use of the thylakoid membrane by both respiratory and photosynthetic components, as the respiratory terminal oxidases have also been shown to help protect the thylakoid from over reduction (Ermakova *et al.*, 2016). A third and very significant pathway in cyanobacteria, functional during illumination is called pseudo-cyclic, or the water-water cycle (Asada, 2000). Electrons in this processes are generated at PSII, pass through the cyt-b_6f complex and are re-energised by PSI. However, under conditions where the acceptors to PSI are not sufficient, a set of flavodiiron proteins Flv1,3, can directly reduce O_2 to H_2O. This is called pseudo cyclic as it helps to rebalance the ATP:NADPH ratio. However, unlike CEF the overall redox state of the photosynthetic system can be reduced with this process. Up to 50 % of electrons generated at PSII has been shown to pass through this pathway under certain

conditions, are also generally associated with carbon limitation or initial irradiance/fluctuating light (Radmer and Kok, 1976, Allahverdiyeva *et al.*, 2013).

Chlororespiration is used primarily to describe the interaction between the respiratory electron transport chain and the thylakoid electron transport chain, defined in chloroplasts, and generally refers to the reduction of O_2 at a 'plastid terminal oxidase' or PTOX (Peltier and Cournac, 2002). This is in eukaryotes with separate chloroplasts and mitochondria, and is generally considered a dark process, responsible for altering the PQ pool redox state to ensure it is optimised for when light returns. In this thesis, the term chlororespiration has been appropriated to refer generally to the function of the thylakoid membrane as a conduit for the transfer of electrons sourced through the oxidation of stored carbohydrates (glycogen). It is an important term in the thesis because a lot of work was done to show that respiration became functional in the light, and in this case the thylakoid based respiratory terminal oxidases (RTOS), such as cytochrome c oxidase, (cox) and cytochrome quinol oxidase (cyd) (Ermakova *et al.*, 2016) were unable to compete for reductant as well as the photosynthetic components (Liu, 2016) . As such, when the term 'illuminated chlororespiration' is used in ensuing chapters, it is significant to recall that the main point being expressed is that the thylakoid membrane is being involved in the transport of respiratory sourced electrons, but these electrons are not necessarily reducing O_2 at a terminal oxidase but may be reducing $P700^+$, the oxidised PSI reaction centre chlorophyll.

1.2.4 *Carbon fixation*

Carbon fixation is obviously a significant component of photosynthesis, and is driven by cytosolic enzymes of the Calvin-Benson-Bassham cycle. The majority of NADPH and ATP generated during photosynthesis are used in this process where CO_2 reacts with ribulose1-5 bisphosphate, catalysed by the ribulose1-5 bisphosphate carboxylase oxygenase (Rubisco) enzyme, followed by the regeneration of trioses to pentoses. Rubisco in cyanobacteria is contained within a protein shell called the carboxysome (Samborska and Kimber, 2012), designed to preclude O_2 from the enzyme's catalytic site, through the concentration of CO_2 into the microcompartment via the CO_2 concentrating mechanism (CCM) (Badger and Price, 2003). The carboxysome is the final component of the CCM, which includes a number of active HCO_3^- and CO_2 pumps which can generally, in freshwater species, be induced under low Ci conditions(Rae *et al.*, 2011).

1.3 The impacts of high temperatures on photosynthesis

Assuming adequate nutrient and water availability, temperature plays a significant role in photosynthetic performance (Levitt, 1980), second only to irradiance. At very low temperatures, growth rate limitations are set by physical parameters such as enzyme kinetics, membrane diffusion limits and substrate affinity (Nedwell, 1999), making them very difficult to overcome through evolution (Brock, 1970). As a result, the optimal temperature for growth of cold adapted phototrophs tends to be much higher than that normally experienced in their native environment (Berry and Björkman, 1980). At optimal temperatures, photosynthesis is limited by the diffusion rate of CO_2, the subsequent regeneration of ribulose bisphosphate (RuBP), and by rates of electron transport across the thylakoid membrane – particularly the oxidation of plastoquinol by the cytochrome b_6/f complex (Whitmarsh, 2000). At supraoptimal temperatures, photosynthetic rate limitation is brought about through heat induced damage. This has been classified under two broad categories termed Indirect and Direct effects by Levitt (1980), or Reversible and Irreversible temperature responses by Berry and Björkman (1980). These damage types and their effect are summarised below:

Indirect/reversible temperature damage:

- *Starvation* – Increased respiration rates at higher temperature outstrips photosynthetic productivity
- *Toxicity* – A buildup of toxic byproducts due to unfavourable metabolic pathways activated in response to thermal stress
- *Protein Breakdown & Biochemical Lesions* – The inhibition of the accumulation/synthesis of compounds and intermediate substances necessary for growth – such as lipids or cofactors
    - Membranes can become 'leaky', disrupting electrochemical gradients
    - Protein repair or synthesis rate impaired to below that of damage rate

Direct/Irreversible temperature injuries:

- *Protein Denaturation* – Proteins denature in an often reversible process – however, irreversible aggregation at high temperature leads to significant/total loss of function
- *Lipid Liquefaction* – Excessive fluidity of the lipids comprising membranes – altering their semi-permeability and leading to the formation of lipid vesicles/membrane destruction
- *Membrane Rupture* – A result of combined lipid and protein deterioration within membranes lead to rupture and irreparable loss of function; a loss of semi permeability and eventually cellular integrity is compromised

1.3.1 *Measuring and interpreting thermal damage in a phototroph*

Although the negative impacts of high temperature stress on photosynthetic performance is probably clear to anyone who has grown a poorly acclimated plant species in a hot environment, a mechanistic understanding of how plants and other phototrophs suffer thermal stress is highly complex. Often high temperatures are exacerbated by other simultaneously occurring stresses, such as low water availability and high irradiance. Even under controlled conditions however, separating damage and regulation when interpreting the reduction of activity in a particular process (Zhang and Sharkey, 2009), particularly in-vivo, can be very difficult. How photosynthetic processes are regulated in response to temperature stress is not well understood (Kruse *et al.*, 2016) and a fundamental shift from supply side (≈ PSII/electron transport activity) to demand side (≈ Rubisco function) models of regulation are debated in the literature, although it currently seems that the demand side model is favoured, at least for C_3 plants.

Owing to the significant difference between reversible and irreversible thermal damage, it is necessary to define the type of damage and the level of stress being studied. 'Moderate' or 'reversible' heat stress, only a few degrees above the optimum temperature, can be encountered frequently in the environment and is directly linked to reduced crop yields. At the mesophilic scale (see Fig. 1-1) organisms tend to possess extensive plasticity for responding to moderate thermal stress (Atkin *et al.*, 2006). This allows them to optimise their performance to suit longer term environmental fluctuations (Inoue *et al.*, 2001). Understanding this type of stress, and a photosynthetic organism's response to it, may have significant implications for efforts to improve agriculture (Sharkey and Zhang, 2010) and for improving models of photosynthetic carbon fluxes into the atmosphere in a warmer future global climate (Heskel *et al.*, 2016).

As is described below, a large amount of work has been published to measure the thermal tolerance of discrete components within cells, based primarily on *in vitro* measurements on isolated components. However, to understand the functional significance of specific thermal tolerances of complexes within the cell, it is necessary to perform *in vivo* measurements. To be able to monitor the activity of specific components, it becomes necessary to measure the impact of a stress on a number of the organism's various cellular components simultaneously, by measuring multiple parameters. For example, in their investigation into moderate heat stress in *Arabidopsis* mutants it was necessary for Zhang

and Sharkey (2009) to simultaneously measure gas flux (net CO_2), chlorophyll fluorescence, P700 and the electrochromic shift signals. Through the integrated analysis of these multiple signals it became possible to interpret the cause of changes in each individual component and thus reconstruct the cause of down regulation of any particular component.

1.3.2 *A summary of thermal damage in mesophiles*

There has been a lot more work to study thermal damage in mesophilic organisms, including plants, and as such it is relevant to examine how these systems cope with thermal stress and damage. In spite of decades of research the primary factors resulting in down regulation of photosynthetic processes in mesophilic phototrophs (those growing optimally in the thermal range ≈ 20 °C to 40 °C, see Fig. 1-1) suffering heat stress are still debated. This is especially true of plants. Some authors subscribe to the idea that Rubisco inactivation at moderately high temperature drives a reduction in net photosynthetic rate. In his review on reversible thermal stress, Sharkey (2005) points out three primary reasons favouring this hypothesis:

- Rubisco activase is inherently heat sensitive
- The ratio of carboxylation:oxygenation, especially in C_3 plants, negatively increases at higher temperatures resulting in the toxic by-product phosphoglycolate
- Plants inhibited in Rubisco activity through activase antisense mutations maintained a higher trans-thylakoid proton gradient and suffered less damage to thylakoid components after repeated thermal stress events, compared to non-inhibited control plants (Sharkey *et al.*, 2001).

Whilst Rubisco activity is seen to be regulated by the thermal lability of Rubisco Activase, the capacity of PSII under heat stress in mesophiles seems to be limited by the binding affinity of the 33 kDa manganese stabilising protein (MSP) (Enami *et al.*, 1994). This external subunit of PSII stabilises the Mn_5CaO_5 catalytic site of water oxidation and has been demonstrated to dissociate from the complex at temperatures that are not high enough to damage other components of PSII involved in electron transport. This has been demonstrated by the addition of artificial electron donors such as diphenolcarbazide after thermal inhibition of the oxygen evolving capacity of the sample (Mamedov *et al.*, 1993).

In vitro work has shown it is possible to wash out the MSP from isolated thylakoid membranes (rendering the system unable to oxidise H_2O) and then reconstitute the water splitting capacity by the re-addition of exogenous MSP – even if it is from another species or type of phototroph (due to the high level of sequence conservation (Williamson *et al.*, 2011)). To demonstrate the significance of the MSP binding affinity on thermal tolerance of PSII water oxidation, Pueyo *et al.*, (2002) isolated spinach thylakoids, washed out the native MSP and reconstituted oxygen evolving capacity through the addition of a thermophilic cyanobacterial MSP. Compared to the native control, this treatment resulted in a significant increase in the thermal tolerance of the thylakoids after incubations of the samples.

Overall the primary cause or component of thermal inhibition in mesophilic phototrophs is not clear cut. Feller *et al's.,* (1998) finding that Rubisco is the primary site of inhibition in cotton and wheat subject to reversible heat stress required a statement acknowledging that the result conflicted with the findings of previous researchers (Havaux and Tardy, 1996, Havaux *et al.*, 1996) who had identified PSII as the initial site of thermal inhibition only two years earlier. In spite of this, Carpentier (1999) , Inoue *et al.*, (2001) and more recently Rowland *et al.*, (2010) again maintain that PSII is the site most sensitive to moderate thermal stress, whilst Sharkey and Zhang (2010) again state that Rubisco activity is the most sensitive site.

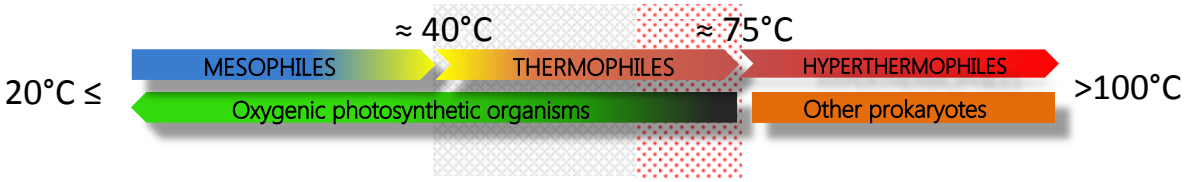

Fig. 1-1: Illustrative definition of mesophiles, thermophiles and hyperthermophiles as they are approximately categorised by temperature.
In comparison to this is a green bar representing the range of temperatures in which phototrophs exist, with the darker colour of the bar representative of fewer species. Other prokaryotes, represented by the orange coloured bar, are found at higher temperatures. The areas of light grey cross-hatching represent the thermal range of moderately thermophilic phototrophs, such as Thermosynechococcus elongatus BP.1, studied in this thesis. The area of red dots represents the thermal range occupied by highly thermophilic cyanobacteria, not studied in this thesis. – Figure is illustrative and not to any scale.

What is reported seems to relate more to the approach taken for defining and studying thermal stress, then the actual processes that thermal stress produce or influence. For example, although the majority of contemporary *in vivo* studies of C_3 plants have found Rubisco activase to be the key regulator responding to moderate/reversible thermal stress, studies undertaken in cyanobacteria, (Yamaoka *et al.*, 1978, Inoue *et al.*, 2001), C_3 plants

measured at elevated CO_2 conditions (Havaux and Tardy, 1996) and C_4 plants (Sage and Kubien, 2007) seem less able to clearly identify Rubisco activity as the primary site of thermal inhibition; or clearly conclude that PSII is the thermally weakest component.

Perhaps it is the elevated concentration of CO_2, found in the carboxysomes of cyanobacteria, in the bundle sheath cells of C_4 plants and generally in C_3 plants subject to elevated CO_2, that allows for spontaneous carbamylation (Salvucci *et al.*, 1986, Feller *et al.*, 1998) of the Rubisco active site, avoiding reliance on activase (where necessary) and making PSII the weakest component in these systems. Allakhverdiev *et al's.*, (2008) review of moderate heat stress in higher plants (therefore, mesophiles) concludes that the oxygen evolving and Rubisco activities are equally heat sensitive. This approach strikes an energetic balance between supply and demand sides of photosynthesis, ensuring redox states do not get pushed beyond a dangerous extreme one way or the other. This mechanism could help localise thermal damage to a smaller and more specific area already subject to high amounts of protein turnover and repair (ie, components of PSII such as the MSP and the D1 protein, or Rubisco activase), whilst protecting those components perhaps more difficult to repair such as PSI (Shimakawa *et al.*, 2016)). This strategy also helps to protect those components of cells that are involved in multiple processes. Consider that PSII participates primarily linear electron transport, whilst PQ,,cyt-b_6/f, PSI and their related redox partners, are crucial to both linear and cyclic electron transport. Furthermore in cyanobacteria, PQ and the cyt b_6/f are also involved in respiration – resulting in the protection of three distinct processes.

Respiration in mesophiles (plants and cyanobacteria) is found to possess consistently greater thermal tolerance than photosynthetic processes (Gifford, 2003, O'Sullivan *et al.*, 2013, Červený *et al.*, 2015). When thinking about and focusing on photosynthesis it is easy to become blinkered into only considering light harvesting, water oxidation, oxygen generation, electron liberation and transfer, the proton gradient, synthesis of ATP, NAD(P)H and the uptake/fixation of inorganic carbon. But when considering the response of entire photosynthetic organisms to a stress like high temperature, which affects all components simultaneously, it can be easily forgotten that the point of photosynthesis is the production of sugars, which phototrophs utilise via respiration. In eukaryotes these two processes occur in separate organelles, the chloroplast and mitochondria, although direct energetic

interactions are reported widely in the literature (Rumeau *et al.*, 2007, Yamori and Shikanai, 2016).

In prokaryotic cyanobacteria, however, where key thylakoid membrane complexes are shared by photosynthetic and respiratory processes (Mullineaux, 2014a), the observation that respiration is more thermally tolerant then photosynthesis (Červený *et al.*, 2015) has a more specific implication for the thermal tolerance of key cellular components. Assuming that the thylakoid membrane can still be used for respiration after high temperature damage, which is data that has not been published by anyone (a conclusion reached after a large effort to find it), the requirement exists for thylakoid complexes in cyanobacteria, such as PQ, cyt b_6/f and cytochrome oxidase, (all downstream of PSII) to exhibit higher thermal tolerance then the water oxidising complex.

It should also be considered that net carbon assimilation is not the 'be all and end all' of photosynthetic electron transfer. Under certain conditions where cells may be suffering stress or even damage, simply pumping protons across the thylakoid membrane can be an end in itself, to ensure survival. This is an idea explored further in the ensuing chapters.

1.4 Understanding thermal damage in thermophiles

Extending research of thermal tolerance and damage in mesophiles is the study of moderate thermophiles (≈ 40 °C to 75 °C – see area of grey cross-hatching in Fig. 1-1) and how they respond to elevated temperatures. Moderately thermophilic cyanobacteria are found to be the upper thermal limit to photosynthesis in the majority of hot springs globally, such as Iceland, Japan, New Zealand and Russia (Castenholz, 1969). Isolated from the Beppu hot springs in Japan, the species *Thermosynechococcus elongtatus* BP.1 (BP.1) has been well studied since the 1970's (Yamaoka *et al.*, 1978). Originally isolated and studied to understand the biochemical changes taking place as phototrophic organisms evolve thermal tolerance (primarily through analysis of cells around temperatures that cause irreversible damage), it is now a fully sequenced (Nakamura *et al.*, 2002) model system for photosynthesis research. In particular, BP.1 and the almost identical strain, *Synechococcus vulcanus* (differing by only a few amino acids), are used extensively for studying protein complexes (due to the extra stability afforded to proteins that allow them to cope with functioning at high temperatures). Most famously, preparations from this organism were

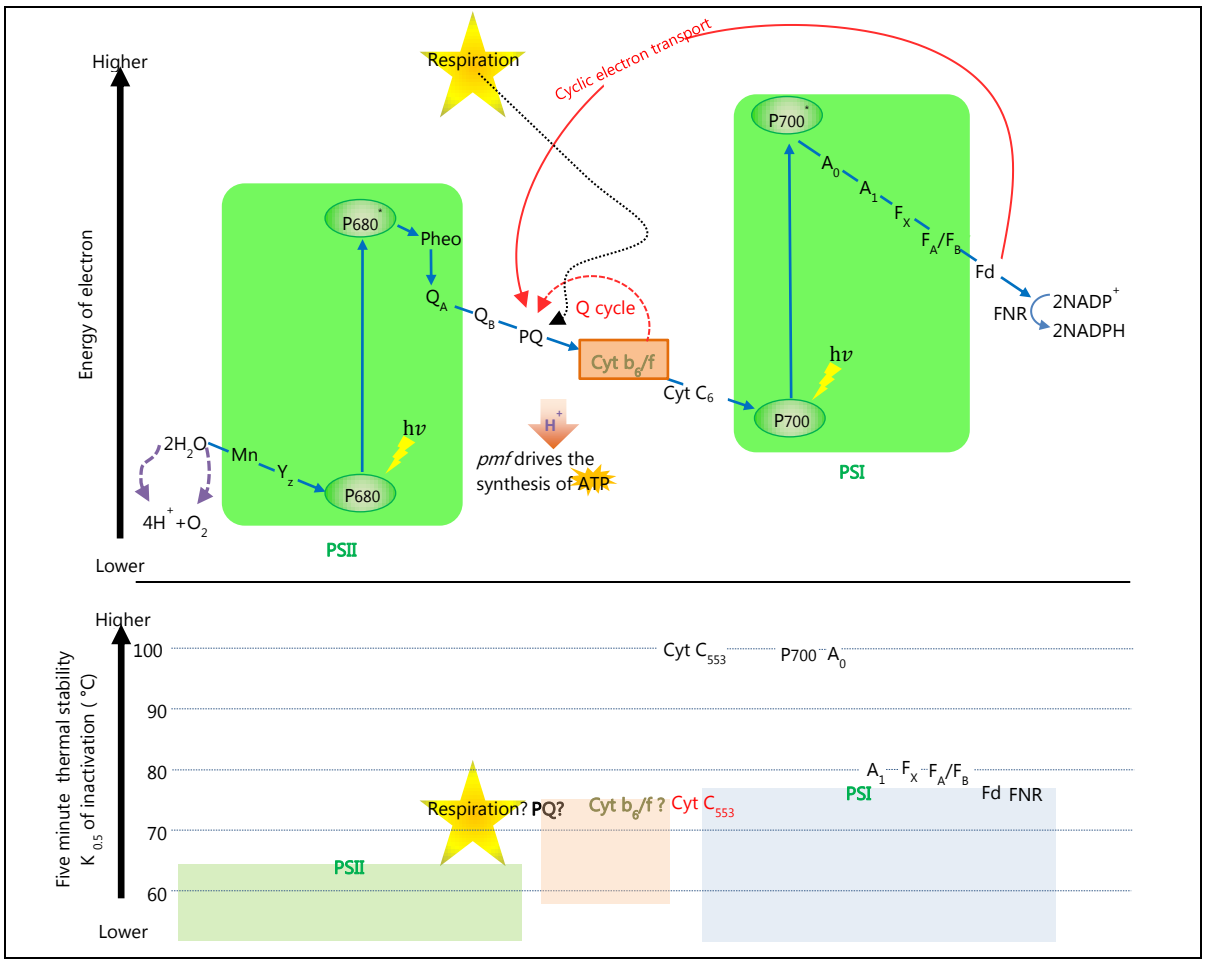

Fig. 1-2: Basic Z scheme of photosynthetic electron transfer from H_2O to $NADP^+$ in upper panel, with values of thermal stability after 5 minute incubations across a range of elevated temperatures for the primary components in the electron transport chain of *Thermosynechococcus elongatus* BP.1 (BP.1) in lower panel.
Note that 'respiration' is not included in the z-scheme's relative scale.
In the upper panel, blue arrows represent linear electron flow, purple dashed arrows illustrate products of water oxidation, the solid red arrow represents cyclic electron flow around PSI, the dotted red arrow represents the Q cycle of the Cyt b_6/f complex and the black arrow represents electron fluxes sourced through respiratory process. The generation of a proton motive force (pmf) by accumulation of H^+ in the thylakoid lumen is represented by the large orange gradient coloured arrow. Abbreviations (left to right): PSI/II, photosystem I/II; Mn, manganese calcium cluster; Y_z, tyrosine 161 in the D1 protein; P680, reaction centre of PSII; hν, photon energy; P680*, excited P680; Pheo, primary electron acceptor of PSII; Q_A, primary plastoquinone electron accepter of PSII; Q_B, secondary plastoquinone electron acceptor of PSII; PQ, plastoquinone pool; Cyt b_6/f, cytochrome b_6/f complex; Cyt C_{553}, cytochrome C_{553} primary electron donor to P700 in BP.1; P700, reaction centre of PSI; P700*, excited P700; A_0,primary electron acceptor of PSI; A_1, secondary electron acceptor of PSI; F_X, F_A, and F_B, three different iron-sulphur centres; Fd, ferredoxin; FNR, ferredoxin-NADP reductase. The star represents reductants reducing PQ via succinate dehydrogenase, it is illustrative of the multiple sources able to reduce PQ and 'not to scale' of the z-scheme voltage potential . Adapted from (Yamori and Shikanai, 2016).
The lower panel represents the published $K_{0.5}$ (temperature where activity was decreased by 50 %)of inactivation in degrees centigrade for key electron transport components in BP.1 after assaying activity/structural integrity of isolated components and/or other(mostly) in-vitro based studies after 5 minute incubations –various authors (see main text). The same abbreviations as the upper panel apply, all components are directly located below their representation in the Z-scheme above. The red font Cyt C_{553} represents the $K_{0.5}$ of photo-oxidation for component assayed *in-vivo*. Black represents the stability of the isolated protein. Green block on the left represents maximal five minute incubation temperature where PSII continued to function (measured with fluorescence signals of PSII complex (Inoue *et al.*, 2000)). Blue block on the left is an estimated maximal temperature of full functionality of PSI based on the thermal $K_{0.5}$ of its key redox components (P700 and the primary acceptor A_0 have been shown to still function after 5 mins of boiling). The central orange block represents my estimate of the unmeasured thermal stability of key electron transport components involved in both photosynthesis and respiration in cyanobacteria – namely the PQ pool and the Cyt b_6/f complex (these components, and respiration, are shown with question marks to represent their unpublished thermal stability). The estimate used is based on the measured stability of Cyt C_{553} oxidation in-vivo, assumes the thermal limitation of Fd and FNR stability sets the upper range for acceptor side activity of P700, which ought not be greater than the donor side components (excluding the possibility of high temperature stability of respiration, for which no data exists). **The uncertainty of these complexes underpins the primary hypothesis in this thesis**

used to generate the high resolution crystal structures of both photosystems (Jordan *et al.*, 2001, Umena *et al.*, 2011).

Research into the impacts of high temperature stress on the photosynthetic processes in BP.1 has revealed that PSII is undoubtedly the most thermally labile component of the organism. Yamaoka *et al* (1978) first proposed this after correlating rapidly decreasing doubling times (and cell death) with the activity of PSII via measurements of net O_2 evolution rates at high temperatures. In a similar study, utilising chlorophyll fluorescence as a measure of photosynthetic performance, Inoue *et al.*, (2000) found that in addition to increased membrane and protein stability (reported in earlier publications), the thermal tolerance of BP.1's photosynthetic apparatus (relative to mesophilic phototrophs) had been increased through an elevated binding affinity of the 33 kDa subunit (MSP) of PSII involved in stabilising the Mn_5CaO_5 catalytic site.

The thermophilic MSP exhibits binding tolerance equal to that of the thermal tolerance of the PSII reaction centre, in contrast to mesophilic organisms discussed above where it is known to be the most heat labile site of the PSII complex (Inoue *et al.*, 2001, Pueyo *et al.*, 2002). By detaching reversibly after even low thermal stress events, the MSP is an excellent candidate for regulating photosynthesis during high temperature events for mesophiles (Enami *et al.*, 1994, Inoue *et al.*, 2001), as discussed above. However, this change in binding affinity is likely to have helped provide the thermophiles with the extra tolerance required for growth at elevated temperatures. The trade-off could be the tight tolerance observed between optimal and lethal growth temperatures in thermophilic phototrophs, where a small increase in temperature above the optimum results in irreversible damage.

Building further upon Yamaoka *et al's.,*(1978) initial reports of PSII lability in BP.1 are numerous biochemical studies of the organism, spanning a number of decades. This work provides a broad view of the thermal tolerance of primary photosynthetic components. These results are summarised in Fig. 1-2 and provide strong evidence that electron transport components downstream of PSII, including the soluble electron carriers, the key components of PSI involved in light reactions and redox coupling, ferredoxin (Fd) and the NADPH:oxidoreductase (FNR) (Koike and Katoh, 1979, Koike and Katoh, 1980, Hirano *et al.*, 1981, Koike *et al.*, 1982, Kaurov Yu *et al.*, 1990, Sonoike *et al.*, 1990, Inoue *et al.*, 2000) all exhibit significantly higher thermal tolerance than the primary source of photosynthetic electrons, PSII.

Although providing an interesting set of data for understanding thermal tolerance of the organism's key photosynthetic components, the majority of this work was conducted in-vitro with isolated membranes, purified proteins and PSI/PSII particles energised with artificial electron donors/acceptors. In addition, the primary basis of these studies was not necessarily to understand the response of BP.1 to thermal stress. Some merely took advantage of the fact that the organism's membrane phase transitions occur at room temperature, allowing their role in regulating electron transport rates to be more easily elucidated (Hirano *et al.*, 1981). This particular work was the first to identify the role of PQ for both photosynthesis and respiration in cyanobacteria.

At no point into research conducted on the thermal stability of BP.1's cellular components, especially that of PSI, has a mechanistic rationale been proposed to explain the observation that PSI and its associated redox components are significantly more thermally stable then PSII. This is especially true of the observation that the trend holds across both mesophilic and thermophile phototrophs.

1.4.1 *What is the thermal tolerance of inter-chain ET complexes?*

In addition to the fact that authors investigating thermal tolerance in BP.1 have not proposed a rationale for the disparity in thermal tolerance between PSI and PSII, it is not possible to find data pertaining to the thermal tolerance of the cyt b_6/f complex or the stability of PQ. As such, it is not possible to speculate on the functional significance of their work pertaining more specifically to PSI. In the lower panel of Fig. 1-2 I have hypothesised that these components exhibit a tolerance that is influenced more by the measured stability of PSI, implicating their role in cellular function at temperatures exceeding that of PSII's stability. Published data on the thermal stability of respiration seems to be missing from the literature, and could shed light on the stability of these significant inter-chain electron transport complexes. This gap in published data is especially significant when considering a

whole cell response to thermal stress, because of the crucial role PQ and the cyt b_6/f complex play as a crossroad between photosynthetic and respiratory electron transport. As such, one of the thesis aims was to provide a context for the findings of previous in *vitro* work, by measuring how the systems functionally interact after high temperature damage.

1.4.2 *Novel methodological approach*

Studying cyanobacterial photosynthetic processes *in vit*ro removes important feedbacks that contribute to regulating the cell's physiology – particularly one can imagine, in response to a stress like heat which affects all systems. It would not be possible, for example, to test the hypothesis that respiration exhibits higher thermal tolerance than photosynthesis, or that it may play a role in survival of transient high temperature events, by simply isolating a component such as the cyt b_6/f complex assaying it, in-vitro. Whole cell, *in vivo* analysis must be performed.

> *However, standard methods of measuring photosynthetic physiology are insufficient to answer the questions posed by the hypotheses stated below in section 1.5. Is it possible to create a system of sufficient complexity, that can operate at temperatures > 60 °C and provide information on multiple individual cellular components simultaneously?*

The primary difficulty associated with measuring the activity of individual cellular components *in vivo* is a result of the very complexity that makes untangling these systems interesting to study in the first place. To monitor each process individually it becomes necessary to simultaneously measure multiple signals, as was conducted by Zhang and Sharkey (2009) in their study of *Arabidopsis* mutants subject to thermal stress. However, where they used chlorophyll fluorescence as a proxy for PSII activity this research work had access to more thorough examination of cellular gas fluxes, membrane inlet mass spectroscopy (MIMS).

In a photosynthetic sample, the separate yet simultaneous measurement of carbon and oxygen fluxes can provide information about the activity of numerous processes and their associated cellular components, from PSII to the Calvin Benson Bassham cycle. However, this is already complicated by the fact that a standard oxygen electrode is unable to de-convolute oxygen production and consumption reactions occurring simultaneously in illuminated samples, providing only a net rate of O_2 evolution (Walker, 1987). Furthermore, such a simple measurement system is unable to provide any information about the rates of carbon uptake in the cell sample, or the actual concentration of total carbon in the measurement buffer. Often work to determine rates of CO_2 fixation in phototrophs relies on the uptake of the radioisotope ^{14}C (Salvucci *et al.*, 1986), which means at best only an

average rate can be determined from a standardised incubation period at an experiment's conclusion. It is not currently possible to use an infrared laser to monitor CO_2 fluxes in a liquid sample, which rules out measurement systems such as the Li Cor, commonly used for carbon flux measurements of leaves.

1.4.2.1 Membrane Inlet Mass Spectroscopy

In principle, a mass spectrometer is capable of measuring oxygen, carbon dioxide and in any biologically relevant gas. However, the sample gas must be introduced into the source under a very high vacuum. This problem was solved by Hoch and Kok (1963) who separated dissolved sample gases from a liquid buffer via a gas permeable membrane. Dissolved gases diffuse directly out of the liquid buffer and through the membrane into the mass spectrometer's high vacuum line, at a rate function of the dissolved gas concentration. This allowed for real time and high precision measurements of multiple simultaneous gas fluxes, limited by the hardware associated with the mass spectrometer. Using this method, termed membrane inlet mass spectrometry (MIMS) (Beckmann *et al.*, 2009), the fluxes of ten gases spanning from mass/charge (m/z) 31 to 46 were simultaneously measured, thanks to ten separate faraday cup detectors of the Thermo-Fisher Ion Ratio Mass Spectrometer utilised. A summary of the cellular processes and components that could be directly measured with gas fluxes is presented in Table 1.

1.4.2.2 Stable Isotopes

Table 1. Quick summary of the broad processes measured for by monitoring each gas

Molecular Mass/Charge	Molecular Structure	Cellular Process/component measured
m/z 32	(^{16}O-^{16}O)	PSII activity
m/z 36	(^{18}O-^{18}O)	Respiration, Alternative Mehler and Mehler type oxidases
m/z 44	(^{12}C-^{16}O-^{16}O)	Calvin-Benson-Bassham Cycle,/ Respiration

The ability to simultaneously measure fluxes of CO_2 and O_2 is not the only advantage of utilising MIMS. This method allows for the use of stable isotopes to further discriminate

between the reactions of a particular gas. In this thesis, samples were enriched with the $^{18}O_2$ isotope to enable the differentiation of oxygen uptake and evolution fluxes during illumination. This provided measurements of true Gross O_2 evolution rates, as O_2 uptake during illumination could be accurately measured – without making assumptions about respiratory activity or the level of function of alternative oxidases and pathways such the Mehler (Badger *et al.*, 2000) and Mehler type (Ermakova *et al.*, 2016) reactions.

By comparing multiple gas fluxes in the light and dark of a single sample, it was possible to begin untangling the convoluted signals produced by intact samples, and to individually compare how each was affected by exposure to thermal stress.

1.4.2.3 Spectroscopy of steady state P700 redox activity

In spite of the power of MIMS, it was not possible to measure the activity of PSI as this is not directly involved in any gas fluxes. It was therefore necessary to incorporate a P700 spectroscopic probe into the measurement cuvette, to follow the redox state and activity of this photosystem. Fred Chow's modified Walz PAM-101 system was used to undertake protocols described by authors such as Klughammer and Schreiber (2008) for steady state measurements of P700. With this set up, which is very similar to that utilised by Zhang and Sharkey (2009), it became possible to include measurements of the activity of PSI and the relative component of donor and acceptor side limitation being experienced by the system - in addition to the multiple gas fluxes provided by MIMS. Furthermore, utilising methods described by Jia *et al.* (2014), it was possible to utilise the P700 probe as a secondary measure of PSII activity, providing a dual set of data to compare from a single set of measurements.

In Chapter Three, the development of equipment and methods necessary for this project are presented . This includes more information relating to the integrated MIMS/P700 system, and how samples were prepared for measurement.

1.5 Hypothesis formulation, thesis aims and structure overview

In mesophilic phototrophs, the functional tolerance to high temperature stress of various cellular components encompassing the photosynthetic system has been heavily researched. Although some debate exists, the overall picture suggests that components downstream of PSII show greater thermal tolerance than the organisms' primary source of reductant.

Previous published work on the physiological impacts of high-temperature stress in the moderately thermophilic cyanobacterium BP.1, has focused primarily on understanding the absolute functional stability of discrete cellular components, exposed to high temperatures, as outlined in section 1.4. The majority of this work was conducted *in vitro*, on isolated components (Yamaoka *et al.*, 1978, Koike and Katoh, 1979, Hirano *et al.*, 1980, Koike and Katoh, 1980, Koike *et al.*, 1982, Katoh, 1988, Kaurov Yu *et al.*, 1990, Sonoike *et al.*, 1990) , or through the addition of artificial electron donors and acceptors to cells (Inoue *et al.*, 2000). The results have clearly shown that PSII is the thermally weakest cellular component of BP.1. Furthermore, the temperatures that inhibit PSII are very close to the optimal temperature for growth in this species (Yamaoka *et al.*, 1978). Strong evidence suggests that thylakoid components downstream of PSII, specifically PSI and primary components of the electron transport chain, exhibit significantly greater tolerance to high temperatures than PSII, and these are illustrated in the lower panel of Fig. 1-2.

There has been no published work investigating the possible physiological significance of this. Furthermore, no data has been published on the tolerance to high temperatures of crucial cellular processes, carbon fixation and respiration.

Hypothesis 1. *The thermal tolerance of respiration is greater than PSII activity in BP.1, consistent with mesophiles.*

To answer this question the thesis set out to complete the first aim:

Aim 1) Utilise membrane inlet mass spectrometry to measure the activity of photosynthesis and respiration in cells of BP.1 under increasing thermal stress to determine if once PSII failed, other cellular systems were still functional. This data are presented and discussed in Chapter Four.

The results led to the conclusion that respiration was indeed able to continue functioning after PSII had suffered thermal inhibition. Furthermore, the data showed that respiration was not subject to down-regulation during illumination, as undamaged samples had been.

Hypothesis 2. *That components of the electron transport chain, shared between photosynthetic and respiratory functions in cells of BP.1, were able to utilise reductant sourced through illuminated respiration to reduce $P700^{+}$ and maintain PSI in a functional state, when PSII was inhibited.*

To answer this question the thesis set out to complete the second aim:

Aim 2) To measure the P700 redox states in cells of BP.1 under increasing thermal stress, to determine if once PSII failed, PSI was still showing evidence of function. This data was generated simultaneously with that presented in Chapter Four, making the two sets directly comparable. This is discussed in Chapter Five.

The results of these measurements provided evidence that respiration was able to reduce the oxidised PSI reaction centre $P700^{+}$, once PSII had been severely inhibited by high temperature exposure.

Hypothesis 3) Can reductant sourced through respiration poise the thylakoid membrane for cyclic electron transport around PSI?

To answer this question the thesis set out to complete the third aim:

Aim 3) Develop/modify a method to estimate steady state fluxes of cyclic electron transport in cyanobacteria, then use this method to estimate the rates of cyclic electron transport around PSI in cyanobacterial cells subject to high temperature treatments.

The work to modify a method used for estimating steady state rates of cyclic electron transport in higher plants, for use with cyanobacteria, and the results of these measurements are presented and discussed in Chapter Six. Although the data supports the finding that respiration can support cyclic electron transport, some problems with the assumptions about the final electron sink under these conditions make the final conclusions less clear. These issues are explored in Chapter Seven, along with a summary of the work carried out throughout this thesis.

Chapter 2.

Materials and Methods

summary of the main techniques used

Chapter summary

In this Chapter, the main methods and hardware utilised during the PhD work are broadly introduced. Within each results Chapter however, more detail of the specific nature of techniques and conditions, relevant to the experiments being discussed, are presented. Furthermore, a number of methods were optimised or developed, for the work conducted during this PhD. Although they are introduced here they are also expanded upon specifically in Chapter Three.

2.1 Cell culturing

2.1.1 *Growth Media*

Growth medium used during the project changed from a commercially procured 50X BG-11 stock from Sigma, to in house made JDM Medium. The change was made early in the project, and growth comparisons indicated that growth was not affected by the change, based on data presented in Fig 3-3. In reality, the components of the two media are very similar. As the majority of the work was conducted with JDM medium, this is described, presented in Table 2.

Table 2: Nutrient composition of JDM Medium

Macro Nutrient	**Final Conc (mM)**
K_2HPO_4	0.18
$MgSO_4.7H_2O$	0.30
$CaCl_2.2H_2O$	0.32
$NaNO_3$	17.65
JDM Medium Micronutrients	
Micro Nutrient	**Final Conc.(mM)**
H_3BO_3	0.02313
$MnCl_2.4H_2O$	0.00174
$ZnSO_4.7H_2O$	0.00040
$Na_2MoO_4.2H_2O$	0.00081
$CuSO_4.5H_2O$	0.00158
$Co(NO3)_2.6H_2O$	0.00008
FeCitrate	0.01362
Na_2EDTA	0.02001

JDM was generally made in bulk batches of 5 L to 10 L. each addition was allowed to fully dissolve before the following ingredient was added to the stirring RO water used to make the stock. Media was divided into 1L shott bottles and autoclaved for sterilisation. The trace metal mix was already available in the lab at 1000 X, it was added at a rate of 1 $mL.L^{-1}$. Post autoclaving, sterile Hepes-KOH at 1.0 M (pH 8.0) was added to the medium, to a final [Hepes] of 20 mM. Note that the reason for changing to an in house made medium was

primarily to allow modification of the constituents. For gas flux measurements, especially work that was conducted at low TCi, it was important to exclude $NaNO_3$, to avoid NO_3^- reduction as an alternative electron acceptor. In this case, the ions were balanced with the addition of 20 mM NaCl and the NO_3^- was excluded. As this buffer was used especially for MIMS measurements, it was significant to minimise pH shifts as this changes the inorganic carbon speciation, and therefore the TCi calibration of the instrument. As such, the measurement buffer contained 50 mM BisTrisPropane-KOH, pH 8.0.

2.1.2 *Growth conditions*

The standard growth conditions for BP.1 cells was 55 °C in approximately 100 mL of growth medium, purged constantly with 2 % CO_2 enriched air in bubble lift tubes suspended in a water bath. These were illuminated constantly at ~ 100 µE with fluorescent growth tubes (NEC, Japan). This method was arrived at, after poor growth rates and culture inconsistency was found with the original cultivation system, in use when the project was started. That system was an orbital platform but suffered from low levels of irradiance and CO_2 enrichment was only able to reach 1 % maximum. More information about the development of the improved bubble lift cultivation system is outlined in section 3.1.2.

For the 6803 WT and M55 mutant strains of Synechocystis, utilised in Chapter Six, the same conditions were used except the growth temperature was reduced to 30 °C.

Culture sterility was maintained, through careful practice and the development of specialised growth equipment. All culture manipulation (dilutions, sampling, inoculation) was performed in a class 2 biological safety cabinet, and all gas entering the cultures was filtered through a 0.22 µm autoclavable filter, which was fixed to the glass gas purge tube. This filter allowed for the gas lines to be aseptically connected, leaving the entire culture tube assembly in a sterile, sealed state, through the use of 'luer' locks. This meant samples were always sealed to the outside, and constant positive pressure kept out contaminants.

To further minimise contamination, the liquid cultures were frequently disposed of, and fresh contaminant free cells from agar plates were used to generate a new starter cultures.

2.1.3 *Agar Plates*

Stocks of BP.1 cells were maintained on 1.5 % Difco Bacto agar plates, made with standard growth medium at pH 8.0 (50 mM Hepes NaOH). These were cultivated in an incubator maintained at ~ 100 % humidity, 2 % CO_2 and approximately 30 µE irradiance, supplied by LEDs. The only change to the medium, besides the addition of the agar, was an increase in buffer concentration to 50 mM Hepes-KOH(pH 8.0), and $Na_2S_2O_3$ at a final concentration of 0.01 mM.

2.1.4 *Contamination checks*

Aliquots from liquid cultures were periodically checked for contamination, particularly when making up a cryo-stock, by adding a small aliquot (100 µL) onto LB plates (Bacto LB, 1.5 % Agar). These plates were available from the main lab supply, and frequently made up fresh. Inoculated plates were incubated at 30 °C in darkness to look for contaminating colonies.

2.1.5 *Cryostorage*

To re-animate -80 °C frozen BP.1 cell stocks, a cryo-tube was rapidly thawed in hot water and heated to ≥ 45 °C. Often an entire tube 1.5 mL tube was added onto a single plate, which was left in a 45 °C incubator under very low light (about 10 to 20 µE, under tissues) at 2 % CO_2. After about a week cells could be observed to be growing. From this plate a swipe was taken, grown under sterile conditions especially carefully in the bubble lift incubator, under standard growth conditions, until approximately OD_{750} of 1.0 was reached (this was when contamination checks were generally made). The sample were concentrated through centrifugation and resuspended in fresh, sterile growth medium containing 20% DMSO. These cells were aliquoted into sterile cryo-tubes, sealed and dropped into LN_2.The tubes were stored at -80 °C.

2.1.6 *Optical density*

Optical density of cell cultures was regularly performed as the primary method for monitoring culture growth. Samples were drawn aseptically from the culture vessel of interest and loaded into 1 mL volume polystyrene cuvettes. Generally the culture was diluted 1/10, so 100µL was taken and diluted with 900 µL with buffer. The absorption of these samples was then determined at 750 nm, with a Pharmacia Ultra Spec Ⅲ. The correlation

between OD_{750} and 'true culture parameters' such as dry cell weight, [Chl] and cell number was established, and presented in Fig 3-4. This confirmed the accuracy of OD_{750} as a proxy for culture growth.

2.1.7 *Measuring Chlorophyll a Concentrations [Chl]*

The concentration of Chl was determined frequently throughout the project, as a method of standardising conditions and results. [Chl] were measured in MeOH, according to the method of either Porra (1989) or Meeks and Castenholz,(1971). Both methods were used throughout the project in order to take advantage of different spectrophotometers available in different parts of the building. Porra's method suited the Carey 50 Bio, as the software 'Simple Reads' was able to automatically record the measured values at each of the three required wavelengths to report the final result. On the other hand, the older Pharmacia Ultra Spec III was only able to measure a single wavelength at a time, and couldn't undertake any automated data processing. As such the Meeks and Castenholz method was useful as it only requires the measurement at a single wavelength. In Fig 3-16, data is presents to show that these two methods gave very similar results, and that 90 % or 100% MeOH didn't make a difference to the result either.

2.1.8 *Dry cell mass*

Sample dry cell mass was determined from cultures in order to collect some fundamental physiological information about the BP.1 strain. The method used involved precisely pre-weighing 50 mL falcon tubes, then filling them with a precise volume of culture at relevant time-points throughout the culture growth. This sample was rinsed three times through a quick spin and resuspension in RO water, to remove excess salts, before a final pellet was frozen in LN_2. The frozen aamples were fully desiccated in a lyophiliser for 3 days, before the tubes were reweighed. The difference was considered the dry cell weight of the culture sample.

2.2 Cell counting

This was undertaken in the early part of the project to collect more physiological information about the BP.1 strain. A 1.0 mL sample of the culture being analysed was collected in an

eppy tube and counted manually, using standard haemocytometery techniques. Samples were diluted as needed.

The results of Cell Counting, Dry Cell Weight, [Chl] and OD_{750} were plotted against each other and showed that the values correlate very highly up to an OD_{750} of approximately 3.0. This showed that simply measuring OD_{750} provided the capacity to report cell culture information in real units of cell.mL^{-1}, µgChl.mL^{-1}, or mg.mL^{-1}. A basic nomogram was developed to easily cross reference these values – presented in the left panel of Fig 3-4.

2.3 Producing Cyano-discs.

'Cyano disc' was the term given to the 'pseudo leaves' made out of cyanobacteria immobilised on glass fibre filter. They were designed to allow measurements of cyanobacteria to be made with systems designed for use with leaves. The method to generate the discs evolved constantly throughout the project, as more was understood more about their properties. In the end a lower [cell] ensured higher rates of gas flux, in a similar way that keeping liquid cultures to a maximum 2 µg.mL^{-1} Chl produced the best gas flux rates, through the minimisation of shading.

The method involved standardising a sample of cells from the incubator and determining the [Chl]. The concentration required would depend on the experiment, but commonly a 10 µg.mL^{-1} stock would be created. From this stock a volume of cells corresponding to whatever was required for the experiment was taken, and added to another volume of assay buffer. For example, 1 mL cell sample would be added to 4 mL of assay buffer – and this 5 mL total volume would contain 10 µg Chl. The vials in which this mixing would occur had a mouth diameter of ≈ 10 mm (see panel A of Fig. 2-1).

A 10 mm diameter glass fibre disc Millipore Class AP, 1.0 µm pore size was cut with a leaf cutter. This disc was placed onto an 8 mm diameter hole cut into a piece of thick polyvinyl tape, stuck firmly down to the filter surface of a syringe driven filter cartridge. The base of the syringe driven filter cartridge was attached to the inlet of low vacuum bellows pump, pulling the glass fibre into the hole in the tape, and holding everything securely. This allowed for the entire apparatus to be inverted and placed onto the top of the 10mm glass vial containing the cell sample diluted to 5 mL tot val. The glass vial and filter apparatus were then flipped quickly over – the buffer was sucked through the glass fibre, leaving the cells

embedded. By stopping the vacuum slightly before all the liquid was pulled through the disc, it remained saturated, ensuring the cells could perform well in measurements.

The now wet, and mostly green 10 mm filter disc was removed from the filter assembly with tweezers, and an 8mm disc was cut from the centre – removing the border area where the glass vial sat, producing an 8mm diameter cyano-disc containing a homogenised sample with no white filter left visible (see panel C Fig. 2-1). Achieving homogenous discs was the reasons the original 10µg.mL^{-1} sample is diluted to 5 mL total volume – as the small concentrated samples would pass unevenly through the disc.

The method of taking a small concentrated sample and diluting it to pass through the filter was a very elegant solution to a problem encountered whilst initially undertaking incubation experiments. Initial data runs showed very inconsistent results and a large error at temperatures where damage started to accumulate. It was realised that the samples were not being evenly incubated, with some heating quicker than others. As such, a method was devised to have the volume of assay buffer, used to dilute the concentrated cell sample, already equilibrated at the temperature of interest. By using even higher concentrations of sample stock a very small volume of cell sample was added to a large volume of thermally equilibrated buffer, bringing the cells instantly to the temperature of interest. By rapidly filtering the cells they were cooled to room temp – stopping the damage. This is how very consistent data across the entire range of incubation temperatures was generated.

2.4 Main MIMS methods

The primary instrumentation underpinning work throughout this thesis was the Membrane Inlet Mass Spectrometer (MIMS), able to make precision gas flux measurements. The instrument used was a Thermo Fisher 'Delta V' Ion Ratio Mass Spectrometer (IRMS). The inlet had been completely modified by the late Warwick Hillier, to enable the high vacuum line to be plumbed through to allow the use of a Teflon membrane within the sample cuvette to be used as a sample inlet port. These Teflon membranes were sandwiched between heavily polished stainless steel plates, with a small amount of Apeizon grease, to ensure a gas tight seal. More information about the cuvettes is presented in section 3.2.2. The method and principles behind the MIMS are outlined more fully by Beckmann *et al.* (2009).

Measurements were conducted in two modes, liquid phase and gas phase samples. Cuvettes for both modes were sealed with a gas tight lid, which provided a port for the integration of a liquid light guide (straight photosynthetic experiments) or a multicore fibre optic (for P700 experiments). In the liquid phase, the lid was sealed by a ring of fluid around its base, in the gas phase an O-ring was sealed against polished stainless steel surface.

In the liquid phase, samples of liquid culture were loaded directly into the stirred and thermostatted cuvette, where dissolved gas was sampled into the high vacuum line through the gas permeable membrane. A stirrer was vital in this mode, to ensure homogenous sampling of the gases dissolved in the sample, to maintain culture suspensions in a homogenous light environment and to avoid the drawdown of gases locally across the membrane surface. The stirrer consisted of a small neodymium magnetic bar, embedded in a Teflon cross shape. It was driven through magnetic induction with switching fields, provided by a 'variomag' stirrer (A+G Labortechnik).

In the gas phase, a solid sample such as leaf disc or 'cyano-disc' was loaded onto a steel mesh suspended above the membrane. The cuvette was sealed with a threaded cuvette top, incorporating an O-ring to create a gas tight seal around the edge. The injection port was sealed with "blue-tac" at all times, with syringes punched through this to introduce new gases to the sample. No stirrer was required in this mode as gas diffusion is rapid enough to ensure homogenous sampling from the entire cuvette, whilst the sample is still, sitting on the mesh. Before any experimental run the instrument was calibrated, taking about half an hour. The following parameters were calibrated: membrane consumption, $[O_2]$/mV, $[CO_2]$/mV, instrument response and background levels (especially for mass 44). These were conducted in the following manner:

2.4.1 *Membrane Consumption*

After reaching the temperature being used for experiments, the cuvette was set up as per experimental conditions, excluding the sample. For cyano disc calibrations, the glass fibre disc was inserted, and all runs included use of the sample buffer, the addition of the approximate $[HCO_3^-]$ or $[CO_2]$and $[^{18}O_2]$ used in the experiment, and the approximate light intensity being used. A background was recorded for light and dark as well, as there was a light effect on the membrane. Ensuring the stirrer was on for liquid runs, the system was left to collect data for a minimum of five mins, but ideally up to ten minutes. During this time,

gas was consumed across the membrane at the approximate rate that would occur during experiments. This rate is a function of the [gas], decreasing over time.

From this data, the following information was taken for each m/z of interest:

$t1$ and $V1$

the signal voltage and time when the measurement begins

$t2$ and $V2$

the signal voltage and time when the measurement finishes

The membrane consumption offset was then calculated in the following manner:

Consumption offset =

$$\frac{\frac{\Delta v\ (mV)}{\Delta t\ (secs)}}{midpoint\ (mV)}$$

Where:

$$\Delta v = V1 - V2$$

$$\Delta t = t2 - t1$$

$$midpoint = 0.5\Delta v + V2$$

The final units of the consumption offset were in the units $mV.sec^{-1}.mV^{-1}$

In the liquid phase there was no need to calibrate consumption for m/z 44, as the HCO_3^- pool constantly replaced the majority of CO_2 drawn through the membrane at around pH 8.0. However, in the gas phase it became necessary to include m/z 44 as the limited CO_2 pool available would be drawn down significantly, particularly if no HCO_3^- reservoir was being utilised (i.e., the addition of some 1.0 M NaHCO3 at pH 9.0, included on a ring of filter fibre within the cuvette, especially required during measurements of leaf disc in 6.1).

2.4.2 *Signal calibration: [Gas]/mV*

In order to convert the raw mV output to a meaningful concentration unit, signal intensity per quantity of gas had to be determined. This was true of any gas being analysed, however it was assumed that the calibration remained the same for different isotopologues, such as between m/z 32 and m/z 36.

For convenience, O_2 was always calibrated with a two-point calibration and CO_2 or TC was calibrated via multiple injections of a known [gas].

2.4.2.1 To calibrate O_2 signals in the liquid

In the liquid phase a two point calibration for O_2 was conducted. An N_2 purge of MQ H_2O in the partly sealed cuvette would provide the zero O_2 offset. The H_2O was then purged with compressed air from the building supply (sourced from the roof), which provided the saturated [O_2] for a given temperature and air pressure in pure water. A table of [O_2] saturated pure H_2O as a function of temperature was sourced directly from Hansatech, and this was used to determine the saturated [O_2] for each calibration. The calibration was then a simple matter:

$$\frac{\Delta\,[gas](saturated\ H_2O\ -\ N_2\ purged\ H_2O)(nmol/mL)}{\Delta V\ (H_2O\ saturated\ mV - N_2\ purged\ mV)(mV)} = mM.mL^{-1}\,.mV^{-1}$$

2.4.2.2 O_2 calibrations in the gas phase

This was very easy and as described above, simply purging the cuvette with N_2 gas to obtain the zero O_2 signal and then purging the cuvette with the compressed air line to find the [O_2] in air, which was then divided by the difference in signal value. The only trick in this calibration was to ensure the freshly purged cold air was able to heat up sufficiently to reach equilibrium in the hot cuvette. For this, it was necessary to keep the cuvette open to the atmosphere and have a VERY slow purge rate into the cuvette. I believe that this method was sufficient to ensure the correct [O_2], corrected for temperature, was found.

2.4.2.3 Calibrating TC ([CO_2] + [HCO_3^-]) in liquid

The calibration value for [TC] was both temperature and pH dependant, and as such the use of liquid buffer required 50 mM buffering to ensure it did not change during experiments. The calibration was conducted through multiple injections of a precisely known number of moles of $NaHCO_3$, generally from a 1.0 M stock made daily. Importantly this injection needed to be into the assay buffer, at the experimental pH. The ΔmV of m/z 44 before and after the injection was determined and the total number of moles injected is divided by this, providing a calibration for mM TC.mV^{-1}.

2.4.2.4 To calibrate $CO_{2\,(g)}$ specifically in the liquid phase

It was still possible to inject known numbers of moles of $NaHCO_3$, however to ensure the equilibrium went completely towards CO_2, the assay buffer in the cuvette was replaced by 0.1 M HCl. In this case the known number of moles of HCO_3^- injected equated to the number of moles of CO_2 produced. So as above, the difference in signal intensity was calculated and the number of moles of C injected were divided by this number – providing a calibration in mM $CO_2.mV^{-1}$.

Importantly, this value must be known to be able to calculate the pH of a buffer solution based on the m/z 44 signal, to be discussed below

2.4.2.5 To calibrate CO_2 in the gas phase

A similar method was used as per the liquid phase. However, the calculations to establish the number of moles of gas injected into the cuvette were slightly more involved. However, assuming one knew the pressure, temperature and volume of gas being injected (and assuming it was a pure gas), then the process was to purge a gas tight syringe a number of times with CO_2 from the building's supply which was left on a constant, slow leak during measurements to ensure purity. A known volume of the gas, assumed to be at room temperature (which was always measured next to the syringe) was injected a number of times into the sealed cuvette. The Hamilton syringe utilised had a valve to seal it from the atmosphere, and ensure the volume injected was accurate. The ideal gas equation could then be used to calculate the number of moles of gas injected into the cuvette, which was of a fixed volume and equilibrated to a known temperature. Once again, the difference before and after in the m/z 44 signal was recorded and divided from the total number of moles injected – to give mM $CO_2.mV^{-1}$.

2.4.2.6 To calculate the pH of a liquid phase sample

This was simply performed by utilising the Henderson–Hasselbalch equation. The measurement takes advantage of the pH dependence of the distribution between $[CO_2]$ and $([HCO_3^-]+[CO_3^{2-}])$. With a fully calibrated instrument it was possible to make injections of a known number of moles of HCO_3^- and look at the resulting $[CO_2]$. It is easy to imagine that if injecting into an acid, the number of moles of CO_2 measured as a proportion of the total amount of Ci injected would be very high, indicating a low pH.

$$pH = pKa + log_{10}\left(\frac{A^-}{[HA]}\right)$$

The pKa of the HCO_3^- ←→ CO_2 for each temperature was found in the CRC handbook of Chemistry and Physics. It was important that the correct pKa for each temperature was selected, when trying to determine the pH of a buffer at different temperatures.

2.4.2.7 Calculating rates of Gross O_2 evolution and uptake

According to the method and equations Radmer and Kok (1976), the enrichment of $^{18}O_2$ into the measurement cuvette allowed for the differentiation of gross O_2 evolution, and simultaneous O_2 uptake rates.

$$U_O = \Delta[^{18}O_2](1 + \frac{[^{16}O_2]}{[^{18}O_2]}$$

$$E_O = \Delta[^{16}O_2] - \Delta[^{18}O_2](\frac{[^{16}O_2]}{[^{18}O_2]})$$

Where:

$U_O =$ Gross Uptake of O_2

$E_O =$ Gross Evolution of O_2

$\Delta[^{16}O_2] =$ The concentration of the $^{16}O_2$ isotope

$\Delta[^{18}O_2] =$ The concentration of $^{18}O_2$ isotope

2.4.2.8 Calculating rates and applying offsets

In Microsoft Excel, raw data from the mass spectrometer was processes to translate data in $mV.s^{-1}$ to real fluxes of µmol(gas).mgChl.hr^{-1}. This required multiple steps. Amplifier gain settings for each of the different detectors had to be standardised to enable accurate determinations of isotope enrichment. The consumption offset was applied and then rates were crudely calculated by integrating 'raw' (including the various offsets) mV data over a time period. This time was changed, depending on the data set and the question being answered. Generally it was kept as short as possible ~ 5 seconds. However, up to one minute was used in the cases that steady state fluxes were required of a single gas. Once a rate in $mV.s^{-1}$ was achieved, the various calibrations were applied for each gas signal being collected. Then they were multiplied to represent an hour, and divided by the [Chl]

concentration of the sample being determined. It was a large spreadsheet, but provided a lot of control over the many steps. Numerous checks were made, such as blank runs, and a check that the calculated enrichment of isotopes always equalled one, (indicating amplifiers offsets were correct) to ensure that the offsets were being accurately applied.

2.5 Spectroradiometer/ cyano-leaf absorptance measurements

In order to calculate an estimate of electron flux through PSI, according to the method of Kou *et al.* (2013), it was necessary to know the absorptance of the sample. For leaves, this was assumed to be 0.85, as discussed in section 6.1.1. However to apply the method to cyanobacterial cells within the MIMS cuvette, a method was developed to enable sufficient P700 measurement beam absorbance, to gain sufficient signal. The development of this technique is outlined in section 3.3, but ultimately lead to the generation of what were termed 'cyano discs', short for cyanobacterial discs, and a reference to the leaf discs they were emulating.

Absorptance is the amount of incident irradiance absorbed by a sample. It is simply the total amount of light a sample is exposed to, minus the fraction of light transmitted and reflected by the sample. Each cyano disc required a value be determined for the amount of light it absorbed, as there was a high variability dependant on the [Chl], determined for each disc. To establish the relationship between a disc's [Chl], and its absorptance, a number of measurements were conducted across a gradient of [Chl] in two cyanobacterial species. This data is presented in Fig 6-4.

To calculate absorptance, it was necessary to measure the reflectance and transmission of a sample. This was calculated as per Bauerle *et al.* (2004) with:

$$100\,\% - (\%\,reflected + \%\,transmitted)$$

To calculate the absorptance, it was therefore necessary to measure both the amount of light transmitted through a cyano disc, and the amount a cyano disc reflected. To perform such a measurement accurately it was necessary to utilise an integrating sphere, collimating light source and for precision, a spectroradiomemter is preferable to a standard PAR meter. I'd like to thank John Evans for his generous loan of the LI 1800-12 Integrating sphere. In Fig. 2-1, a summary is presented of the method used to generate the cyano discs, and the how the measurement was conducted.

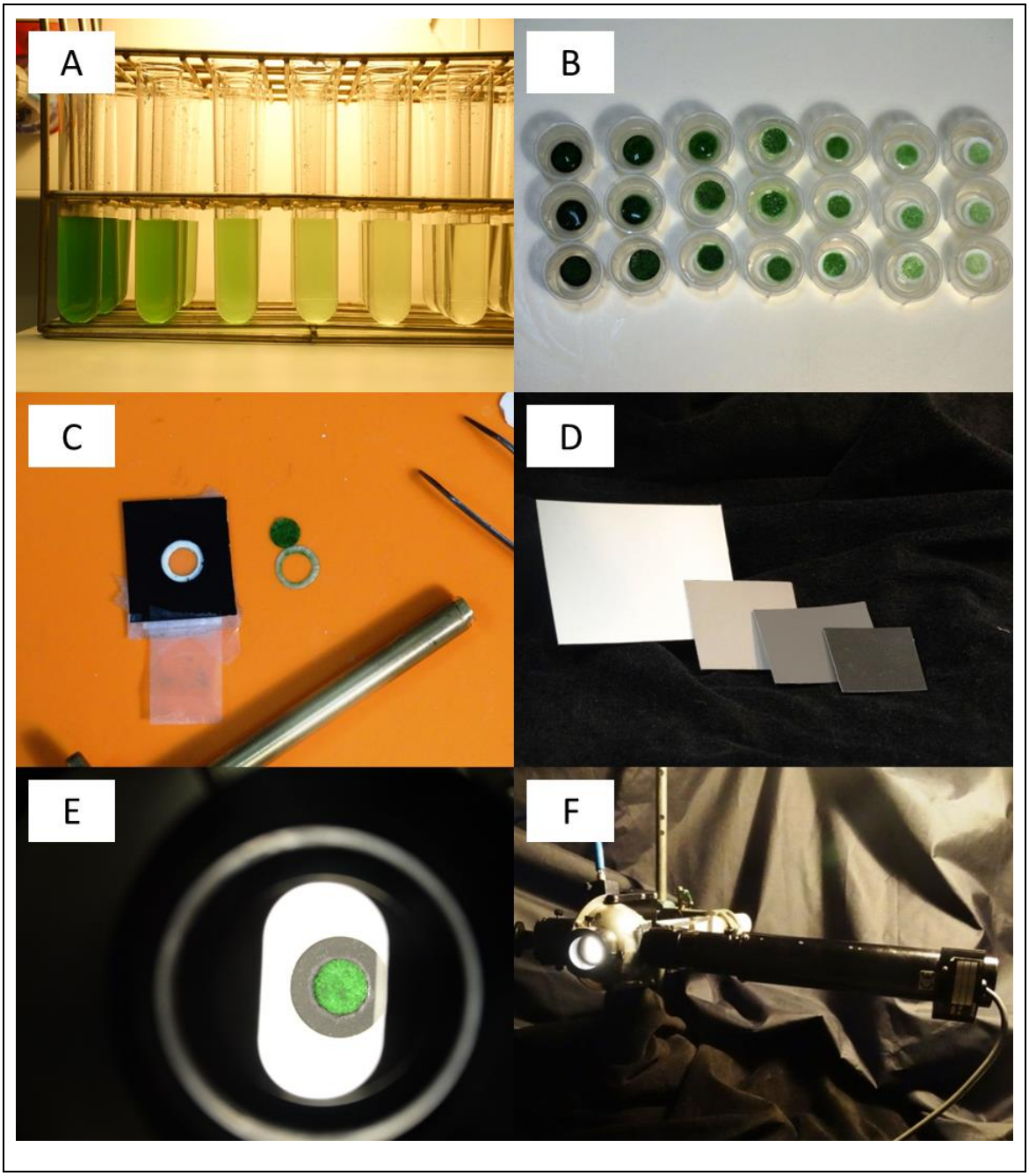

Fig. 2-1: Summary of cyano disc generation, and absorptance measurements

A: dilution series of cell culture made up to standardised volume. B: Each sample was vacuum filtered into a 10 mm glass fibre disc. C: The white masked area of each 10 mm disc was removed to leave a homogenous 8 mm diameter 'cyano disc'. This exact method was used to generate the discs used in gas flux/P700 measurements, however in measurements the cell density was standardised. The 8 mm disc was loaded into a sample holder, which included a masked edge and glass backing. The masked edge maintained a standardised border around samples for reflectance, and the glass backing allowed for transmission measurements to be made, without needing to move the disc into a different sample holder D: The reflectance of a number of calibrated standards were recorded, before the cyano disc samples were measured. E: View into the integrating sphere during reflectance measurement. Care was taken to standardise the orientation of the black card sample mask, which was used for both cyano discs and calibrated reflectance standards. F: The integrating sphere set up for transmission measurement. The long black cylinder to the right is the collimated light source. The sample port facing the camera has been opened, but during transmission measurements contained a calibrated 99 % reflectance card. The blue vertically pointing shaft is the Ocean Optics spectroradiometer fibre optic.

For details on the method for measuring reflectance and absorbance, I refer the reader to the instruction manual for the Li 1800-12 https://www.licor.com/documents/c0vkjb20o7r4lekvm21p.

To summarise: For reflectance, the sample was placed in the holder (panel E, Fig. 2-1), and the light source was aimed on the wall of the integrating sphere. This meant an integrated signal was reaching the sample, and the detector. For transmittance, the light source was moved to behind the sample (panel F, Fig. 2-1), so that it had to shine through the cells. To remove the effect of the glass fibre disc, a number of blanks (filter with no cells) were also included to find the effect of cells only. Where the light had been for reflectance measurements was replaced with a 99 % reflectance standard, which was not moved at all between samples, and hence a standardised measurement environment was maintained.

The fractions of light reaching the detector for each standard were compared against control runs, with zero and 100 % transmittance (i.e. the blank disc in the light path), and for reflectance, against a standard curve generated with calibrated reflectance standards, in the place of the cyano discs.

2.6 P700 measurements

The application of P700 measurements allowed for the simultaneous monitoring of both gas fluxes, to determine the function of PSII, carbon fixation and respiration, and the redox state of the reaction centre of PSI, P700. The spectrophotometric method used has been described in detail by Klughammer and Schreiber (2008). In section 3.3, the methods developed to integrate this measurement into gas fluxes of cyanobacterial cells are described in detail. Then in section 5.2, how the technique was used to monitor the activity of P700 activity is described in detail, including details of the hardware components and all equations. In section 6.1.1 the methodology is described for using P700 to estimate the flux of electrons passing through PSI, under steady state photosynthetic conditions, as described by (Kou *et al.*, 2013). As such, no further description of the system is included in this section.

Chapter 3.

Technique Development and Optimisation

New methods for unique measurements

Chapter Summary

Throughout this PhD, work has been ongoing to improve existing techniques, methods and hardware: or else entirely new approaches have been developed.

A number of experimental considerations, relating to work at much higher than average biological temperatures, are presented and discussed. The idea is to provide the reader with confidence that experimental conditions selected throughout this thesis have been done so based on evidence, and can be supported as such. Furthermore, a number of improvements were made to existing systems:

Areas of development covered include:

- *Cell culturing: Where the original system was producing variable growth rates, generally at much lower than published maximums and produced poorly performing cells – a new one was developed. Data is presented to show various improvements gained through use of this new system.*
- *MIMS hardware: where the existing cuvettes were unable to cope with very high temperatures, and were generally quite prone to noise, a new set of cuvettes were developed – encompassing both liquid and gas phase sampling.*
- *P700 data acquisition: The original system was designed for use with leaf samples. After trying a number of approaches, an artificaial leaf produced with cyanobacetria fixed into a glass fibre filter was found to work well. Data presented provides evidence that the samples performed as standard, even once the 'cyano disc' was samples in the gas phase. This lead to the unexpected benefit of clearer gas flux data for CO_2.*

A number of comparisons are also presented to demonstrate that various methods ,or techniques, were similar enough to be considered the same. This included the methods for the determination of [Chl] in samples, and different growth mediums, which changed over the course of the PhD.

Finally, some of the people with whom I have interacted during this PhD, who have helped both conceptually, and materially, are acknowledged.

Developing & optimising hardware & protocols

To my knowledge, no work had been conducted with thermophilic phototrophs in the Research School of Biology (RSB) when I started my PhD. As such a lot time and effort was required to optimise the growth conditions and to develop methods for accurate physiological measurements at temperatures exceeding the design limits of equipment already available for use. It was also necessary to develop a new approach for P700 measurements of cell cultures using our system, which was optimised for leaves. The results presented in this chapter underpin all further work in the thesis and provides evidence that experimental conditions selected were based on evidence.

3.1 Cell Culturing

In 2010 Warwick Hillier visited Miwa Sigura at the Ehime University, Japan, to take possession of the thermophillic cyanobacterial strain *Thermosynechococcus elongatus* BP.1 (BP.1). This strain was made famous when PSII cores prepared from it possessed the structural integrity to produces X-ray diffraction data to a resolution of 1.9 Å (Umena *et al.*, 2011). Warwick enjoyed recounting the story of keeping the cells warm in his breast pocket as he caused havoc passing through Australian customs.

During his time in Japan he took note of the conditions being used to cultivate the cells – conical flasks on orbital shakers housed in cabinets of enriched CO_2 at 45 °C and approximately 80µE illumination (Boussac *et al.*, 2008). In order to replicate these conditions a number of orbital incubators were purchased – however required modification to achieve a controlled CO_2 environment. David Barwick of the RSB workshop developed a system to do this, through the integration of a Vaisala CARBOCAP (Helsinki, Finland) CO_2 measuring probe integrated with a small programmable controller/solenoid system. Although capable of reaching 2% CO_2 with this hardware, [CO_2] > 1% were not realised due to the high leak rate from the cabinets.

3.1.1 *Selecting a Standard Cultivation Temperature and [CO_2]*

A post-doctoral researcher already working in the Hillier Lab when I arrived, Alison Winger, had undertaken initial growth characterisation work to establish optimal conditions for culturing the thermophilic cells in our system. With reference to the work conducted by Yamaoka, Satoh et al.(1978) she focused on growth at higher temperatures than those

utilised in Japan, to achieve higher growth rates and possibly healthier cells. The results of her initial experiments in Fig. 3-1 show clearly that growth at 55 °C supplemented with elevated CO_2 produced preferable results. Cells were able to grow very slowly at 60°C however this data is omitted for the sake of clarity.

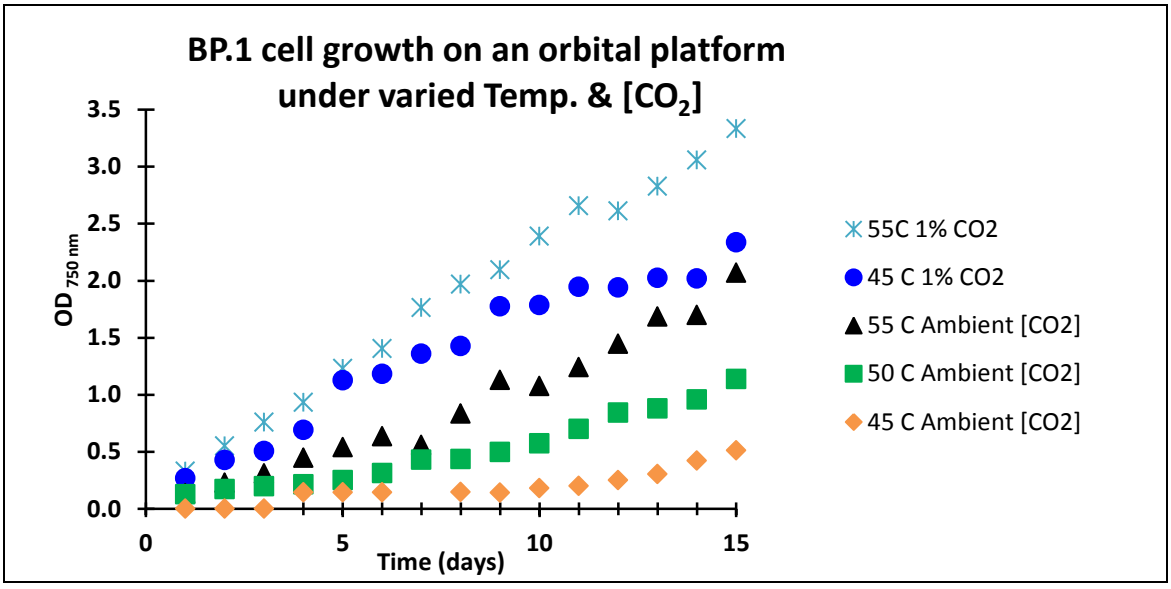

Fig. 3-1: Comparison of growth of BP1 under varying conditions of temperature and [CO_2] on an orbital platform at 120 rpm, illuminated at 80 µE in BG-11 medium at pH 8.0.
Cell density was measured by optical density measurements at 750 nm, with dilutions to ensure instrument linearity. Values represent means of multiple replicates (n= 3 to 6), however large variance resulted in error bars being excluded. Measurements conducted by Alison Winger.

3.1.2 *Comparing Orbital Platform vs Bubble Lift Cultivation*

Although the condition Alison defined was optimal for growth in the orbital platform incubators, the maximal doubling rate of 73 hours was very low compared to the literature value of only 4 hours. Cultures were also temperamental, requiring initial inoculums of a sufficient density (OD_{750} > 0.2) to avoid a propensity to bleach, whilst growth between replicates was highly variable, the error bars in Fig. 3-1 have been excluded due to the large error associated with standard cultivation techniques in those early days.

It was hypothesised that limitations in the solubility of CO_2 at elevated temperatures combined with the relatively low light levels available in the commercially bought system (with only 'top down' illumination) to result in poor cell growth in the orbital incubators. In an attempt to grow cells at rates closer to the published rates, I constructed a pair of bubble lift incubators. This consisted of a glass aquarium custom built by Gem Aquatics (Canberra) to my specifications (230 x 250 x 600 mm) on which a sheet of 20 mm thick Perspex was fit as a lid, see lower panel of Fig. 3-2. Into the lid a number of holes were cut: two rows of circles from which cultivation tubes (aprox. 30 x 300 mm) were suspended into the

aquarium's water. A single large square hole provided a location to suspend a "Julabo" (Germany) immersion heater into the water for thermal regulation. Fluorescent growth tubes (NEC, Japan) running the length of the incubator ensured even illumination across its length.

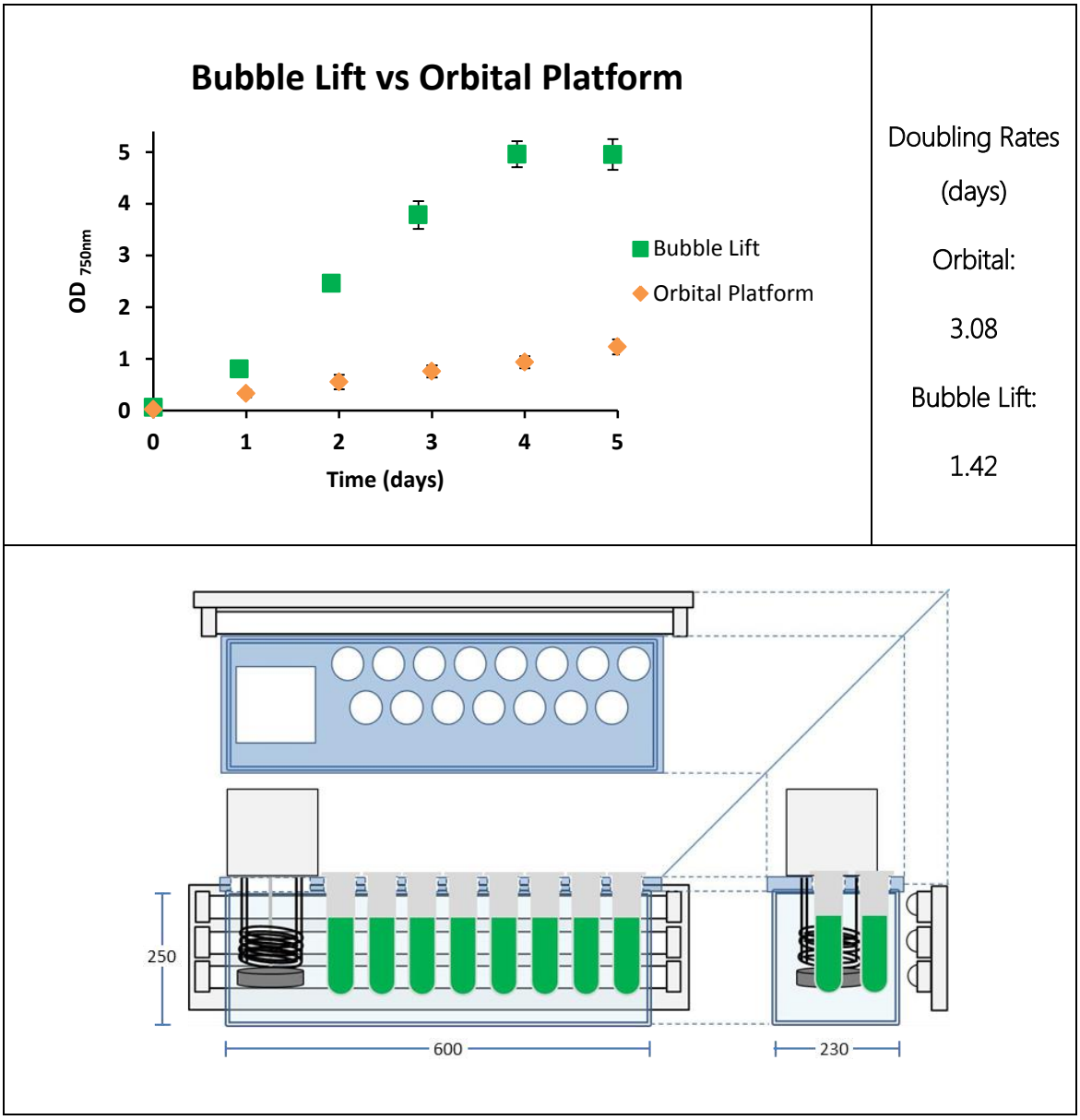

Fig. 3-2: Comparison of BP.1 cell growth when cultivated in bubble lift or orbital incubators.
To compare the advantages of the bubble lift cultivation method directly with the optimal conditions available within the orbital platform. The two set-ups resulted in orbital cells being grown at 80 µE and a 1% CO_2 atmosphere shaking at 120 rpm, whilst the bubble lift cells were grown at 85 µE and 2% CO_2, in BG-11 at pH 8.0. Error bars show standard deviation of three replicates. For a direct comparison, the calculated doubling times are presented in the top right panel. The lower panel contains an orthogonal layout of the bubble lift incubator. Dimensions refer to the glass aquarium, in mm. Sitting on the glass was a 20 mm thick Perspex lid, with holes cut as presented in the top down view. The square hole held the Julabo water heater, with round holes holding the 35 x 200 mm glass tubes used for cultivation. A light panel containing three fluorescent growth lamps (NEC) could provide up to 150 µE irradiance was controlled by adjusting the number of tubes illuminated, or moving the location of the light array. The layout of the holes for holding tubes allowed for eight essentially identical locations to grow cells, under very close to identical irradiance, and temperature, and gas was all sourced from a single source, split via a manifold with needle valve dials to manage bubbling rate.

A gas mixing system was developed utilising "Brookes" flow rate meters, to deliver compressed air enriched to 2 % with CO_2, (calibrated with the Vaisala CO_2 probe). Gas was delivered via a 'luer lock' system, devised out of 1 mL syringes and silicone tubing which attached to 0.22 µM hydroscopic autoclavable syringe filters (Merck-Millipore, Melbourne, Australia). These were modified by way of an autoclavable rubber tip, to provide a gas-tight seal into glass pipettes, pierced through autoclavable silicone-foam bungs in the top of the glass cultivation tubes. This provided a method to aseptically connect/disconnect the gas lines and to sterile filter gas delivered into the cultures.

The resulting improvements to growth rates were considerable and clearly visible in upper panel of Fig. 3-2. Most likely a result of improved availability of light and CO_2, doubling times at 55°C of 34 hours, less than half of the original system – yet far from the optimal rates achieved by Yamaoka *et al.*,(1978). Nonetheless, culture stability saw a marked improvement - inoculum densities of OD_{750} < 0.01 were capable of growing at the standard light intensity used (100 µE) and very low variance between replicates was obtained. Cultures in this system continued to grow linearly to maximal densities of around OD_{750} 5.0, approximately 2.5 x 10^8 cells.mL^{-1} or 1.3 mg.mL^{-1} - as determined through correlations between OD_{750}, Dry Cell Weight (DCW) and Cell Number, as shown in Fig. 3-4. By simply marking a line on the tubes, it became very easy to accurately replace evaporated growth medium when undertaking growth curves, with sterilised MQ H_2O.

3.1.3 *Growth Medium: comparing the options*

The growth medium initially used in the lab for culturing cells was a commercially procured 50X stock of BG-11 produced by Sigma Aldridge (St. Louis - USA), to which an autoclaved 1 M stock of TES (Sigma Aldridge, St Louis - USA) at pH 8.0 was added to 20mM. As the project moved forward, the inability to modify the makeup of this purchased medium, such as the exclusion of NO_3^- necessary to perform accurate O_2 evolution measurements in low Ci conditions (avoiding O_2 produced via NO_3^- reduction to NH_4^+), made it desirable to utilise a self-made growth medium. Already in use in the department was DTN (Muhlenhoff and Chauvat, 1996), making it the obvious choice. To ensure consistency of results between the commercially procured and self-made growth media, it was necessary to test that cell performance was not altered. Cells in the bubble lift incubator were cultured at 55°C in BG-11 and DTN media under both ambient and 2% CO_2 conditions. The results in Fig. 3-3

clearly show that the change in medium did not have an impact on growth under either condition and so throughout this thesis the two media are used interchangeably.

3.1.4 *Growth Measurements: Confirming their Accuracy*

Optical density measurements at either 730 nm or 750 nm is the standard method for rapidly determining cell culture density (Ermakova *et al.*, 2016). However, there are assumptions about cell size and health vs time that must be made to utilise this simple measurement as a proxy for actual culture growth. In order to determine that these assumptions are valid in the thermophillic cells it was deemed useful to measure the correlation between OD_{750} and actual measurements of cell number, dry cell weight and [Chl]. This data allowed for the rapid estimation of these more complex values from the simple OD_{750} measurements.

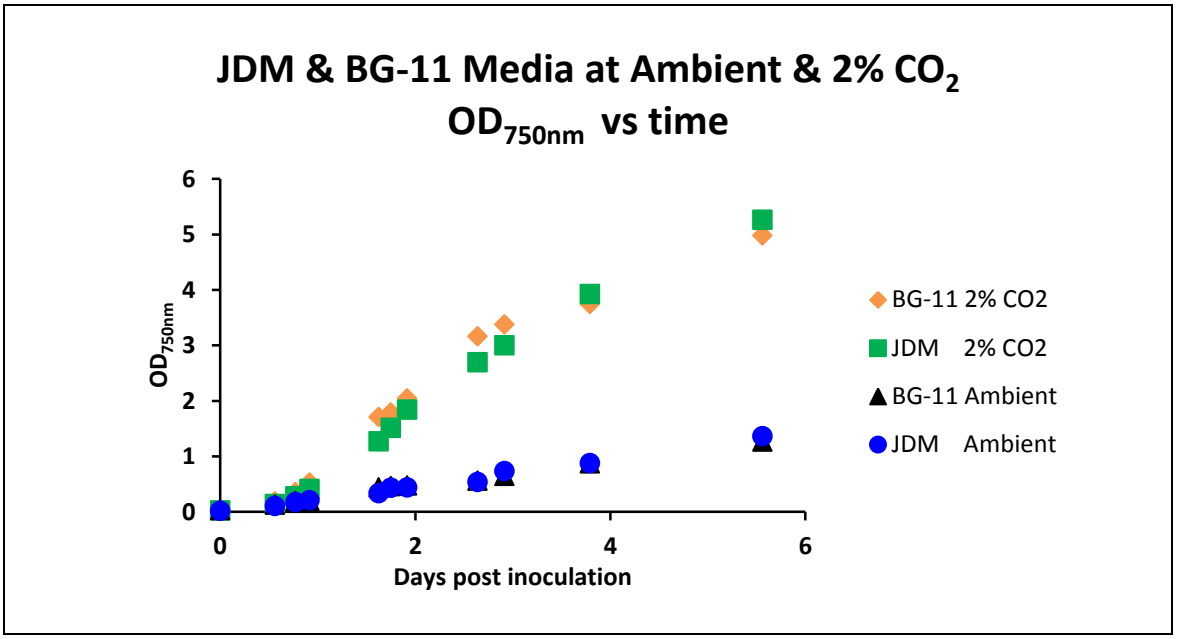

Fig. 3-3: A comparison of growth of *BP.1* cells when cultured in BG-11 and JDM media - bubbled with air containing ambient [CO_2] or 2% CO_2 enriched air at 55 °C and 85 µE.
Cell density was determined through optical density measured at 750 nm from aliquots taken at numerous time-points, diluted to ensure measured value remained within the linear range of the instrument. In this quick development test only a single tube of each culture was inoculated, hence n=1.

Eight growth tubes were inoculated simultaneously in the bubble lift system under optimal conditions as previously defined. At various time-points one tube was used to make measurements of OD_{750}, [Chl], Cell Density and Dry Cell Weight (DCW). The data displayed in Fig. 3-4 shows that the relationship between each parameter and OD_{750} was very highly correlated, and linear when constrained through zero. This information was used to construct a simple nomogram – a tool enabling rapid estimation of each parameter from the simple measurement of OD_{750}, displayed on the left panel of Fig. 3-4. The data confirms

that the assumptions inherent in the utilisation of optical density measurements for the tracking of culture growth are valid for BP.1.

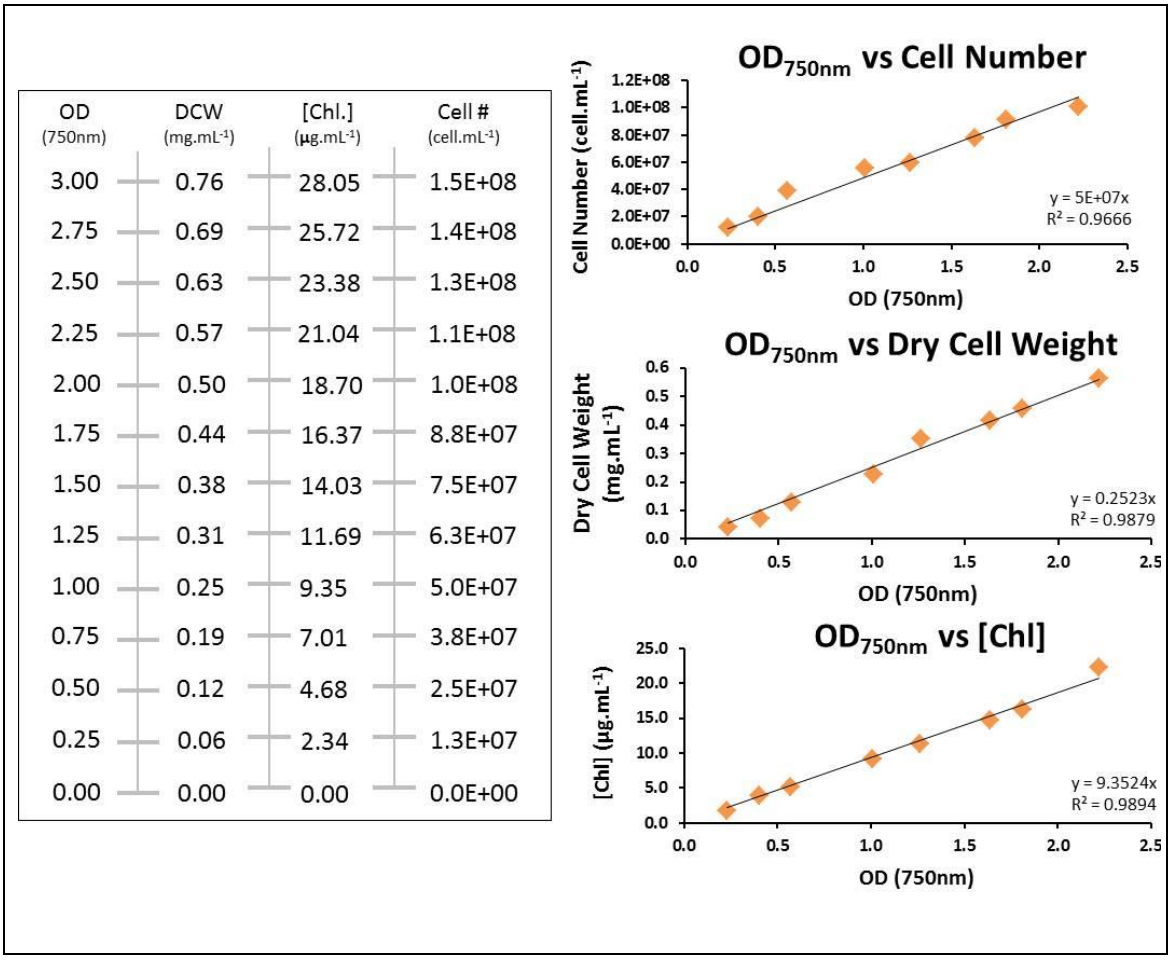

Fig. 3-4: Quantifying the relationship between OD_{750} vs Dry Cell Weight, Cell number and [Chl] in cultures of BP.1 The raw data collected from cultures grown under optimal conditions of 55°C, 2% CO_2 enriched in bubble lift cultivator is displayed down the right hand side – each parameter as a function of its OD_{750}. Strong linear correlations were found with linear regression constrained through zero, up to an OD_{750} of 2.5. Equations determined with linear regression were used to generate the simple nomogram displayed on the left, allowing for simple determination of three key parameters of a cell culture from one measurement. Cultures reaching stationary phase lost linear correlation, likely due self-shading, cell death and cell swell in stationary cultures (data not shown). [Chl] refers to Chl,a - $\mu g.mL^{-1}$.

3.2 Membrane Inlet Mass Spectrometry (MIMS)

Although MIMS has a long history within the Research School of Biology (RSB), no one had attempted using the membrane inlet system at temperatures exceeding 35°C before this project was commenced (a thorough literature search suggests no one has used MIMS at such high as in this thesis). With an optimal growth temperature of 55°C it was clear that work with BP.1 would require 'turning up the dial on the MIMS thermostat'. It quickly became evident that the original brass cuvettes and magnetic stirrers were not up to the

task. A combination of rapid oxidation of the brass surface leading to membrane noise combined with an inconsistent stirrer speed (as the small electric motor suffered at higher temperatures), to produce very noisy data. From the beginning a lot of work was required to improve the cuvette and associated hardware for performance at high temperatures.

Work was then able to start on developing an understanding of the effects that varied temperatures have on membrane properties, such as consumption rates, and how these interacted with chemical considerations such as gas solubility, which becomes sparing at higher temperatures, and equilibrium constants. This was especially relevant for inorganic carbon speciation. Moving the lab from the old Robertson Building to the new Linnaeus building was very disruptive and cost a lot of time: but provided an opportunity to set up a beautifully customised space for MIMS/P700 physiology.

Fig. 3-5: The MIMS and P700 equipment as set up after the building move from the Robertson to the Linnaeus Building.
The Thermo *Delta V* IRMS on the bottom right hand side of the screen. Warwick Hillier's custom valve assembly and ice trap are visible to the instrument's left. Gas plumbing for N_2, CO_2, Compressed Air and argon is located along the back wall. The Gas phase cuvette used to undertake measurements of 'cyano-discs' is set up and attached to the multi-core fibre optic, in front of the orange mat on the bench in the image centre. Four power supply units, side by side, each drove an LED lamp for the P700 measurements, as did the large flash unit on the shelf above them, with the actinic light power source in a blue box on the shelf centre right/top of the image. The laptop on the desk, left, was used to drive P700 acquisition software, the BNC pulse/delay generator next to it. Above this is the Walz PAM 101 and a voltage meter to balance the measurement signals with greater precision. Incubation water baths, the MIMS PC are out of the field of view. A higher detail image of the P700 apparatus is presented below in Fig. 3-10.

3.2.1 *MIMS Flux Measurements at High Temperatures*

Temperature affects numerous physical parameters of the MIMS system and a number of these are synergistic. The key parameters relevant to physiological measurements that

required consideration were the membrane consumption rate, which increases with temperature, gas solubility which decreases with temperature and equilibrium constants, particularly for inorganic carbon. Fig. 3-6 presents a number of fundamental measurements as functions of temperature, primarily for O_2 but also TC.

Although none of this data is new, it was important to keep these effects in mind when conducting measurements, particularly as the mass spectrometer and software only presented raw, uncorrected readouts of mV versus time, having no offsets for these effects. For example, the synergy between decreasing gas solubility, increasing membrane permeability and associated increase in signal versus gas concentration: generated complexity for the analysis and acquisition of signal at high temperatures.

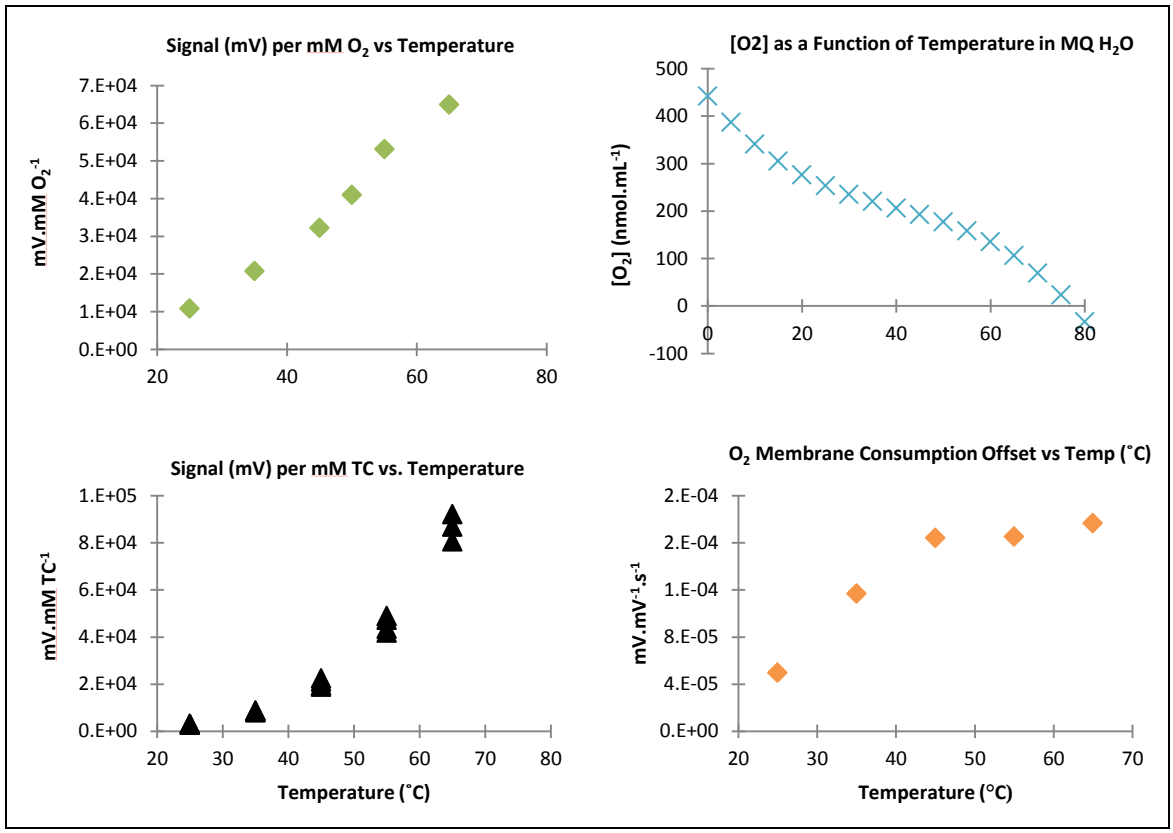

Fig. 3-6: Data illustrating the thermal effects on fundamental measurement parameters.
Figures on the left present the signal measured by the mass spec per mM of dissolved gas at each measurement temperature. The clear increase in signal for a given gas concentration is a result of the increasing membrane consumption rate, shown in the bottom right panel. The membrane consumption offset value, based on measurements of the membrane consumption rate, which is a function of temperature and [gas] is used to correct rates when analysing data. The plateau around 45°C is probably a result of the decreasing concentration of oxygen at higher temperatures, which decreased the amount of gas able to diffuse through the membrane. This is illustrated in the top right panel, which shows the maximum solubility of O_2 between zero and 80°C in pure water. This data is based on Henry's law and provided by Hansatech. It shows how difficult oxygen evolution measurements close to 80°C, or anywhere over 60°C are to perform. All measured data was collected under measurement conditions in BG-11 medium, without cells. Each data point represents an n=1. This data is here to illustrate the effects of temperature on the techniques and data was not used for analysis.

This was particularly true at temperatures > 60° C, where gas solubility rapidly declines (Fig. 3-6, top right panel). The very large signal intensity versus gas concentration

resulted in increased noise of calculated rates due to the resultant very high calibration value. In later stages of the project, this was a factor that helped change the methodology from one of rate measurements at a given temperature to one of measurements at a single optimal temperature.

A constant problem with low gas solubility at elevated temperatures was the formation of bubbles in liquid medium, as cells photosynthesised and oxygen levels reached saturation, or growth medium at lower temperature heated in the cuvette and dissolved gas came out of solution. These bubbles formed on both the stirrer and sidewalls, generating noise and altering the flux of gas through the membrane by providing a competing location into which gas diffusion could occur. At very high temperatures it became necessary to vacuum purge dissolved gas out of pre-thermally equilibrated buffer to minimise bubble formation.

3.2.2 *Cuvette Problems: developing a new system*

As briefly described, the MIMS cuvettes available upon starting this project were unable to cope with the temperatures required when working with thermophilic cyanobacteria. Two key problems were identified that required a new cuvette concept to be developed, capable of performing the elevated temperatures.

1) the bronze used in the original cuvettes rapidly oxidised, producing a rough surface for membrane adhesion/sealing, resulting in noise.

2) The original stirrer consisted of a small DC electric motor, rotating a magnet. The cuvette sat on this stirrer, as shown schematically in Figure 2 of Beckmann et al. (2009). This design subjected the electric motor to the cuvette's temperature and I found that at around 55 °C the stirrer motor became erratic, resulting in stirrer noise. This is clearly illustrated in the top two panels of Fig. 3-8, where net O_2 evolution and TC uptake rates of BP.1 are measured in the bronze cuvette at 45°C and 60° C. It is clear that levels of noise beyond 55° C were too high to make any clear conclusions.

These problems were solved by designing and manufacturing a new cuvette from stainless steel, and replacing the DC motor based magnetic stirrer with an inductively coupled magnetic stirrer system. The development of this system was time-consuming but the results were impressive, as can be seen from a comparison of gas fluxes at high temperatures in Fig. 3-8. We achieved a cuvette that suffers very low levels of membrane

noise, in part through a very highly polished stainless steel, corrosion resistant surface (see Fig. 3-7), which provided excellent sealing qualities for the membrane, combined with the digitally controlled inductive magnetic stirrer "Variomag" (H+P Laborteknic) providing consistent magnet rotation across the entire thermal range. I would like to acknowledge the efforts of Link Williams in helping to design and build the system. The lowest panel in Fig. 3-8 shows that even a 65 °C measurement temperature generated reasonable data, the majority of the measurement noise at this point is coming from the effects of high temperature on solubility and equilibrium constants, particularly for TC distribution, described above.

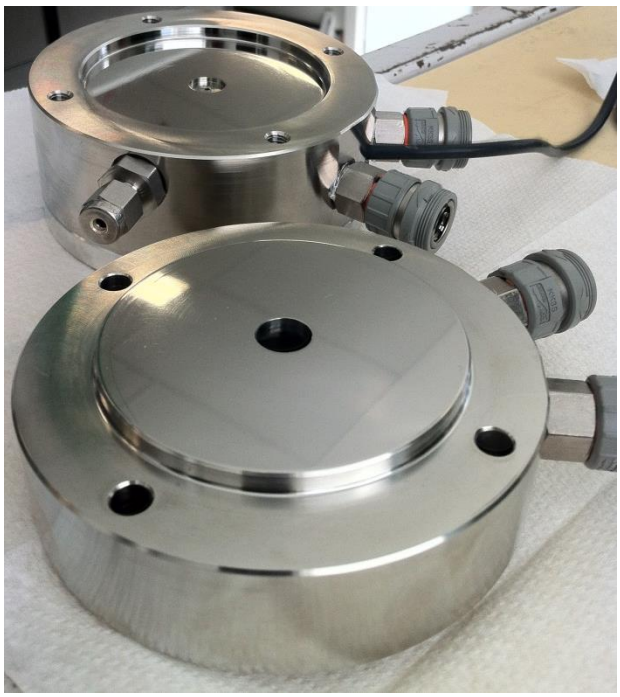

Fig. 3-7: A new stainless steel cuvette: Photograph shows the highly polished surface onto which a tiny volume of 'Apiezon' N, the cryogenic tolerant, high vacuum grease was applied. I found this was less likely to liquefy at high temperatures and was preferred over the other forms of Apeiezon. Grease helped seal the Teflon membrane between the two faces to form the 'membrane' component of the MIMS. The high vacuum outlet can be seen on the further back component, which was covered with a sintered plastic 'frit' to support the membrane. The membrane sealed between the two heavily clamped together faces. The four outlets on the right of the cuvette are quick release/self-sealing valves for the water bath. The cable visible between the two water connections was attached to the induction magnetic stirrer, integrated into the base. The top of cuvette (hidden) contained the location where samples were entered, and different lids were used according to the phase of the measurement sample.

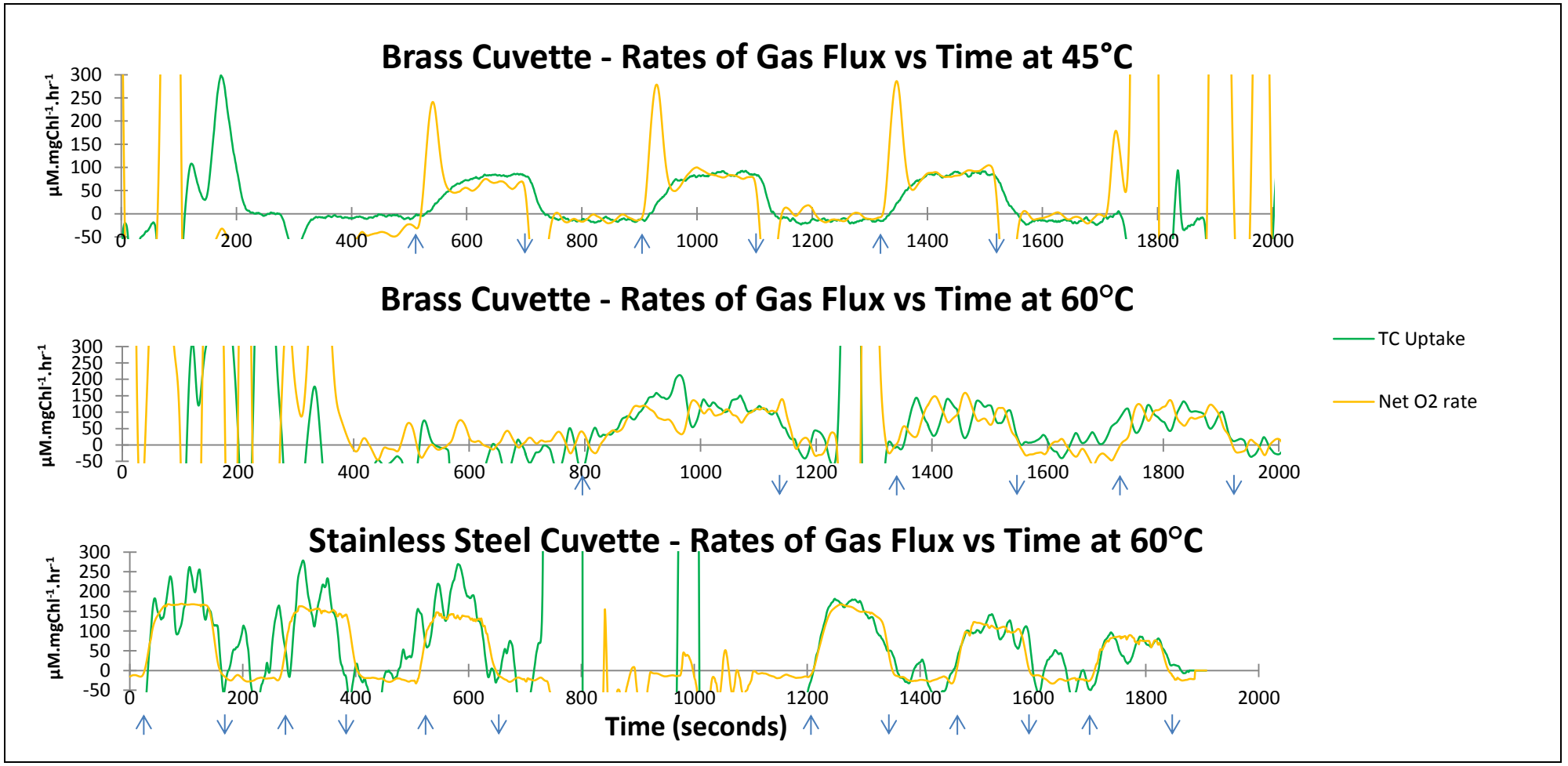

Fig. 3-8: Comparison of the rates of gas flux vs time, in the liquid phase, generated at two different cuvette temperatures in the original brass cuvette.
These panels are representative of data utilised to generate Fig. 3-9, and illustrates the noise encountered when measuring gas fluxes in the original brass cuvettes 45 °C vs 60 °C, in the upper and middle panels, and then at 60 °C in the stainless steel cuvette in the lower panel. Three minute illumination periods, in triplicate per sample. The increased general noise, but specifically the large 'bleep' at 1200 seconds in the middle panel, were characteristic of the results when brass cuvettes were used above 50°C. This was found primarily to be a function of the magnetic stirrer being utilised, which became unstable at higher temperatures. It is clear that the data in the lower panel is much clearer, with 'extra' noise in the 700 s to 1200 s time due to loading a new sample. That said the general noise, especially for TCi uptake rates is quite high. Cells were grown at 55 °C on an orbital platform at approximately 70 µE, atmospheric CO_2 enriched to 1%. Measurements were performed at natural abundance of O_2 — hence only Net O_2 evolution rates are presented. Up arrows indicate actinic light on, down arrow indicates light off. [Chl] = 4 µg.mL^{-1}.n=1, representative data.

3.2.3 *MIMS vs O_2 Electrode: Validating the Data Analysis Spreadsheet*

The software package (Delta V) supplied with the Thermo Fischer mass spec was not able to perform rate calculations or provide live feedback regarding gas concentrations. A certain level of experience was therefore required to undertake experiments, particularly in light of the effects of temperature on the chemical properties within the cuvette mentioned previously. It also required the creation of a spreadsheet capable of performing quite a large number of data calculations, including offsets for parameters such as membrane consumption, amplifier gain settings and isotope enrichment, before calculating final rates.

To validate the spreadsheet's accuracy, a comparative measurement between the MIMS and a Hansatech O_2 electrode was undertaken. The results showed similar figures, accounting for the fact that different illumination was provided for the respective samples. A second check was made by comparing O_2 evolution rates measured in my system against literature values, once again showing 'ballpark' maximum net values of 350 µmol.mgChl^{-1}.hr^{-1} at 55 °C (Yamaoka *et al.*, 1978). The spreadsheet went through numerous iterations over the course of the project, and is now a fairly straightforward to use tool for precisely calculating rates of various gas fluxes (Net O_2 evolution, Gross O_2 evolution, TC uptake) and the [TC] in a number of different units, including µMol/mgChl/hr and µMol/m^2/sec.

3.2.4 *Temperature and Cultivation Method vs Cell Performance*

In the early days of the project cells were being grown in the orbital platform and these cells were used to generate a temperature response curve, comparing O_2 evolution rates to cuvette temperature. The results of these early experiments in Fig. 3-9 clearly show that O_2 evolution rates were maximal at 55° C. However at only 150 µMol.mgChl^{-1}.hr^{-1}, this rate was less than half of published values.

These low rates, in conjunction with the low growth rates described in Fig. 3-2, were the reason a bubble lift cultivation system was trialled and ultimately utilised. It should be noted that these early experiments were conducted at 4 µgChl.mL^{-1}, whilst later experiments were conducted at 2 µgChl.mL^{-1}, (to minimise self-shading), and this discrepancy accounts for some of the lower rates measured. Repeating the experiment with the bubble lift cells resulted in a very similar to the published literature, indicating the correct method had been

developed. Cells cultivated in the bubble lift system at 55 °C, 2% CO_2 standardised to 2 $\mu gChl.mL^{-1}$ became the standard condition for measurements in the liquid phase. This temperature was also adopted as the optimal temperature in later experiments where the sample was pre-incubated at the temperature of interest and then measured at their 'optimal' temperature.

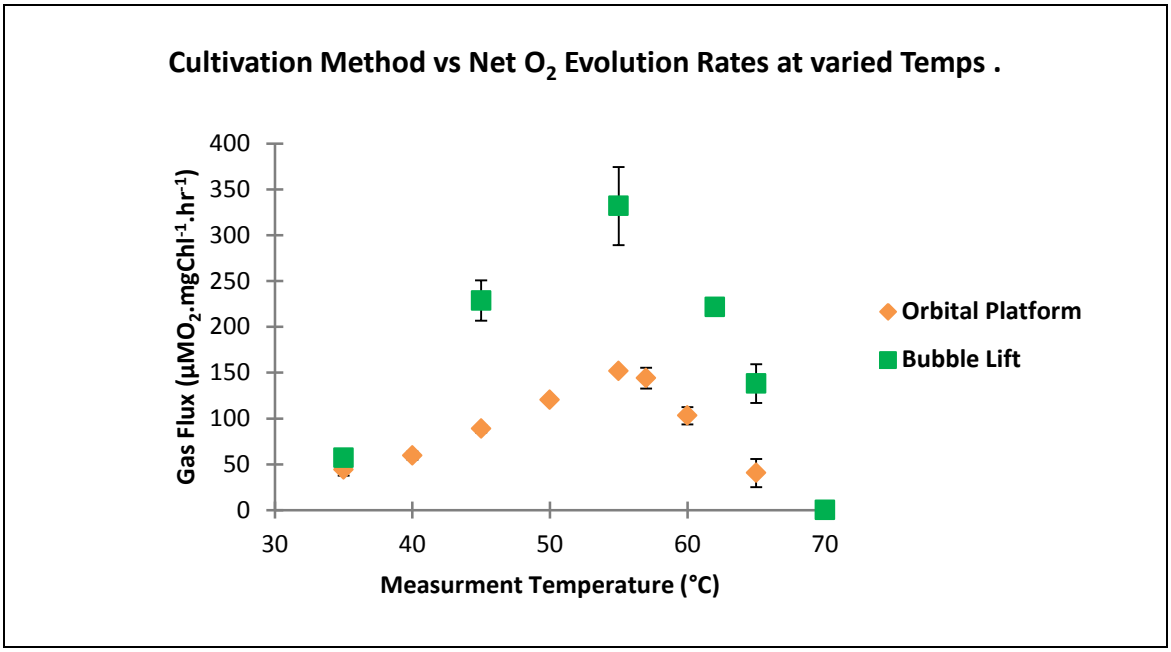

Fig. 3-9: Impact of cultivation method on rates of Net O_2 evolution measured in MIMS, with cuvette set to each of the indicated temperatures: note different [Chl] between samples.
Orbital platform cells grown at 55°C, 1% enriched CO_2 on an orbital platform at 80 µE, were standardised to 4µg.mL^{-1} chl a. Bubble lift cells were cultivated at 55° C and 2% CO_2 enriched air at 100 µE, final [chlorophyll] was standardised to 2 $\mu g.mL^{-1}$. Four mL of both samples were loaded into the cuvette, incubated five mins in the dark before measurements were made (except at 65°C as this was lethal, so measurements made rapidly after signal stabilisation) with saturating light (300 µE) at around 500 µM HCO_3^-. Error bars show St Dev of at least 3 measurements. Difference in growth conditions due to the capabilities of the two systems.

3.3 Integrating MIMS with P700 measurements

Although gas flux data alone was capable of providing a lot of information regarding the relative activity of key cellular components, it was not possible to monitor PSI activity. As a significant cellular component, this was a problem. If any positives can be taken from the tragic passing of Warwick Hillier, it was Fred Chow's addition to my panel as a co-supervisor.

We immediately began working together, adapting his leaf based P700 measurement system for use with cyanobacteria and integrating this with the MIMS to enable simultaneous measurements. The problems generated and solved during this process resulted in an enhanced cell physiology measurement procedure for both gas fluxes and the incorporated P700 data. In the section below I will describe the numerous problems

encountered and how they were solved, starting with spinach as a well understood control, before moving to measurements of cyanobacteria

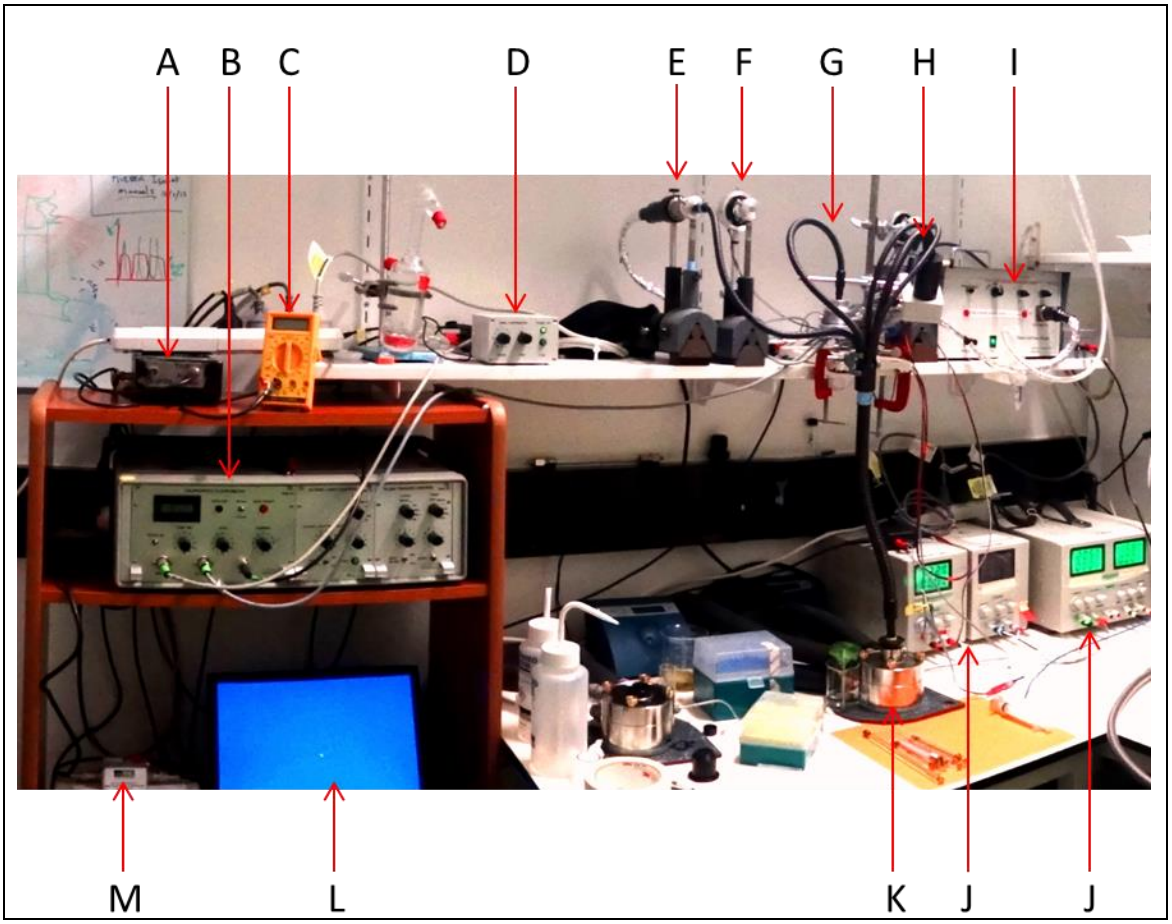

Fig. 3-10: Integrated set up of P700 system and MIMS cuvette, focus on the P700 system.
Numbers and arrow correspond to the following components: A) Analogue to Digital converter B) Walz PAM 101 system C) Voltmeter for monitoring signal with improved precision D) Signal balance control to match absorptance between the 810 nm measurement beam and the 870 nm control signal E) Xenon flash lamp for P700max saturating flash F) Actinic Light for pre-illumination of spinach samples G) Far Red Light with low voltage for weak constant illumination of P700max and high voltage for strong pulse used in Y(I) H) PAM emitter and detector I) capacitor for Xenon flash lamp J) Current supply for various LEDs K) MIMS cuvette L) Laptop for running P700 acquisition software M) Switch for selecting P700max or Y(I) components. Missing from this image: BNC pulse generator programmed to switch light flashes and acquisition software and the associated electrically actuated switches between power supplies and light emitting components.

3.3.1 *P700 with MIMS, Proof of Concept with Spinach*

The P700 set up was designed for use with leaf discs in a custom cuvette sitting in Fred Chow's laboratory. The first step was to rebuild the P700 system in Warwick Hillier's MIMS laboratory, then to create a gas tight MIMS cuvette for work in the gas phase and integrate the multicore fibre into the MIMS cuvette lid. The initial aim was to recreate data already generated with spinach leaf discs. The specific method used to generate P700 data is explained in section 5.2, where data generated with this technique is discussed. The problems found and solved during this process resulted in an enhanced cell physiology

measurement procedure for both gas fluxes and the incorporated P700 data, also discussed in Chapter 5

Measuring gas fluxes of spinach discs with the MIMS provided an opportunity to observe numerous assumptions made using standard Hansatech O_2 electrodes, such as the true [CO_2] of the atmosphere when equilibrated to a reservoir of 1.0 M HCO_3^- at pH 9.0 – standard procedure in Hansatech O_2 electrodes (Walker, 1987). Although the basic spinach measurements were quite easy to establish they took some time to perfect. An electronically triggered shutter system needed to be incorporated into the existing actinic light source for steady-state Y(I) measurements, which was further modified to reach sufficient illumination for saturation of the discs (> 2000µE). Results from these measurements are presented and discussed in Chapter Six.

An initial problem of consistently low O_2 evolution rates was eventually solved through analysis of the Δ [CO_2] over the course of each experiment. I was not used to the rapid rate of CO_2 drawdown that the leaf discs were capable of (compared to cyanobacterial rates), so my assumption that an initial [CO_2] of 5% would be sufficient to conduct a full set of P700 measurements for each sample, whilst excluding photorespiration, was incorrect. This necessitated the incorporation of the 1.0 M HCO_3^- reservoir at pH 9.0, commonly utilised in oxygen fluxes from leaf discs as described by Walker (1987), although this removed the ability to monitor CO_2 uptake fluxes simultaneously from the spinach disc samples.

Eventually success was achieved, both $P700_{Max}$ and steady-state Y(I) measurements could be consistently performed with numerous concordant technical repetitions, laying the foundation to make these measurements with cyanobacteria.

3.3.2 *Initial Set up and Measurements; Creating a "Leaf" with Cyanobacteria*

Initial attempts to measure P700 in cyanobacteria involved the use of a four mL volume, 27 mm path-length stainless steel MIMS cuvette, the same one used for liquid phase gas flux measurements. The first problem encountered pertained to signal intensity, as the 820 nm measurement wavelength is poorly absorbed by cells in a diffuse solution (not a problem in leaves thanks to the internal reflectance and associated extended path-length that is a feature of leaf architecture (Hu *et al.*, 2013)). As such, the first P700 measurements of

cyanobacteria suspended in liquid at 2 µg/mL^{-1} chlorophyll provided no information, as illustrated in the top left panel of Fig. 3-11. In fact, light at this wavelength is so poorly absorbed that concentrating the [Chl] by 18 fold, to 36 µg.mL^{-1}, resulted in no change to the level of measurement beam absorption.

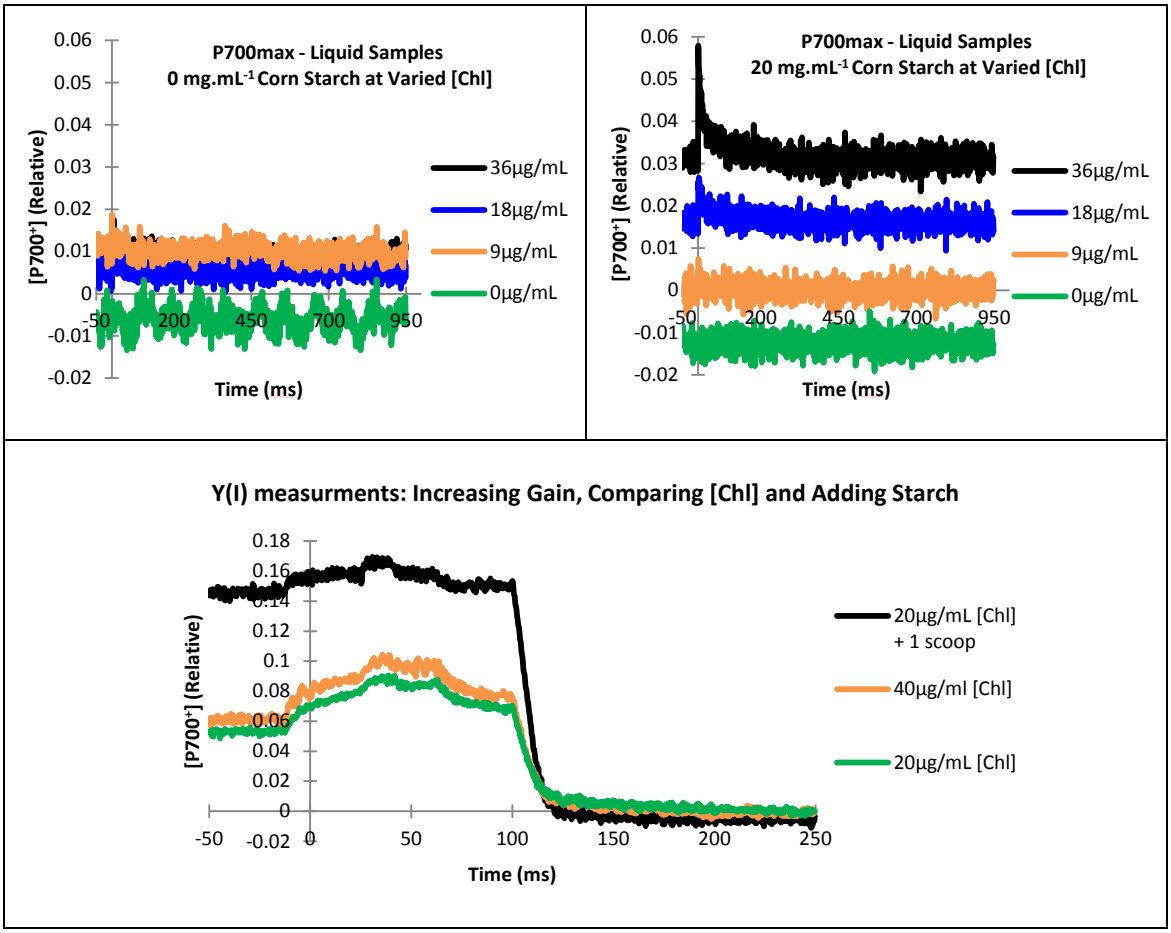

Fig. 3-11: P700 signals measured in liquid samples of BP.1 cells in the MIMS cuvette.
Initial efforts to integrate the P700 measurements with the MIMS. Top left panel shows attempts to measure $P700_{max}$ across a range of [Chl], and a blank with only the stirrer on. The blank shows the stirrer generated signal noise. Top right panel shows same samples, measured after the addition of 20 mg.mL^{-1} corn starch: in a bid to increase the internal reflectance of the sample and improve the absorption of the measurement beam. Bottom panel shows measurement of $Y(I)$ in liquid samples, comparing two different [Chl] and the addition of 10 mg.mL^{-1} of corn starch. Signal intensities not directly comparable, due to different gain settings between the $P700_{max}$ and $Y(I)$ measurements – data was used to asses usefulness of increasing [Chl] or starch addition, no analysis is based on this data and n=1, it is included to illustrate the processes of development undertaken during the research project.

In order to increase the measurement beam path-length and ultimately absorbance in the liquid sample, corn starch was added to imitate leaf architecture: with a hope to increase the sample's internal reflectance. The results for P700 measurements, shown on the top right panel of Fig. 3-11 were an improvement on the original trial, and as such further work to develop this approach was initiated. Through increasing the gain settings of the detector and adding starch it became possible to measure $Y(I)$ with a reasonable signal intensity and

resolution, at a [Chl] of just 20µg.mL^{-1}, as shown on the lower panel of Fig. 3-11. As this is a [Chl] that could possibly be worked with, it looked initially like the problem of signal intensity had been solved.

However, two important reasons made it necessary to determine the level of actinic light attenuation by the starch needed to be investigated.

1- Gas flux measurements assume a (relatively) homogenous sample of cells, with each equally illuminated at any given light intensity. Self-shading results in a reduction of gas flux rates when corrected for [Chl] for a given light intensity, inverse to the [Chl] (which is why 2 µg.mL^{-1} is the [Chl] used for the majority of work conducted in the liquid phase, in this thesis).
2- The P700 measurements require that all cells in a sample (or chloroplasts in a leaf) are homogeneously and fully saturated with light when the saturating pulses are applied.

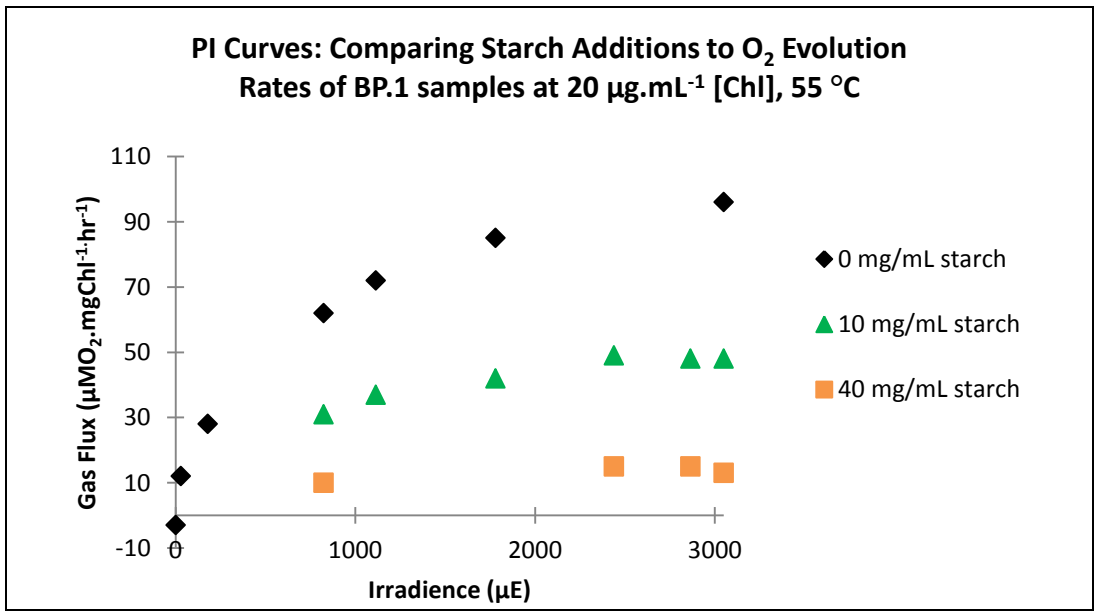

Fig. 3-12: The effect of corn starch additions on the rates of net O_2 evolution from BP.1 cells at 20 µg.mL^{-1} [Chl] at 55 °C.
The [Chl] used is already 10X that used in standard gas flux experiments, as such the maximum rates are very low at only 100 µMO$_2$.mgChl^{-1}.hr^{-1} compared to the standard net rate around 300 to 350 µMO$_2$.mgChl^{-1}.hr^{-1}, whilst the irradiance is also close to 10X higher. n=1: No analysis is based on this data, it is only a component of the technique development and the result was very clear from this single trial.n=1

Measurements to test the effect of starch additions to the gas fluxes of samples were conducted. The first consisted of a series of PI curves to compare the maximal rates of O_2 evolution of samples set at 20µg.mL^{-1} [Chl] with varying concentrations of starch. The results presented in Fig. 3-12 were not promising. Under the conditions used to generate the successful $Y(I)$ results in Fig. 3-11, O_2 evolution rates plateaued at 40 to 50 µmolO_2.mgChl^{-1}.hr^{-1} — at 2000 µE irradiance! The exclusion of starch, which resulted in no P700 signal (Fig.

3-10) did not reach a plateau until 3000 µE irradiance, and even this was only around a rate of 100 µmolO_2.mgChl^{-1}.hr^{-1}. Adding 40mg of starch (2 small spatulas) resulted in essentially no O_2 evolution, with a maximum rate of < 20 µmolO_2.mgChl^{-1}.hr^{-1} recorded.

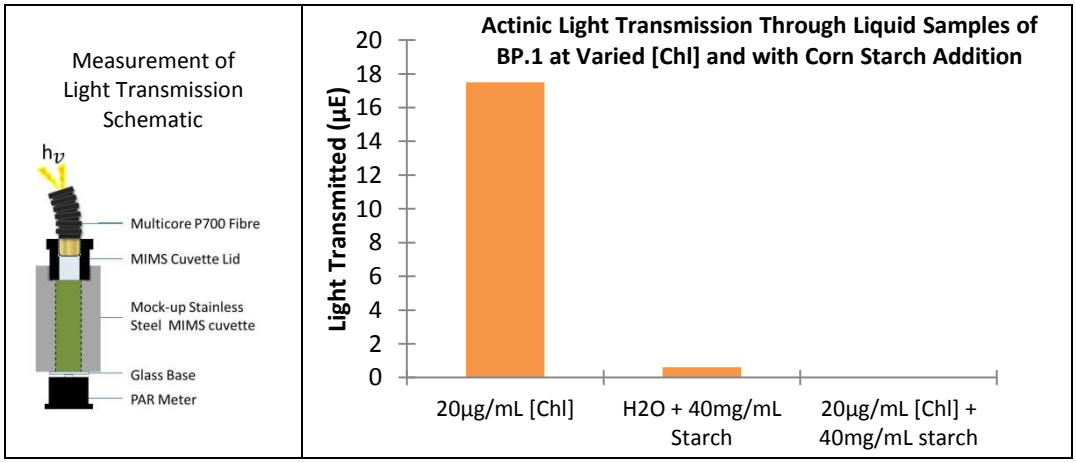

Fig. 3-13: measurement of transmitted light through BP.1 sample culture at 20 µg.ml^{-1} [Chl], with and without starch.
Measured with PAR sensor in a mock-up of identical dimensions (path length of 27 mm) to actual MIMS cuvette, schematically described in the left panel. Control measurement performed using MQ H_2O = 670 µE transmitted, showing that cells without starch attenuate almost 98% of light, whilst starch on its own at 40 mg.mL^{-1} attenuated >99% compared to the control. The combination blocked 100% of light from reaching the detector. Only a single measurement was conducted for each condition, hence n=1. The result was clear and has not been used in further analysis.

The second measurement was to determine how much light was attenuated by the samples along the path-length of the cuvette. It required the construction of an identical stainless steel cuvette 'mock-up', able to support the actual MIMS cuvette top, with a glass base – shown schematically in the left panel of Fig. 3-13. The results of this measurement, in the right panel of the same figure, were unambiguous. At 20 µg.mL^{-1} Chl, and without starch, the sample absorbed over 98% of illumination. When including starch 100% of light compared to the control was absorbed. Starch on its own at 40 mg.mL^{-1} absorbed 99% of light compared to control.

With such a high level of absorbance, it was clear that the P700 measurements would never be accurate, as saturating pulses were attenuated too quickly within the sample length. There was no way to limit the measurement beam to the cells that were actually experiencing a saturating pulse of light. In an attempt to resolve this problem, a short pathlength cuvette (10 mm) was trialled, however the results of PI curves indicated the same problem was occurring (results not shown).

3.3.3 *Cyanodiscs – Good for P700 AND absorptance measurements!*

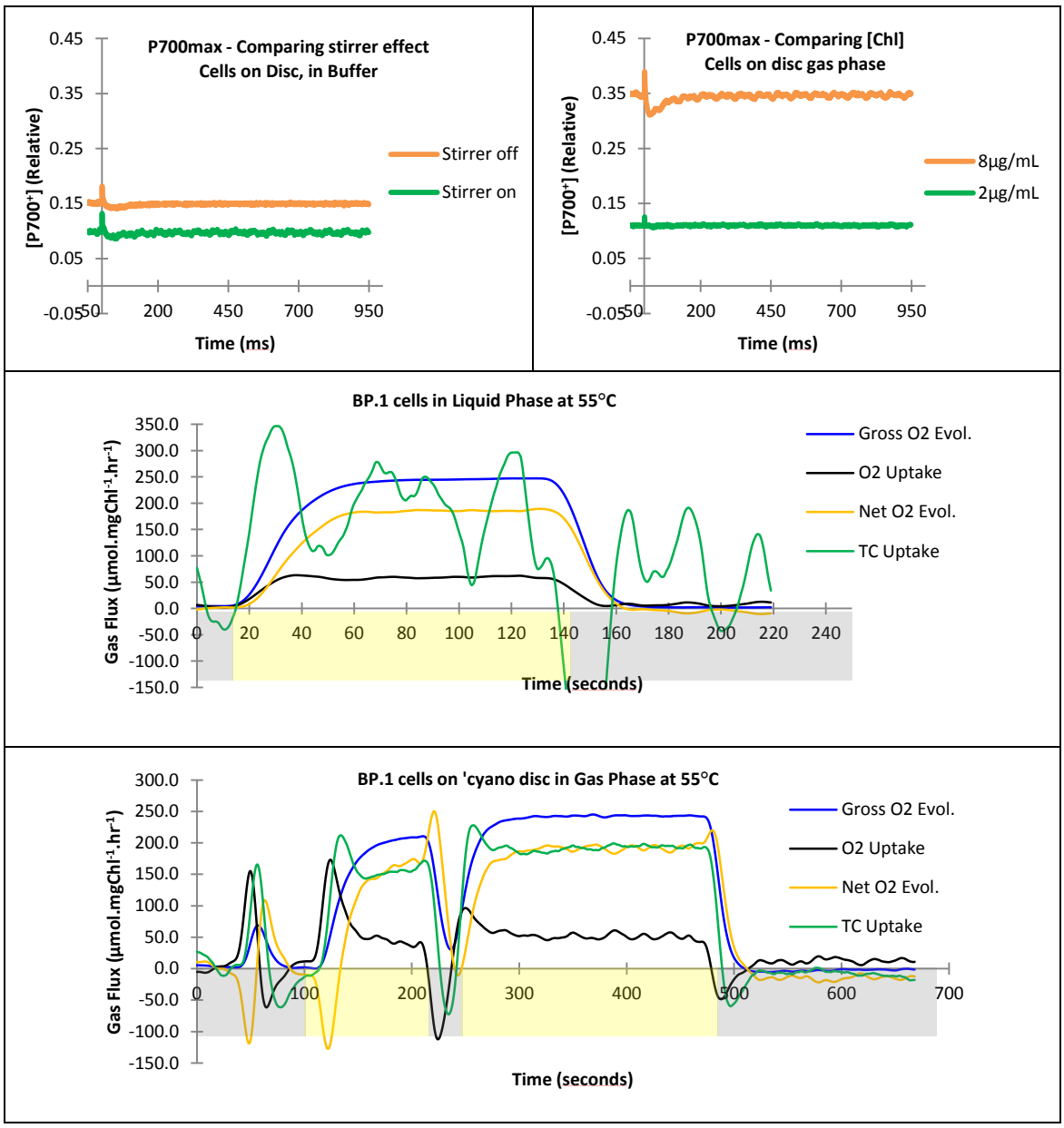

Fig. 3-14: P700 signals and gas fluxes measured from BP.1 cells fixed into a glass fibre filter disc.
Top left panel: $P700_{max}$ signal measured from a cyano-disc, created through vacuum infiltration of cells into glass fibre filter disc, submerged in liquid buffer with and without cuvette stirrer activated. Observe level of noise generated by the stirrer. Top right panel, same sort of cyano-disc, however $P700_{max}$ was measured from a disc mde with either 1 mL of 2 µg.mL^{-1} or 8 µg.mL^{-1} Chl. Compare to left hand panels and see how much better the P700 signal was in the gas phase. Middle panel: Gas fluxes from a submerged cyano-disc, for comparison with gas fluxes in the bottom panel from a gas phase cyano—disc of identical cell density. The noise in the gas phase panel is clearly much reduced in comparison to that measured in the liquid phase. This was especially true of the CO_2 uptake rates. To minimise noise in the middle panel, integration times have been increased: as can be clearly seen in the signal for O_2 uptake. An excellent check of the lower panel's accuracy is the concordance between rates of Net O_2 evolution and TC uptake. Grey colour bar represents darkness, the yellow represents illumination at 500 µE. Each represents a single run, conducted for development of methods and not used in analysis, n=1.

The first attempts to produce a clear P700 signal from cyanobacteria in the MIMS cuvette were abject failures. However, a conversation I had whilst visiting Graham Peers, at Colorado

State University in Fort Collins, sprang to my mind one morning. We were introduced during the 2012 Photosynthesis Congress and he invited me to visit his lab.

Whilst there we discussed the problems associated with determining absorptance of micro-organisms, and he mentioned suspending them on a filter disc to measure reflectance and transmission. I realised that immobilising cells on a filter disc was a much better approach to simulating a real leaf disc than adding starch to a liquid sample. As such I began trials to create a 'cyano-disc'.

A new one mL volume, short path-length but wide diameter cuvette was constructed, into which a steel grid could be placed to support the cyano-disc. This cuvette design allowed the cyano-disc to sit at only a short distance (≈ 2 mm) from the quartz glass window through which the measurement beam and actinic light was passed. From the very first trial, the P700 data resolution matched that expected from a real leaf, around 0.3. Even with the detector at the lower gain settings, it was possible to achieve measurement beam absorbance values around 0.35 from filtering an 8 $\mu g.mL^{-1}$ [Chl] sample onto an 8 mm disc, seen top right of Fig. 3-14. The previous best maximum was only 0.06 with a [Chl] of 36 $\mu g.mL^{-1}$. That represents almost 60 X increase in signal with 4.5 X fewer cells! Although the problem of achieving a P700 measurement with the cyanobacteria had been achieved, the issue now turned to ensuring gas flux measurements from cells immobilised in a glass fibre matrix were accurate, and representative of those suspended in liquid medium.

In the first approach to achieve this I trialled immersing the 'cyano-disc' into the measurement buffer, in effect maintaining a liquid sample. I envisaged this would minimise the number of development issues encountered as the experimental method was essentially

Unchanged, and none of the MIMS equipment or techniques at that time was designed for work in the gas phase. After embedding the cells into the glass fibre disc through vacuum filtration, the glass fibre disc, embedded with cells, was loaded into the cuvette (sitting on a steel mesh) and buffer was carefully added. Very few cells detached from the disc when the cuvette was filled with measurement buffer, and gas fluxes from this set up (bottom panel of Fig. 3-14) seemed reasonable.

However the stirrer, required for use in the liquid MIMS phase measurements to ensure sampling of homogenous dissolved gas, created problems for the P700 data: which can be seen in the top left panel of Fig. 3-14. In this panel, the $P700_{max}$ signal of a single disc is compared, initially measured without the stirrer, and then with the stirrer activated.

The stirring buffer resulted in a large decrease in signal intensity and an increase in signal noise so significant; it swamped the post saturating pulse 'PSII kinetic area curve'.

The other obvious problem with the liquid measurement of immobilised cells was that the signal intensity was affected by the liquid, as can be seen by comparing the clarity of the PSII kinetic curve in the gas phase (top right panel of Fig. 3-14) to the liquid phase (top left panel of Fig. 3-14). It quickly became obvious that excluding liquid medium from the MIMS cuvette resulted in much higher P700 signal intensity from the 'cyano-discs', however the cuvette needed to be modified and a new lid created before gas phase flux measurements could be trialled.

3.3.4 *Do Cyano-discs in gas phase perform like a liquid culture?*

Thankfully a comparison of data generated with cells in liquid compared to cells on a disc in the gas phase, presented in the bottom two panels of Fig. 3-14, showed that the gas fluxes between the two methods (especially for oxygen) are essentially identical. Excitingly, the TC uptake rate in the gas phase was much clearer than in the liquid phase, a result of issues discussed earlier pertaining to the measurement of TC_i uptake from a liquid sample at pH 8.0. I have been asked, and had to consider - for such a radically different environment why aren't the cells performing any differently and how do they access Ci?

The way I think about this result is that although the disc is sitting in the 'gas phase', conceptually the cells on/in the moist disc (discs were always left 'saturated' with buffer after filtration was completed) are still in a liquid phase, with a liquid layer of buffer surrounding them. Gases must diffuse into or out of the cells and into this medium – as they must in the liquid phase. This layer of surrounding medium contains a pool of CO_2 and HCO_3^-, just as the liquid phase measurements; however the key Ci pool in the gas phase is CO_2, not HCO_3^- (elevated with an injection to > 2% before each run). The Ci pool is kept in equilibrium at high temperature via quite a rapid equilibrium constant, ensuring cells are able to utilise both HCO_3 and CO_2 at their will. At lower temperatures (<45 °C) this equilibrium was maintained by the addition of CA to the buffer.

Gases must also diffuse from the liquid phase into the gas phase, before diffusion into the membrane for sampling. However the results show that this process must be similar enough to the diffusion of gas out of liquid and directly into the membrane – as occurs during liquid phase measurements. An additional advantage came from the fact that in the

gas phase, natural diffusion was sufficient to ensure sample homogeneity, removing the need for a stirrer, which was a significant source of noise and reduced the membrane sample area – hence sensitivity.

Although the move towards working in the gas phase required yet more hardware, method and calculation development (including new offsets for the analysis spreadsheet) then had been initially anticipated, the quality of results: for both gas fluxes from immobilised cyanobacteria and the P700 data, meant the time and effort were well spent.

3.3.5 *Chlorophyll extraction and quantification comparison*

Chlorophyll *a* concentrations ([Chl]) were used to standardise gas flux rates and other values, such as the determination of cyano disc absorptance (discussed in section 6.2.2), across a range of experiments and methods. Accordingly, [Chl] was determined from a number of different sample types including whole cells in culture, thylakoid preparations and from immobilised cells on glass fibre discs. Although the [Chl] was always determined spectrophotometrically, different spectrophotometers were utilised dependent upon their proximal convenience to a given experiment's location within the building. On some instruments it was only possible to scan a single wavelength, whilst others were able to automatically measure a number of wavelengths and perform simple calculations to determine [Chl]. For the single wavelength mode it was useful to utilise Meeks and Castenholz (1971) chlorophyll determination method (absorption at 665 nm x 12.7 for μg(Chl *a*).mL^{-1}), and for the latter mode Porra *et al's.*, (1989) equation, ([Chl a] = 16.29 x A $^{665.2}$ - 8.54 x A $^{652.0}$) was used.

To simplify chlorophyll analysis from these different sample types, the most convenient method was used in each instance, such as 100% MeOH extraction and then [Chl] determination from cyanodiscs, compared with 90% MeOH extraction from liquid culture samples. To ensure concordance between the different methods used, and therefore the accurate comparison of results standardised to [Chl], the extraction and determination of [Chl] was compared between 90 % vs 100 % MeOH, and between the techniques of Meeks and Castenholz from discs and liquid samples. It can be observed in the upper and middle panels of Fig. 3-15 that there was concordance within each method, for the 90 % and 100 % MeOH tests. A further test was conducted to gauge the 'saturation' of cells being filtered into the glass fibre discs. The glass fibre used was not fine enough to capture 100% of cells,

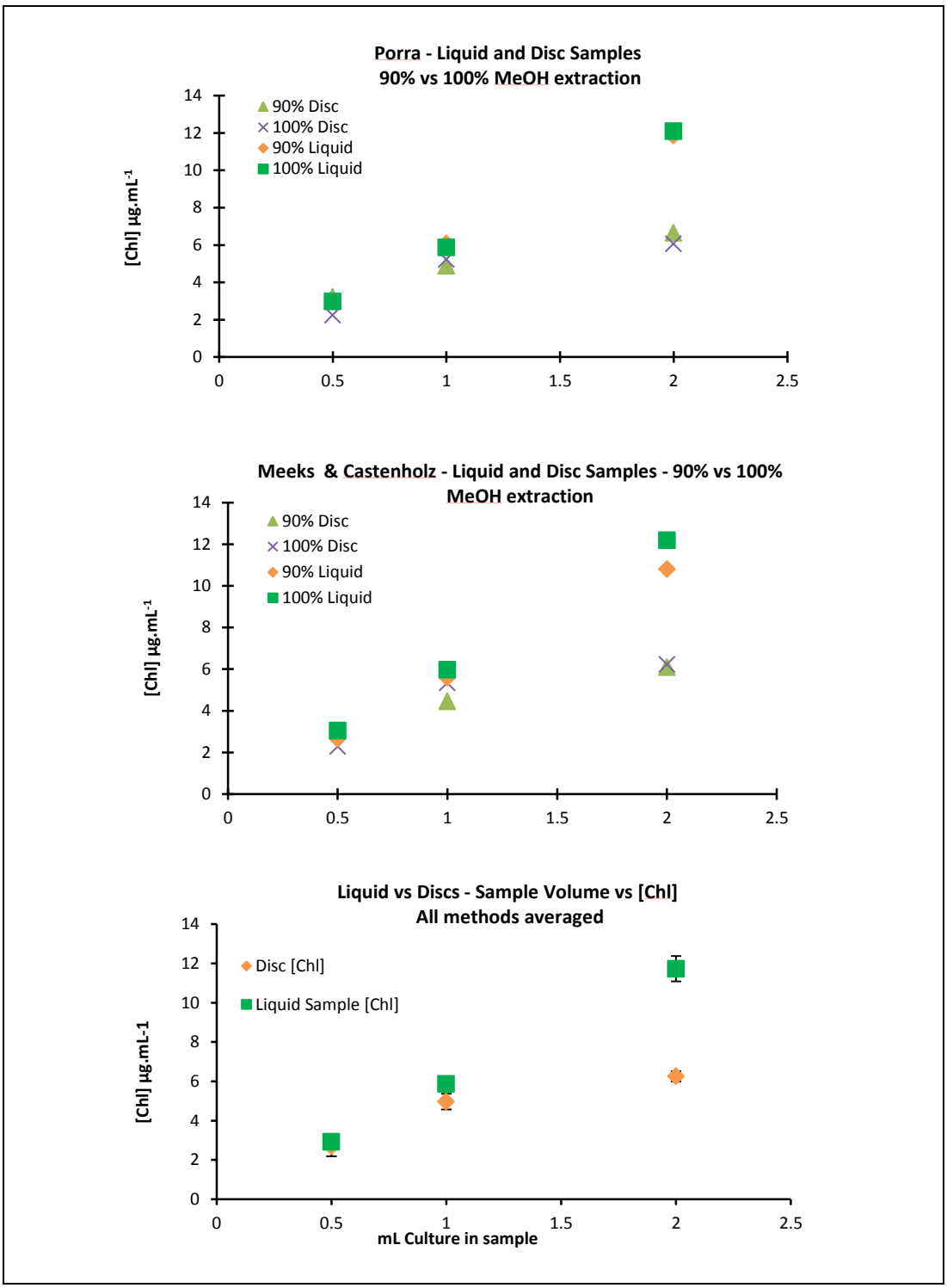

Fig. 3-15: Comparison of the Porra *et al's*. (1989), with Meeks and Castenholz (1971) methods for Chlorophyll a determination in MeOh, and test of capacity for glass fibre discs to hold cells.
A further comparison was made to ensure that the use of either 90% vs 100% MeOH did not affect the results. A single sample of cells was used, from which 0.5, 1.0 or 2.0 mL aliquots were added to both an eppy tube, and filtered onto an 8 mm glass fibre disc, which were then also placed into an Eppy tube. This allowed a comparison of the total [Chl] to that 'fixed' into the disc. Liquid samples in tubes were pelleted and the medium removed before 1.0 mL of 90% or 100% Methanol (MeOH) was added to all samples. Samples were incubated for 5 mins at room temp before being centrifuged to pellet solid material. Supernatant was transferred to a quartz glass cuvette of 1cm path length absorbance measurements were performed in a spectrophotometer according the methods outlined for each author in the text, for determining [Chl]. Error bars in final figure are St Dev. of 4 samples.

as this lead to clogged filters and inconstant outcomes. It was deemed better to use a standard, but slightly excess number of cells to try and generate consistent discs. A plateau in the data of [Chl] on the discs, compared the liquid aliquots, in the lower panel of Fig. 3-15, indicated that maximum amount of chlorophyll from in cells able to be fixed to an 8 mm glass fibre disc was around 6 µg. As such, all experimental discs were produced with around 10 µg total Chl, usually diluted into a large volume for rapid thermal equilibration of the cells (as discussed in section 4.2).Strong concordance between the two methods and the preparation of different discs was also evident, from data in the bottom panel in Fig. 3-15.

3.4 Carboxysome isolation for *in vitro* ^{14}C assays in 4.1.4

In order to measure the activity of Rubisco after thermal incubations that had inhibited PSII, an isolation of intact carboxysomes from BP.1 cells was attempted. Two methods to isolate the protein compartments that make up a critical component of the CCM in cyanobacteria (Badger and Price, 2003) were trialled. It was hoped that the thermal stability of the proteins from the thermophilic cells would enable the first ever published isolation of intact, *β*-carboxysomes. These are relatively larger, and tend to denature during biochemical isolation, in comparison to the smaller α carboxysomes which can be purified intact via a sucrose gradient method. As a result, the method to isolate *β*-carboxysomes relies on a precipitation with Mg^{2+}, pelleted together with percholl. It was hoped that any intact compartments, on the other hand, may indeed separate into a layer within the 10 % – 50 % sucrose gradients.

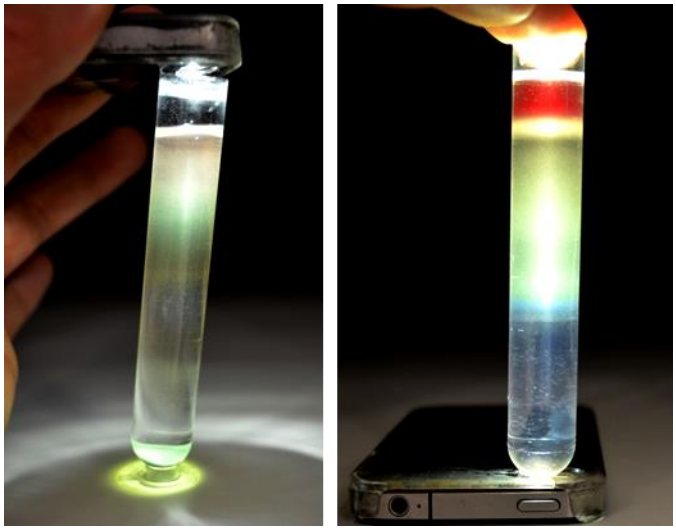

Fig. 3-16: comparison of attempts to purify carboxysome samples with sucrose gradients, prepared with the β-method left, and α-method right.
The need to illuminate the left tube from above results from the solid pellet formed in the base, indicative of the nature of the material being isolated using the β-method. The presence of strong chlorophyll fluorescence the top of the right tube, not evident in the left tube, clearly illustrates the very different cell fractions being isolated through the two methods, before any sucrose gradient separation occurs.

As such, the sucrose gradient method was trialled, and after numerous attempts, found to fail. An example of two sucrose gradients, containing samples prepared under the more standard α-method, (right) and from the β-method (left) are presented in Fig. 3-16. In it, the clear difference between the cell fractions targeted by the α and β methods can be observed.

A solid pellet in the base of the tube on the left containing an enrichened fraction of ruptured carboxysomes, and likely a large amount of membrane material, formed from a sample generated with material from the β method, made it necessary to illuminate from the top for the photograph in . In contrast on the right, light was transmitted all the way through the gradient, indicating the aliquot of α method material, separated by the sucrose gradient, contained mainly soluble, or freely associated components of the cell. Although some 'promising looking' bands can be observed in both gradients, consistent with what would be expected from intact carboxysomes, the results of SDS (BioRad pre cast, 4 – 15 % Protean TGX Stain Free , imaged on Bio rad Gel Doc EZ imager) and Western Blots, presented in Fig. 3-17, were consistent with the conclusion that no intact carboxysomes were found in the sucrose gradient from either method.

To summarise the method used, cells were cultivated in large (2.5L) vessels sparged with 2% CO_2 at 55 °C at 100 µE irradiance. They were left to reach high cell density before harvesting through centrifugation (10,000g for 10 mins). Cells were lysed at 18,000psi, using a French press in 'thylakoid buffer' (50mM MES (pH 6.0), 10mM MgCl2, 5mM CaCl2, 25% glycerol and protease inhibitor cocktail). A gentle spin to remove cell debris, 3000 g 5 mins, is the step that separates the standard α – method from the β-method. For the α – method the pellet from this initial spin was taken and 'cleaned' twice through incubations with cell lysis compound ('bug buster', Merk Millipore) and centrifugation, to remove membrane components etc from the carboxysomes. This final pellet from this process was then loaded onto a 10 %-50 %a sucrose gradient containing 0.5 % Triton X-100 and spun at 105,000 g for 30 minutes.

The β-method utilised the supernatant from the initial low speed spin, which was resuspended in EM buffer (40 mM EPPS–NaOH, pH 8.0 & 27 mM MgSO4), then spun at 12,000 g for 15 minutes. The Mg^{2+} w as supposed to interact with the broken carboxysomes, precipitating them into a loose pellet. Supernatant was discarded and the pellet was resuspended in EM buffer with 20 % percholl, 0.133 TritonX-100, then incubated for 20

minutes on ice. The addition of percholl increased the stability of the carboxysome enriched pellet. The sample was then centrifuged again, this time at 40,000 g for 20 minutes, the supernatant discarded and the pellet resuspended in 0.75 % EM buffer, 1 % Triton X-100: this step was repeated twice. The final pellet was called the TP (Tris-percholl) pellet, containing an enriched carboxysome fraction. For detailed methods, refer to Long *et al.* (2005) in their Figure 2.

To test if the possibility that carboxysomes were isolated intact, a number of different experiments were conducted., with various products generated during the above mentioned steps. One worth noting here, was that a number of sucrose gradients, some containing the 'initial pellet' and some containing the 'initial supernatant', after the low speed spin post initial lysis, were compared. Each sample was loaded into a standard 10 – 50 % sucrose gradient with 0.5 % Triton X-100 and spun at 105,000 g for 30 minutes. Fractions were separated from along the length of the column, and run on an SDS page, followed by Western blots.

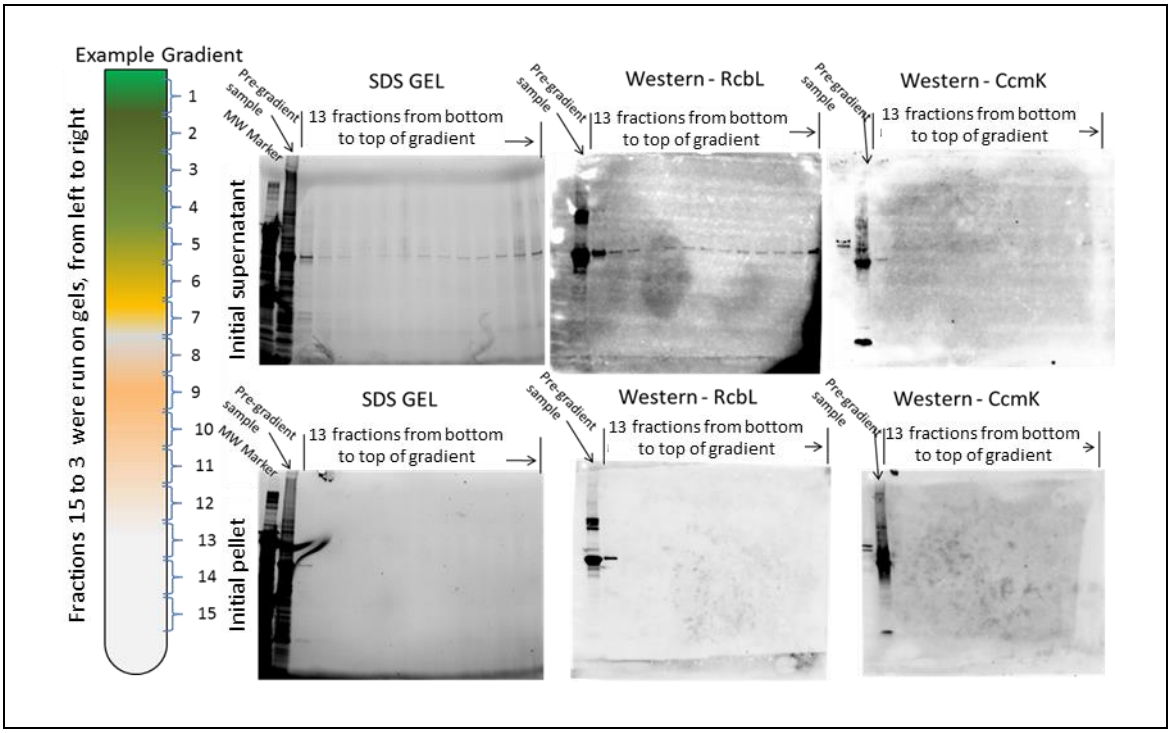

Fig. 3-17: A comparison of the protein content obtained from the pellet vs the supernatant of the initial spin of cbx isolation.
The step that separated the α or β carboxysome isolation methods was a low speed spin following cell lysis. To test if intact carboxysomes could be found in either fractions, both the pellet and supernatnat were treated with the α-carboxysome isolation method, described in text, and run on 10 %– 50 % sucrose gradients. Those gradients were roken into 15 fractions, as demonstrated on the example tube, and 13 of the fractions were run on SDS and Western Blots to identify components associated with intact carboxysomes.
Samples fractions 1 and 2 separated from the gradients were not loaded onto SDS gels, allowing for a molecular weight marker (Bio Rad "Precision Plus" protein) and a sample of the final product before loading onto the gradient, to be loaded into lanes one and two respectively of each gel. Western blots, located to the right hand side of each of the two SDS page gels, were used to confirm the presence of RbcL- the 55 kDa Rubisco large subunit and CcmK , the 10 kDa carboxysomal shell proteins.

In Fig. 3-17, a comparison of the SDS gels from the two gradients shows clearly that the β method gradient has the RbcL (Rubisco Large subunit, as can be seen by comparison with the adjacent Western Blot, targeting this protein) throughout the each of the fractions measured. However, the carboxysome shell protein CcmK could not be detected in any of the fractions, except for the bulk sample before being loaded. This suggests that the carboxysomes were not pure, or in-tact and were therfore unable to uniformely settle at a specific densitiy in the sucrse gradient.

The results of a similar analysis, combining SDS page and Western blotting on the TP pellets generated after completing the standard β method (i.e. no sucrose gradient step), showed that all of the components required for a carboxysome were found. This supported that a carboxysome enriched fraction had been formed. This sample was used for ^{14}C fixation assays, describe in section 4.1.4, and these results further supported that active rubisco was isolated in the TP pellet..

3.5 Key Points and Ideas from Chapter 3

To conclude this Chapter, a number of methods required development in order to conduct the measurements presented in the ensuing Chapters. This included a number of new cuvette designs incorporating new materials, stirrers, and layouts.

A large amount of development went into the creation and testing of a new cultivation system, that was able to generate cells capable of greater rates of growth (over five times more growth over a four day period (see Fig. 3-2), with far more consistence when cultivated and measured ((Yamaoka *et al.*, 1978) indicate that their cell growth was highly variable, whilst the cultures in this thesis were very stable), and generated greater photosynthetic rates (over double the Net O2 evolution rate under optimal conditions (Fig. 3-9).

The physical and chemical limitations of working with MIMS at temperatures where the solubility of gas in water became very low, led to a range of problems that were overcome with ingenuity in the lab, including vacuum evacuation of heated measurement buffer before addition to the cuvette and the development of a new excel based platform for analysing complex Mass Spec runs: including the large number of offsets for changing physical constants, membrane consumption, amplifier gain, isotopic enrichment etc.

The desire to measure simultaneous P700 dynamics and gas fluxes lead to the development of a 'cyano disc', an emulation of leaf discs used commonly in plant physiology. These discs potentially open up a range of instrument opportunities, to measure micro-organisms in systems generally designed for used with leaves. The data in Fig. 3-15 suggests the physiology of the cells were not adversely affected by being suspended in the 'gas phase' and furthermore the data resolution on CO_2 fluxes was significantly improved.

The data in this chapter demonstrates that great effort was made to ensure measurements were performed under conditions selected via testing: and not simply based on the literature. This was in part through necessity, as many of the measurements conducted have not previously been published under such conditions. There was also no precedent to follow in the lab, or the research institute, when this project was started.

The extra time required to perform so much development was worth it, in the end. The data presented in this thesis is robust and precise. I am proud of the work that went into this process of development, and have learned a lot in conducting it. I hope that these skills will set me apart from many PhD graduates, who have performed 'technically' more straightforward projects and I sincerely thank the many people in RSB, around the campus more generally, and also international colleagues, with whom conversations have helped spark ideas.

Chapter 4.

Deconvoluting cyanobacterial gas fluxes:

determining activity of specific components *in vivo*

Chapter Summary

Two broad observations of oxygenic photosynthetic organisms exposed to transient thermal stress underpin the main hypotheses in this Chapter. The first; non-photosynthetic processes (such as respiration) exhibit a higher thermal tolerance than photosynthetic oxygen evolution. The second; photosystem I (PSI) and its primary redox partners exhibit a significantly higher thermal tolerance than photosystem II (PSII). Whilst these are well measured phenomena in plants, algae and cyanobacteria growing optimally in the mesophilic range, little information exists in the literature pertaining to this in thermophillic phototrophs, namely the cyanobacteria found growing in geothermal hot springs. Does this trend hold up in these systems?

A number of in vitro studies examining the thermal tolerance of cellular components critical to photosynthesis, isolated from the moderately thermophilic cyanobacterium BP.1, have been published. These have shown unequivocally that PSI (Sonoike et al., 1990), and its associated redox partners (Koike et al., 1982), possess marked thermal tolerance, whilst PSII is comparatively labile. Little supporting data exists from in vivo work, to describe the function of moderately thermophilic cells subject to transient thermal stress: nothing has been published on key functions such as respiration and carbon fixation.

The first hypothesis being tested is that, based on the published in vitro work, these functions will exhibit higher thermal tolerance, than PSII function, just as in mesophilic cyanobacteria.

As respiration in cyanobacteria shares a number of downstream electron transport components of the thylakoid membrane, the second hypothesis is that the high temperature tolerance of PSI allows it to actively participate in respiration, when PSII has been inhibited.

Through precision, real time gas flux measurements performed with MIMS, including the use of isotopic discrimination for oxygen production and uptake processes, the activity of individual cellular functions were measured in BP.1 cells. The results of the gas flux data, analysed through a mass balance framework, provided strong evidence to support the first hypothesis, and some evidence that the second is possible. Further support for the second hypothesis is provided in the following Chapter (Five).

Measuring thermal damage in photosynthetic systems

In this chapter a number of approaches were used to elucidate the damage caused by high temperatures. The initial approach was to measure cells at the stress temperature of interest, where both the cell's response to sub-optimal and supra-optimal temperatures could be explored. Although this method provided some information, and was shown to be a useful approach to study physiology of sub-optimal temperature effects, it was concluded that the measurements were not precise enough to provide the data required to answer both of the hypotheses being explored

In response to the fact that more information was required about the specific activity of PSI, the 'cyano disc' method was developed, as discussed in section 3.3.3. This had the unintended consequence of improving the resolution of CO_2 fluxes. As such, the majority of conclusions drawn from this Chapter come from the second half, where cells were incubated for a time period and then measured at a single optimal temperature: in combination with a simultaneous P700 measurement.

4.1 Measuring continuous thermal stress and acclimation in BP.1

The initial question of 'how' to measure thermal damage of various cellular components *in vivo* seemed like an obvious one to answer; heat up and calibrate the MIMS cuvette, load a standardised sample, turn the actinic light on and off a few times and measure the respective gas fluxes. Repeat this process, at progressively higher temperatures and record the maximum rates for each of the various fluxes being measured. It seemed logical that simply plotting these fluxes against the temperature they were measured at would yield interesting and clear results. It also copied a methodological precedent set by original measurements of the BP.1 thermophile by Yamaoka *et al.*, (1978), see Fig. 4-1. Unfortunately technicalities of measuring gas fluxes in this manner, particularly at very high temperatures (> 60 °C) where low gas solubility combines with numerous shifts in the membrane properties to generate significant signal noise (discussed in the previous chapter), thereby reducing the effectiveness of this initial approach.

Nonetheless, it was trialled and the results are presented in Fig. 4-2. This early work included an additional experimental condition that is not repeated in any other experiment throughout this thesis, a comparison of two growth temperatures. This was performed

in order to investigate a curious phenomenon published by Yamaoka *et al.*, (1978) but dismissed as 'statistically insignificant', see Fig. 4-1. The authors show that cells grown at the lower temperature, 40 °C, produced a higher net oxygen flux then cells grown at the optimal temperature of 57 °C. Growth rates reflected the opposite trend, increasing with temperature. When compared to more recent characterisation papers dealing with thermal acclimation (Inoue *et al.*, 2001) these results are curious as such a difference is not usually seen. Generally in mesophiles a measurement of net O_2 flux will yield a similar rate when the measurement temperature matches that of the growth temperature (ie a 25 °C grown culture will record a rate at 25 °C that is the same as the rate measured by a 35 °C culture measured at 35 °C).

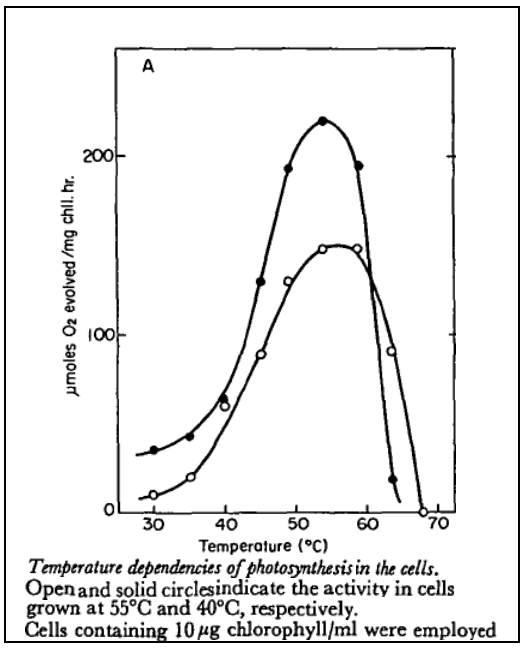

Fig. 4-1: Yamaoka *et al's.*, original figure (1978) comparing net O_2 evolution rates in BP.1 at a range of temperatures.
A comparison of net O_2 evolution rates from cells grown at 40 °C and 55 °C, measured with a Clarke type electrode at each temperature of interest after incubating there for five minutes.
Sourced from the original figure.

The second thought behind generating a comparative set of measurements undertaken with samples acclimated to either 45 °C and 57 °C was to garner more information from the *in vivo* data set, through an analysis of the similarities and differences in the responses of the various gas fluxes.

4.1.1 *Method summary*

- Fresh samples of BP.1 were inoculated from glycerol stocks and checked for contamination though addition of an aliquot of culture onto LB plates.
- Cells were cultivated in BG-11 medium, buffered to pH 8.0 with 10 mM Hepes-NaOH in autoclaved and silicone foam-stoppered bubble lift tubes. This was supplied with humidified air enriched with 2% CO_2, filter sterilised on entry into the vessel. Irradiance of approximately 100 umoles(photons).$m^{-2}.s^{-1}$ (μE) was supplied by fluorescent growth tubes (NEC, Japan).
- The cultivation temperature was maintained through the suspension of the growth tubes in a thermostatted water bath, at either 57 °C or 45 °C.

- Culture density was maintained around OD_{750} of ≤ 1.0 to ensure consistent growth conditions (both nutrients and irradiance) through daily dilutions, conducted under strictly sterile conditions within a recirculating laminar flow hood.
- Aliquots of culture were taken for measurement through transfer into a sterile 50 mL falcon tube, centrifuged at 2000 g for 3 mins, to form a cell pellet.
- The pellet was resuspended in Assay Buffer (growth media: minus $NaNO_3$ (replaced with 20 mM NaCl to maintain osmotic balance) and an increase to 50 mM Hepes-NaOH,(to resist pH changes during MIMS experiments as [$HCO3^-$] are changed)) and transferred into a sterile eppy tube, returned to an incubated water bath at 57 °C or 45 °C in darkness. The [Chl] of this concentrated sample was determined spectrophotometrically in 90 % MeOH (Porra *et al.*, 1989).
- Assay buffer was pre equilibrated to the temperature being measured – this ensured excess dissolved gas was minimised for high temperature measurements. Aliquots were purged with N_2 to remove excess O_2 and were then vacuum purged to remove as much gas as possible before being injected into the thermally equilibrated and calibrated MIMS cuvette via a syringe. This was necessary, especially at high temperatures to avoid the formation of bubbles within the cuvette. Total assay volume was (3300 µL).
- A volume equal to the calculated volume of the required sample was removed from the cuvette, before the sample was injected to produce a final cell concentration of 2.0 µgChl.mL^{-1}. In comparison to many papers, where up to 10 µg.mL^{-1} is used, the relatively low [Chl] was used to minimise self-shading in the cuvette and maximise gas flux rates. This approach came at the cost of noise, however, especially when rates were low (in the dark or at damaging temperatures).
- $NaHCO_3$ was injected to ensure a saturating concentration of total carbon (TCi) 5mM. The thermal stability of available carbonic anhydrase (bovine) was not clear at the elevated temperatures, testing seemed to show its enzymatic function declining with time at this temperature (data not shown). It was considered better to avoid a changing equilibrium in the sample, and as such, it was hoped that the elevated temperature would result in a sufficiently rapid interconversion of HCO_3^- to CO_2 to enable accurate measurements of TCi uptake (the results show that this was partly true).

- Cells were left to dark adapt for five minutes whilst an initial background rate of dark respiration was measured. Samples were then illuminated for three minutes at 300 µE, as determined through an independent set of light response curves, to measure steady state gas fluxes. This was repeated three times for each sample with three minutes of darkness in between. At damaging temperatures, this approach was problematic as damage was progressive, and in practice, the actual timing was changed to enable the damage occurring to samples be monitored. In these cases a representative rate was taken, from only the first period of illumination and the initial dark adaptation was shortened to two minutes.
- Data sets in which bubbles, or other large sources of noise were encountered, were discarded as they were not useful. As a minimum, three independent experimental runs were used to generate figures. Unlike previous literature on work with BP.1 that report wide variability between batches, the samples were very consistent in both growth and gas flux responses between batches, which I attribute to the development put into optimising growth conditions at the start of the project (described in section 3.1).

4.1.2 *Results of gas fluxes under continuous thermal stress*

The results presented in Fig. 4-2 include rates of Gross O2 evolution, Net O_2 evolution, TCi uptake, Illuminated O_2 uptake and Dark O_2 uptake; as a function of the temperature at which the samples were measured. Cells cultivated at 45 °C are presented in the top two panels (panels A and B), those cultivated at 57 °C data are shown on the lower two panels (C and D). The actual gas flux rates in µmol(gas).mg $Chl^{-1}.hr^{-1}$ are presented on the left hand side (panels A and C), whilst rates normalised to the maximal value are presented on the right hand side (B and D). The term 'sample' with respect to this dataset refers to either cells cultivated at 45 °C or 57 °C, whilst the temperature at which samples were measured at was termed the 'treatment'. This compound figure contains a lot of information and is quite dense; however, it pays to be able to make direct comparisons of the trends in the data.

Net Oxygen Evolution

Note that the oxygen electrode used by Yamaoka *et al.*, (1978) could only measure Net Oxygen evolution, as such this was the first parameter to be compared with the data generated by the MIMS. Overall the trends in Fig. 4-2 match those previously reported,

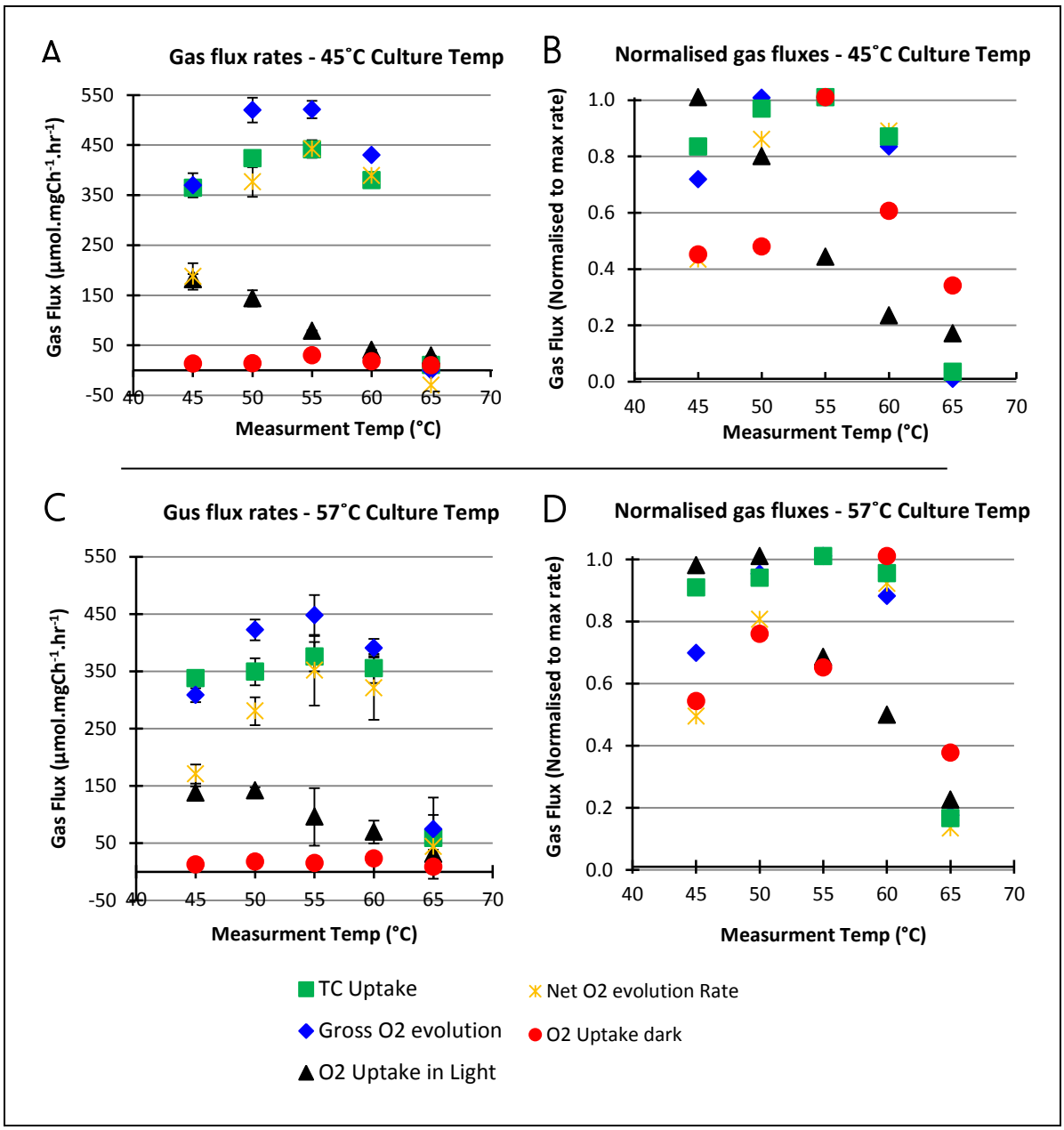

Fig. 4-2: Comparison of total gas fluxes at varied measurement temperatures from cells cultivated at 45°C and 57°C. Samples of BP.1 cultivated at either 45 ˚C (panels A, raw rates and B, normalised rates) or 57 ˚C (panels C, raw rates and D, normalised rates) were diluted to 2 µg.mL^{-1} chlorophyll in the calibrated and thermally equilibrated to the value presented on the x-axis MIMS cuvette. Measurement buffer was pre-thermally equilibrated, N_2 purged to remove oxygen and vacuum purged to remove excess gas before loading. Samples were left in darkness for 5 minutes whilst 5 mM HCO_3^- and a bubble of $^{18}O_2$ air was injected into the cuvette. The bubble was removed before measurements were started. Light provided by a halogen globe via a liquid light guide at 300 µE illuminated samples until a steady state rate of gas flux was observed. This was cycled three times per sample. Gas fluxes presented in left panels (A and C) are the mean of three separate samples. Right panels are the values normalised to the maximal value, which can be observed in the respective panel A or C. n=3plus/minus standard deviation.

although the high [Chl] used in the original experiments (10 µg.mL^{-1}) likely resulted in self-shading of cells, producing lower rates on a per mg Chl. basis. At the low temperature treatment of 45 °C in the current dataset, net O_2 evolution rates between the two cultivation samples (panels A and C) were very similar, 150 µmolO_2.mgChl^{-1}.hr^{-1}. Net O_2 evolution rates of both samples rose with increasing treatment temperature, with both peaking at 55 °C, before dropping at 60 °C and collapsing rapidly as measurement temperatures reached >60

°C. In Panel A, the cells cultivated at 45 °C recorded a negative evolution rate at 65 °C, suggesting the cells were net consumers of oxygen, possibly an indication of respiration occurring in the light.

Although a comparison of normalised values between the low and high temperature samples show proportionally similar increases with each measurement temperature, a comparison of actual rates shows that cells cultivated at 45 °C recorded a highly significant increase ($P<0.005$) in the net rate of O_2 evolution across the optimal temperature range, compared to those cells cultivated at the optimal temperature of 57 °C (Results of Single-tailed Student's T-test n =3). This finding suggests that the result presented in the original data set of Yamaoka et al. (1978) was also significant. As rates of dark oxygen uptake when assayed at the respective growth temperatures were very similar (discussed below in 0), the data suggests that a change in [Chl] was not responsible for the increased rates measured.

In line with existing literature the overall thermal tolerance of cells cultivated at 45 °C was lower (Berry and Björkman, 1980). Cells cultivated at 45 °C lost 100 % of net oxygen evolution by 65 °C, where it became negative so was 'set' to zero (panel B). Cells cultivated at 57 °C however, still exhibited approximately 15 % functionality (panel D) at this treatment temperature. Although it must be notes that the rates were declining during the course of the measurement, making a 'steady state' value difficult to ascertain accurately.

Gross Oxygen Evolution

Gross oxygen evolution broadly trended rates of Net O_2 evolution. However, the difference between the two values changed with temperatures, being more pronounced at sub-optimal temperatures, and becoming much closer to parity at optimal temperature. (panels A and C). Irrespective of incubation temperature, both samples exhibited maximal Gross O_2 evolution rates at 50 °C and 55 °C, and were marked by sharp declines beginning at 60 °C. However, samples acclimated to 45 °C lost double the gross O_2 output compared to those acclimated to 57 °C, the former losing 20 % of maximal activity at 60 °C (Panel B), compared to only 10 % loss of the latter (Panel D). This trend continued with increasing temperature. Samples acclimated to the lower temperature suffered complete loss of PSII function at 65 °C , whilst those cultivated at the higher temperature still maintained almost 20 % (Panel D) of the maximal capacity. However, looking at the raw data it is very clear that even rates of the high-temperature-grown cells were subject to a progressive decline at the higher measuring temperature. The rate presented in Fig. 4-2 (panel C) was extracted from a

time point that is earlier than had been used for lower temperature samples. This problem is part of the reason why subsequent measurements were made at a single assay temperature (post-thermal-stress incubations), to ensure a consistent assessment of thermal stress.

The stark difference in trends between the Net and Gross O_2 evolution rates at suboptimal temperatures highlights an issue with some previous data presented for thermophiles, based on Net O_2 fluxes. The low rates measured at suboptimal temperatures were interpreted as representative of photosynthetic activity itself (Yamaoka *et al.*, 1978), and this was considered the cause of depressed growth rates at sub-optimal temperatures. Clearly the Gross O_2 data suggests that PSII itself was less affected then Net O_2 values imply. This is consistent with the idea that a different component of the biochemistry, possibly relating to CO_2 fixation or membrane permeability to electron carriers (Hirano *et al.*, 1981), limits the growth rates at sub-optimal temperature.

The result excludes the conclusion that activity of PSII limits capacity for BP.1 cells to acclimate to sub-optimal temperatures (see Fig 3-1, where growth rates at lower temperatures were vastly slower). This is a trait of thermophiles that differentiates them from mesophiles, which tend exhibit a 'broad peak' of temperatures that may be considered optimal, or exhibit greater acclimation capacity (dependant on growth temperature) (Berry and Björkman, 1980). This finding highlights the significance of utilising MIMS, and stable isotope discrimination of consumption and evolution processes, when interpreting O_2 fluxes in whole cells. This is particularly true in cyanobacteria, capable of such efficient O_2 consumption via the Flv1-3 proteins (Allahverdiyeva *et al.*, 2013, Bersanini *et al.*, 2014).

Net Total Carbon Uptake

Data for total carbon (TCi) uptake in Fig. 4-2 is likely to be inaccurate at the lower temperature measurements of 45 °C and 50 °C, based on the observation that for both high and low temperature grown cells the TCi uptake rates do not match (and in fact greatly exceed) the net O_2 evolution rates. This could be indicative of a disequilibrium between the [CO_2] being measured by the MIMS, and the [TCi] ([HCO_3^-]+ [CO_2]) in the sample (Badger *et al.*, 1994), occurring even under steady state conditions. Such a situation may occur if the cells were preferentially consuming CO_2 compared to HCO_3^- in the non-catalysed assay buffer, keeping the [gas] 'low' due to impeded reaction rate between the two Ci pools. At mesophilic temperatures (≈ 25°C to 30 °C) commercially available (Sigma Aldrich) bovine carbonic anhydrase (CA) is often included in the measurement buffer to avoid this

phenomenon. However, bovine CA was found to be thermally unstable for these experiments, as discussed above in method summary. The data in panels A and C of Fig. 4-2 indicated that at temperatures >50 °C, the equilibrium kinetics seemed high enough to generate close to 1:1 for Net O_2 evolved and TCi consumed. As such, the results of TCi uptake for these higher temperatures were deemed accurate for the steady state rates reported.

The rates of Net CO_2 fixation measured were once again higher in cells cultivated at the lower temperature. Significantly, the rates of TC uptake and of Net O_2 evolution were very highly correlated across the upper range of temperatures, including at temperatures that show clear damage to PSII, based on Gross O_2 evolution rates in Fig. 4-2. This observation was reinforced through comparison of the normalised values in panels B and D, implying a very strong functional correlation existed between the activity of PSII and carbon fixation. As a result, it was not possible to use this data set to conclude whether TC uptake rates decrease due to damage to the carbon fixation components, or if it was a result of diminishing levels of energy available to perform this task.

In Fig. 4-4 of section 4.1.4 below, *in* vitro measurements of incubated samples of carboxysome enriched fractions, isolated from the BP.1 cells, indicated that isolated Rubisco function was still highly active after a ten minute incubation at 60 °C, and still possessed 20 % of maximal function after a 70 °C incubation. This was consistent with the idea that a loss of reductant to drive carbon fixation underlies the loss of TCi uptake observed in Fig. 4-2, and therefore the activity of Rubisco was not necessarily impeded by temperatures that inhibit PSII.

Illuminated Oxygen Uptake

Enriching the measurement buffer with $^{18}O_2$ prior to illumination provided an excellent method to measure real time rates of O_2 uptake in illuminated samples (Radmer and Kok, 1976). Broadly, it was found that a negative correlation existed between the illuminated rate of O_2 uptake and increasing temperature in Fig. 4-2, observed in both samples cultivated at 45 °C and 57 °C. The samples cultivated at 45 °C (panels A and B) showed the highest rate of illuminated O_2 uptake, 182 $\mu molO_2.mgChl^{-1}.hr^{-1}$, measured at the 45 °C assay temperature. This was followed by a fairly constant decrease in uptake rates with increasing temperature, until a minimum of 30 $\mu molO_2.mgChl^{-1}.hr^{-1}$ was recorded at 65 °C.

The samples grown at 57 °C showed a slightly different trend. At assay temperatures of both 45 °C and 50 °C, the rate of illuminated O_2 uptake was constant at around 140 $\mu molO_2.mgChl^{-1}.hr^{-1}$. The rate then declined in a steady manner, similar to the 45 °C cultivated cells, to reach a final uptake rate equalling cells cultivated at the lower temperature of 30 $\mu molO_2.mgChl^{-1}.hr^{-1}$.

Rates of illuminated O_2 uptake, recorded at 45 °C in samples cultivated at both 45 °C and 57 °C, almost matched the rate of net oxygen evolution (panels A and C, Fig. 4-2). Therefore, half of all oxygen produced by PSII was being consumed by the cells, an observation supported with literature generated with other cyanobacteria (Kana, 1992). This was likely through either, or as a combination between, respiration, photo-respiration (Ermakova *et al.*, 2016) and/or Mehler-type reactions (Badger *et al.*, 2000, Allahverdiyeva *et al.*, 2013). As cells were in a saturating HCO_3^- environment (precluding photo-respiration), and dark oxygen uptake values suggested a maximum respiration rate of only around 13 $\mu molO_2.mgChl^{-1}.hr^{-1}$ (section 0), activity of the Flv1-3 proteins were a strong candidate to explain the high illuminated oxygen uptake rate. This was consistent with a potential sink limitation, possibly some limitation in the Calvin-Benson-Bassham cycle that decreased with increasing temperature.

Dark Oxygen Uptake

The rate of dark O_2 uptake in panels A and C in Fig. 4-2 were very similar between cells cultivated at 45°C or 57 °C. At sub-optimal temperatures, the values were equally around 13 $\mu molO_2.mgChl^{-1}.hr^{-1}$, consistent with respiration rates measured by Zilliges and Dau (2016) (13 to 16 $\mu molO_2.mgChl^{-1}.hr^{-1}$ with two separate strains of BP.1 measured at 38 °C). This rate increased with assay temperature; however, the rate of increase was offset between the two cultivation temperatures. Between assay temperatures 45 °C and 55 °C, cells cultivated at 45 °C climbed from 13 to 30 $\mu molO_2.mgChl^{-1}.hr^{-1}$ in panel A. This was consistent with a Q_{10} (the # fold increase in respiration rate for each 10 °C increase in temperature (Atkin and Tjoelker, 2003)) of ~ two, expected from non-acclimated phototrophs exposed to rapidly increased temperatures. The rate declined again to 18, then 10 $\mu molO_2.mgChl^{-1}.hr^{-1}$ as the assay temperature increased to 60 °C, then 65 °C.

In Fig. 4-2 panel B it can be observed that this was consistent with a decrease in other gas fluxes, although rates of dark oxygen uptake showed greater resilience to increased assay temperature, especially in comparison to the rate of Gross oxygen evolution

(which had ceased completely). This supports the conclusion that illuminated uptake rates of oxygen, occurring once PSII has ceased generating O_2, may be illuminated respiration.

Evidence of acclimation to a higher growth temperature can be observed in data from the cells cultivated at 57 °C, which peaked in respiration at 60 °C (Fig. 4-2 panel C). However, the values were not consistent with a Q_{10} of 2, climbing only from 17 to 23 $\mu molO_2.mgChl^{-1}.hr^{-1}$ between assay temperatures of 50 °C and 60 °C in panel C.

Unfortunately, a combination of low cell density and relatively low flux rates resulted in high signal to noise issues for the dark fluxes. Furthermore, the TCi evolution rates were unmeasurable, due to strong buffering at pH 8.0 which resulted in the small CO_2 gas efflux being driven rapidly into the HCO_3^- pool, becoming 'invisible' to the MIMS. As such, it was impossible to compare the two fluxes and confirm respiration rates were accurately recorded. This issue was overcome in the gas phase experiments discussed below 4.2.

There was a strong similarity in respiratory rates between samples cultivated at the two different temperatures, when assayed at their respective growth temperature (45 °C in panel A and 55 °C panel C). This was evidence for a phenomenon known as homeostasis, as described by Atkin and Tjoelker, (2003). Interestingly, this response has also been described for rates of photosynthetic processes in mesophilic cyanobacteria, as measured by activity of PSII evolution (Inoue *et al.*, 2001). That the gas fluxes between the cultivation temperatures were similar in darkness, but significantly different in the light, suggests that changes to [Chl] per cell were not behind the increased values measured in the 45 °C grown cells.

4.1.3 *Fluorescence data supports interpretation of Gross O_2 evolution*

As a secondary measurement of PSII activity, to provide some supporting evidence that the MIMS system was producing reliable data, a set of basic variable fluorescence measurements were conducted across a wide range of sample temperatures. This was only conducted on cells cultivated at 57 °C. Thermal control was provided to the samples via the use of a 'thermal gradient' heating block. In this system a Peltier heater was attached to one end of an aluminium block and a heat exchanger, connected to a water bath, was connected to the other. By setting differential temperatures at each end a gradient of temperature was eventually established across the block, into which sample holders had

been drilled. These sample holders were filled with water to ensure rapid heat transfer into the 5000 µL cell samples, at 4 $\mu g.mL^{-1}$ Chl, in thin walled open topped glass vials. A thermocouple was used to measure when temperatures equilibrated in each sample. A timer was then started to ensure that five minutes had passed, before the fibre optic of the Walz PAM 2500 was inserted into each glass vial and the measurement was initiated. Measurements were replicated three times, providing F_o values. Following the determination of F_o, samples were then incubated with 10 µM DCMU and the same procedure was used to determine F_m – (Schuurmans *et al.*, 2015).

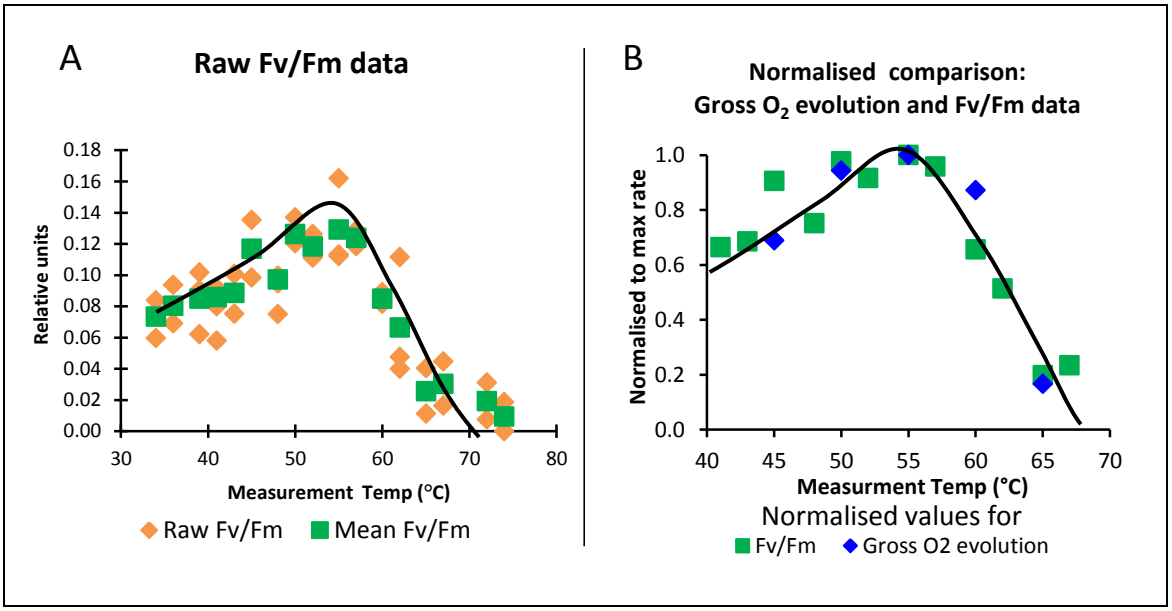

Fig. 4-3: The efficiency of photosynthesis, determined via Fv/Fm fluorescence data of BP.1.
Panel A shows measurements at temperatures ranging from 34°C to 74°C after 5 mins of reaching the indicated temperature, with raw values individual measurements from one run in orange diamonds, the averaged data of three runs in green squares. In panel B, the normalised average Fv/Fm values from Panel A (normalised to the maximum value of 0.13) are compared to the normalised Gross O_2 evolution rates, taken from data displayed in Panel D of Fig. 4-2. All cells being compared were cultivated at 57 °C. Fluorescence measurement conducted at 4 $\mu g.mL^{-1}$ [Chl a], with 10 µM DCMU used to ascertain Fm values, see Fig. 4-2 for information on the Gross O_2 values.

A representative set of 'raw data' and the averaged data from three runs is presented in panel A of Fig. 4-3. The broad trend is highlighted with a line, fitted by eye to simply help observe the data. In panel B, the mean Fv/Fm data was normalised to the maximum value (0.13) and compared directly with the normalised Gross O_2 evolution data (447.5 $\mu molO_2.mgChl^{-1}.hr^{-1}$) from panel D of Fig. 4-2.

The Fv/Fm data in panel B was limited to 67 °C, as there was no gas flux to compare it with at higher temperatures. It can be observed that the Fv/Fm values seem to remain elevated at temperatures > 70 °C in Panel A. However, gas flux data after 10 minute incubations discussed, in 4.2, showed that PSII had ceased to function by this temperature. The trend in Fv/Fm supports the finding that PSII began suffering damage at around 60 °C,

and overall fluorescence data seems to support the use of Gross O_2 fluxes as a proxy for PSII function. This is supported still further from measurements of PSII kinetic area through P700 data in Chapter Five.

4.1.4 *In vitro check of Rubisco's thermal stability*

The rate of CO_2 fixation in panels A and C of Fig. 4-2 could be seen to correlate strongly with the decrease in activity of PSII, at temperatures > 60 °C, as determined through values of Gross O_2 evolution. From that data set alone, it was not clear if this was simply due to a loss of energy to drive the Calvin-Benson-Bassham- cycle, or due to an inherent thermal limitation in key enzymes utilised by the cycle.

It was not possible to isolate and determine the activity of each enzyme of the Calvin-Benson-Bassham cycle, however, an attempt was made to isolate intact carboxysomes from the Beta cyanobacteria: something that until this point has not been possible (so far it has only been possible to isolate intact carboxysomes of the smaller alpha variety). It was hoped that the extra stability afforded by the thermally stable proteins would enable an intact Beta carboxysome to be isolated, and characterised (as was successfully performed with isolation of the oxygen evolving complex of PSII for high resolution crystal structures (Umena *et al.*, 2011)).

Unfortunately, after considerable time and effort, it was determined that the project had to move on and as such, only 'tris percholl' (TP) pellets of carboxysome enriched fractions were produced (Long *et al.*, 2005). However, this preparation contains active Rubisco, so a test of relative $^{14}CO_2$ fixation activity of the enriched fractions, following incubations at a range of temperatures, was conducted. The results of these experiments are presented in Fig. 4-4. More details of the isolation procedure and assay method are discussed in Chapter 3.

All aliquots tested were drawn from a single bulk sample, using a high precision 'Hamilton' syringe. All incubations were conducted in triplicate with their respective procedural blanks, reaction lengths were carefully managed and everything possible was done to ensure only the incubation temperature differed between samples. As such, it is possible to make direct comparisons between the raw data of the samples in 'counts per minute' as determined by the scintillation counter without worrying about [total protein]. The

aim of this experiment was simply to obtain a measure of the 'relative Rubisco activity' at increasing temperatures.

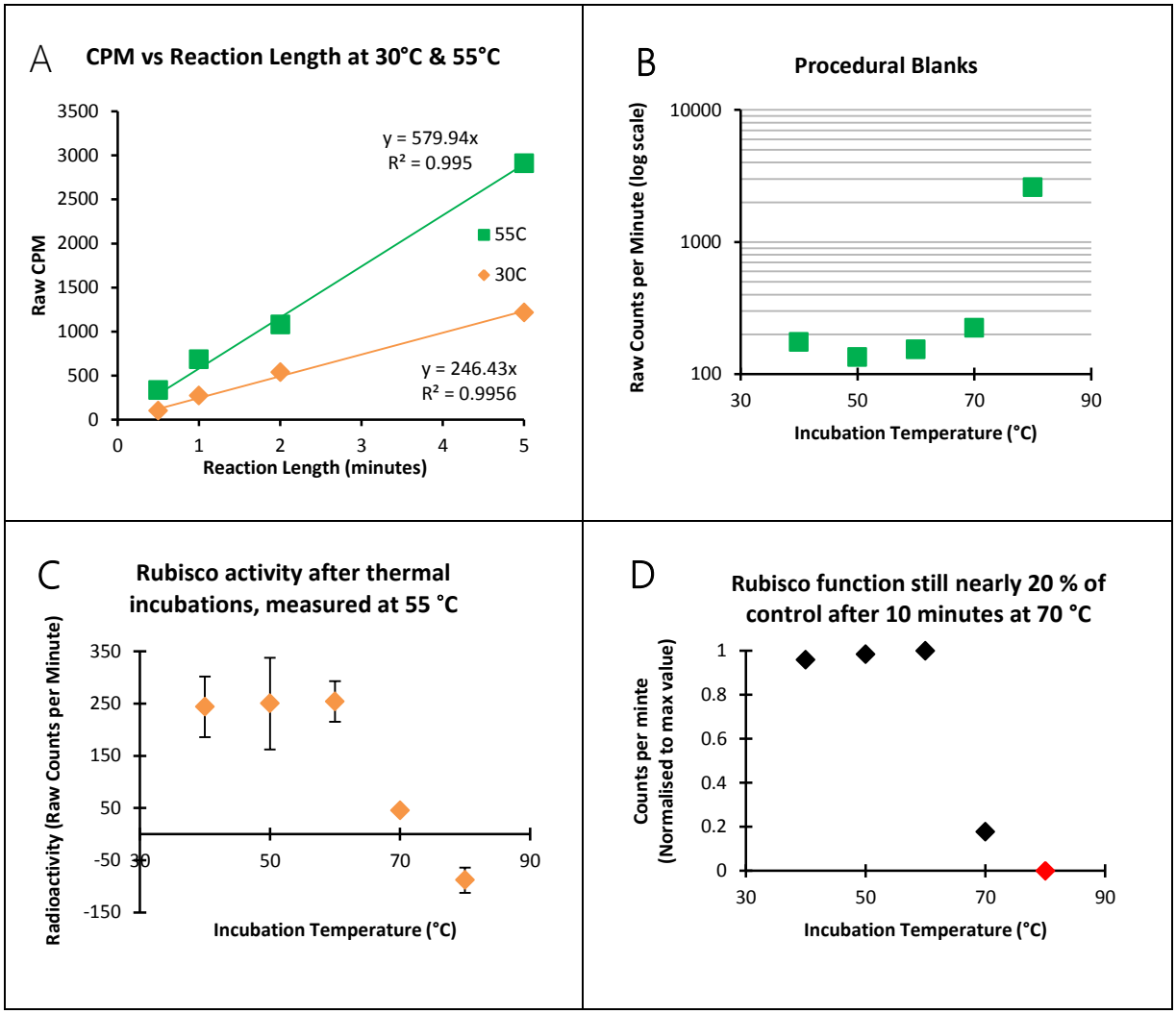

Fig. 4-4: *In vitro* measurements Rubisco function after 10 minute incubations, determined through measured through ^{14}C fixation of carboxysome enriched fractions of Tris Percholl (TP) pellets isolated from BP.1 cells.
Panel A, comparison of reaction rates at 30 °C and 55 °C assay temperature, without pre-incubation, to parametrise experiments (n=1, quick test to compare relative rates and area of linear reaction rate). B, The effect of 10 minute thermal incubations on the activity measured from procedural blanks, including each reagent except RuBP, later subtracted from final data. Only a single procedural blank tube was included in each experimental set, n=1. C, TP pellets were incubated at the indicated temperatures for 10 mins, aliquots of sample were moved to reaction mixture at 55 °C for 5 mins before RUBP addition. Reactions progressed for precisely 1 minute before addition of 10% formic acid. Error bars = St Dev of three repeats. D, values normalised to maximum counts (254 cpm) in panel C. Red point 'set' to zero, as the procedural blank was > than final result, making it negative. Normalised values of C, subject to same error as panel C, but not shown.

The first experiment performed was a simple comparison between assay temperatures and reaction lengths, at the more standard 30 °C and the thermophilic 55 °C. This was to determine which time point would ensure linear fixation rates were being achieved for comparison between samples, and which temperature was more reactive. In panel A of Fig. 4-4 it can be clearly observed that reaction lengths up to five minutes were still within the linear range, and that the rates at 55 °C was more than double that at 30 °C,

based on the linear regression presented in the figure. As such, assay lengths of 1 minute at 55 °C were used for the thermal incubation comparisons.

Procedural blanks, including every step and reagent used in the assay, excluding the addition of RuBP (which started the Rubisco enzyme's function), were conducted at each incubation temperature. This was fortunate because the high temperature incubations seemed to drive spontaneous carbamylation (Caplow, 1968), resulting in enormous background signals at the upper temperatures – as presented in Panel B of in Fig. 4-4.

Subtracting the 'blank' baseline value from each experimental result, produced the values presented in Panel C of in Fig. 4-4. This was considered to be correlated to the number of molecules of $^{14}CO_2$ fixed by Rubisco to an acid stable form, during the one minute of incubation with RUBP. Direct comparisons could be made between the samples due to the care taken to ensure each contained a homogenised concentration of protein and received the same amount of reagents and time. Hence, the terminology of 'raw' in the y-axis of Panel C, refers to the fact that the data was not standardised back in any way to, for example, total protein concentration.

In panel C it is very clear that the activity of Rubisco was unchanged by incubations at up to 60 °C, that between 60 °C to 70 °C this level of activity dropped significantly, and reached a 'negative' value after an 80 °C incubation (where the noise became so high it ultimately swamped the small signal of the result, considered 'zero' activity).

In Panel D, the values were normalised to the maximal counts per minute (254 cpm at 60 °C), and here it could be observed that although the rate of CO_2 fixation reduced markedly between 60 °C and 70 °C, approximately 20 % of the maximal activity still remained at the latter temperature. It was unfortunate that an incubation was not conducted at 65 °C, as later in this chapter (Fig. 4-5), incubations of whole cells suggest that Rubisco activity still seemed to function at rates equal to 100 % of the < 5 % activity measured for PSII at this temperature. It would have been good to make a comparison to the remaining activity of *in vitro* Rubisco at that same temperature.

4.1.5 *Summarising results of gas fluxes at the temperature of interest*

Although it initially seemed like a sensible approach to investigate the impacts of high temperatures on the physiology of BP.1 cells; conducting measurements at the temperature of interest proved quite problematic. The precision of measurements at damaging temperatures was negatively impacted by a combination of physical, chemical and biological parameters. This was driven by decreasing solubility of analyte gases, the increasing Teflon membrane permeability of the MIMS (discussed in section 3.2.1, Fig. 3-6), combined with decreased gas flux rates from the damaged cells, to result in a very high signal to noise ratio. Furthermore, the damage to cells was being constantly added to, making the reporting of 'steady state' data very difficult (actually impossible). As such, making conclusive statements about the relative activities between samples as a function of temperature was compromised.

A comparison between Fv/Fm and Gross O_2 evolution rates of cells cultivated at 57 °C (Panel B Fig. 4-3) supported the use of this gas flux as a measure of PSII activity. Furthermore, an initial *in vitro* assay of Rubisco activity after incubations up to 70 °C suggested this primary enzyme of the Calvin Benson cycle still possessed 20 % function after a 10 minute incubation at 70 °C. This supported the idea that a loss of reductant for CO_2 fixation, and not necessarily the loss of CO_2 fixing enzyme function, was responsible for the tight correlation between decreasing rates of Gross O_2 evolution and the fixation of CO_2 in Fig. 4-2.

In summary however, the primary findings support the hypothesis that PSII exhibited lower thermal tolerance than other cellular components. This was based primarily on the observation that O2 uptake continued at greater rates then O_2 evolution in thermally damaged cells, especially obvious in panel B of Fig. 4-2. This conclusion is consistent with the literature on moderate thermophiles (Yamaoka *et al.*, 1978, Hirano *et al.*, 1981, Koike *et al.*, 1982, Kaurov Yu *et al.*, 1990, Inoue *et al.*, 2000), suggesting that PSII is the thermally weakest component of the cells. Significantly, the data places the context of this data back into an *in vivo* system.

The experimental approach and data presented in Fig. 4-2 provided the only opportunity within this thesis to examine the response of BP.1 cells to suboptimal

temperatures. Although not a primary focus of the research, there was an interesting trend in illuminated oxygen uptake data, presented in Fig. Fig. 4-2, to help further the understanding of the physiology of BP.1 cells to thermal stress generally. This was the result that at sub-optimal temperatures, the samples recorded very high rates of illuminated oxygen consumption (~ 50 % of total PSII activity). This was consistent with a sink limitation downstream of PSI, requiring the function of an alternative acceptor (such as the Flv1-3 proteins) to protect the PSI complex from over reduction (Shimakawa *et al.*, 2016). Whether this was caused by the actual availability of CO_2 to the cells, an internal limitation based on chemical/enzyme kinetics (Kruse *et al.*, 2016), membrane diffusion (Koike *et al.*, 1982) or some other cause is not known, and not investigated further in the thesis.

Based on a comparison of illuminated O_2 uptake between cells cultivated at 45 °C, with those cultivated at 57 °C, I speculate an internal enzyme kinetic/membrane diffusion issue was the cause. Where the 45 °C cells reduced their uptake of O_2 by 20 % at 50 °C, the cells cultivated at 57 °C maintained an elevated uptake of O_2 until 55 °C. The available CO_2 in the buffer should have been equal between the samples at each incubation temperature, implying an internal biological cause for the sink limitation that drove elevated O_2 consumption in the cells acclimated to higher temperatures.

Also clear in Fig. 4-2, and a follow on from the observation of a potential sink limitation at sub-optimal temperatures, was that PSII activity was much higher when determined with Gross O_2 fluxes than measurements based on Net O_2 evolution would suggest, visible at the lower assay temperatures in panels A and C. This suggests that the low growth rates at 45 °C compared to 57 °C, presented in in Chapter Three, was unlikely to be caused by a lack of PSII function.

Cells cultivated at 45 °C recorded significantly higher gas fluxes, both O_2 evolution and CO_2 fixation, than those cultivated at 57 °C. Interestingly the illuminated rates did not seem to match theories of homeostasis. Homeostasis is the observation that the organisms will acclimate to their growth temperature and modulate rates to be optimal at that temperature, ie: cells grown at 25 °C and 35 °C record similar rates when measured at 25 °C and 35 °C respectively, see Fig 2, panel A in Inoue *et al.* (2001). However, homeostasis did seem to occur for respiration, as cells from both cultivation temperatures (panels A and C Fig. 4-2) had similar rates of dark O2 uptake rates (13.3 and 14.8 µmol.mgChl-1.hr-1 for cells cultivated at 45 °C and 57 °C, measured at 45 °C and 55 °C respectively) at their

respective cultivation temperatures, in line with other phototrophs (Atkin *et al.*, 2005). This suggests that the differences in rates of illuminated gas fluxes were not simply a result of changed [Chl] between incubation temperatures.

That being said, the noise associated with the comparatively low gas flux rates in the dark reduced the reliability of this data. In fact, it was found overall that measuring cells at the temperature of interest was not overly useful with respect to answering questions regarding the key hypotheses. Data became difficult to interpret with any precision at elevated temperatures, due to a combination of constantly accumulating damage and the physical properties of the experimental system. As such, a different approach was adopted, to provide better control of the thermal damage inflicted upon cells, and to increase the resolution of CO_2 fluxes. This was achieved by pre-incubating cells for a specified time, filtering the cells onto a glass fibre disc, and then performing measurements in the gas phase, as if on a leaf disc. This is discussed in the following section.

4.2 Post incubation measurements of transient thermal stress

As discussed in 4.1.5, measurements of gas fluxes at the temperature of interest were not as useful for understanding how cells respond to high temperature stress as I had initially thought they would be. In response, it was decided to utilise the incubation approach to generate thermal damage, standardising the 'amount ' of accumulated thermal stress or damage, based on the time period that samples were exposed to damaging temperatures (Inoue *et al.*, 2000, Inoue *et al.*, 2001, Bukhov *et al.*, 2002). After a standardised stress period the level of the damage, and the cell's response to it, could be investigated through measurements at a single, optimal temperature at which undamaged cellular performance provided a benchmark for comparison.

For this study the optimal temperature was set at 55 °C, close to the optimal temperature for growth yet slightly lower to reduce some of the effects that raised temperatures could have on the experimental set-up, such as elevated Teflon membrane diffusion rates. This approach made working with the MIMS much easier, and perhaps more reliable too. Instead of recalibrating the entire system between each new temperature a single calibration run was sufficient for each day. This meant that only a single 'membrane consumption offset' value was used between runs, reducing the possible variability that high temperature measurements, presented in Fig. 4-2, were subject to. It was also an assay

temperature that data presented in Fig. 4-2, indicated is high enough to ensure the kinetics of TCi uptake were not impeded, ensuring no requirement for carbonic anhydrase to obtain accurate total carbon fluxes.

Although literature into thermal stress often utilises a five minute incubation period, for both thermophilic (Yamaoka *et al.*, 1978, Sonoike *et al.*, 1990, Inoue *et al.*, 2000) and mesophilic (Enami *et al.*, 1994, Aminaka *et al.*, 2006) samples, it was considered more useful to conduct 10 minute incubations in this thesis. This incubation length generated strong changes to monitor across a shorter thermal range, provided a sufficient time period to stagger experiments efficiently which lead to increased efficiency of the experimental work and reduced the time required to occupy the heavily used instrument.

A further, and highly significant, addition to the following data sets was the addition of simultaneous P700 spectrophotometric difference measurements to the gas fluxes. This provided relative information on the redox activity of PSI. In order to generate sufficient signal for this measurement, the samples were no longer measured in dilute liquid culture, rather cells were embedded into a glass fibre filter disc and saturated with measurement buffer. This was termed a 'cyano disc' – in reference to the 'leaf disc' its design was trying to emulate. Data to support the accuracy of this measurement approach was provided in a discussion of the evolution of the P700 measurement, and the eventual development of a 'cyano disc' in section 3.3.3 Fig 3.15.

An added advantage of the 'cyano-disc' method was that a much smaller volume of measurement buffer remained in the sample. This made it was possible to measure the CO_2 efflux from cells into the cuvette, as it was more likely to exchange with the CO_2 gas in the atmosphere around the disc, then stay as HCO_3^- in the very small pool existing in what was likely a HCO_3^- saturated buffer. One limitation of the pre-incubation approach however, was that no information could be elucidated about processes that were not damaging, such as cellular regulation in response to sub-optimal temperatures.

Whereas the data in Fig. 4-2 provided some information as to what may be a stress response to sub-optimal temperatures, incubating cells at low temperatures for 10 minutes and measuring them at the optimal temperature resulted in no change to fluxes. As such the temperature range measured with the transient heat stress approach covers temperatures from only from 50 °C up to 75 °C.

4.2.1 *Method summary for transient stress analysis on cyano-discs*

- Samples of BP.1 were cultivated as for previous experiments, except the cultivation temperature was standardised to 55 °C, matching the 'optimal temperature' utilised during measurements.
- An aliquot of sample was aseptically taken from the growth tubes, pelleted through centrifugation, made up to a low volume with measurement buffer (0.5 M [Hepes], excluding NO_3^-, replaced with 20 mM NaCl), the [Chl] was determined before adding sample buffer to dilute samples to 100 µg Chl/$mL^{-1.}$
- Samples were loaded into a septum sealed 10 mL vial, a syringe pierced through the vial to maintain the cultures gently bubbling with compressed air whilst a second syringe penetrating only to the head space acted as a gas vent. The compressed air line kept the vial suspended in a water bath maintained at 55 °C whilst a tungsten desk lamp provided constant low light, through the Perspex wall of the water bath of about 30 µE at the sample. These conditions were determined to maintain the cells in a stable state, no obvious differences were noticed between cells taken from this sample stock early or late in a day. A separate water bath was set to the incubation temperature of interest containing a number of septum sealed glass vials, each filled with 5 mL of measurement buffer. One septum lid, supporting a Pt 100 (platinum difference thermometer) probe, was placed onto the glass vial to be used. 100.0 µL, or 10 µg of chlorophyll *a* was taken from the bulk sample at 55 °C and injected into the incubating vial (based on the data in Fig. 3-16, that about 6 µg was the maximum retained on the discs). Darkness was maintained by covering the incubator in an opaque black cloth. The large volume of pre-equilibrated sample buffer ensured that the low volume of injected cell sample reached the required incubation temperature almost instantly, as confirmed by monitoring the Pt100 readout.
- After precisely 10 minutes, the sample, kept in darkness by illuminating the room with only dim 'green light', was filtered under light vacuum into a glass fibre disc of 10 mm diameter, sitting in an 8 mm diameter vacuum filtration mask. The fibre was kept saturated with buffer by stopping the vacuum before completely removing all of the buffer.
- To remove the masked edge an 8mm disc was cut from the 10 mm disc, producing a fully incubated, highly homogenous, green 'cyano disc' of 8 mm diameter.

- The 8 mm disc was loaded onto a small gauge steel mesh within the thermally equilibrated and calibrated MIMS cuvette. The mesh sat upon on a ring consisting of two layers of glass fibre filter, saturated with MQ H_2O to ensure the chamber remained at saturating humidity to ensure full saturation of the cyano disc was maintained.
- The cuvette was then closed, purged briefly with N_2 gas before the injection port was sealed with 'blue tack'. Through the blue tack 20 µL of CO_2 gas (≈ 2 % v/v final) and approximately 50 µL of $^{18}O_2$ gas (≈ 5 % v/v final) was injected with a gas tight, valve sealed syringe. The actual final concentration of the gases was calculated via the MIMS calibrations; as such the calculated fluxes were not contingent upon the precision of these injections.
- Including the time spent setting gas concentrations, cells were left in the dark at 55 °C within the cuvette for five minutes, to allow equilibration for cells back to the 'optimum' temperature, and to allow gases to reach an equilibrium state between the various phases within the cuvette.
- Initially a $P700_{max}$ measurement (low irradiance (12 µE) Far Red (FR) light at 723 nm), followed by the Y(I) measurement (requiring a total time of 1.7 minutes of almost constant actinic illumination) were undertaken. These are discussed more thoroughly in Chapter Five. A further period of 3 mins of straight actinic light (500 µE, from the same source as the Y(I) measurement) was then used to ascertain the steady state gas fluxes. Gas fluxes reported here were determined during this three minute period of actinic illumination – to ensure they were a true 'steady state' flux.
- Dark rates reported were taken from data after the actinic light period. This avoided the disequilibrium effects on calculated rates that occurred within the five minute dark period before sample illumination as gases were being dissolved into liquid phases within the sample and the cuvette.
- To determine the [Chl] on discs, at the conclusion of the MIMS experiment each was loaded into an eppy tube containing 1000.0 µL of MeOH, placed on ice until all gas fluxes had been measured. Samples were then left overnight in the fridge to extract chlorophyll, then determined spectrophotometrically according to (Porra *et al.*, 1989).

4.2.2 *Data from cyano-disc gas fluxes, post incubations*

Overall fluxes from cyano discs presented in Fig. 4-5 were lower than the rates measured in liquid cultures of Fig. 4-2, although they were still in line with published values (Yamaoka *et al.*, 1978).

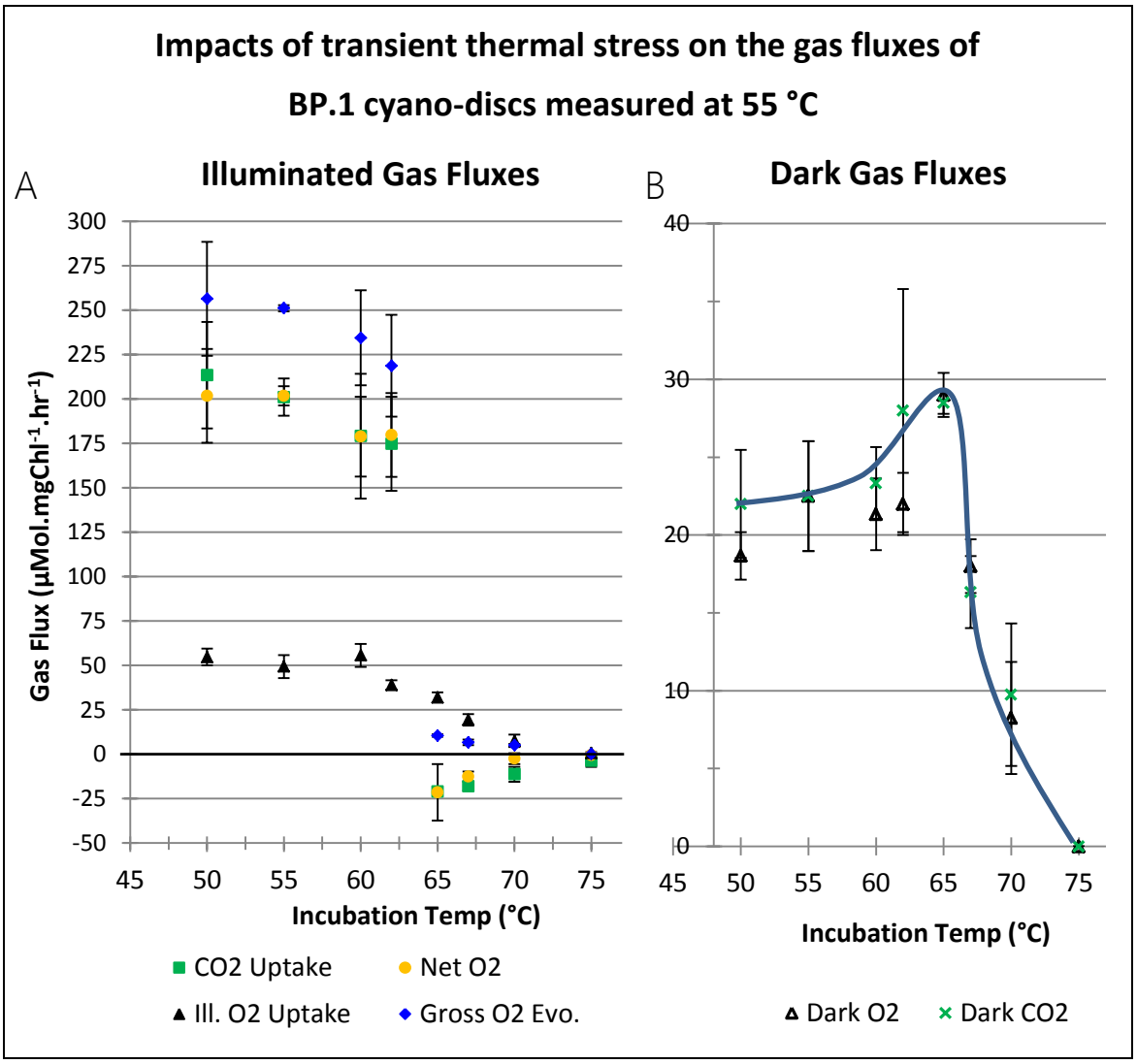

Fig. 4-5: Post incubation steady state gas fluxes of thermosynechococcus elongatus BP.1 'cyano discs' in the light (Panel A) and dark (Panel B).
Samples were incubated at temperatures displayed on the x – axis for 10 minutes in the dark, after almost instant heating from the standard temperature of 55 °C. After precisely 10 minutes, samples were vacuum filtred into a glass fiber disc (10 mm) to create a 'pseudo leaf'. From this an 8 mm disc of homogenous cell density was cut, called a 'cyano disc'. All steps performed in dim green light. This was loaded into the gas phase MIMS cuvette calibrated to the standardised temperature of 55 °C. In darkness the gas atmosphere of the measurmenet cuvette was purged breifly with N_2 gas, 2 % v/v CO_2 and ≈ 3 % v/v $^{18}O_2$ was injected. Samples were left for five minutes total time in darkness at 55 °C in cuvette, whilst the gases were injected, before P700 measurements were conducted (see the following chapter for results). This provided an intial period of almost two minutes actinic illumination (500 µE). P700 measurements were immedietly followed by a further three minute period of actinic illumination, designed specifically to achieve steady state photosynthesis: from which the rates presented in panel A were extracted. At the cessation of illumination, a period of darkness was used to extract the values presented in Panel B.. Values in both panels are the mean of at least three replicates, presented with the standard deviation. Examples of the raw fluxes versus time are presented in Fig. 4-8 for the temperature 62 °C to 75 °C.

In most probability, this was a result of self-shading on the relatively dense disc, which was not optimised for maximal photosynthetic rates but a compromise to maximise

signal to noise ratios of the P700 system (requiring a nice green cell density). This may have depressed rates on a 'per chlorophyll a basis'. In Chapter Three, Fig 3-15 provided evidence that the 'cyano-discs' function as well as 'standard' liquid cultures.

The rates of **net O_2 evolution** presented in Fig. 4-5 compare well with those shown in Fig. 4-2, maintaining a steady rate across the optimal temperature range before dropping rapidly at temperatures > 60 °C. The higher resolution of this data set makes it possible to see that rates don't reduce enormously between 60 °C and 62 °C, however, it can be seen in panel A of Fig. 4-5 that 10 minutes in the dark at 65 °C was enough to eliminate all net oxygen evolution. At this temperature the rate became negative – implying a net uptake of oxygen. The negative rate trends towards zero in the range of 67 °C to 70 °C, and finally reached zero at 75 °C.

Unsurprisingly, the rates of gross oxygen evolution trended very closely against net oxygen evolution in Fig. 4-5, showing the same response across the optimal range, before dropping slightly between 60 °C and 62 °C. After 10 minutes in the dark at 65 °C, the rates reduced to only about 5% of maximal rates, however, they did not become negative (which would be impossible by definition of the fact this is a gross measurement). Between 65 °C and 75 °C, the rate dropped slowly but consistently, reaching zero at 75 °C. Although instrument noise became problematic as the rates dropped, an excerpt of processed data showing rates as a function of time, covering 62 °C, 65 °C, 67 °C and 70 °C, is presented below in Fig. 4-8. There it can be observed that even very low rates of oxygen evolution were quite accurately measured by the MIMS method in the gas phase.

The **net Ci uptake rate,** measured during steady state photosynthesis was most probably a useful measurement of photosynthetic CO_2 fixation. These values both matched and trended with the net oxygen evolution fluxes very closely (well within the reported error) across the entire range of temperatures investigated. This included the net uptake rate becoming negative at 65 °C, where the negative value implied a net efflux of CO_2 from the sample. As with rates of net O_2 evolution, this negative rate trended back towards zero in a consistent way with temperature, reaching almost zero at 75 °C.

Illuminated rates of oxygen uptake in Fig. 4-5, panel A, were steady across the 'optimal' thermal range, where incubations caused no damage (50 °C to 60 °C) in. There was no obvious correlation between the uptake of oxygen and other fluxes in this figure, when one considers the scale of the change that occurred with transient temperature stress.

Although the rate of oxygen *uptake* decreased in a similar fashion to the rate of oxygen *evolution*: where only 5 % of gross oxygen evolution remained after the 65 °C incubation, almost 60 % still remained of the uptake value. The majority of the decrease in oxygen uptake activity occurred gradually at temperatures > 60 °C and did not experience the 'step change' observed for both oxygen evolution and carbon fixation.

Dark rates of oxygen uptake and Ci efflux from the cells, in Fig. 4-5, panel B, matched each other closely and remained steadier than other values measured in the light across the thermal range investigated. Both rates tended to increase with increasing temperature between 50 °C and 65 °C, although the data was relatively noisy. That said, a single tailed T-test of the difference between the rates at 50 °C and 65 °C indicated a significant increase overall (P = 0.05 and 0.001 for O_2 and CO_2 fluxes respectively, n=3). Beyond 65 °C the flux rate of both gases declined sharply, but consistently across 67 °C and 70 °C, before also reaching zero at 75 °C.

4.3 Analysing the physiology behind steady state gas fluxes

The key goal of setting up the mass spectrometer to measure real time gas fluxes from a photosynthetic sample was, in this case, to elucidate the physiological functions that underpin those gas fluxes under steady state conditions. This approach was used to make a comparison between the physiologies of samples that had suffered thermal damage, relative to undamaged controls. As the generation or consumption of gases were driven by chemical reactions within the cells, and due to the redox nature of cellular chemistry, these reactions were ultimately linked to the movement of electrons from oxidative sources such as PSII, to reductive sinks such as Rubisco. As such, the chemistry driving each gas flux measured with the mass spectrometer was considered within the context of it being an electron source or sink.

The simplified equations for photosynthesis and aerobic respiration provide the foundations on which gas fluxes ought to balance:

$$\text{Photosynthesis: } 6CO_2 + 6H_2O \rightarrow C_6H_{12}O_6 + 6O_2$$

$$\text{Respiration: } C_6H_{12}O_6 + 6O_2 \rightarrow 6CO_2 + 6H_2O$$

In this *simplified* version of photosynthesis, the oxidation of $6H_2O$ by PSII liberates 12 electrons and the reduction of $6CO_2$ by Rubisco consumes 12 electrons. Reversing this processes through aerobic respiration results in the same values, with 12 electrons liberated

by the oxidation of each glucose-equivalent being used to reduce $6O_2$ molecules to H_2O. Whilst the mass balance exercise was performed in units of µmol(gas).mgChl^{-1}.hr^{-1}, the idea that each gas term making up the total flux is an electron source or sink was required in order to parametrise the mass balance equations.

Interpreting gas fluxes in the context of electron sources and sinks was considered a robust analytical framework with which to ascertain the responses of cells to the loss of PSII activity, (which was predicted to be severely inhibited after incubations at around 65 °C (shown in Fig. 4-2). It is an analysis framework built upon that used by Radmer and Kok (1976), which was used by them to investigate the dynamics of O_2 and CO_2 fluxes on the onset of illumination, in an early application of the MIMS method.

4.3.1 *Using a mass balance approach to investigate gas fluxes*

The mass balance approach relied on a number of assumptions that must be clearly understood. The mass spectrometer accurately measures gas fluxes, however, these gas fluxes were only proxy measurements of highly complicated and convoluted processes occurring within the cells. Although the stoichiometry of electrons being generated or consumed with relation to a specific gas flux may be the largest single assumption, there is a precedent for such an approach (Radmer and Kok, 1976). Whilst there exists no better way to directly measure the flux of electrons through an intact sample, the instrument can only measure gases that are entering or being removed from the atmosphere around the sample within the cuvette.

Furthermore, the number of reactions and pathways are considerably complex and this analysis attempts to reduce the entire organism's biochemistry to a handful of primary reactions. This may be an unreasonable assumption to make, particularly once cells suffer severe damage.

The location of these reactions within the cell is also contentious. For example, it is well documented that cyanobacterial respiration utilises the thylakoid membrane, however, there is a proportion that also take place on the cytoplasmic membrane (Lea-Smith *et al.*, 2016), which presumably has little impact on the photosynthetic electron transport chain.

Great effort was made to provide evidence to support all claims regarding changes to the biochemistry observed in the following section. Although the mass balance approach may not result in a perfect outcome, the conclusions drawn at the end of this section were

not considered 'in a vacuum'. They were used as a foundation, to which further measurements were added, especially the results of from the simultaneously measured P700 data, analysed and discussed fully in Chapter Five.

4.3.2 *Explaining the mass balance estimation*

In simplistic terms, the mass balance estimation was a summing up of all activities that generate and consume electrons, considered under steady state conditions of either illumination or darkness, and measured through the proxy of gas fluxes. It is an approach used early in the evolution of applying MIMS techniques to photosynthetic physiology (Radmer and Kok, 1976). In the simplified form, PSII activity was considered the only source of electrons, the primary sink was CO_2 fixation and any excess was consumed through the 'regulatory' O_2 consumption of the water-water cycle (Asada, 2000), which is also considered as a 'pseudo cyclic' pathway, primarily mediated in the cyanobacterial cells by the Flv1,3 proteins (Allahverdiyeva *et al.*, 2013). It is described in the following:

Eqn. 1

$$GrO_2ev - NetCO_2up - GrO_2up \sim 0$$

Where:

GrO_2ev = Gross O_2 Evolution rate

$NetCO_2up =$ Net CO_2 Uptake rate

GrO_2up = Gross O_2 Uptake rate

In the dark, a lack of PSII activity allowed this to be further simplified to:

Eqn. 2

$$NetCO_2up + GrO_2up \sim 0$$

as the $NetCO_2up$ rate became both negative, and the primary electron source, it cancelled out the respiratory GrO_2up, which remained the electron sink. The use of capitalisation for these terms denotes that they were directly measured by the instrument.

Applying this analysis, especially to damaged cells, required slightly more detail of the biochemical processes underpinning each of these major gas fluxes be considered, so that the separate functions underpinning each could be derived. As such, the full equation considered in this thesis was:

Eqn. 3

$$(GrO_2ev - rspCO_2ev) - (fixCO_2up + regO_2up + rspO_2up) \sim 0$$

Where although:

$GrO_2ev =$ (Water oxidation: *electron source*)

The other two measured values were comprised of multiple terms:

$$NetCO_2up = fixCO_2up - rspCO_2ev$$

$$GrO_2up = regO_2up + rspO_2up$$

Where:

$fixCO_2up =$ rate of CO_2 fixation (Calvin Benson cycle: *electron sink*)

$rspCO_2ev =$ rate of CO_2 evolution (a negative value = Respiration: *potential electron source for thylakoid energisation*)

$regO_2up =$ rate of regulatory O_2 uptake (Mehler type reactions of the water - water cycle: *electron sink*)

$rspO_2up =$ rate of respiratory O_2 uptake (Respiration: *electron sink*)

4.3.2.1 Working through an undamaged example

It is useful to examine an example data set comprising undamaged cells, where changing fluxes were driven instead by altering the irradiance. The data in Fig.4-6 provided an example to illustrate that the concept broadly works, and the significance of analysing steady state fluxes to maximise the probability that assumptions being applied are valid. The data were generated during trials of the cyano-disc concept, to establish the optimal [Chl] on discs, and the irradiance to be used for the measurement data presented in Fig. 4-5. This is an example of how the 'raw' MIMS data looked once the mass spectrometer's $mV.s^{-1}$ output, was translated into *gas flux rates.sec*$^{-1}$. To my eye, it is a beautiful set of data: it illustrates the dynamics of the cyanobacterial samples over the course of light dark transitions, and how they cope with excess to needs (of the Calvin-Benson-Bassham cycle) PSII activity, by increasing regulatory O_2 consumption with increasing irradiance.

The light cycles involved three minutes illumination at an irradiance level illustrated above each 'peak' in the figure, followed by one minute in darkness. The data summary extracted from this figure, ie. the rates determined for each irradiance, are presented in Table 3. The first four columns of this table are self-explanatory. The column titled "Result Eqn. 1" presents the result from applying this analysis to the data in the first three columns. The final column titled "% of data unaccounted" is calculated with Eqn. 4 as:

Eqn. 4

$$\left(\frac{GrO_2ev - NetCO_2up - GrO_2up}{GrO_2ev}\right) \times 100$$

This is an approximate measure of the 'accuracy' of the mass balance 'estimation', determined by dividing the gas flux remainder, by the fluxes of gases assumed to be the 'total input of electrons'. The idea of using this check was that it highlights when assumptions about the application of the simple mass balance equation were appropriate. For example, when PSII was the only source of electrons, then GrO_2ev was used as the denominator, as above in Eqn. 4Error! Reference source not found.. However, when a more etailed approach was required to explain the data, and Eqn. 3 was utilised, it became necessary to test the idea that both PSII activity and respiration were functioning in concert under illumination (see below), in which case Eqn. 4 was modified to become:

Eqn. 5

$$\left(\frac{(GrO_2ev - rspCO_2ev) - (fixCO_2up + regO_2up + rspO_2up)}{GrO_2ev - rspCO_2ev}\right) \times 100$$

In this thesis the threshold for 'acceptable' error was set arbitrarily to 5%, to account for instrument/sample error resulting in the rates measured being subject to noise. In other words, the result of applying Eqn. 1 to any condition tested (irradiance on a light curve or incubation temperature, for example) must have fallen within 5% of the total input flux of electrons to the thylakoid being considered in the analysis (ie. GrO_2ev or $(GrO_2ev - rspCO_2ev)$) to be considered fully explained, as this was considered the 'total energisation available' to thylakoid based processes. When data fell outside of this range using Eqn. 1 the more detailed version, Eqn. 3, was applied. Different options, such as changing assumptions about illuminated rates of respiration were then tested to find a scenario that could fit the data. This is explained in more detail in subsequent sections where it was applied.

It can be observed that the majority of irradiances measured, presented in Fig.4-6, were fully explained by the application of Eqn. 1 in Table 3 . However, the first irradiance at 45 µE, fell a long way out of the 5% boundary. As such, the data highlighted that these conditions required further analysis and consideration, that in this case it was not necessary to utilise the comprehensive Eqn. 3, to test if processes such as illuminated respiration (which would include irradiances below the light compensation threshold for net oxygen fluxes

(Walker, 1987)) were causing the imbalance, because clearly in Fig.4-6 there was little to no illuminated oxygen uptake measured at 45 µE. So why did the fluxes not balance?

The most likely explanation was that rates at the lower irradiance had not yet reached a steady state of photosynthesis. A measure of cells reaching steady state in this experiment was when the 'net' rate of O_2 evolution equalled that of net CO_2 fixation. In Fig.4-6 the cells do not seem to have reached a steady state of photosynthesis (by this definition), until nearly the end of the 130 µE irradiance. Before this time-point, it could be observed that the values for $\mathrm{GrO_2up}$ were decreasing steadily over time, as the rate of $\mathrm{NetCO_2up}$ increased. Eventually this matched the Net O_2 evolution rate, just before the light was extinguished.

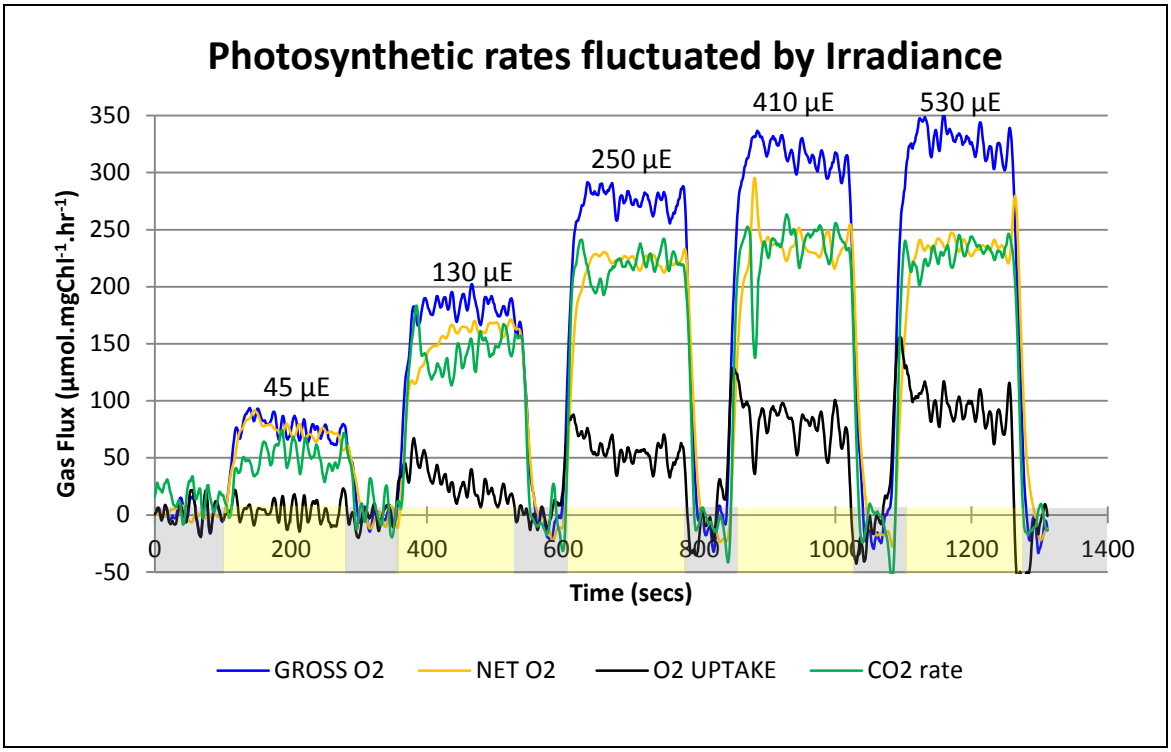

Fig.4-6: Photosynthetic irradiance curve of a BP.1 cyano-disc illustrating the concept of 'regulatory' oxygen uptake. A disc containing a relatively low, (compared to the incubation experiments in Fig. 4-5) 3.8 µg chlorophyll was created with a fresh cell sample. There was no pre-incubation, the saturated disc was loaded into the 1000 µL cuvette, purged briefly with N2 which was then sealed with blue tack and 20 µL of CO_2 and 30 µL of $^{18}O_2$ were injected. After five minutes sitting at 55 °C in darkness a three minute to one minute sequence of actinic light to darkness was initiated (illustrated in the figure by light yellow and grey colour bands along the x-axis). Through adjusting the calibrated halogen lamp's power supply during each dark period, the irradiance was altered for each period of illumination. The first period at 45 µE, then climbing through 130 µE, 250 µE, 410 µE and 530 µE respectively. The five minute pre-illumination period has been excluded from the figure

In their paper exploring this phenomenon, entitled "Photoreduction of O_2 Primes and Replaces CO_2 Assimilation", Radmer and Kok (1976) describe the dynamics of the induction of carbon fixation, as cells are initially illuminated after dark adaptation. They demonstrate that oxygen reduction to water can be used to quench excitation from PSII, in

excess of the capacity of the Calvin Benson cycle to utilise it (termed 'regulatory' O_2 uptake in this thesis). They also demonstrate that the extent of this response was dependant on irradiance, the two were positively correlated.

This could be the reason that rates presented in Fig.4-6, at 45 µE presented such low O_2 uptake rates, as the initial irradiance seemed low enough to be balanced solely by the fixation of CO_2. However, the second curve at 130 µE seems to be initially subject to excess irradiance, although the cells begin to adjust and after three minutes they reach a steady state with very low regulatory O_2 consumption. Recall they were cultivated at 100 µE. Higher irradiance seemed to require the reduction of oxygen to balance PSII sourced reductant, even once steady state has been achieved, as O_2 consumption increased with each increase in irradiance. Even once the rate of CO_2 fixation plateaued at ~ 400 µE, the Gross evolution of O_2 is able to increase, in step with an increased rate of O_2 uptake/reduction as a counter balance.

Table 3: data points extracted from Fig.4-6 used as an example for a mass balance analysis of gas fluxes. '% of data unnacounted" is a measure of the capcity of the basic Eqn. 1 to account for the data. A value < 5 % is considered accurate enough to warrant no further investigation. > 5% requires the use of the more detailedEqn. to perform some hypothesis testing.

Irradiance (µE)	GrO_2ev *µmol gas.mgChl^{-1}.hr^{-1}*	$NetCO_2up$ *µmol gas.mgChl^{-1}.hr^{-1}*	GrO_2up *µmol gas.mgChl^{-1}.hr^{-1}*	Result Eqn. 1 *µmol gas.mgChl^{-1}.hr^{-1}*	% of fluxes unaccounted
45	83	62	3	18	21.7
130	174	158	16	0	0
250	282	226	56	0	0
410	332	236	96	0	0
530	310	232	76	2	0.6

This was taken as strong evidence for the need to ensure cells were fully equilibrated with their measurement environment (to ensure equilibrium between the injected isotopes within the cells and their environment, also highlighted by Radmer and Kok (1976)), and in a steady state of photosynthesis, before gas rates were recorded for analysis with the mass balance estimation. All data in Fig. 4-5 was accordingly recorded after about five minutes of actinic light exposure, (and before that, expose to weak FR light) which can be seen in raw plots of the *gas flux rate versus time* from the incubation temperatures between 62 °C and 70 °C, presented in Fig. 4-8.

This example analysis of a single set of data was intended to help the reader better understand how the gas flux measurements presented in Fig. 4-5 were generated, and what considerations were given to the timing of defining steady state fluxes. It was also intended

to demonstrate why the mass balance framework was selected as a tool for the objective assessment and description of the data. In the following sections, where assumptions about the sources and sinks of electrons become more complex as a result of damage to PSII, the value of this approach hopefully becomes clearer.

4.4 Applying the mass balance to thermally damaged cells

In the following section, data presented in Fig. 4-5 was analysed utilising the mass balance approach discussed above. Through simple deduction it will be shown that respiration must have been functioning in the light, after incubations (> 65 °C) that severely inhibited PSII. Although this observation answers one of the key questions asked in this thesis, the hypothesis being tested in these experiments was more expansive, asking: *do thylakoid based cellular components downstream of PSII continue to function when PSII is severely inhibited by high temperatures?*

The major systems referred to include the b_6/f complex, PSI and perhaps even the Calvin Benson cycle. In their combined ^{13}C-metabolic flux and RNA sequencing analysis of Synechocystis 6803, You *et al.*, (2015) suggest that the Calvin-Benson-Bassham cycle, and various respiratory pathways, are still functional when linear electron transport is inhibited by the addition of DCMU to cells. Was it possible to observe this in the BP.1 cells exposed to temperatures that had inhibited the great majority of PSII function?

Table 4: 'Baseline values' for gas fluxes from non-damaged cells, generating by combing fluxes after incubations at 50 °C, 55 °C and 60 °C.
All fluxes in units of µmol(gas).mgChl^{-1}.hr^{-1}. Yellow cells = illuminated fluxes. Grey Cells = Dark fluxes

	Gross O_2 Evol.	Net CO_2 Uptake	Ill. O_2 Uptake	Dark O_2 Efflux	Dark CO_2 Uptake
Averaged fluxes at 50 °C, 55 °C & 60 °C	*247*	*198*	*53*	*22*	*24*
Terms describing each 'measured' gas flux	GrO_2ev	$NetCO_2up$	GrO_2up	$DarkO_2$	$DarkCO_2$

It was first necessary to set the baseline levels of function after incubations that had caused the cells no damage, as defined by a significant change in fluxes from the 'optimal' temperature at 55 °C. For this, data from incubations at 50 °C, 55 °C and 60 °C were grouped together as 'not damaged', to be used as the control group. Although there was a slight decrease in the overall GrO_2ev rate at 60 °C, according to a single tailed T-test comparing this rate to that at 55 °C, the difference was insignificant (P = 0.2, n=3).

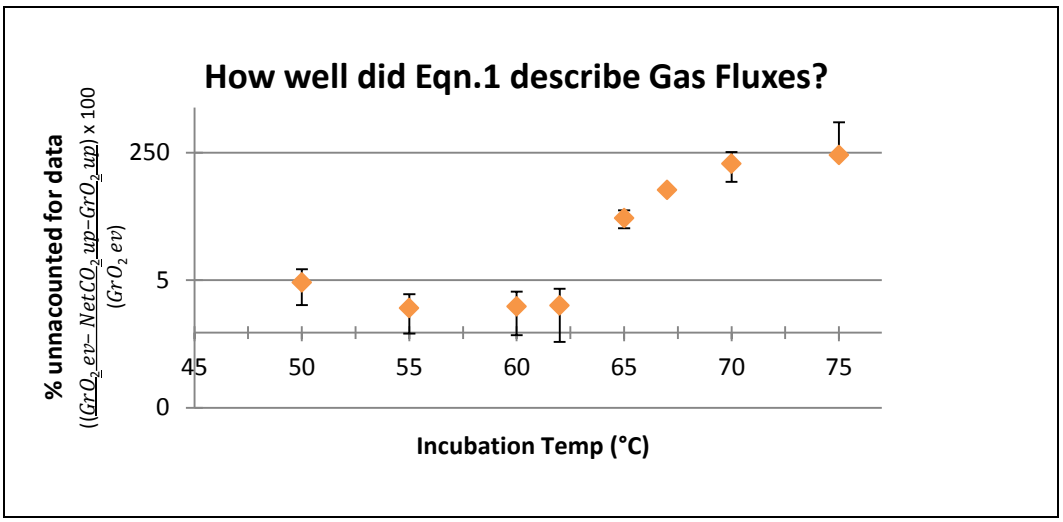

Fig. 4-7: Accuracy of assumptions behind Mass Balance equation:
The mass balance equation described in Eqn. 1 assumes that PSII is the primary electron donor to the system and that the MIMS measurements were accurate enough to stoichiometrically balance. To test the validity of these assumptions, Eqn. 4 was applied to each experimental repeat with the results averaged and presented above. A 5 % threshold was applied to the data to allow for error associated with reproducibility of MIMS measurements/ incubations etc. Results > 5% indicated the assumptions had possibly broken down. Data is presented on a semi-log plot to show where data becomes > 5 %. Incubations at 65 °C, 67 °C , 70 °C and 75 °C are clearly > 5%. Data points are the averaged result of applying Eqn. 4 to each replicate individually, with the standard deviation.

Furthermore, no significant change in the GrO_2ev rates at 62 °C were determined, however, the GrO_2up rate at 62 °C significantly decreased when compared to that rate at 60 °C (single tailed T-test: P= 0.008, n=3). As such data at 62 °C was excluded from the group that were defined as 'not damaged', because the driver of reduced oxygen uptake was unknown. Data for each flux across the 'not damaged' group was averaged, producing the values presented in Table 4.

To this data, the simple Eqn. 1 was applied:

$$GrO_2ev - NetCO_2up - GO_2up \sim 0''$$

$$247 - 198 - 53 = -4 \quad \text{(all units in µmol(gas).mgChl}^{-1}\text{.hr}^{-1}\text{)}$$

∴ the output from the mass balance estimation is out by 4 units from reaching the expected 'zero' value. To this result Eqn. 4 is applied:

$$\left(\frac{247-198-53}{247}\right) * 100 = -1.6\,\%$$

The final value was transformed to a positive number, to make it an 'absolute' value, or else variance between positive and negative results could reduce the final averaged result to within 5% .

$$\therefore final\ result = 1.6\,\% = < 5\% = valid\ assumptions$$

The results of each sample replicate were analysed in this manner, the results were averaged and used to produce the results presented in in Fig. 4-7. It shows a very clear trend, with cells exhibiting high PSII function (those exhibiting high rates of GrO_2ev in Fig. 4-5) fitting within the 5% tolerance, and those incubated at temperatures > 62 °C rapidly trending upwards from 0%, reaching up to 250%. These results indicated that the primary assumptions broke down as the cells suffered thermal damage. This indicated a different approach, or set of assumptions, was needed to explain the data in thermally damaged cells.

4.4.1 *What happened when PSII failed due to heat stress?*

As discussed briefly when describing trends in Fig. 4-5, the flux of GrO_2ev dropped precipitously by 95 % between incubations at 62 °C and 65 °C. This correlated strongly with the flux of $NetCO_2up$, which became negative (implying a net efflux of CO_2 from the cells). However, the rate of GrO_2up deviated from this trend, being reduced only marginally at 65 °C, compared to measurements conducted after incubations at 62 °C. As the GrO_2ev flux was a proxy for PSII activity, and typically this is considered the only source of reductant entering the thylakoid during illumination, (assumes respiration is down regulated in the light), then it makes no sense that the flux of GrO_2up can remain relatively unaffected when PSII failed.

Stoichiometrically, this is impossible under the initial set of assumptions, because it would require a different source of reductant to enable the terminal oxidases to function. A strong clue to the new source of reductant driving the GrO_2up rate, once PSII had ceased the majority of its function, was that $NetCO_2up$ became negative, not simply zero (implying a net release of CO_2). The simple explanation for these observations was activity of the respiratory pathways. If correct, it became a significant flux during illumination, much higher in activity then PSII under these conditions. To enable a more detailed analysis of the gas fluxes and related physiological processes in this changed scenario, it was

Table 5: Gas flux data averaged from cells incubated at 65°C.
Note that applying Eqn. 1to these numbers actually balances out perfectly. However, the data in Fig. 4-7 calculated the mass balance for each experimental repeat and as such the values presented are an average of those results. All fluxes in units of µmol(gas).mgChl^{-1}.hr^{-1}. Yellow cells = illuminated fluxes. Grey Cells = Dark fluxes

$Temp$ (°C)	GrO_2ev µmolO_2.mgChl^{-1}.hr^{-1}	$NetCO_2up$ µmolCO_2.mgChl^{-1}.hr^{-1}	GrO_2up µmolO_2.mgChl^{-1}.hr^{-1}	$GroCO_2ev$ µmolCO_2.mgChl^{-1}.hr^{-1}	GrO_2up µmolO_2.mgChl^{-1}.hr^{-1}
65 °C	11	-21	32	29	29

necessary to employ Eqn. 3. The data for fluxes after a 65 °C incubation are presented in Table 5.

Two hypothetical scenarios were tested with the application of Eqn. 3, to investigate if the gas fluxes support the hypothesis. In the first scenario, it was assumed that CO_2 fixation was 100 % inhibited by the high temperature incubation. In the second scenario, CO_2 fixation was assumed to still function at 100% of remaining PSII activity.

As a reminder Eqn. 3:

$$(GrO_2ev - \ rspCO_2ev) - (\ fixCO_2up + regO_2up + rspO_2up) \sim 0$$

Where: $$NetCO_2up = fixCO_2up - rspCO_2ev$$

$$GrO_2up = regO_2up + rspO_2up$$

4.4.2 *Testing scenario one: Zero CO_2 fixation.*

In scenario one, none of the energy entering the thylakoid membrane from PSII activity could be used to drive carbon fixation, requiring that 100 % of this energy be consumed through $regO_2up$. As such:

$$fixCO_2up = 0 \therefore \ regO_2up = \ GrO_2ev$$

$$\therefore rspO_2up = GrO_2up - \ regO_2up$$

$$\therefore rspO_2up \ = GrO_2up - \ GrO_2ev$$

and $rspCO_2ev = NetCO_2up$

Inserting the values from Table 5:

$$rspO_2up = 32 - \ 11 = 21 \ \mu molO_2 .mgChl^{-1}.hr^{-1}$$

$$rspCO_2ev = -21 \ \mu molCO_2 .mgChl^{-1}.hr^{-1}$$

$$regO_2up = \ 11 \ \mu molO_2 .mgChl^{-1}.hr^{-1}$$

Applying Eqn. 3Eqn.

$$(GrO_2ev - \ rspCO_2ev) - (\ fixCO_2up + regO_2up + rspO_2up) \sim 0$$

$$(11 - \ -21) - (0 + 11 + 21) = \ 0 \ \mu molCO_2 .mgChl^{-1}.hr^{-1}$$

Where Eqn. 1 was deemed too simple because it explained less than 95 % of the gas flux data through a mass balance approach at a temperature that has inhibited the majority of

PSII activity, the more complex Eqn. 3 seems to have worked very well under this set of assumptions, explaining 100 % of the flux data.

4.4.3 *Testing scenario two: CO_2 fixation = 100 % PSII activity.*

In the second scenario tested, 100 % of the activity at PSII resulted in electrons being transferred across the thylakoid membrane to generate NADPH and drive the Calvin-Benson-Bassham cycle. As such, 100 % of electrons generated at PSII were assumed to be driving CO_2 uptake, discounting regulatory O_2 consumption: in a similar manner to the 45 µE irradiance discussed in Fig.4-6.

Assuming that:

$$fixCO_2up = GrO_2ev \therefore\ regO_2up = 0\ \mu molO_2.mgChl^{-1}.hr^{-1}$$

$$\therefore rspO_2up = GrO_2up$$

and $rspCO_2ev = NetCO_2up - fixCO_2up$

Using the values from Table 5:

$$rspO_2up = 32\ \mu molO_2.mgChl^{-1}.hr^{-1}$$

$$rspCO_2ev = -21 - 11\ \mu molO_2.mgChl^{-1}.hr^{-1}$$

$$fixCO_2up = 11\ \mu molCO_2.mgChl^{-1}.hr^{-1}$$

Applying Eqn. 3

$$(GrO_2ev - rspCO_2ev) - (fixCO_2up + regO_2up + rspO_2up) \sim 0$$

$$(11 - -21) - (0 + 11 + 21) = 0\ \mu molCO_2.mgChl^{-1}.hr^{-1}$$

Once again, the more comprehensive equation accounts for 100 % of the flux data, indicating that both hypothetical situations are possible after PSII has suffered severe thermal damage.

4.4.4 *Selecting which scenario matches the data*

A choice had to be made as to which of the two scenarios was more valid, as both seemed to explain the data very well. This is where the value of deriving fluxes for each sub-process that made up the measurements determined by the MIMS system can be illustrated (refer to the explanation of Eqn. 3 in 4.3.2 for a reminder). Comparing the two scenarios, it was clear that estimations of $rspO_2up$ in the light were the differentiating factor.

- In the first scenario with no carbon fixation

$$rspO_2up = 21\,\mu molO_2 .mgChl^{-1}.hr^{-1}$$

- In the second scenario, with CO_2 fixation rate = '100%' of PSII activity

$$rspO_2up = 32\,\mu molO_2 .mgChl^{-1}.hr^{-1}$$

Earlier in this chapter the assumptions about respiration in the dark were described with Eqn. 2 that rates of $rspO_2up$ = $rspCO_2ev$.

In Table 5 the dark flux of:

$$rspO_2up = 29\ \mu molO_2 .mgChl^{-1}.hr^{-1}$$

$$rspCO_2ev = 29\,\mu molCO_2 .mgChl^{-1}.hr^{-1}$$

The second scenario seems to fit the measured fluxes for dark respiration more closely than in the first scenario. However, this implies that respiration was functioning at 100 % dark rate during illumination.

4.4.5 *Can dark rates of respiration occur during illumination?*

It is well accepted that cyanobacterial cells share components of the thylakoid membrane for both respiratory and photosynthetic electron transport (Mullineaux, 2014a). However, this is a big question, and one that extends far beyond a simple subsection of a thesis. Debate has surrounded the issue of regulatory mechanisms of respiration between light and dark in phototrophs since at least 1949, when Kok (1949) first described his 'effect', which can be summarised as the photoinhibition of respiration.

To summarise my point of view, and how I approach the issue with respect to the results I have from my experiments: I agree with the conclusion of Schuurmans *et al.* (2014) that the redox state of the PQ pool is under strict homeostatic control. As such, its redox state (or that of components in close proximity to it) is a feedback to multiple systems, such as transition between S-states (Ma *et al.*, 2010). When PSII was inhibited by high temperature, incubations during experiments discussed in 4.2, the PQ pool likely became highly oxidised by the activity of PSI in subsequent periods of illumination. A highly oxidised PQ pool, under strong irradiance with a functional PSI system, would result in a highly oxidised P700.

A high level of oxidation of P700 is presented in Fig 5-5, which correlated to a strong PSI donor side limitation, in Fig 5-2, which suggests a strongly oxidised PQ pool. This strong oxidation could have up-regulated the activity of complexes such as the Succinate

Dehydrogenase (SDH), which is able to reduce a highly oxidised PQ pool (Cooley *et al.*, 2000), in order to maintain the PQ pool in a lower level of oxidation. Other feedbacks, resulting from a general increase in the level of cellular oxidation, could have added pressure for the respiratory systems to upregulate the oxidation of sugars. What happened to the reductant sourced through illuminated respiration must also be considered. Under the conditions tested here, PSI would have a stronger affinity for reductant then terminal respiratory oxidases (Peltier and Sarrey, 1988, Liu *et al.*, 2012, Ermakova *et al.*, 2016). This issue is considered in more detail in the Chapters Five and Six.

The PI curves in Fig.4-6 suggest strongly that there was no little to no respiration occurring at 45 µE in undamaged cells, as the Gross O_2 uptake rate, determined with $^{18}O_2$ ($Gr O_2 up$), was very low to non-existent. There is no evidence that respiration must function in cyanobacteria during light and dark: in fact a mutant of 6803 lacking PSII and all terminal respiratory oxidases has been shown to survive on cycling reductant, sourced exogenously (glucose uptake), around PSI (Howitt *et al.*, 2001). So in that case, respiration can be seen as a system primarily tasked with ensuring cellular energy is available during periods that PSII cannot provide the necessary reductant: such as darkness, or perhaps when the photosystem is damaged.

Lajkó *et al.* (1997) suggested that elevated temperatures (40 minutes at 47 °C) downregulated the input of reductant from PSII, and upregulated that from respiration. However, their work at elevated temperatures to measure Cyt f oxidation in KCN treated cells did not produce an independent measurement, to show PSII itself was not damaged. I suspect the 40 min treatment at 47 °C of their *Synechoccocus* 6301, would have damaged the photosystem directly (based on data from (Inoue *et al.*, 2001)). As such, I believe their results support my interpretation, that reductant sourced from respiration 'replaces' lost PSII activity, as a simple feedback to the loss of reductant entering the thylakoid membrane, and an overall depression of cells redox state.

So, bringing this back to the interpretation of the data discussed in 4.4.4, if the PQ pool's redox state can play a significant and rapid regulatory role in respiration, than the fact PSII was no longer functional suggests that the pool was likely to be in an oxidised state and able accept electrons readily from alternative sources. This includes a potentially elevated cyclic electron flux, and from respiratory complexes such as SDH.

This lends weight to the second of the two hypothetical scenarios tested, because the derived rate of respiration in the light in scenario two:

$$rspO_2up = 32\,\mu molO_2.mgChl^{-1}.hr^{-1}$$

Was much closer to the dark respiration rate measured

$$rspO_2up = 29\ \mu molO_2.mgChl^{-1}.hr^{-1}$$

then the derived rate in scenario one, at only

$$rspO_2up = 21\ \mu molO_2.mgChl^{-1}.hr^{-1}$$

In the following section, more evidence is presented from observation of the raw gas fluxes, to support the conclusion that cells inhibited in PSII function were subject to elevated rates of illuminated respiration, but also that CO_2 fixation was functional at rates limited by the remaining activity of PSII.

4.4.6 *Drawing out nuances in the raw gas flux data*

Although the previous section presented literature evidence supporting the idea that illuminated rates of cellular respiration in thermally damaged cells, suffering severe PSII inhibition, 'could' function at rates measured in the dark: what experimental evidence supports the scenario described in 4.4.3?

The assumption was that CO_2 fixation could still function at 100 % of the rate measured for remaining PSII activity after the 65 °C incubation. This implied there was no energy remaining to drive 'regulatory' O_2 consumption, and therefore 100% of O_2 uptake measured during the light = respiration. This would imply that the rate of net CO_2 fixation, measured by the instrument, would be offset by the respiratory release of CO_2 (ie, the negative rate, implying net CO_2 efflux, should be depressed/be less negative, by the uptake of CO_2). This utilises a similar logic to that used by Yamamoto *et al.* (2016) to demonstrate that transgenically expressed Flv1-3 proteins in *Arabidopsis* were not competing with CO_2 fixation for photosynthetically sourced reductant. What would this look like in the raw data, and was it observed?

During a transition from light to dark, these predicted affects should be visible: if the only driver of O_2 uptake was respiration, occurring at a steady rate between light and dark, then no change should be observed in this flux. If the efflux of CO_2 measured in the light would be reduced by the rate of carbon fixation, then this should increase (become more

negative) when the light turns off. Significantly, this decrease should be equal to the measured rate of Gross oxygen evolution.

A selection of representative examples of the 'raw' data, that generated after conversion of the instrument's raw $mV.s^{-1}$ output to the $\mu mol(gas).mgChl^{-1}.hr^{-1}$ output (the same as that presented in Fig.4-6), used to determine the rates plotted in Fig. 4-5, are presented in Fig. 4-8. These panels cover measurements from 62 °C to 70 °C, including slightly impaired (62 °C) to increasingly severely damaged sample (65 °C to 70 °C). As discussed with reference to Fig.4-6, these plots provide an excellent illustration of the cellular dynamics over time, as the experimental measurements were conducted. A comparison of the data presented in panels labelled 62 °C and 65 °C in Fig. 4-8 strongly supports the predicted observations, discussed above.

Comparing cells at 65 °C (severely impaired in PSII function) to the cells at 62 °C (considered relatively undamaged), fluxes of gas were very similar under low intensity far red light conditions of the $P700_{max}$ measurements. Rates of O_2 uptake in both samples just before the initiation of actinic light at t ~ 60 sec were 18 to 20 $\mu molO_2.mgChl^{-1}.hr^{-1}$. Once the Y(I) max measurements was started in both samples (62 °C and 65 °C), as denoted by the 'red/yellow' stripes at the bottom of the figure (which involved actinic illumination at the steady state irradiance, interspersed with high intensity far red light and saturating actinic light pulses), the difference in activity of the cells became clear. The gas fluxes in the lower temperature cells climb towards a steady state rate of PSII activity, statistically similar to undamaged cells, whilst the 65 °C cells rapidly reached their maximal flux of gross O_2 evolution at ~11 $\mu molO_2.mgChl^{-1}.hr^{-1}$.

Focusing on the fluxes of O_2 and CO_2 across the transition from actinic light to darkness at t ~ 415 sec, in both the 62 °C and 65 °C panel of Fig. 4-8, evidence to support the predictions described above can be observed. Whereas a relatively large decrease in the uptake of O_2 between the light and dark (from ~ 37 to ~20 $\mu molO_2.mgChl^{-1}.hr^{-1}$) was observed in the cells incubated at the 62 °C, the damaged cells changed only marginally, from ~ 32 to ~29 $\mu molO_2.mgChl^{-1}.hr^{-1}$, *matching the values derived for respiratory uptake in the previous section 4.4.3.*.

The very low $Gr O_2 ev$ flux, recorded in the cells at 65 °C, implied the much higher O_2 uptake rate *must* have been driven by respiration (an insufficient level of reductant was generated at PSII to drive this uptake). With such a small change between light and dark in

the uptake of oxygen recorded, further credibility was given to the notion that respiration in the light was functioning at the same rate as in the dark.

Superficially though, the $NetCO_2up$ rate of illuminated cells did not support this, operating at a flux that is nearly 30 % lower than the O_2 consumption rate (when a close to 1:1 ratio can be expected (Fogg, 1973). Recall however, that this outcome would be predicted, if the flux of CO_2 efflux from the cells was reduced (made less negative) by still functional CO_2 fixation. Recall that in this scenario being tested, the fixation of CO_2 was assumed to be operating at 100 % of remaining PSII activity.

Looking at the values for data across the light to dark transition in the 65 °C fluxes of Fig. 4-8:

GrO_2ev Dropped from ~ 11 to ~ 0 $\mu molO_2 .mgChl^{-1}.hr^{-1}$

GrO_2up Remained stable at ~ 30 $\mu molO_2.mgChl^{-1}.hr^{-1}$

$NetCO_2up$ Dropped from ~ -21 to ~- 30. $\mu molCO_2 .mgChl^{-1}.hr^{-1}$

If the flux of CO_2 uptake driven by PSII activity would have reduced any respiratory CO_2 efflux in the light by the rate of CO_2 fixation, ie:

$$NetCO_2up = fixCO_2up - rspCO_2ev$$

Let: $fixCO_2up = GrO_2ev = 11\,\mu molCO_2.mgChl^{-1}.hr^{-1}$

Solving for: $rspCO_2ev = -NetCO_2up + fixCO_2up$

$$\therefore rspCO_2ev = 21 + 11 = 32\,\mu molCO_2.mgChl^{-1}.hr^{-1}$$

This relationship was indeed evident in Fig. 4-8, as the light turned off, the $NetCO_2up$ rate dropped by exactly the amount it should if PSII activity was driving the Calvin Benson cycle.

Two thin red lines have been inserted into the 65 °C panel of Fig. 4-8, denoting the $NetCO_2up$ and GrO_2up rates in the *dark*. These lines are a visual guide, to make a clear comparison between the illuminated and dark fluxes. Whereas the GrO_2up line fits both light and dark curves equally well, the $NetCO_2up$ in the light is clearly less negative (i.e. does not even interfere with the margins of the signal noise) when PSII was functional. This could imply a down regulation of respiratory CO_2 efflux, but that is discounted by the derived

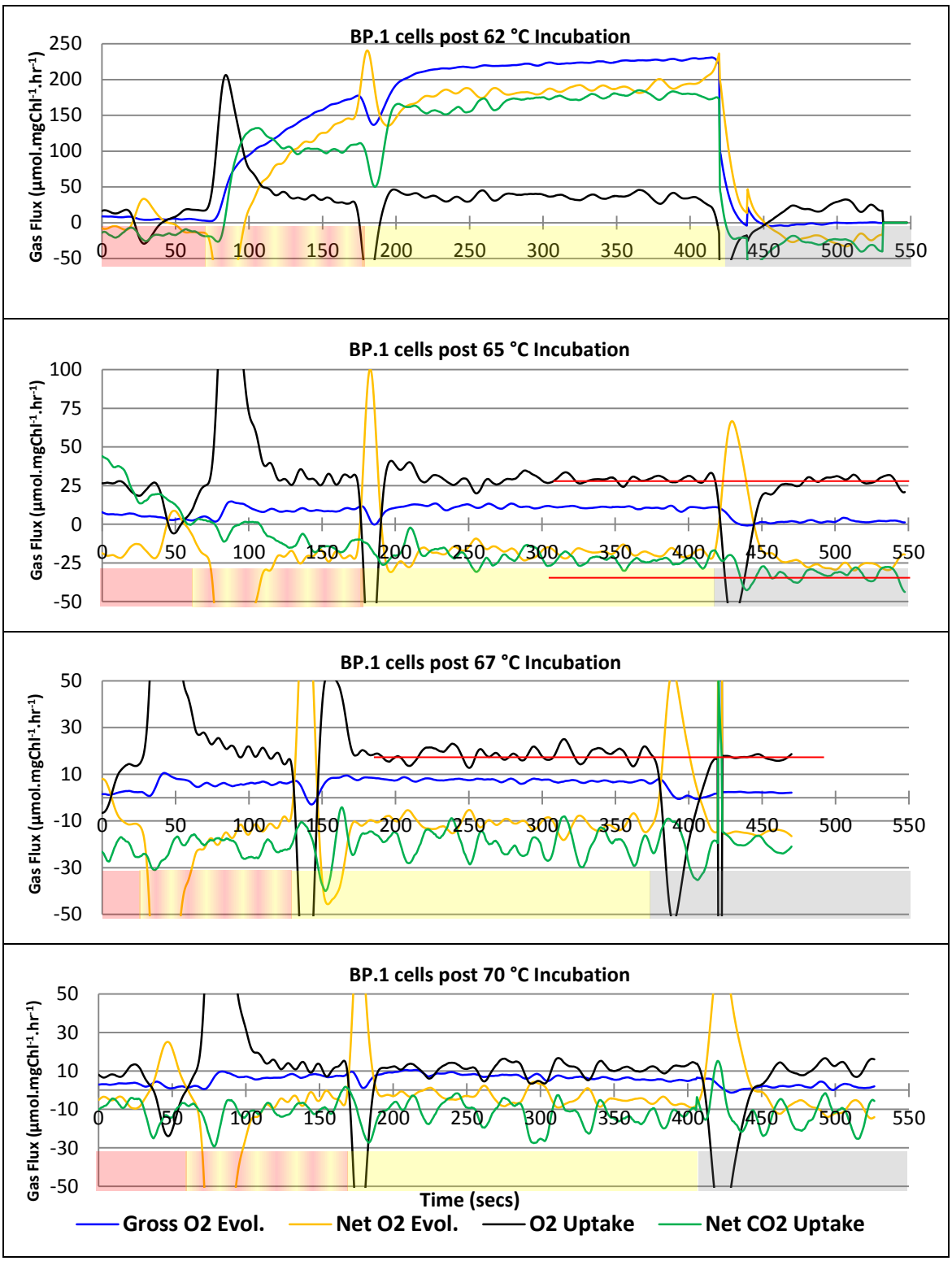

Fig. 4-8: Comparison of gas flux versus time data, used to generate Fig. 4-5 (gas flux vs incubation temperature) illustrating change in fluxes with incubation temperatures at 62 °C, 65 °C, 67 °C and 70 °C.

This is how experiments look once raw values had been converted into real rates and concentrations. From this data it is possible to really observe how cells were responding to light with respect to their gas fluxes. The important point to note is the red line in the 67 °C panel shows between light and dark there is no difference in the O2 uptake rate, consistent with the data in the 65 °C, however in the 65 °C panel the Net CO2 flux is clearly different between light and dark.

Conditions as per summary of Fig. 4-5. Five minute period of darkness not shown preceding $P700_{max}$ measurement not shown. P700 measurements were conducted simultaneously, as such a coloured bar is included beneath the x-axis to show what gas flux correlates with what condition of illumination: red = $P700_{max}$ measurement, yellow/red stripes = Y(I) max measurement. Yellow = actinic light at 500 µE. Grey = Darkness. The thin red line in some panels is there as a visual aid to help see if a flux has dropped or remained steady between the actinic light and dark, as discussed in the text. Data in each panel is a representative sample of experimental measurements.

values for $rspCO_2ev$ – hence CO_2 was possibly being fixed in the light, and therefore the $NetCO_2up$ rate 'seems' less negative. In future this could be examined by the enrichment with a second stable isotope, $^{13}CO_2$, to determine the gross flux of CO_2 uptake and release from cells in addition to O_2 rates (Haupt-Herting and Fock, 2002).

Nonetheless, this result was very strong support for the second scenario tested, in which cells exposed to temperatures that severely damaged PSII were still able to fix CO_2 at rates equal to the remaining PSII activity: as opposed to the first scenario tested, where PSII activity drove the water-water cycle.

4.4.7 *Incubation temperatures > 65 °C: severe damage and signal noise*

As cells suffered increasing levels of damage, and their gas flux rates decreased still further at incubations > 65 °C, assumptions used to undertake the mass balance estimations became invalid. The decrease in signal to noise ratios at 67 °C and 70 °C incubations could have contributed to the fact that the gas fluxes no longer seemed to balance. However, a comparison between the data in 67 °C and 70 °C panels in Fig 7-8, with the data generated by the blank cuvette data, presented in Fig 7-9, illustrated that the presence of cells in the

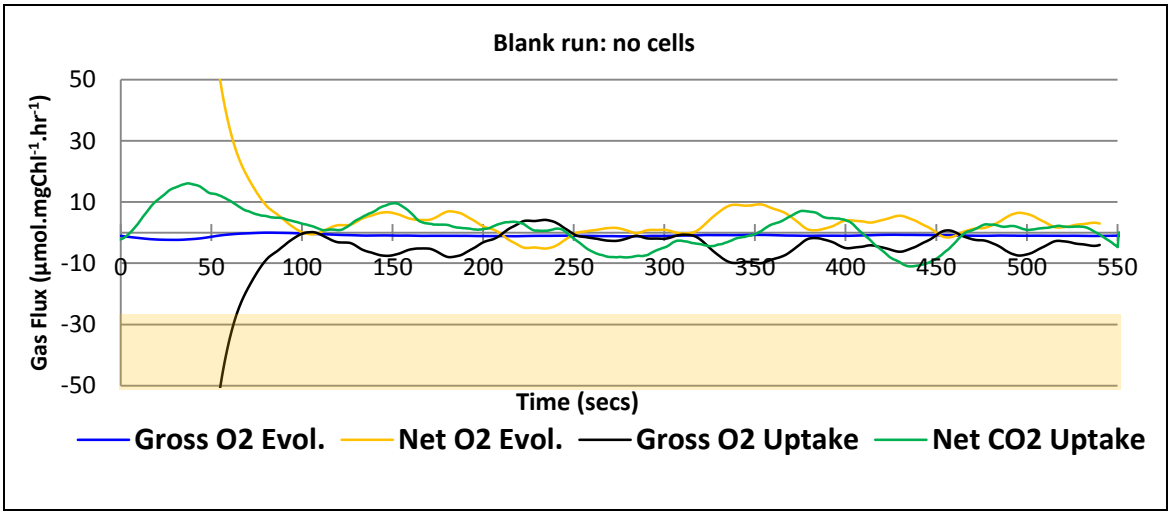

Fig. 4-9: Blank run, an example of data generated each day to validate the 'instrument consumption offset'. This offset is required to compensate for the loss of gsses across the Teflon membrane to be measured by the Mass Spectrometer. The data is generated by setting up the cuvette exactly as for a measurement, however the filter disc does not contain cells. This data was generated using illumination at the actinic measurement irradiance: however an offset was determined for both illuminated and darkened samples, due to light effects on the membrane that became significant when determining very low fluxes from damaged samples. The first 100 seconds shows the stabilisation of gases following injection of the $^{18}O_2$ isotope. Yellow bar denotes 'actinic light on'.

cuvettes significantly influenced the gas fluxes measured.

The blank cuvette data was an example of that generated each day, to ascertain background consumption rates of the instrument across the Teflon membrane. The cuvette was set up as though an experiment was being conducted; including the same volumes of measurement buffer, on the same sized blank filter disc (without cells on it), identical gas injections and levels of irradiance. Each time data was analysed, the background offsets were checked, to ensure the values were coming out at around zero. As can be seen in Fig 7-9, the data for each of the fluxes of interest centred around zero (as expected). The associated noise with each gas flux was not considered random, but consistent across the measurement time shown – which is representative of a standard blank run.

Table 6: gas flux data averaged from cells incubated at 67°C and 70 °C.
All fluxes in units of µmol(gas).mgChl^{-1}.hr^{-1}. Yellow cells = illuminated fluxes. Grey Cells = Dark fluxes

Temp (°C)	GrO_2ev *µmolO_2.mgChl^{-1}.hr^{-1}*	$NetCO_2up$ *µmolCO_2.mgChl^{-1}.hr^{-1}*	GrO_2up *µmolO_2.mgChl^{-1}.hr^{-1}*	GrO_2up *µmolO_2.mgChl^{-1}.hr^{-1}*	$GrCO_2ev$ *µmolCO_2.mgChl^{-1}.hr*
67	7	-18	19	18	16
70	5	-11	8	8	10

Comparing this data to that in the 67 °C and 70 °C panels of Fig 7-8, it was clear that the gas fluxes were significantly influenced by the presence of the cells. These damaged cells were still generating 'real' gas fluxes, in response to the light and dark conditions. Especially clear was that Gross O_2 evolution rates were largely absent of noise, and stepped up as illumination was instigated, before stepping down again the light was extinguished. Although the other fluxes were much noisier, in that blank data centred around zero, there can be confidence that the values around which the signal noise centred were 'true values'.

The values presented in Fig. 4-5 and reported in Table 6, were the result of triplicate measurements, and in Fig. 4-5 the tiny range of the error over the three replicates, and the clear trends in the data, support that there was strong concordance between each run. This result was considered an excellent example of the resolving power of the MIMS approach, especially in the gas phase, where no stirrer was required (which tends to contribute greatly to noise), combined with the higher total number of molecules (compared to the relatively low [gas] in a high temperature liquid sample) being sampled, which significantly reduced the signal noise.

As such, the results of the mass balance estimations performed with this data from severely damaged samples could be considered with confidence. At this point, however, the application of Eqn. 1 failed to describe over 80% of the fluxes, as can be observed in Fig. 4-7. As above, the more comprehensive Eqn. 3 was applied to the data, and a number of hypothetical situations were worked through. However, there was no way to balance the data, assuming that the biochemical assumptions described earlier were still valid, also resulted in a set of outcomes that simply don't balance anymore. Interestingly, the cause of the imbalance was consistent at both 67 °C and 70 °C, where it became impossible to balance the uptake of O_2 with the evolution of CO_2. However, this was only in the light. The strongly overlapping standard deviation associated with the dark gas flux rates in panel B of Fig. 4-5 shows that there was no significant difference between the dark values of net CO_2 and O_2 fluxes at both temperatures, and as such those reported in Table 5 were not statistically different. However, to establish whether the differences between illuminated rates of 'net' CO_2 and O_2 rates were significant or not, a Student's T-test was conducted. The result of a two-tailed T-test at 67 °C was a P-value of 0.015, and at 70 °C 0.013, (n=3), suggesting a significant difference was indeed observed. Therefore, the values of net O_2 evolution and net CO_2 efflux were clearly not balanced in the light. This result set the data at these two incubations apart from all other incubation temperatures, where the net values of these two gases were not seen to be significantly different. It suggested that some physiological processes (within the damaged cells) were not being considered under the highly simplified assumptions used in the gas flux estimations. For example, Havaux (1996) hypothesised an alkalisation of the lumen lead to an increased rate of CO_2 uptake, which was converted to HCO_3^- in leaves, after PSII was severely inhibited by high temperature exposure in samples of potato leaf.

Data generated after cells were incubated at 67 °C makes this point very clear, and as such, analysis of this data set in the following section is used to provide an example of how and perhaps why, the masses no longer cancelled each other out. The approach taken was very similar to cells incubated at 65 °C, in that two hypothetical scenarios were tested. In scenario-one it was assumed once again that there was no CO_2 fixation occurring. In scenario-two, the assumption was again that CO_2 fixation functioned at the rate of PSII activity. All values used in this analysis were drawn from those presented in Table 5.

4.4.8 *Testing the two scenarios with mass balance estimations in highly damaged cells*

Testing scenario-one: the assumption that cellular damage had inhibited CO_2 fixation ($fixCO_2up$), as a result none of the energy entering the thylakoid membrane from remaining PSII activity could be used to drive carbon fixation, requiring that 100 % of this flux be consumed through $regO_2up$. As such:

$$fixCO_2up = 0$$

$$\therefore\ regO_2up = GrO_2ev$$

$$\therefore rspO_2up = GrO_2up - regO_2up$$

$$\therefore rspO_2up = GrO_2up - GrO_2ev$$

and $rspCO_2ev = NetCO_2up$

Using the values from Table 6:

$$regO_2up = 7\ \mu molO_2.mgChl^{-1}.hr^{-1}$$

$$rspO_2up = 19 - 7 = 12\ \mu molO_2.mgChl^{-1}.hr^{-1}$$

$$rspCO_2ev = -18\ \mu molCO_2.mgChl^{-1}.hr^{-1}$$

Applying Eqn. 3

$$(GrO_2ev - rspCO_2ev) - (fixCO_2up + regO_2up + rspO_2up) \sim 0$$

$$(7 - -18) - (0 + 7 + 12) = 6\ \mu mol(gas).mgChl^{-1}.hr^{-1}$$

Applying Eqn. 5 to test the 'accuracy' of the assumptions and the estimation:

$$\frac{((\mathrm{Gr}O_2ev - rspCO_2ev) - (fixCO_2up + regO_2up + rspO_2up))}{GrO_2ev - rspCO_2ev} \times 100$$

$$\frac{((7 - -18) - (0 + 7 + 12))}{7 - 18} \times 100 = 24\ \%$$

The result that 24 % of data remained unaccounted for implied that the assumptions used were not supported by the analysis. Looking simply at the derived values for respiratory fluxes of O_2 and CO_2 provides evidence that even the basic assumption:

$$rspCO_2ev = -1 \times rspO_2up$$

was not supported, as the derived values from scenario one, just tested was that:

$$rspCO_2ev = -18\ \mu molCO_2.mgChl^{-1}.hr^{-1} \neq -12\ \mu molO_2.mgChl^{-1}.hr^{-1} = rspO_2up \times -1$$

A quick check of how far proportionally the mass difference is out shows that:

$$\frac{\Delta respiratory\ fluxes}{larger\ of\ the\ two\ fluxes} \times 100 = \frac{-18--12}{-18} \times 100 = 33\ \%$$

$$\therefore \textit{The key assumptions have broken down completely in scenario one.}$$

Unfortunately the same was true when the second set of assumptions used to define scenario two was tested, whereby the CO_2 fixation rate = O_2 evolution rate, assuming the thylakoid membrane and Calvin Benson Bassham cycle was still functioning well:

$$fixCO_2up = GrO_2ev$$

$$\therefore\ regO_2up = 0$$

$$\therefore rspO_2up = GrO_2up$$

$$rspCO_2ev = NetCO_2up - fixCO_2up$$

$$\therefore rspCO_2ev = NetCO_2up - GrO_2ev$$

Again, using the values from Table 6:

$$fixCO_2up = 7\ \mu molCO_2.mgChl^{-1}.hr^{-1}$$

$$rspO_2up = 19\ \mu molO_2.mgChl^{-1}.hr^{-1}$$

$$rspCO_2ev = -18 - 7 = -25\ \mu molCO_2.mgChl^{-1}.hr^{-1}$$

Applying Eqn. 3Eqn.

$$(GrO_2ev - rspCO_2ev) - (fixCO_2up + regO_2up + rspO_2up) \sim 0$$

$$(7 - -25) - (7 + 0 + 19) = 6\ \mu mol(gas).mgChl^{-1}.hr^{-1}$$

Finally applying Eqn. 5 to test the 'accuracy' of these assumptions:

$$\frac{((\mathrm{Gr}O_2ev - rspCO_2ev) - (fixCO_2up + regO_2up + rspO_2up))}{GrO_2ev - rspCO_2ev} \times 100$$

$$\frac{((7 - -25) - (7 + 0 + 19))}{7 - 18} \times 100 = 24\ \%$$

Once again the final result was out by 24 % and the same values fail to balance:

$$rspCO_2ev = -25\ \mu molCO_2.mgChl^{-1}.hr^{-1} \neq -19\ \mu molO_2.mgChl^{-1}.hr^{-1} = rspO_2up \times -1$$

4.4.9 *Selecting and interpreting the more probable scenario*

A significant difference between the outcomes of scenarios one and two, tested above, was the that by assuming the rate of $fixCO_2up = GrO_2ev$, the total flux derived for

$rspCO_2ev$ became much larger than the unambiguous dark measurements of respiration, in Table 6. This sort of outcome is why the mass balance estimation was a useful framework for analysis. In the dark, significantly, the CO_2 and O_2 fluxes were very close to parity. When compared with their error in panel B of Fig. 4-5, they can be considered equal. According to the mass balance estimations performed at 65 °C in section 4.4.5, the rates of dark respiration seemed to equal the rate of illuminated respiration. There is no evidence, or reason to suggest that the illuminated respiration rate would be higher than in the dark. As such, the results lean towards scenario-one, where CO_2 fixation has been inhibited.

However in scenario one, there was a clear imbalance remaining in the gas fluxes, with 33% more CO_2 being released than the derived value for $rspO_2up$ could account for. This result can be observed directly, where the Net O_2 fluxes became less negative then the CO_2 rates in Panel A of Fig. 4-5 at 67 °C and 70 °C.

One possibility to explain this result was that oxygen was in competition as a terminal acceptor during illumination, and under the very low fluxes generated by the damaged cells, this alternative pathway became significant. There is evidence that the cyt-b_6f complex competes with the activities of respiratory terminal oxidases within the thylakoid membrane, particularly under heat stress in cyanobacteria, algae and plants (Lajkó *et al.*, 1997). There is also evidence that $P700^+$ will be preferentially reduced over respiratory terminal oxidases (Bukhov *et al.*, 2002), and that this outcome is promoted by the physical movement of key respiratory complexes within the membrane (Liu *et al.*, 2012). In other words: electrons available from the PQ pool will preferentially drive photochemistry, when PSI is oxidised, compared to reducing O_2 to H_2O.

There are a number of possible electron sources available to reduce the PQ pool. Combined evidence in this thesis, and from the literature, suggests they are still likely to be functional after the 67 °C incubation. There was the small, but clear remainder of PSII activity (observe the 67 °C panel of Fig. 4-8, Gross O_2 evolution is very clear, just a tiny fraction of maximal rates however).There was likely to be the oxidation of succinate, and generation of fumarate by the SDH complex, which directly reduces the PQ pool through an NADH type intermediate step (Vermaas, 2001) and in cyanobacteria there is the NDH-$1_{1,2}$ complex, able to utilise reduced Fd from either PSI, or possibly via the oxidation of NADPH through FNR_s (Peltier *et al.*, 2016).

Data in Chapter Five supports that respiration was still able to re-reduce $P700^+$ after the 67 °C incubation, supporting the function of at least one of these 'respiratory' pathways. In the literature, data of Cyt C_6 and P700 photooxidation in cells suggested that both reached maximal functionality at around 67 °C (Koike *et al.*, 1982), whilst the $K_{0.5}$ of inactivation for FNR_L and Fd was about 76 °C, based on *in vitro* measurements of isolated components prepared from BP.1 cells (Koike and Katoh, 1979, Koike and Katoh, 1980). As such, sufficient evidence exists to reasonably claim that the majority of electron transport pathways to reduce PQ would still have had at least some functionality after a 67 °C incubation.

As mentioned, the data in Chapter Five (specifically that presented in Fig 5-5, discussed in section 5.1.3 and generated simultaneously with this gas flux data), clearly showed that P700 was still functional at 67 °C. When oxidised, it was most likely reduced with reductant sourced via the PQ pool, and as just described, there were a number of possible sources available for these electrons. As PSI function reduces Fd directly, and this carrier can be used to drive many enzymes, there were multiple possible routes for the reductant to take, once it has reduced $P700^+$. These do not necessarily end in the reduction of O_2, which would upset the balancing of electrons based on gas flux data.

One of these routes is back to the PQ pool as stated, via activity of the NDH-$1_{1,2}$ complex, the primary route for cyclic flux around PSI in cyanobacteria (Xu *et al.*, 2016). Another route could be to a terminal oxidase, such the Flv1,3 complex, although the mass balance does not support this. The most common pathway, under optimal conditions, is the reduction of $NADP^+$ at the FNR_L. Although this pathway is a primary component of standard linear electron transport to CO_2 fixation in undamaged cells, the NADPH generated in the damaged cells lacking CO_2 fixation would be highly sought after by the mechanisms re-building thermally damaged cellular components (Spaans *et al.*, 2015). Should the strong reductant be used in some sort of anabolic process, like protein repair, there seems to be no need for the electron to find O_2 as a terminal acceptor.

In fact, such an outcome could be considered an energetically wasteful one. With functional PSI, there is no need to drive electrons to O_2 to generate a proton gradient and ATP. Cells could simply drive electrons around PSI, keeping the system poised with reductant from respiration (this concept becomes a hypothesis tested in Chapter Six). As such, the idea that respiratory O_2 uptake was in competition with $P700^+$ seems justifiable. After incubations

at 67 °C, the apparent respiratory quotient in the light dropped from the expected 1.0 (Fogg, 1973), down to 0.7. However, it returned to 1.0 in the dark. It could be simply concluded that the remaining activity of PSII drove this linear pathway through to NADPH, which was then used in cellular anabolism. However, with PQ's role as an intermediate step in such an array of pathways (Hirano *et al.*, 1980), it cannot be ruled out that reductant from respiratory products, such as SDH activity, was also involved.

To conclude therefore: The mass balance estimation was able to reject the idea that CO_2 fixation was still functional at rates anywhere close to remaining PSII function, as this resulted in a derived rate for respiratory CO_2 efflux that far exceeded that measured in the dark. Assuming instead that the remainder of PSII function was driven to a terminal oxidase for regulatory O_2 uptake drove the balance for the respiratory quotient of CO_2 and O_2 in the light out from 1.0, to 0.7. It didn't matter how the assumptions were tested, when the light was on, a competition for reductant between O_2 and an alternative was observed. What the implications of this conclusion may have for cells suffering PSII inhibition more broadly, will be elaborated upon in the following sections.

4.4.10 *Conclusions of the gas fluxes due to transient heat stress*

Based on analysis of the data presented in Fig. 4-5, cells incubated in darkness for ten minutes at temperatures up to 60 °C did not suffer significant levels of damage to primary photosynthetic components. At temperatures between 62 °C and 65 °C, over 95 % of PSII activity (as defined by the Gross O_2 evolution rate, Fig 4-5) was inhibited, compared to the undamaged samples.

Once cells suffered this damage, evidence from gas flux data (specifically panel B of Fig. 4-5) indicated that dark rates of respiration functioned at significantly higher levels than undamaged cells (all measured at the optimum 55 °C). Furthermore, the elevated rates of respiration were maintained in both the light and dark. Primary evidence for this was found after 65 °C incubations in Fig. 4-5. Net CO_2 became negative (implying evolution of the gas) and rates of Gross O_2 uptake became greater than the activity of PSII in the light. Furthermore, the rate of O_2 uptake did not change in the dark (see the red line inserted into the 65 °C panel of Fig. 4-8, raw flux data for Gross O_2 consumption).

The rates derived for respiratory CO_2 efflux in the light through the mass balance estimation in 4.4.4 equalled the Gross O_2 uptake, with the difference found to be equal to

the rate of PSII activity. For this to work out,, there had to be zero 'regulatory' O_2 uptake. Data in Fig.4-6 at 45 µE irradiance provided evidence that regulatory O_2 uptake was insignificant when the activity of PSII was low enough to be safely utilised by the cells without the need to divert reductant to O_2. As such, the low rates of PSII activity after damaging thermal incubations likely resulted in a similar outcome, especially considering the relatively higher rate of PSI activity that would have been occurring at the 500 µE measurement irradiance.

Finally, the idea that PSII activity was still driving CO_2 fixation could be shown with the raw data in the 65 °C panel of Fig. 4-8. In that panel, a second 'red line' was fitted manually through the data for dark rates of CO_2 uptake (negative values, as it was an efflux). With this it could be observed directly that the illuminated rate of net CO_2 uptake was less negative, as the red line did not even enter into the area of the data considered 'noise' during illumination. The change in the CO_2 efflux rate between light and dark was exactly equal to the expected amount, for rates of respiration occurring in the light being underestimated by CO_2 fixation at rates equal to PSII activity. This was strong support for the assumptions made in the second set of mass balance estimations.

At incubation temperatures ≥ 67 °C, however, evidence suggested that assumptions relating to electron sources and sinks within cells, on which mass balance estimations were based, failed. Using data from 67 °C incubations presented in Table 6 for mass balance estimations showed that the dark data was still sensible, and estimations seemed unaffected. However, during illumination the rate of CO_2 efflux still matched the dark flux, but O_2 uptake became a problem to balance. It was clear from the raw data in the 67 °C panel of Fig. 4-8, that the red line fitted to dark O_2 uptake also equalled illuminated O_2 uptake. However, there was a small flux of O_2 still being generated by PSII. This upset the mass balance equation and provided evidence that the electron transport components were possibly in competition with O_2 as a terminal acceptor during illumination, as discussed by authors such as Lajkó *et al.,*(1997) and Liu (2016).

It was suggested that $NADP^+$ acted as a 'terminal acceptor', in so far as the re-oxidation of P700*. As part of this, it was suggested that if this strong reductant was used for anabolic processes (besides CO_2 fixation, which was deemed inactive), such as protein synthesis, then there was no need specifically for that electron's terminal acceptor to be O_2. As some of the reductant entering the PQ pool was likely sourced through respiration, this

may have implications for how the cells can utilise respiratory sourced reductant to supplement lost PSII function (discussed above in 4.4.9, and further in chapter Five, where P700 data is used to support this idea, and in the conclusion section 7.5 where further explanation is provided).

The clearest outcome from the analysis of gas fluxes after thermal incubations is that, as is well established in plants and mesophilic cyanobacteria, the respiratory pathways of *Thermosynechococcus elongatus* BP.1 were found to be more thermally tolerant than PSII. This is a major conclusion from the work presented in Chapter Four, as evidenced by the gas flux data presented in Fig. 4-5, that shows dark rates of O_2 consumption and CO_2 efflux (respiration) were not inhibited by temperatures that significantly inhibited the generation of O_2 in the light. It also seems that the thylakoid membrane, and its associated protein complexes, were still capable of functioning after PSII was significantly inhibited. This result supports some of the work conducted *in vitro* by authors like Koike and Katoh (1979) and Sonoike *et al.* (1990).

However, using the gas flux data alone, it was not possible to determine if PSI played any significant role in helping the cells manage high temperature stress once PSII was inhibited. This was partly because it was not possible to differentiate between respiration occurring along the thylakoid or plasma membranes (Mullineaux, 2014a) with the gas flux data. In the following Chapter, P700 data acquired simultaneously with the gas flux data examined here, are analysed and discussed. Through the combination of these two data sets, especially the data and analysis in section 5.5, strong support is given to the notion that $P700^+$ could be re-reduced by respiratory based electrons, implying a proportion of respiration took place along the thylakoid membrane, and PSI still played a role in PSII damaged cells.

4.5 Final summary and conclusions of Chapter Four

In this Chapter two hypotheses were set out to be answered. The first, that cellular systems downstream of PSII in the moderate thermophile BP.1, such as PSI, carbon fixation and respiration, possess equal or greater thermal tolerance than PSII.

Analysis of data generated through assaying cells at the temperature of interest, presented in Fig. 4-2, suggested that O_2 uptake rates were more stable than O_2 evolution rates. This indicated the stability of respiration was greater: however, also raised the prospect

that respiration was functional during illumination. It was clear however that dark rates of O_2 uptake were more stable than PSII function: hence the hypothesis gained its first support.

This was further confirmed through mass balance estimations of the data generated post incubations, discussed in 4.4.4.Evidence supported the idea that both CO_2 fixation and respiration were functional after greater than 95 % of PSII function had been inhibited by a 10 minute incubation at 65 °C.

The second hypothesis being tested was that PSI played an active role in cells once PSII was severely inhibited. This could not be answered fully with the gas flux data alone, and a more thorough comparison of combined gas flux and P700 data in the following chapter will show that this hypothesis is supported. However, what could be gleaned from the gas fluxes alone was that respiration became highly functional in the light, and literature was used to support that idea that the PQ pool is shared by both PSI and various respiratory steps. As such, the gas fluxes provided a foundation for supporting this idea.

Furthermore, the mass balance estimation suggested that a decrease in the respiratory quotient from 1.0 in the dark, to 0.7 in the light, may imply that oxygen was in competition as a terminal acceptor once cells were severely damaged by a 67 °C incubation. This idea is elaborated upon further in Chapter Five, and in the final discussion in section 7.5. If correct, this provides further support for the idea of an active role for PSI once PSII has been severely, and preferentially damaged, by an environmental stress like temperature.

Chapter 5.

PSI's potential support role in cellular respiration

Once PSII is severely inhibited by high temperatures

Chapter summary:

In the previous Chapter, a gas flux analysis of BP.1 cells exposed to a range of transient high temperature stresses found the cells lose >95 % of PSII activity at an incubation temperature of 65 °C. At this temperature however, rates of dark respiration were not only found to function at levels higher than undamaged cells, but this was not suppressed in the light. In addition, CO_2 fixation continued to function. These findings provide strong evidence for the initial hypothesis posed in this thesis; that respiration, and the primary functions of the thylakoid membrane downstream of PSII, possesses a higher thermal tolerance than the primary source of reductant in cells of the moderate thermophile BP.1.

In this Chapter the hypothesis is extended: that a component of aerobic respiration not only occurred along the thylakoid membrane, but was capable of supplementing some reductant otherwise provided by PSII. It thus proposes an 'active role' for PSI in respiration of BP.1 cells that have lost PSII activity through thermal stress/damage.

To explore the hypothesis, P700 data generated simultaneously with the measurements of gas fluxes from Chapter 4 were analysed in a number of ways. Initially the photochemical yield and variable levels of donor and acceptor side limitation, experienced by the P700 photosystem, were considered with respect to gas flux data. This provided evidence that after PSII was thermally inhibited, PSI still functioned at higher rates than PSII alone could support. An examination of the raw P700 measurements were then conducted to provide further evidence that electrons, likely sourced from the oxidation of sugars, were indeed reducing $P700^+$.

The results were consistent with the hypothesis, and suggest that PSI is able to re-energise reductant sourced through the oxidation of sugars. This could generate high energy protons for use in anabolic cellular metabolism. It further implies a possible pathway in which cells could re-cycle electrons around PSI, as respiratory electrons poise the redox balance: explored in the following, Chapter Six.

5.1 The response of PSI to transient thermal damage

As discussed in the introduction of Chapter 1, PSI is considered a thermally robust protein complex. This is especially true when compared to the thermal stability of PSII in most probably all oxygenic phototrophs (although, this is unknown, would be very interesting to measure in the extreme thermophiles of Yellowstone National Park, seemingly unable to evolve greater thermal tolerance). Cellular components isolated from cells of the moderately thermophillic cyanobacterial strain *Thermosynechococcus elongatus* BP.1 (BP.1) have been thermally incubated and biochemically assayed for activity ((Koike and Katoh, 1979, Koike and Katoh, 1980, Hirano *et al.*, 1981). It was observed that some components, such as cytochrome C_{550} exhibited barely measurable changes after 5 mins of boiling (Koike and Katoh, 1979). However, this does not imply that the protein complex, the electron transport system with which it functions or the broader cellular environment can withstand such extreme temperatures.

In the introduction to this thesis, an estimation was made that the maximal fully functional temperature that can be managed by the PSI and its redox partners is around 70 °C. This was based on Hirano *et al's.*, (1981) finding from *in vitro* measurements that cytochrome C_6 oxidation was still observed at 72 °C, but methyl viologen photoreduction rapidly ceased at around this incubation temperature. This *in vitro* data provides evidence to support the hypothesis that PSI maintains functionality at temperatures that inhibit PSII. It suggests further that PSI would be able to utilise electrons released through respiratory reduction of the PQ pool, once PSII has been inhibited.

In this Chapter, the P700 measurements conducted simultaneously during gas flux measurements of cells incubated at a range of damaging temperatures, (described in the previous chapter), are analysed in order to examine the redox activity of PSI *in vivo*. No whole cell measurements of PSI activity in BP.1 subjected to high temperature stress have been published. Furthermore, the response of PSI to thermal stress, in the context of being a component within the broader cellular system, has not been investigated in this organism.

The primary aims of the P700 analysis were therefore:

- to observe the function of PSI after standardised thermal incubations, *in vivo*

- to investigate the thylakoid membrane's functionality, via PSI redox activity, to provide evidence that cellular respiration within BP.1 can utilise thylakoid components after PSII has been inhibited by thermal damage
- to find evidence in support of the idea that PSI may still play a significant functional role in cells suffering severe thermal inactivation of PSII

As PSII is the primary electron donor to PSI under optimal conditions, it could be easily and justifiably assumed that increasing incubation temperatures which result in decreased PSII activity, would lead to a highly correlated decrease in PSI function. This was found to be the case for rates of CO_2 fixation in Chapter 4. Although *in vitro* assays of Rubisco itself (Fig. 4-5) provided evidence of its functionality at relatively high rates, even after incubations that inhibited PSII, the measured rate of CO_2 fixation by whole cells was correlated very strongly to the activity of PSII as determined by Gross O_2 evolution rates.

The primary question being answered in this Chapter can therefore be rephrased to: what does the activity of PSI look like in comparison to the activity of PSII after thermally damaging incubations, and what drives this? Answering this question can provide the information necessary to achieve the aims stated above. Therefore, two broad outcomes being tested, with respect to the answer of this question are:

1- *If the P700 data correlates very strongly with the activity of PSII, as determined through the Gross O_2 evolution proxy of PSII activity, it can be concluded that PSI does not play any significant role in helping cells to cope with damage to the PSII complex, and is simply subject to PSII's level of activity - just as CO_2 fixation was.*
2- *If on the other hand, the values for $\boldsymbol{Y(I)}$ (photochemical yield of PSI) do not trend PSII activity (i.e. activity is still measured in PSI after the severe inhibition of PSII activity) the data would be consistent with the idea that PSI plays a physiological role in cells with damaged PSII.*

The results presented, analysed and discussed in this Chapter are consistent with the second of these outcomes. That is, at incubation temperatures ~65°C to 70 °C, the following conclusions could be drawn from P700 data in Fig. 5-2, normalised to maximal values and compared to the activity of PSII and respiration in Fig. 5-3:

- The donor side limitation ($\boldsymbol{Y(ND)}$) of PSI was driven entirely by a loss of PSII function

- The photochemical yield of PSI ($Y(I)$) became uncoupled from PSII function as PSII was inhibited and
- The probable source of reductant to reduce $P700^+$, once PSII has been severely damaged, is respiration which was still functioning very strongly
    - This final point is supported specifically with data in Fig. 5-5 and Fig. 5-6

5.2 Monitoring the activity of PSI post thermal incubations

Gas flux data in the previous Chapter provided strong evidence that exposure to elevated temperatures inhibited the function of PSII and invoked a large rate of illuminated respiration in the cells of BP.1. Simultaneously, what little reductant still entering the thylakoid membrane from those PSII centres still capable of generating oxygen seemed able to drive the Calvin-Benson-Bassham cycle to fix CO_2.

These measurements and their analysis provided strong support for the first key hypothesis proposed in this thesis; that respiration has a higher thermal tolerance in this cyanobacterial species then the activity of PSII. However, gas fluxes alone were insufficient to provide evidence for the possible involvement of PSI in the response to high temperature damage of PSII, the second key hypothesis of this thesis. In this Chapter, P700 data acquired simultaneously during measurements of the gas fluxes discussed in Chapter Four are analysed to provide supporting evidence for claims already made with respect to the activity of PSII versus temperature, and to further elucidate the response of BP.1 cells to damaging temperatures. The P700 measurement itself is a non-destructive spectroscopic method able to determine the relative concentration of the oxidised form of the reaction centre chlorophyll of PSI, termed $P700^+$. Where the ground state of the P700 chlorophyll does not absorb light at 830 nm, the cationic species does. The change in absorption of an 830 nm measurement beam can be correlated back to the relative proportions of oxidised versus reduced P700 centres in a given sample, for a given set of conditions.

To correct for the fact that there may be some absorption by other redox active species such as plastocyanin at 830nm (although the BP.1 strain does not utilise this soluble redox carrier), P700 is measured in the dual-wavelength mode (where the difference in intensities of 875 nm and 830 nm pulse-modulated measurement beams, reaching the photodetector are reported).

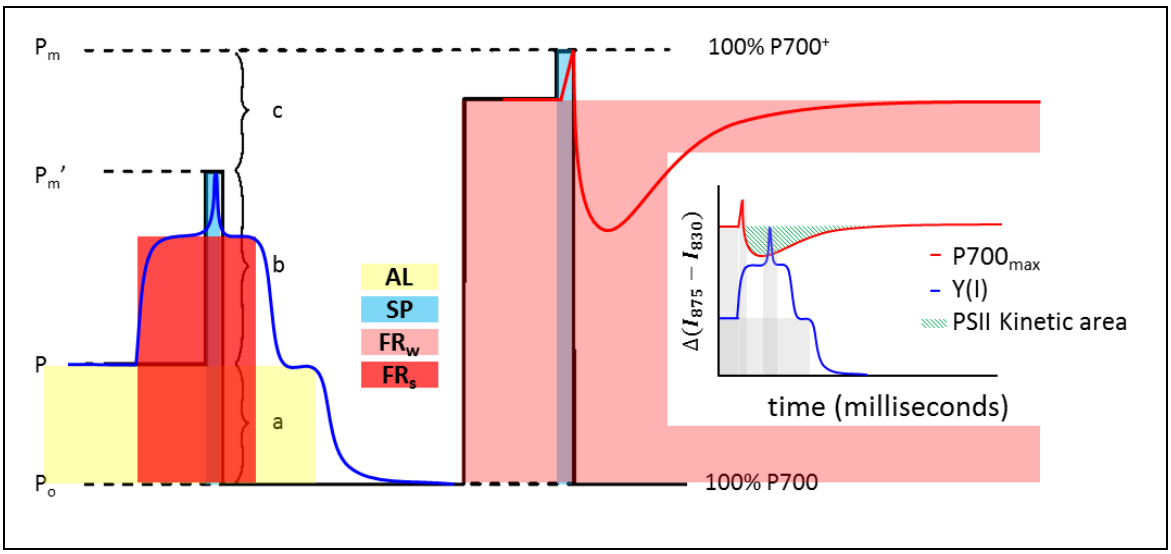

Fig. 5-1: Schematic ilustration of the P700 measurement protocol.
This figure of the Saturation Pulse method for determining the efficiency, or yield, of energy conversion in PSI is modified directly from the original publication on these measurements by Klughammer and Schreiber (2008). Relative P700 oxidation is measured with a Walz PAM 101 in the dual-wavelength mode, by measuring the difference of intensities at 875 nm and 830 nm, in measuring light reaching the photodetector. P700 oxidation was considered positive signal change (ie, the greater the proportion of $P700^+$, the higher the signal, 1.0 = 100% = Pm). To determine $\mathbf{P_m}$, the complete P700 oxidation in the sample (presented on the right hand side of the figure with red curve), samples were illuminated in weak FR light (FR_w) to preferentially drive PSI photochemistry. A Saturating Pulse (SP - blue component of the figure) was triggered over this FR_w background, driving the final component of unoxidised P700 centres to be fully oxidised. This represented the maximal P700 signal, or **Pm**. This measurement protocol was termed the "$P700_{max}$ " measurement. The FR_w was kept on and as such, electrons from PSII resulting from the SP were rapidly re-oxidised at P700, resulting in the trough observed in the figure following the blue SP component
To determine the proportion of centres closing during actinic illumination, and the dark value for full reduction, the second measurement termed $Y(I)$ was conducted (shown in the blue curve on the left). In the presence of Actinic Light (Yellow, AL) a fraction of donor-side limited, closed centres $P700^+$ (fraction **a**), was oxidized. This resulted in an intermediate P700 signal, denoted by **P**. A strong FR light (FR_s) was then applied to maximise oxidation of the active fraction of P700 centres, before a further SP ensured complete oxidation of any remaining fraction (fraction **b**) (open centres P700), with this maximal P700 signal achieved during actinic illumination denoted by **Pm'**. The remaining fraction (fraction **c**) (acceptor-side limited closed centres $P700^+$) that could not be oxidized, corresponded to the difference between **Pm** and **Pm'**. All light was then extinguished and the $P700^+$ was rapidly fully reduced by the intersystem electrons, leading to the value **P** (the fully reduced value). The inset figure provides an approximation of the signals generated under ideal/non damaged conditions, with a time scale of 1000 milliseconds total. Note that within this inset, a green shaded area is depicted. The integrated area of this component is denoted as the PSII Kinetic area Jia *et al.* (2014) and is driven by intersystem electrons re-reducing $P700^+$ after the SP.

As such the raw data is often reported as $\Delta(I_{875-I\,830})$. These relative signals were balanced to zero before each measurement in the dark. P700 oxidation was characterized by a positive signal change (Klughammer and Schreiber, 2008). Fig. 5-1 presents an illustrated description of the P700 measurement methodology used to monitor the relative redox states of PSI during steady state conditions.

The description of how P700 terms were defined and measured in Fig. 5-1 are based on the literature. In this thesis; however, some significant deviations were made to the standard approach for determining the P_m and P_o terms at temperatures that severely inhibited PSII function. The specific reasons for these changes are discussed and justified in section 5.5.3 and 5.5.4 below, and only applied to samples at incubation temperatures 65 °C to 75 °C.

5.2.1 *Determining the maximum level of oxidisable P700 (P_m)*

Whilst illuminating the sample in constant but weak far red (FR) light (723 nm at 12 μmol.m^{-2}. s^{-1}), PSI was preferentially stimulated compared to PSII and as a result became highly oxidised. This condition tends to oxidise approximately 85 % to 90 % (Hu *et al.*, 2013) (also see the data points at 50 °C and 55 °C of the upper panel in Fig 5-6) of the P700 in a sample, over which a saturating single turnover pulse of actinic light (high intensity xenon flash lamp) was applied to fully close the remaining PSI centres. In Fig. 5-1 this is demonstrated on the right hand side: the red trace illustrates an example of the data, determined by a relative change in reflected light at 830 nm recorded over time (1000 ms total measurement time). The higher value recorded equates to a higher absorbance of the measurement light by the sample, thus a higher concentration of the oxidised P700$^+$ in the sample. The maximal value, or peak, occurring when both the weak far red light and actinic pulse were combined (as illustrated with a light red coloured box overlayed with skinny light blue rectangle), is considered the maximum level of P700$^+$ in the sample and is assumed to be the full oxidation of P700 (or closing of 100 % of PSI centres). This peak is defined in the literature (Klughammer and Schreiber, 2008) as:

P_m = maximum level of P700$^+$

In this thesis the protocol used to generate P_m is referred to as the $P700_{max}$ measurement. During the gas flux measurements the $P700_{max}$ was acquired after the five minute period of incubation at 55 °C in darkness, preceding actinic illumination measurements. This can be observed in Fig 4-8, by the red coloured portion of the 'irradiance bar' placed under each panel of gas fluxes versus time. Significantly, at incubations > 65 °C, assumptions on which this measurement was based, fell apart. Analysis of the data suggested that the weak FR light was unable to sufficiently oxidise the high flux of electrons sourced, most probably, from the oxidation of sugars. This made up a component of the data considered to be consistent with the idea that chlororespiration seemed able to reduce P700$^+$, in the absence of PSII function (see section 5.5.4).

This extra electron flux required that the strength of the baseline FR light should have been increased. As PSII was inhibited anyway, increasing this irradiance would not have jeopardised the basic assumptions of the measurement, and could have avoided the problems identified later in this Chapter. These stemmed from the fact that the baseline

oxidation state in weak FR light was too low to reach full P700 oxidation during the saturating pulse. Unfortunately this was not realised/appreciated during the experiments. As such, the data analysis takes the lack of full P700 oxidation into account in another way. Although this is discussed below in section 5.5.4, to summarise the main point: the P_m value was no longer determined through the $P700_{max}$ saturating pulse method at elevated temperatures ≥ 65°C. Instead, it was taken to equal P_m'as determined through the $Y(I)$ measurement (refer to the left hand side of Fig. 5-1). This is because the activity of PSII was severely inhibited, and as such it is probable that the oxidation of P700 was likely maximal even under actinic light conditions – especially with the addition of the strong FR light before the saturating pulse.

5.2.2 *The Yield of PSI and its Donor & Acceptor side Limitations*

Following the $P700_{max}$ measurement to determine a sample's P_m, a second measurement was conducted to determine the parameters required for calculating the photochemical yield of PSI, and its complimentary quantum yields of donor and acceptor side limitations. In this thesis this is referred to as the $Y(I)$ measurement, and it was undertaken according to the method of Kou *et al.*, (2013) to maintain the sample in a steady state of actinic illumination. To summarise the overall measurement, as illustrated on the left hand side of Fig. 5-1, or clearly visible in the black trace of the 60 °C panel of Fig. 5-5, this measurement relied on a sequence of light pulses.

After 9700 mS of actinic illumination of the sample, the Walz PAM detector and computer acquisition software were activated (at t= -50 s in Fig. 5-5) by a BNC (Berkeley Nucleonics Corporation) pulse/delay generator. In actinic light the level of P700 oxidation is a balance between the formation of $P700^+$ through PSI turnover, and the re-reduction of $P700^+$ by electrons generated at PSII (and of course, any other alternative electron source including cyclic electron transport and possibly respiratory electrons). It is not difficult to imagine that if PSII lost function, through causes such as thermal damage or chemical inhibition, then this intermediate value would be much higher, indicating a "donor" side limitation, when P700 is in the oxidised form. At the same time if electrons were not removed from the acceptor side of P700 for some reason, such as limiting CO_2 and the absence of an alternative electron sink, then the intermediate level would be much lower, considered an "acceptor" side limitation.

$$Y(I) = 1 - Y(ND) - Y(NA)$$

Where:

$$Y(I) = Photosynthetic\ yield\ of\ PSI$$

$$Y(NA) = \textit{acceptor side limitation}$$

$$Y(ND) = \textit{donor side limitation}$$

The term to describe the level of $P700^+$ related absorption of 830 nm light under steady state actinic illumination is:

P = absorbance of 830 nm measurement beam during steady state photosynthesis

In order to increase the turnover rate of PSI relative to PSII, and increase the relative P700 oxidation level in actinic light, a strong FR pulse (~ 800 µE) lasting 100 mS was initiated (t = 0 ms lasting to t = 100 ms in Fig. 5-7) to oxidise the inter-chain electrons and therefore help oxidise any P700 centres able to be oxidised during steady state photosynthesis actinic light, to which a further saturating pulse (10 µSec, ~9000µmol.m^{-2}. s^{-1}) was applied at t=50 ms (Fig. 5-7.) In Fig. 5-1 this light sequence can be observed under the blue trace on the left hand side. In this case it should be imagined that if there was an unlimited electron acceptor operating downstream of PSI the enormous amount of PSI specific excitation (strong far red light and a saturating pulse) should be able to oxidise the P700 centres to the full extent of the $P700_{max}$ value (P_m). However, if this same level is not reached it can be inferred that an acceptor side limitation ($Y(NA)$) is impeding the oxidation of P700. This value of 830 nm light absorbed when the pulse reaches its maximum is termed:

P'_m = maximum oxidation of P700 in steady state actinic light

At the cessation of the strong FR pulse the actinic illumination continued for a further 50 ms, before a shutter extinguished it and the sample entered a 100 ms period of darkness to fully reduce all $P700^+$ in the sample. This was assumed to be the value corresponding to 100 % P700 reduced, the lowest absorption of 830 nm light. It is termed:

P_0 = value where 100 % of PSI is reduced (centres are open)

This measurement and associated light cycle was performed following the $P700_{max}$ measurements, as can be seen in Fig 4-8, denoted by the red/yellow striped component of the light bar representing constant actinic with a superimposed strong far red light pulse.

Through determining the terms described above for P_m, P_m', P & P_0, the values a, b & c, as illustrated in Fig. 5-1, were then derived:

$$a = P - P_0$$

=intermediate P700 oxidation level in actinic light – level in darkness.

$$b = P_m' - P$$

=maximal value in actinic light – intermediate level in actinic light.

$$c = P_m - P_m'$$

= maximal value under weak far red light with saturating pulse – intermediate level with saturating pulse superimposed on strong FR and actinic light.

As indicated earlier the data presented in Fig. 5-5 and discussed below provided evidence that samples damaged by thermal incubations at ≥ 65 °C required a slightly different interpretation. In these cases, P_m = P_m' and the value of P_0needed to be defined at zero, as the re-reduction time took much, much longer than 100 ms in the absence of inter-chain electrons derived from PSII. Whilst the rationale for this is fully discussed below in sections 5.5.4 and 5.5.3 respectively , note that the results presented in Fig. 5-2 for temperatures 65 °C to 75 °C used this altered analysis, whilst lower temperatures used the standard set of assumptions.

Once values for a, b & c were determined it was possible to calculate the Photochemical Yield of PSI, which as a reminder is:

$$Y(I)_{(photosynthetic\ yield\ of\ PSI)} = 1 - Y(ND)_{(donor\ side\ limit.)} - Y(NA)_{(acceptor\ side\ limit.)}$$

Where:

$$Y(I) = \frac{b}{a+b+c}$$

$$Y(ND) = \frac{a}{a+b+c}$$

$$Y(NA) = \frac{c}{a+b+c}$$

In the following sections, the dynamics of these three terms are discussed with reference to incubation temperature, whilst a few of the more salient points regarding the data's trends are commented upon. However in sections following this, a more thorough analysis is conducted including comparisons with the gas fluxes from Chapter Four.

5.3 Impacts of thermal incubations on Yield of PSI ($Y(I)$)

The $Y(I)$ data in Fig. 5-2 is presented as blue diamonds and on the second x-axis, to differentiate it from the values of donor and acceptor side limitation, both impediments to electron flux (although the scales are the same on both axes). For there to be any value measured, some electrons must be transferring between the donor and acceptor sides.

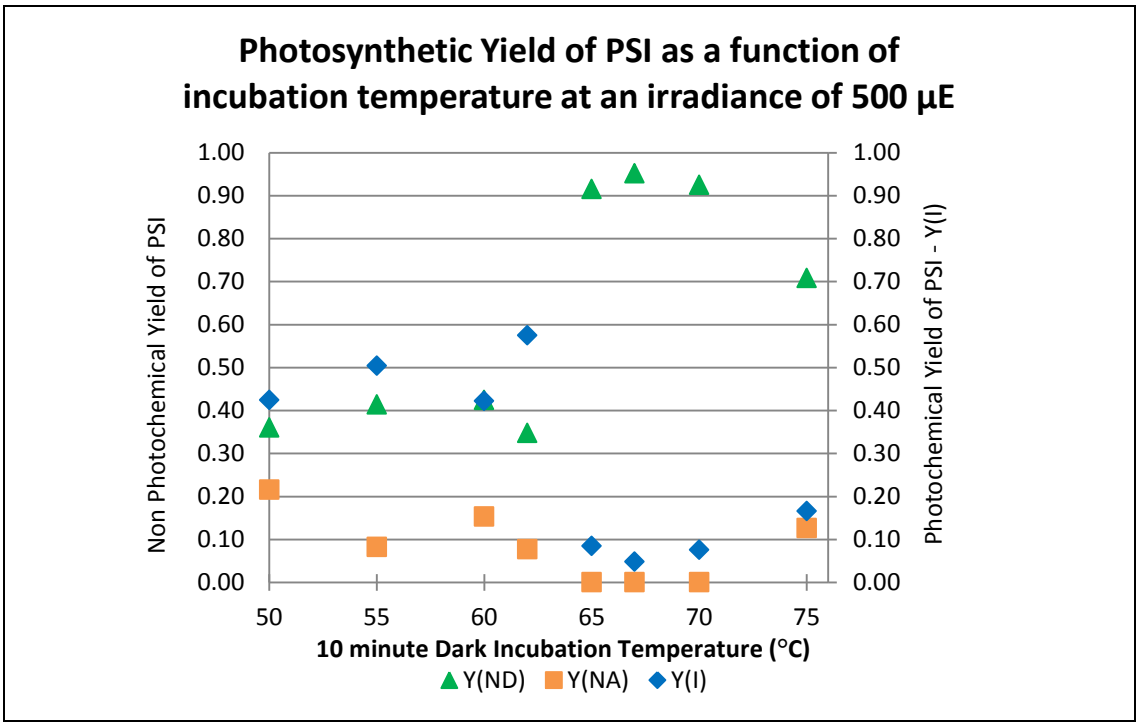

Fig. 5-2: The photochemical Yield of PSI (Y(I)) as a function of incubation temperature, compared to its complimentary yields of Donor (Y(ND)) and Acceptor (Y(NA)) side limitations.
P700 measurements were conducted at the same time as gas flux measurements presented Chapter Four, Fig 4-5, as such all conditions are identical. The data presented are the mean of 3 replicates.

The overall trend shows a lot of variance in the data at temperatures that were, according to analysis of the gas fluxes, not damaging (50 °C to 60 °C). It is therefore not possible to make a clear statement about any trend at these non- damaging temperatures, except to say that in all probability the $Y(I)$ value was around 0.45, broadly in-line with published values from other cyanobacteria. It is slightly low compared to Shimakawa *et al.,'s* data (2016) from *Synechococcus sp. PCC* 7002, although it would make sense, as Gross O_2 evolution rates measured from the cyano-discs in Chapter Four (Panel A, Fig 4-5) were also found to be slightly lower than in the liquid cultures (Panel C, Fig 4-2), likely due to self-shading on the dense discs. Furthermore, the values are higher than those published from measurements of *Synechococcus WH8102* by Bailey *et al.,* (2008).

At 62 °C the value peaks to almost 0.6, before dropping precipitously at 65 °C to 0.08 and further still to just 0.05 at 67 °C. Although these values are low, this is evidence that electrons were still being transferred through the system, a claim supported further in following sections. Although the value climbs again to 0.08 at 70 °C, and then further to 0.17 at 75 °C, the latter value can be discounted as cell membranes seemed to begin severely rupturing (based on electrolyte leakage in Fig. 5-7), whilst a loss of P700 redox dynamics (discussed below in section 5.5.4), discount its physiological relevance.

5.3.1 *Dynamics of acceptor side limitation* ($Y(NA)$)

The acceptor side limitation ($Y(NA)$)presented in Fig. 5-2 exhibits a similar level of variance as the $Y(I)$ data at temperatures between 50 °C and 60 °C. That the $Y(ND)$ data shows comparatively little variance suggests that changes in the value determined for $Y(NA)$ drove the variance of $Y(I)$ data discussed above. If a 'line of best fit' were drawn through the three $Y(NA)$ points between 50 °C and 60 °C, a steady state of approximately 0.15 is apparent for non-damaging temperatures. This low overall value, especially considering the relatively high irradiance of the measurements (500 µE), is evidence to support the conclusion that Flv1,3 proteins were able to facilitate oxygen reduction downstream of PSI, driving the high flux of 'regulatory' O_2 uptake in Panel A of Fig 4-5 (Allahverdiyeva *et al.*, 2014).

A clear decreasing trend in $Y(NA)$ is evident from 60 °C through to 67 °C. This implies that the amount of acceptors available to oxidise P700*, the excited state of P700, were not limiting and became even less so as incubation temperatures increased. This does not necessarily imply that the system was able to handle more electrons, more efficiently. It could simply be a result of fewer electrons arriving at the donor side that require being accepted, a more likely scenario. This helps keep the P700 complex oxidised and limits it potential to suffer photo-damage (Shimakawa *et al.*, 2016).

At 75 °C the level climbed to 0.13, close to the level measured under non-damaging conditions. However as mentioned, this data point is likely un-informative, due to cellular damage which can be observed easily in the 75 °C panel of Fig. 5-5 and the membrane rupture data in Fig. 5-7

5.3.2 *Dynamics of donor side limitation* ($Y(ND)$)

As mentioned above, the donor side limitation determined at non-damaging temperatures was slightly more consistent than both $Y(I)$ and $Y(NA)$, remaining within the range of 0.35 to 0.42 between incubation temperatures of 50 °C and 62 °C. The $Y(ND)$ value climbs very sharply at 65 °C, to 0.92, then 0.95 and back to 0.92 at temperatures of 65 °C, 67 °C, and 70 °C respectively. This indicates that nearly 100 % of inhibition of $Y(I)$ was driven by a limitation on the donor side of PSI. It suggests the very low values determined for acceptor side limitation ($Y(NA)$) recorded across this temperature range were indeed a result of PSI undergoing fewer turnovers. In the following section, these trends are discussed with comparison to the gas fluxes of Chapter Four, to provide evidence that it was the loss of PSII function that primarily drove the increase in $Y(ND)$.

5.4 As PSII failed, PSI activity maintained relatively more activity

Data analysis in Chapter 4 provided strong evidence that after a ten minute dark incubation at 65 °C the activity of PSII, as determined by gross O_2 evolution, was reduced by over 95 %. In Fig. 5-2 of this Chapter it can be seen that this trend coincided with a substantial increase in the donor side limitation ($Y(ND)$) of P700 data. Simultaneously by this temperature, the remainder of PSI's photochemical yield ($Y(I)$) appeared to be active turnover, as $Y(I)$ did not reach zero in contrast to $Y(NA)$ which did. Can the ~5 % of PSII function still measurable, and found to be driving the Calvin-Benson-Bassham cycle in Chapter 4, be sufficient to account for the level of $Y(I)$ still observable at 65 °C in Fig. 5-2? Or is the level recorded for $Y(I)$ too high to be driven solely by the remaining PSII activity?

To investigate this, the gas fluxes from Chapter 4 and the P700 data were normalised to maximal values for comparison in Fig. 5-3. A component of this normalisation was the inversion of the $Y(ND)$ data, to account for the fact that a decrease in PSII activity lead to an increase in $Y(ND)$ values. Comparing the processed values for PSII activity (as measured through the proxy of Gross O_2 evolution), dark respiration, the photochemical yield of PSI ($Y(I)$) and $1 - Y(ND)$ (the inverse value of donor side limitation) provided support for two key findings:

The first of these findings is not surprising, and serves as a check that the data comparisons make sense. A strong correlation exists between diminishing rates of Gross O_2 evolution and $1 - Y(ND)$ at temperatures greater than 65 °C, until the cells begin to show severe damage at 75 °C (see discussion of Fig. 5-7 in section 5.6).

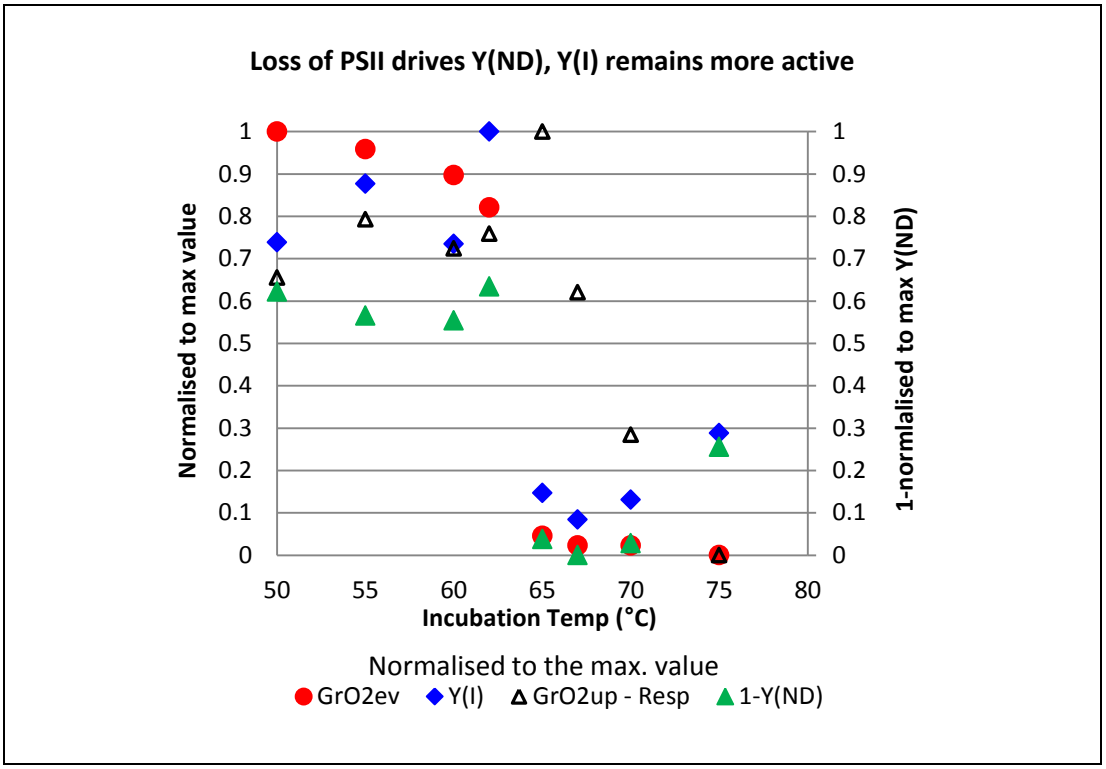

Fig. 5-3: Comparison of normalised activity of PSII, PSI, respiration rates and 1-(normalised to maximal rate of Y(ND)) (donor side limitation of PSI).
Displayed on the primary y-axis are values normalised to the maximal activity for: the gross flux of O_2 evolution: the rate of dark respiration (both from Chapter Four) and the photochemical yield of PSI. On the secondary y-axis is **1-(the normalised to maximum value for Y(ND))** – by inverting the values for Y(ND) in this way, it is possible to directly compare the correlation between **GroO_2Ev** and the donor side limitation of PSI (**Y(ND)**), which ought to be inversely correlated when PSII activity is limiting the flux through PSI.

This is consistent with the idea that PSII is the primary donor of electrons to PSI at non-damaging temperatures. It implies that once PSII was severely inhibited, the loss of reductant to PSI produced a severe donor side limitation. This would result in it becoming highly oxidised under actinic illumination, with a large acceptor side capacity. That zero acceptor side limitation was found has already been noted in Fig. 5-2 at >65 °C. That P700 became highly oxidised in actinic light can be seen in Fig. 5-5 (from the 65 °C panel upwards) and discussed in section 5.5.4, where the entire curves of $Y(I)$measurments became increasingly oxidised with increasing temperature. The value of Pm' reached or indeed exceeded the level of Pm.

The second finding is more interesting, as it suggests that PSI in cells with inhibited PSII function (caused by exposure to high temperatures), continues to function at higher rates than could be driven solely by the remaining activity of PSII. Where PSII activity

recorded only 4.6% of the maximal value at 65°C, $Y(I)$ still recorded a value of 14.7 %, over three fold higher. Discussion of data in section 4.4 suggested that after a 65 °C, incubation the small number of electrons still generated by PSII were able to reduce CO_2, via the Calvin-Benson-Bassham cycle. This presumably involved the PSI complex, however this small flux from PSII seems insufficient to maintain $Y(I)$ at such a relatively high level. A number of electron sources alternative to PSII, able to reduce the PQ pool, could explain this discrepancy (Bukhov and Carpentier, 2004). The first comes from cyclic electron transport (CEF) and the second from the direct reduction of PQ via the oxidation of sugars.

If electrons generated at PSII were indeed being used to generate NADPH for the reduction of CO_2 in the Calvin-Benson-Bassham cycle, as the conclusions to Chapter 4 suggest, then a constant and significant bleed of reductant required to maintain the redox poising necessary to allow cyclic electron transport (Alric, 2015) would occur. Although a slight inhibition of PSII is known to enhance the relative amount of CEF occurring in cells, excess inhibition leads to a significant drop in the capacity of the cells to perform CEF. This is due to the oxidation of ferredoxin (Fd), which becomes unable to re-reduce the PQ pool. This concept was already a finding from the original *in vitro* data published by Tagawa et al., (1963), who used DCMU to inhibit the re-reduction of Fd. *In vivo* however, the capacity of the cells to reduce the PQ pool with reductant sourced from the oxidation of succinate, via the SDH complex (Cooley *et al.*, 2000), could result in two possibilities. Significantly, these are not mutually exclusive and both could be active.

The first option is that these electrons simply continue in the linear photosynthetic pathway. They reduce $P700^+$, then Fd and finally $NADP^+$, itself a non-oxygenic terminal acceptor. This extra source of reductant alone could increase the measured $Y(I)$ values. This pathway could also be an efficient method to translate 'low energy' NADH, generated through respiration, feeding into the PQ pool via complexes such as SDH, into the high energy NADPH required for reduction steps in anabolic processes which according to Spaans *et al*,. (2015) is required in large amounts by cyanobacterial cells. This would be particularly true of cells working to repair damaged proteins etc. A specific enzyme, Pyridine nucleotide transhydrogenase is able to perform this role. Knocking out this complex in 6803 cells had no clear physiological impact in illuminated cells. However when relying on heterotrophic pathways for energy, the cells were severely disrupted in growth (Kämäräinen *et al.*, 2016). The authors speculate that a loss of NADPH to indirectly drive the NDH-1

complex to generate a proton gradient for ATP synthesis, was likely the cause of the low growth rates measured in the mutant cells. The authors also speculate that the activity of this enzyme translocates a proton from the thylakoid lumen into the cytoplasm. This is an energetic cost, with respect to a situation where PSII is severely inhibited and respiratory sources of reductant are required to energise the cells. The linear pathway being proposed, from a source such as SDH, via the PQ pool to NADPH at PSI would in fact increase the number of protons across the thylakoid membrane.

The terminal acceptor in this pathway suggests a non-oxygenic respiratory route, consistent with the data in Chapter Four that a non-oxygenic respiratory process began to function at temperatures that severely inhibited PSII, section 4.4.4.

The second option is that by reducing Fd, these electrons provide the necessary poising to enable cyclic electron transport. As such the PQ pool was re-reduced and electrons are re-cycled around the photosystem (Yamori and Shikanai, 2016). This would enable a large increase in the relative proportion of flux through the $Y(I)$ complex, compared to that available from PSII. Such a process would also enable cells to maximise the energy available to them from their environment, by driving photochemistry with internally sourced reductant. This energisation of the thylakoid membrane would generate maximal ATP through respiration whilst minimising the usage of a cell's stored carbon.

Such a system has been proposed for phytoplankton growing in oligotrophic oceans. When unable to source sufficient nitrogen to maintain active PSII, they can revert to cycling externally sourced reductant from assimilated organic compounds (Grossman *et al.*, 2010) to generate ATP and maintain primary cellular function. It has also been proposed to explain the observation that a 6803 mutant, inhibited in activity of PSII and respiratory terminal oxidases and growing heterotophically, still managed higher growth rates in the light (Howitt *et al.*, 2001). From thorough literature searching only one example was found where authors have clearly proposed that respiratory reductant has been used to poise the thylakoid for cyclic electron transport in the absence for PSII function. Lu *et al.* (2016) proposed NADPH, sourced from the oxidative pentose phosphate pathway, was being used to reduce $P700^+$ in a brown macro algae inhibited in PSII function by osmotic stress.

As such, any of these proposed outcomes would make it possible for the relative Yield of PSI to be so much higher than the relative activity of PSII. Further analysis of raw P700

data in the following sections provides more evidence for the reduction of $P700^+$ through respiratory reductant. Furthermore, in the following Chapter (Chapter Six), data analysis suggested that thermally damaged cyanobacterial cells can re-cycle respiratory sourced reductant around PSI. Although these experiments were conducted with *Synechocystis* 6803cells, there is sufficient literature around the activity of cyclic electron transport between different species to suggest these results apply to BP.1 cells as well.

To summarise the key point from this section, the analysis of normalised data in Fig. 5-3 provides a good foundation that PSI was more active at temperatures that had severely inhibited PSII, and that respiration was still functioning strongly. That this could be used to reduce $P700^+$, as already demonstrated by authors such as Grossman *et al.*,(2010), is investigated in the following sections where the raw P700 data is examined to provide more evidence that the $P700^+$ system was reduced by the oxidation of sugars.

5.5 Unlocking hidden data in the raw $P700_{max}$ and $Y(I)$ curves

As PSII was inhibited with increasing incubation temperature, changes can be observed in a number of characteristics in the raw data of both the $P700_{max}$ and $Y(I)$ components of P700 measurements. As with the gas fluxes discussed in Chapter 4, the raw data can provide a level of detail to what was happening in the samples, compared to simply looking at the broad trends of extracted values (presented in Fig. 5-2). It pays to remember that before each measurement, the level of the Walz PAM 101 system was re-zeroed in the dark, to balance absorption between the 875 and 830 nm measurement beams. This implies that the level of oxidised P700 in FR or actinic light should be consistently comparable to the zero starting value, and that when fully reduced the P700 should come back to approximate zero. It certainly did during experiments - if enough time was allowed to pass in darkness, discussed below in section 5.5.3.

One of the conclusions to be drawn from the analysis of data in the following sections is that I failed to account for physiological changes within cells that upset the assumptions underpinning aspects of the P700 measurements. Specifically, it was a failure to realise that setting up and testing the equipment with undamaged cells did not ensure that the assumptions held true once cells suffered damage. For example, ensuring the saturating pulse was really saturating, and the weak FR light was driving sufficient oxidation to be

around 85 % to 90 % of the maximal saturating pulse's level (explored in 5.5.2). It was not the original plan to investigate a potential role for PSI in respiration when designing the experiments. The conclusions drawn at the end of the following sections are not in line with what I had initially set out to investigate, as such my failure to consider this in designing the experiments was due to the unforeseen nature of the circumstances.

However it must be stressed that the data work-around used for deriving the values of $Y(I)$, $Y(NA)$ and $Y(ND)$, presented in Fig. 5-3, was based on solid consideration of the changed conditions that occurred within cells, as discussed below in sections 5.5.3 and 5.5.4. As such, this data is accurate, up until the cells began to rupture at ≥70 °C, based on data presented in Fig. 5-7. Most importantly the observation that $Y(I)$ is still functioning at temperatures where PSII was severely damaged, discussed above in 5.4, was without doubt correct as the assumptions made to determine the value of a, discussed above in section 5.2.2, would if anything underestimate that value.

That I failed to take into account the changing redox pressure faced by PSI turnovers, caused by what I argue to be the increased rate of respiratory electrons reducing the PQ pool, has resulted in a wonderful set of data to investigate. As the intensity of the weak FR light used to oxidise PSI was not changed under any conditions, the redox response of the cells measured by the P700 system can be directly compared, discussed and ultimately used to provide the evidence required to show that PSI was being reduced by respiratory electrons.

As such. in the following section, raw P700 data is examined to draw out further evidence for the two key claims being made in this thesis: that PSII fails before other processes within the cell, and that PSI continues to function after PSII had failed. It achieved this using reductant sourced from respiration and hence, for all intents and purposes, became a component of the respiratory pathway. Some of the data analysis discussed in the following sections are based on published interpretations of P700 data, such as the PSII kinetic area (Jia *et al.*, 2014) described in the inset of Fig. 5-1. Other interpretations combine my own observations, based on first principles underpinning how the measurements function, with established ideas in the literature regarding the drivers of P700 redox relaxation kinetics (Bernát *et al.*, 2011, Fan *et al.*, 2016). These processes are examined with respect to changes in the data between incubation temperatures, and how this may reflect what was happening within the cells.

It is not intended that any of the observations made in this following section be considered as conclusive evidence in their own right. These observations are considered primarily as support for the key findings already discussed in this Chapter and concluded in Chapter Four. However, by the end of this section it is hoped that the consistency found between the different components of data interrogation becomes evidence in itself, for the accuracy of the examination and its conclusions.

5.5.1 *Loss of PSII Kinetic area consistent with gas flux data*

The raw $P700_{max}$ data contained the easiest-to-interpret changes occurring with incubation temperature. The first phenomenon to observe in the signal is the component of the curve termed the PSII Kinetic area (Jia *et al.*, 2014). This 'trough' component (see the green hashed area of the red curve in the inset in Fig 5-1), subsequent to the saturating pulse, was driven by intersystem electrons derived from PSII turnovers during the saturating pulse. As they arrived to reduce $P700^+$ to P700, the absorption of the 830 nm measurement beam was decreased. However, the constant illumination of the samples by weak FR light continuously drove P700 oxidation rapidly (~ 250 mS) back towards the steady state $P700^+$ level, seen before the pulse. At least this was true in samples that were not excessively damaged (< 65°C, based on the Gas flux data in Chapter 4).

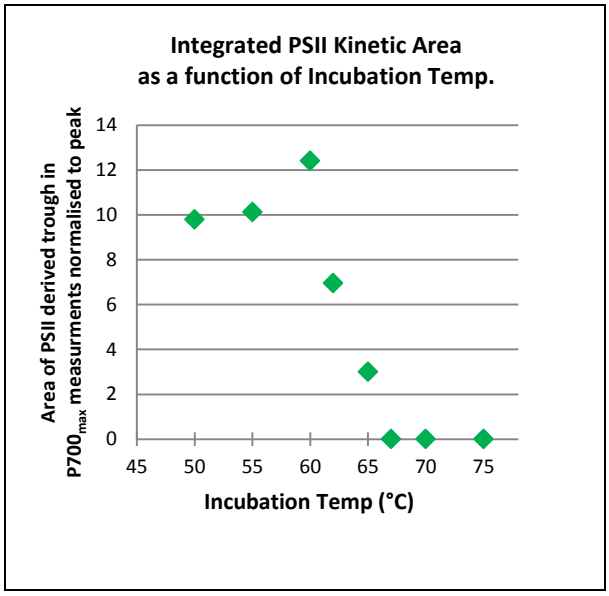

Fig. 5-4: Integrated PSII Kinetic Area as a function of incubation temperature.
The area of the trough described in Fig. 5-1 from $\boldsymbol{P700_{max}}$ measurements normalised to the $\boldsymbol{P_m}$ peak. At temperatures >65 °C the value was set to zero because the calculated area was a negative due to the complete loss of function in PSII which can be seen in Fig. 5-5 to no longer drop below the steady state value of oxidation, hence there is nothing to subtract from the steady state to make up the area inside the curve. Conditions were as described in other figures describing both gas fluxes and the P700 measurements. n =3

A representative raw plot of both the $P700_{max}$ and $Y(I)$ measurement data at each temperature from 60 °C to 75 °C is presented in Fig. 5-5. The thin blue line in each panel is a visual aid for making subjective comparisons between the steady state levels of oxidation in weak FR light during the $P700_{max}$ measurement, compared to the PSII driven trough formed after the saturating pulse. As PSII lost function the area of this trough decreased, until incubations ≥ 67 °C,

where the trough was clearly no longer visible. In its place was a response reminiscent of samples inhibited in PSII function by DCMU: a peak followed by a slow decline back to the steady state $P700^+$, but not driven below it (Jia *et al.*, 2014). A more objective analysis is presented in Fig. 5-4, the integrated area of these troughs, calculated after the data was normalised to the peak values.

The trend in this data is already very familiar, correlating broadly with the Gross O_2 evolution data presented in Fig 4-5. The values at temperatures > 65 °C were set to zero, as the derived values became negative when calculated using the standard data analysis protocol. This was because, as can be seen in Fig. 5-5, the curves never drop below the steady state value and as such, there is nothing to integrate below the 'blue line' in these panels.

The results from analysis of the PSII kinetic area provides good support for the conclusions drawn from the already discussed gas flux and the fluorescence data of Chapter 4, with respect to the thermal lability of PSII.

The precision of this analysis became questionable as PSII was severely damaged, caused likely by an alternative source of reductant which delayed the rate of re-oxidation in weak FR light.

More support is given to this idea below in each of the following sections, but if correct it may have slowed the re-oxidation of P700, artificially enlarging the area of the trough. This can be seen in Fig. 5-5 by comparing the data in the 60 °C panel with that in the 65 °C panel. Where the former is fully oxidised again (or at least very close compared to the large response) after only 250 mS, the latter did not return by this time-point and the upward slope of the curve towards the blue line is very shallow.

This is especially true when considering that the PSII driven response in damaged samples was small to begin with. Bear in mind that the total measurement lasted for 1000 ms (-50 to 950 ms), so the impeded re-oxidation of P700 had time to accumulate a relatively large amount of error. In spite of the possible over estimation, the area calculated at 65 °C is 6 fold smaller than at 60 °C. However, this is not ~5 % of the maximum, as would be expected if the measurement accurately reflected Gross O_2 measurements, as can be seen in Fig. 5-3. This is not to say the measurement is inherently imprecise. It is in fact consistent with the idea that $P700^+$ was being re-reduced by a larger flux of respiratory electrons than the weak FR light was able to efficiently oxidise.

5.5.2 *Higher respiration correlated to lower PSI oxidation*

A comparison of the proportion of P700 oxidised by weak FR light with respect to the maximum peak (Pm) obtained with the saturating pulse, provides another example from raw $P700_{max}$ data that an alternative source of reductant to PSII was reducing $P700^{+}$ in thermally damaged cells.

It is expected that 85 % to 90 % of the total population of PSI should be oxidised under the weak FR light (Kou *et al.*, 2015) before the saturating pulse was applied to determine P_m. This was indeed observed in the cyanobacterial samples. See the proportion of oxidised P700 centres in the upper panel of Fig 5-6. In the top panel of Fig. 5-6, a plot of the relative change in oxidation level between the steady state in weak FR light and the peak at Pm, shows a clearly negative trend with incubation temperatures up to 67 °C. This value shifts from the expected 85 % to 90 % range, down to 75 % at 67 °C. From 67 °C the value climbed rapidly back up to almost 100 % by 75 °C. However this latter point correlated with severe cellular damage, as determined through conductivity measurements of cell leakage and lysis in Fig. 5-7. The decreasing proportion of P700 centres being oxidised in the weak FR light, whose intensity was not changed during experiments, is consistent with the idea that an increasing amount of reductant was entering the thylakoid with increasing temperature. If this is accurate, could this reductant have been sourced from respiration?

The gas flux data in Panel B, Fig 4-5, provided evidence that the rate of respiration also climbed with increasing temperature. It peaked at 65 °C then dropped again towards zero from 67 °C, as can be observed in Fig. 5-3. Bernát *et al.*, (2011) state that PQ is an integral component of all respiratory pathways in cyanobacteria and present evidence that different *'NADPH'* plastoquinone oxidoreductase (NDH-1) complexes are responsible for reducing PQ at different levels of oxidation. Further, C*ooley et al.,* (2000) proposed succinate dehydrogenase (SDH) is capable of reducing the PQ pool, primarily when the pool is mostly oxidised. Recently however, NDH-1 has been reclassified as a Fd-PQ reductase (Peltier *et al.*, 2016), as more evidence is produced suggesting it most likely accepts electrons directly from Fd.

The specific complex or the specific variant of each complex, and which specific condition favours the activity of which, is still being discussed in the literature.

Suffice to say, there is plenty of evidence to support the idea that PQ can be reduced by respiration in cyanobacteria.

Under the experimental conditions of weak FR illumination and with PSII being severely damaged, the PQ pool would have likely been subject to severe oxidation in cells ≥ 65 °C. This would have certainly promoted its reduction by one of the many possible candidate complexes and pathways summarised above. As mentioned, the following Chapter (Chapter Six) provides evidence that these respiratory electrons may even be re-cycled around PSI.

Taken on its own, this is not a conclusive piece of evidence that PSI is involved in respiration. Combining evidence from the literature regarding the reduction of PQ through respiration with (1) the concrete gas flux findings that increased incubation temperatures correlated with the stimulation of illuminated respiration at elevated rates in Chapter Four and (2) a lower level of steady state oxidation between 65 °C and 70 °C in the upper panel of Fig. 5-6 — suggests that the change to P700 measured may be driven by reductant sourced from the oxidation of sugars. Therefore, the data is certainly consistent with the hypothesis that PSI can be involved in cellular respiration as PSII becomes inhibited by high temperatures.

5.5.3 *Respiratory electrons altered rates of dark $Y(I)$ re-reduction*

In this section, data trends in the rate of $P700^+$ re-reduction of $\boldsymbol{Y(I)}$ measurements during the 100 mS dark period are explored to show that they correlate well with the conclusion that an alternative source of reductant was able to reduce the PQ pool in the absence of PSII function. Recall that the $\boldsymbol{Y(I)}$ measurement was conducted in accordance with a method designed to maintain samples in a 'steady state' of photosynthesis, achieved by only darkening the samples for 100 mS out of every 10 sec (Kou *et al.*, 2013). This dark period was used to 'check' that the 'dark level' ($\boldsymbol{Po}$) of P700 did not shift due to instrument drift or physiological changes. In the lower panel of Fig 5-6, rates of re-reduction in the final 50 ms of darkness (out of 100 ms total darkness) are compared (although rate values are inverted to make a comparison clearer). At the initiation of this dark period, $P700^+$ was re-reduced to P700 in a manner that changed substantially with increasing incubation temperature (see lower panel of Fig 5-6, the rate of re-reduction drops substantially at 70 °C and 75 °C).

Looking at the black $Y(I)$ curve in each panel of Fig. 5-5, it is clear when the actinic light was extinguished at 150 ms. This is especially true of undamaged samples in the 60 °C and 62 °C panels, where the $Y(I)$ curve rapidly returns to approximately zero. The reduction of $P700^+$ in the dark followed a biphasic curve, which became more obvious as PSII damage increased(according to gas flux data in Chapter 4).This constituted an initially rapid phase (initial 50 ms), which reduced the substantial majority of P700 centres in undamaged samples, followed by a slow linear phase. This initially rapid phase is due to the reduction of $P700^+$ by intersystem electrons. At temperatures where PSII had been severely damaged (≥65 °C), however, the relative contribution from each component became inverted. The rapid initial phase contributed a smaller percentage of the total, with each increase in incubation temperature. The slower linear component of undamaged samples became the major contributor to $P700^+$ reduction where PSII had been inhibited. Due to the slow rate of the linear phase however, samples were unable to reach an equilibrium within the short 100 ms dark period, which under the basic assumptions used with undamaged cells was defined as zero or P_o. However, at the end of the experiments the signal would eventually return to the starting value of zero, which was set in darkness before the experiment began, although this could take up to 10 seconds in severely damaged cells. As such the assumptions used to calculate $Y(I)$ data had to be changed for these temperatures, as discussed in section 5.2.2, with P_0 'set' to zero, as opposed to the value for zero being determined through data analysis.

Interpreting the two phases of the $Y(I)$ re-reduction curves, and why they differ, provided further evidence that the system was being re-reduced by electrons sourced through respiration.

The initial and rapid phase of the biphasic re-reduction of $P700^+$ was analogous to the formation of the trough used to determine the PSII kinetic area, without the constant weak FR background to re-oxidise it (Maxwell and Biggins, 1976). It was driven by PSII derived inter-chain electrons, making their way through the numerous complexes and carrier molecules involved in the photosynthetic electron transport systems operating under the conditions of steady state and high irradiance (500 µE). In most likelihood this would have constituted both the large PSII driven linear flux and a component of cyclic electron flux (Suorsa, 2015). As the sample entered darkness these electrons arrived at, and reduced, the large majority of the closed P700 centres resulting in their rapid re-reduction.

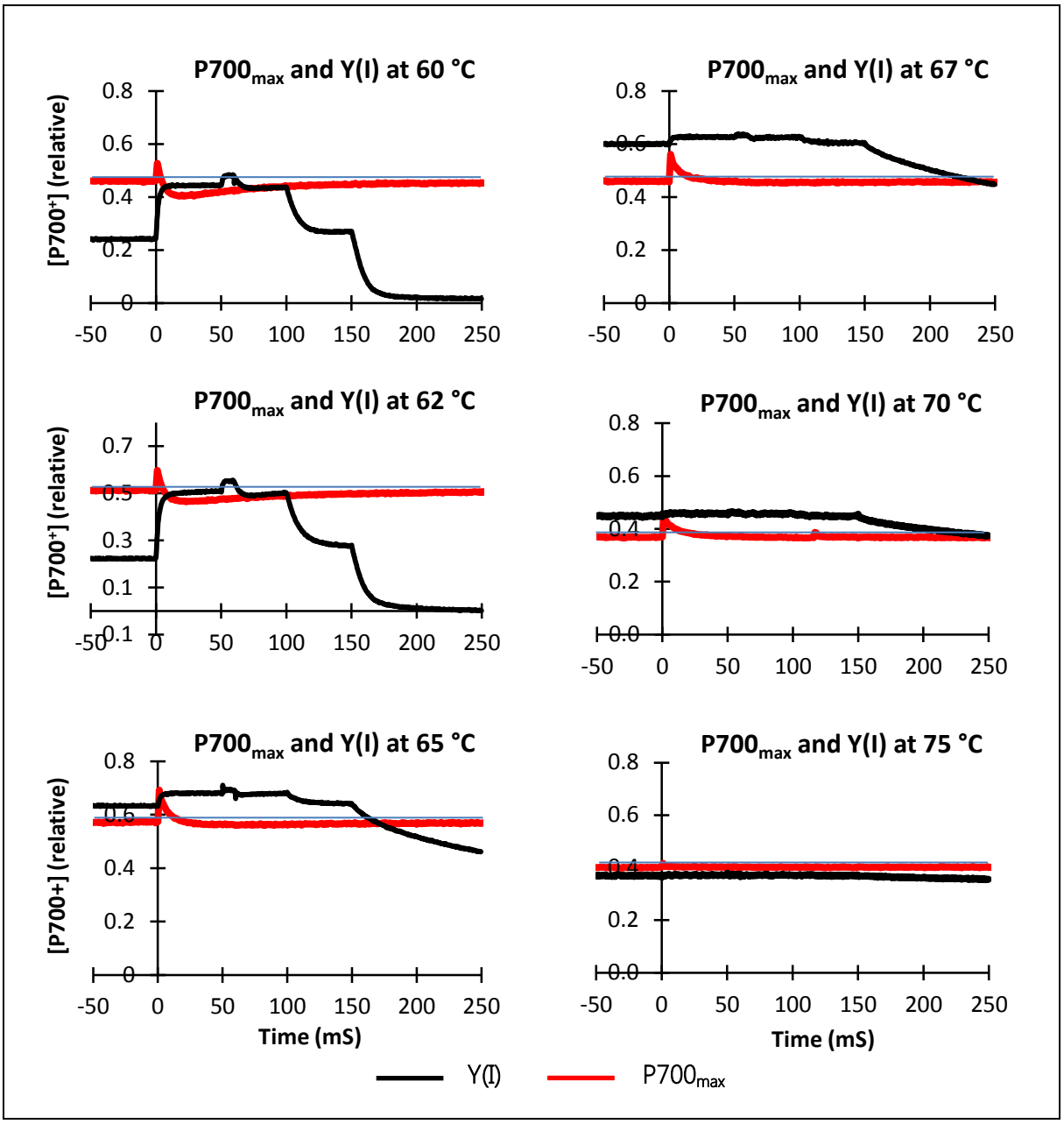

Fig. 5-5: Comparison of $\boldsymbol{P700_{max}}$ and $\boldsymbol{Y(I)}$ raw signals at increasing incubation temperatures.
A representative measurement from each incubation temperature is displayed to illustrate the changes occurring to P700 signals resulting from thermal damage to BP.1 cells. What can be observed in this comparison of is that the level of Fm, the maximal level of P700 oxidation shown with the red curve at each temperature is less oxidised then the Y(I) data shown in the black curve at temperatures >65˚C. This indicates that something was 'reducing P700' in the low FR light that competed to minimise the rise in P700 oxidation. As such, at temperatures ≥65 ˚C, the Fm' was used in place of Fm to define the maximal P700 oxidation. Conditions for each sample were the same, except for the temperature of the 10 minute dark incubation period. $P700_{max}$ signals were ascertained by oxidising P700 under weak far red light. 50 ms after recording was started a saturating actinic light pulse fully oxidised the total P700 in the sample with the weak far red light maintained, reoxidising those P700 reduced by electrons flowing from PSII in the period immediately following the saturating pulse. Total acquisition time was 1000 mS, only the first 300 ms are displayed. Y(I) data was generated under steady state actinic light (500 µE). After the signal was recorded for 50 ms a strong far red light was applied to oxidise as much P700 as possible in the presence of strong actinic light. After a further 50 ms, a saturating pulse of white light at 9000 µE was used to oxidise as much of the remaining P700 centres as possible. The Strong far red light was turned off after a further 50 ms and the actinic light was rapidly darkened via a shutter after 200 ms from the start of the acquisition. This period of darkness lasted for 100 ms, before the actinic shutter reopened, effectively keeping the sample in constant illumination. Other conditions as described in gas flux data in Fig 4-5. lower panel, Each of the Y(I) measurements from the four upper panels are normalised to the maximum value and compared to each other

The transition from the rapid phase to the slow phase could have been driven by a number of processes, including the delayed arrival of the PSII derived inter-system electrons passing through the thylakoid, a shift in the electrochemical gradient around the $P700^+$ Cyt-C_6/plastocyanin docking site, potentially caused by the rapid cessation of illumination (Fan *et al.*, 2016), and simply back reactions within the PSI complex (Rutherford *et al.*, 2012) . The final slow phase is consistent with the steady relaxation of DCMU infiltrated samples, published by Maxwell and Biggins (1976).

As noted, when PSII became severely damaged (especially visible in the 65 °C panel of Fig. 5-5), the proportion of $P700^+$ re-reduction contributed by the two phases became inverted. The initial rapid phase produced a much smaller portion to the total measured change, whilst the steady linear phase became the primary contributor. The linear nature of the decrease in oxidised P700 centres observed during this slow phase of the re-reduction is consistent with the idea that it was driven by a steady flux of reductant. Recall from Chapter Four that gas flux data provided very strong evidence of respiration rates that were not only elevated at 65 °C, but were equally functional in the light and the dark. A constant rate of electron flow from respiration, entering the thylakoid via SDH and/or NDH-1 and reducing the PQ pool would be a good candidate to describe the constant rate of $P700^+$ re-reduction observed during the slow phase.

To provide a more objective comparison of the dark re-reduction rates, a linear regression analysis was performed on the final 50 ms of the dark phase for each of the $Y(I)$ measurements presented in Fig. 5-5. This final 50 ms period was selected to avoid the component of re-reduction likely driven by inter-chain, PSII derived electrons. The results from these linear regressions are presented in the column graph in the lower panel of Fig. 5-6.

The overall trend of this figure is interesting as it broadly mirrors the data presented in the upper panel; a comparison of the proportion of P700 oxidised in weak FR light compared to the saturating pulse (discussed in 5.5.2). Where the lower values in the upper panel correspond with a potentially higher rate of reductant entering the thylakoid from an alternative electron source (as discussed in more detail in the previous section 5.5.2), the higher value in the lower panel may also correspond to a greater contribution from alternative electrons. As such, the mirroring of the data's trends adds strength to the individual claims made about each.

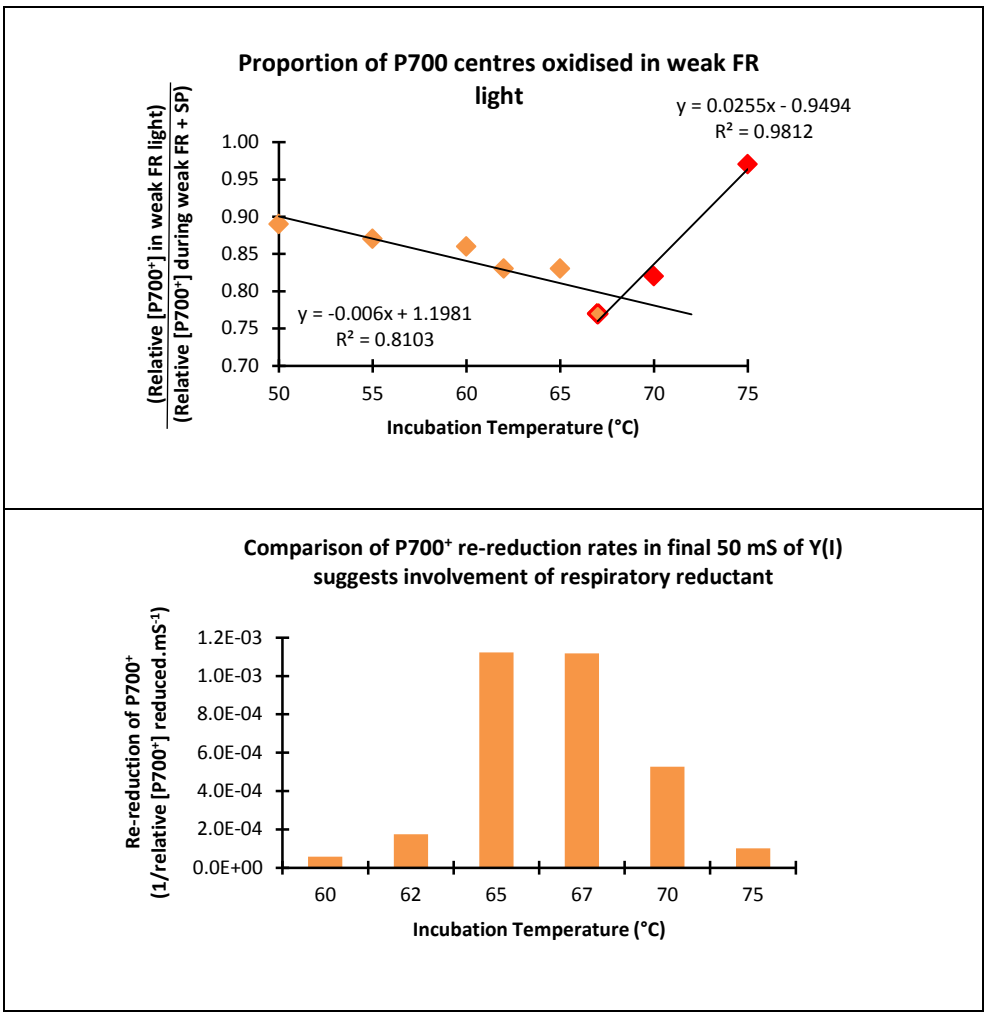

Fig. 5-6 : Support for the hypothesis that respiratory reductant was reducing $P700^+$ at temperatures where PSII had been inhibited, found through a further comparison of raw $P700_{max}$ and Y(I) data. In the upper panel the proportion of P700 oxidised by weak FR light as a proportion of the total oxidisbale P700 (P_m) is plotted against the incubation temperature. That this is declining, given the conditions between samples during measurments were kept unchanged, suggests something was reducing the $P700^+$ as it was generated by the weak FR light.
In the lower panel, the rate that $P700^+$ reduced back to P700 in the final 50 ms of data acquisition during Y(I) measurements (at the beginning of the dark period) are compared for each incubation temperature. The rates were determined using a linear regression analysis of the raw data and *has been inverted* to be a positive value, for easier visual comparison. Where PSII was functional, little to no $P700^+$ should be remaining in the final 50 ms of data acquisition, as the samples are nearly fully reduced by the activity of PSII, immediately following the light off. analysis of interpreting this figure is provided in the text. The data in both panels is considered a representative sample for each temperature, selected at random and therefore n=1. The raw data traces for each temperature, from which all of this data was extracted, are presented in Fig. 5-5.

The bell shape of the data describing linear regressions of the final component of P700 re-reduction may be representative of different phases of cellular damage. Functional PSII had already re-reduced the vast majority of $P700^+$ at the beginning of the linear regression in samples at 60 °C and 62 °C. Hence, the re-reduction rate in the final 50 ms was very low, representative of the fact that the $P700^+$ population was very low. From this data set alone (n=1, these curves are a representative sample of the data acquired during measurements), the level of significance of the increase in rate between 60 °C and 62 °C

cannot be determined. However, there is a strong similarity between this and the decrease in PSII activity clearly visible in the normalised gross O_2 evolution rates presented in Fig. 5-3.

In the centre of the bell curve are samples incubated at 65 °C and 67 °C. These showed very similar rates of $P700^+$ re-reduction that were much higher than either of the two samples possessing high PSII activity. The primary reason for the increase in re-reduction rate was likely a result of the much larger population of $P700^+$centres still requiring re-reduction, compared to the less damaged samples. So although impossible to exclude a simple $P700^+$ back reaction resulting in the same rates between the samples, it is clear that the rates at these temperatures were much higher than the rates at 70 °C. At this temperature respiration rates were significantly lower (Panel B, Fig. 4-5), and the cells were also beginning to suffer structural damage (Fig. 5-7). As such, the 70 °C rate was more likely closer to that of a pure back reaction at P700 – providing support to the idea that 65 °C and 67 °C rates were accelerated by respiratory processes. Undoubtedly the rates at 75 °C were confounded by the degradation of cellular integrity, discussed in 5.6. The entire Y(I) curve at this temperature in Fig. 5-5 shows that the system was suffering severe damage.

Measurements of altered P700 re-reduction kinetics are one of the primary methods used to measure and determine the processes defined as chlororespiration, the reduction of the PQ pool by oxidation of either stored or externally obtained carbohydrate substrates. It is a well-documented metabolic pathway in cyanobacteria, plants and green algae (Hirano *et al.*, 1980, Bennoun, 1982, Peltier and Sarrey, 1988, Peltier and Cournac, 2002). As such, a substantial body of literature supports the possibility that the increased rate of P700 re-reduction could have been driven by the oxidation of stored sugars, particularly once the samples had been exposed to elevated temperatures (Bukhov *et al.*, 2002).

Furthermore, it is probable that any reductant entering the PQ pool at this initial onset of darkness would have reduced $P700^+$ over any respiratory terminal oxidases (RTOs) as the distribution of complexes such as SDH and NDH-1, with respect to PSI within the steady state system, would have likely maximised this probability. A wonderful paper from Liu *et al.*, (2012) demonstrated that these complexes physically transfer their location depending on the conditions, to be close to terminal oxidases in the dark, or PSI in the light.

Unfortunately, no comparison was made with samples inhibited in PSII function by DCMU, or perhaps with KCN to inhibit respiration in the cells more broadly. This could have provided a useful comparison. In their recent paper, Aihara *et al.*,(2016) produced similar

results to those described above, in *Symbiodinium.* However the authors concluded the increased rate of re-reduction with elevated temperature was driven by cyclic electron flux. I argue that they have insufficient evidence to rule out some form of 'illuminated chlororespiration', as will be discussed more thoroughly in section 6.2.6. The cyclic flux they observed was not inhibited by Antimycin A, implicating the NDH-1 complex, they don't present gas flux data and they did not consider that the final acceptor may not have been oxygen, but rather $NADP^+$, as proposed in this thesis, which could explain their result that the rates were elevated under anoxic conditions.

The data in this section provides, at the very least, anecdotal evidence to further support other analyses throughout this chapter. If some form of 'illuminated chlororespiration' was in-fact an important contributor to the rates of re-reduction observed at 65 °C and 67 °C, then it discounts a direct correlation between the rate of respiration and the rate of electrons entering the thylakoid membrane. Recall that respiration rates dropped significantly between 65 °C and 67 °C (Fig. 4-5). This could suggest that the cells may maximise their capacity to involve PSI in respiratory activity, preferring to use this pathway when available over others. Or else some rate/capacity limiting step in the pathway may have been reached in both of these samples, which was saturated at respiratory rates lower than those exhibited by the cells.

There is not a lot of literature exploring the partitioning of respiration between different pathways. In Liu's (2016) recent article titled the "distribution and dynamics of electron transport complexes in cyanobacterial thylakoid membranes" examining this, and other electron transport related dynamics, Liu states that "our current understanding of the functional and structural dynamics of electron transport pathways needs to be substantially improved". One issue I see in the literature on the subject is a lack of gas flux data to corroborate assumptions. In their otherwise excellent paper exploring the functionally distinct roles of the different NDH-1 complexes (NDH-1L and NDH-1L') Bernát *et al.*, (2011) rely solely on the addition of inhibitors to mutants for comparison with WT cells of 6803 when elucidating P700 redox kinetics, whilst the recent paper from Aihara *et al.*, (2016) mentioned above, failed to provide gas flux data to corroborate their findings.

Without gas flux data, and having a complete reliance on the assumptions of the efficacy of the inhibitors, I question whether they can really make some of the claims they do – and more importantly, I wonder what findings they have missed. Without gas fluxes they

cannot correlate specific cellular processes back to the P700 redox kinetics, and how the changing gas flux rates may or may not change the kinetics. Another issue with Aihara *et al's.*, (2016) paper, and many papers on this subject, is that relative estimates of CEF are being performed under FR light, and not in actinic light. Therefore, the resulting data could be of questionable biological significance to 'photosynthetic' electron transport dynamics. This critique is mostly designed to highlight the power of the integrated MIMS/P700 system. With such a system, it was possible to begin ascribing specific processes, and their level of function, to changes in redox values in PSI.

5.5.4 *Alternative electrons depressed value determined for P_m*

An obvious problem with the P700 data collected during measurements discussed in this Chapter was the depression of the relative level of P700 oxidation under weak FR illumination, discussed in 5.5.2. This became especially apparent at temperatures that resulted in significant damage to PSII and as discussed above, were possibly subject to a high influx of alternative electrons via the oxidation of carbohydrates. In the 60 °C and 62 °C panels of Fig. 5-5, the 'ideal' data set was achieved. There, the red curve of $P700_{max}$ data is clearly higher than the black $Y(I)$ curve. However as the incubation temperatures increased, especially in the 65 °C and 67 °C panels, the relative height of the red curve was depressed compared to the black one, indicative of a lower level of P700 oxidation during the$P700_{max}$ measurement, in comparison to the $Y(I)$ data. This is an unusual set or results, at face value, considering the $P700_{max}$ measurement was designed specifically to maximise P700 oxidation.

The $P700_{max}$ data relies on preferential oxidation of P700 to develop a highly oxidised baseline, which ought to be around 85 % to 90 % of the maximal value obtained after the saturating pulse. Recall the analysis of the relationship between these two values presented in the top panel of Fig. 5-6. Especially for data at 65 °C and 67 °C, it was suggested that an alternative source of reductant to PSII seemed to depress the steady state level of P700 oxidation under weak FR illumination. A comparison of the 65 °C and 67 °C panels of Fig. 5-5 not only adds weight to this conclusion, but implies that the extent to which P700 oxidisation was depressed was far more significant than data in Fig. 5-6 suggests.

Consider the level of P700 oxidation that would occur in the following situation: samples suffering inhibition to over 95 % of PSII activity were then exposed to the 500 µE actinic illumination, to which strong FR and a saturating pulse were added. It is a fair assumption to state that the population of P700 oxidised under these conditions would be close, or equal, to 100%. In fact, in the 65 °C panel of Fig. 5-5 it is clear that the value of P_m and P_m' reach parity. This is why in 5.2.1 it is described that assumptions about P_m were changed and $P_m = P_m'$ was used in the calculation of values for b and c. This is also the reason that the value for $Y(NA)$ reaches zero in Fig. 5-2.

At 67 °C the situation is yet more pronounced. As the data in the 67 °C panel of Fig. 5-5 clearly illustrates, the entire $Y(I)$ curve has reached a higher level of oxidation then the entire $P700_{max}$ measurement. Furthermore, the level of change occurring in the $Y(I)$ values between solely actinic illumination and the addition of the strong FR light and saturating pulse becomes increasingly negligible – evidence that PSII derived electrons were contributing very little to almost zero reductive capacity to the system. As such, the claim that the value for $P_m = P_m'$ is very strong. These observations are highly consistent with the idea that an alternative source of reductant, most probably the oxidation of stored sugars, was efficiently reducing $P700^+$ under weak FR light, to a level that severely depressed the signal.

At 70 °C the difference between the curves in Fig. 5-5 reduced markedly once again. The Y(I) measurement = the P700max peak. This is consistent with the analysis of the reduced proportional oxidation in weak FR light between the steady state and the saturating pulse, discussed in 5.5.2 and presented in the top panel of Fig. 5-6. There, at 70 °C the level of oxidation in the weak FR light was returning to levels less affected by alternative electrons. It is also consistent with the reduced rate of dark re-reduction discussed in 5.5.3 and presented in the lower panel of Fig. 5-6.

On the one hand it would have been ideal to realise during experiments a need to increase the strength of the weak FR light. On the other hand, not changing the irradiance provided the opportunity to observe the increased flux of alternative electrons on levels of $P700^+$.

As such, the sum of the data interpretation of the $P700_{max}$ and $Y(I)$ signals discussed in sections 5.5.2, 5.5.3 and 5.5.4 is greater than the parts. Further conclusions that:

- examination of the data presented in Fig. 5-3 suggested that PSI turnover functioned at rates exceeding that driven by remaining PSII activity
- correlations were found between rates of respiration (discussed in Chapter Four) and rates of alternative electron re-reduction of $P700^{+}$

provide a number of data sets consistent with the hypothesis that reductant from the oxidation of sugars replaces the flux from PSII, as this complex suffers inhibition due to thermal damage.

5.6 Conductivity measurements of electrolyte leakage & cell lysis

In all of the data presented and discussed throughout this chapter the trends seem to relax back, disappear, or become otherwise nonsensical at around 70 °C, and certainly by 75 °C. Including gas flux data in the previous Chapter (Four), there is strong evidence that something catastrophic happened to cells at this range of temperatures.

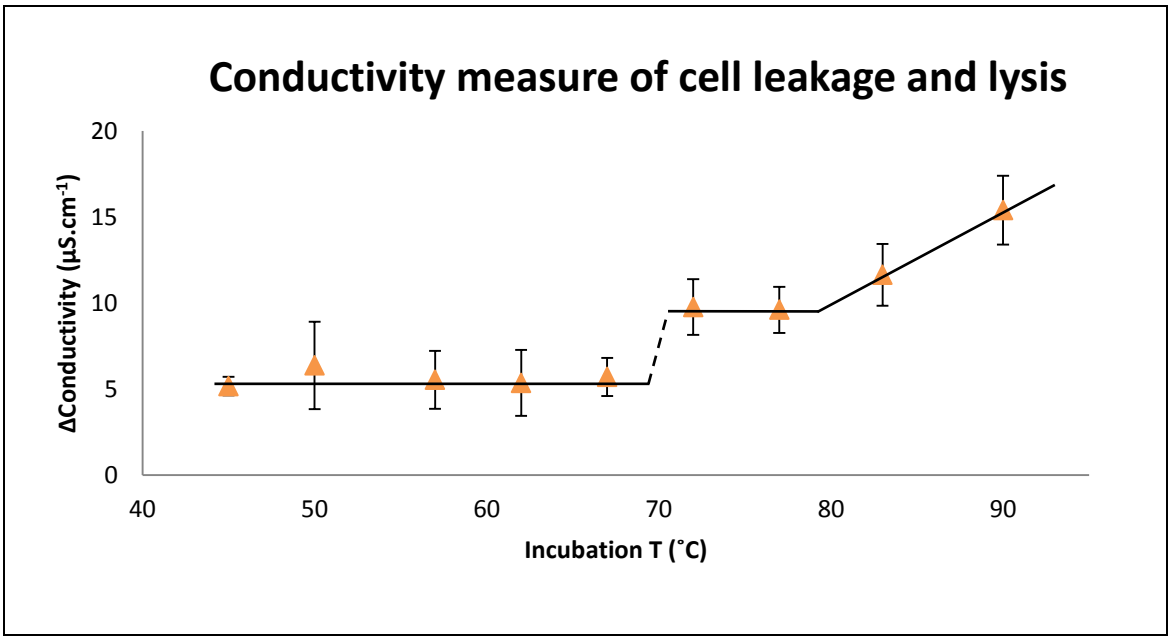

Fig. 5-7 : Conductivity measurements versus incubation temperature: a proxy for membrane rupture and cell lysis, measured after five minute dark incubations of liquid samples at the temperatures stated.
Three independent cultures were harvested, pelleted and rinsed twice in MQ H_2O, standardised to a [Chl] of 14 $\mu g.mL^{-1}$ before an initial measurement was made. Samples were then incubated for five minutes in darkness, before being spun back down and a final measurement was made. Data reported is the difference in initial and final conductivity, averaged from the three independent experiments, reported with Standard Deviation. The lines were drawn in to help illustrate the changes and define the period of the 'plateau' discussed in-text.

In order to gauge the relative level of cellular damage through a somewhat physical means, the level of electrolyte released by the cells into their medium was estimated through

changes in its electrical conductivity after incubations. This experiment is a repeat of that conducted by Inoue *et al.*, (2000). Increased conductivity was considered evidence for increased electrolyte leakage. Changes to cellular permeability versus complete lysis were subjectively made, due to the limitations of this measurement.

It can be observed from the data presented in Fig. 5-7 that there was no change to the amount of cellular leakage across incubations, until between 67 °C and 72 °C where the broken line indicates a 'step-change'. This suggests that temperature somehow increased the amount, or rates, of electrolytes exiting the cells at around 70 °C, resulting in an approximate doubling of the conductivity measured. This 'step' remained level until some temperature between 77 °C and 83 °C, where it then started to climb steadily with further increases in incubation temperature.

That no change occurred to samples at the lower temperatures is consistent with the idea that there was no significant structural cellular damage/membrane rupturing at these temperatures. The single step up between 67 °C and 72 °C suggests that ions were leaking across the membrane through potential lesions, or an increased activity of some form of ion exchange pumps, perhaps during the period of elevated temperature during the incubation. At temperatures > 77 °C however, the constant increasing trend in the data is consistent with some severe damage, possibly lysis. It is hard to know exactly from this method alone.

Frustratingly, this experiment was conducted early during the research period, at a time before the 10 minute incubation protocol had been determined to be best for examining the impact of thermal damage on cells. As such these cells were incubated for only five minutes in the dark, in contrast to all other data in this chapter where the incubation was for a 10 minute dark period. Furthermore, these cells were not left for five minutes at the optimal temperature before measurements, as was conducted with other incubation experiments in this thesis, and by Inoue et al., (2000).

It is difficult to know for certain what the impacts of increasing the incubation period would have had on the results, specifically:

- Would the level of ionic leakage have potentially been detected at a lower temperature? (Say, 67 °C?)
- Would the 'plateau' observed between 72 °C and 77 °C have still occurred?

The analysis of data in this chapter suggests that significant cellular rupture or significant leakage would not have occurred at temperatures lower than 70 °C. For example, gas fluxes in Fig. 4-5, and P700 data of both $P700_{max}$ and $Y(I)$ curves in Fig. 5-5, all show clear data at 67 °C (after ten minute incubations). However, these same sets of data indicate a large decrease in activity at 70 °C and then effectively zero functionality at 75 °C.

This suggests that the 'plateau' was lost after a longer incubation period, and cell rupture/lysis that began at 70 °C was severely exacerbated by 75 °C. This is more consistent with the original experiment performed by Inoue *et al.*, (2000). In their results two clearer phases of damage are also found, without the plateau. The first is considered a slow but constant increase correlating to temperature: increasing between 50 and approximately 73 °C. Then a second, higher rate was determined for > 75 °C.

5.7 Chapter 5 conclusions: oxidation of stored carbohydrates seemed to reduce $P700^+$ as PSII failed due to high temperature

In Chapter Four, evidence based on an analysis of gas fluxes in cells incubated at a range of damaging temperatures was used to support the conclusions that PSII activity ceased in BP.1 cells at temperatures that were lower than the functional activity of other key cellular processes: namely carbon fixation and respiration. Respiration, (as defined broadly in this thesis as the net efflux of CO_2 and uptake of O_2 in the dark, relating to various pathways involved in the oxidation of energy storage molecules such as glycogen) was not only found to function at elevated rates where PSII had been severely damaged, but remained active during illumination.

In Chapter Five, evidence based on the redox kinetics of P700 was used to expand upon these initial findings, to conclude that the *in vivo* activity of PSI was not causatively correlated with PSII, in the way that Rubisco based carbon fixation seemed to be in Chapter Four. This was determined primarily by the observation that values of the photochemical yield of PSI remained much higher than the activity of PSII alone could likely have supported (Fig. 5-3). The source for reductant utilised by the P700 photosystem was hypothesised to be that which was liberated by the oxidation of sugars, and enhanced potentially by cyclic electron transport. The former point was supported by a large number of observations revealed

through comparative examination of raw P700 data across the range of thermal damage including that:

- Increased rates of illuminated respiration correlated with a decrease in the level of steady state P700 oxidation under weak FR light, determined through a comparison to the saturating pulse, but especially obvious against the oxidation levels measured in full actinic irradiance when cells possessed only a small fraction of functional PSII.
- Cells inhibited in PSII function exhibited rates of dark P700 re-reduction consistent with the idea that it was driven by an alternative source of reductant to PSII. This rate did not correlate to measured rates of respiration, as a significant decrease in respiration rates did not change the rate of re-reduction between samples at 65 °C and 67 °C. This led to the further hypothesis that the alternative pathway for reductant to drive PSI activity has a limited capacity, compared to the total capacity for cellular respiration. Simple $P700^+$ back reactions were discounted as a source of the similarity between rates of re-reduction at 65 °C and 67 °C, through comparison with cells that had suffered severe damage (70 °C and 75 °C) and a loss of respiration, in which P700 was nonetheless able to undergo oxidation, but re-reduced at a much slower rate.
- The PSII kinetic area was reduced approximately six fold at 65 °C compared to the maximal value. This was consistent with the overall trend in the activity of PSII determined with gas fluxes, but not close to matching in magnitude. This was interpreted to be consistent with the idea that an alternative reductant was inhibiting the rate of re-oxidation in the weak FR light.

To specifically answer the three aims, stated at the start of this chapter:

- to observe the function of PSI after standardised thermal incubations, *in vivo*
    - This was achieved, and provided a large amount of data to support conclusions based on the gas flux data analysed in Chapter Four
- to investigate the thylakoid membrane's functionality, via PSI redox activity, to provide evidence that cellular respiration within BP.1 can utilise thylakoid components after PSII has been inhibited by thermal damage
    - Based on the conclusion that respiratory reductant was likely able to reduce the PQ pool, and from there drive $P700^+$ re-reduction, the P700 data

strongly supports the conclusion that primary thylakoid membrane components were still functional post PSII inhibition.

- to find evidence in support of the idea that PSI may still play a significant functional role in cells suffering severe thermal inactivation of PSII
    - That the P700 system was undergoing turnovers in excess of what the very small proportion of remaining PSII activity could support, and evidence was provided to exclude these electrons (PSII sourced) being cycled around PSI, there is support to the idea that PSI may play an active role in maintaining the system's energetic supply once PSII has been inhibited by thermal damage.

The final conclusion from analysis of data in this chapter is that the hypothesis is well supported: As PSII suffers damage leading to inhibition from elevated temperatures, alternative sources of reductant were sourced to maintain a sufficient level of PQ reduction to enable numerous complexes downstream of PSII to continue functioning. As these electrons were likely sourced from carbohydrates stored in the cells, this conclusion is consistent with the hypothesis that PSI became a component of the respiratory processes. This outcome may enable the maintenance of a pH gradient across the thylakoid membrane, potentially increasing the amount of ATP generated per sugar oxidised, and could also elevate lower potential NADH into highly reductive NADPH (without using cellular energy). The final outcome of this is the possibility that the cells could then use this system to poise the thylakoid membrane to enable cyclic electron transport.

This latter point is considered further in the following chapter. A mutant of Synechocystis 6803 (inhibited in the function of Ndh-1 complex resulting in impaired respiration and lacking a cyclic electron pathway) is used to compare fluxes through PSI in the WT. The results support the hypothesis that cells are able to cycle electrons sourced from the oxidation of sugars through the cyclic pathway

Chapter 6.

Cyclic Electron flux around PSI

Recycling respiratory reductant?

Chapter summary:

In Chapters Four and Five, evidence was presented to support the hypothesis that the tolerance to transient damaging high temperatures of key cellular processes in BP.1 cells, including respiration, carbon fixation and PSI activity, was greater than PSII. This result supported the published in vitro measurements of isolated components, downstream of PSII (Koike and Katoh, 1980, Koike et al., 1982, Sonoike et al., 1990). A key finding in Chapter Five, presented in Fig 5-3, was that the photochemical yield of PSI ($Y(I)$) exhibited a proportionally slower decrease with damaging temperatures, then the functionality of its primary donor, PSII.

Analysis of gas flux data (in section 4.4.2), generated simultaneously with P700 data that enabled the comparison to be directly made, suggested CO_2 fixation still occurred at rates equal to the very small remaining proportion of PSII function (< 5%) after 65 °C incubations. This implied all PSII derived electrons were progressing linearly through to the Calvin Benson Bassham cycle, leaving no reductant spare for poising of the thylakoid for cyclic activity around PSI. This would have been the obvious explanation for greater fluxes through PSI, than was generated at PSII. Most authors lacking such comprehensive gas flux data would likely have reported elevated cyclic electron transport through PSI as a final conclusion. However due to the MIMS data, a different hypothesis was sought.

That respiratory activity was found to be functional during actinic illumination, once PSII has suffered severe inhibition (section 4.2.2), the hypothesis was formed that PSI became an active component in respiration. This hypothesis was supported through the analysis of P700 data in section 5.5.

The conclusions led to the proposal of a third hypothesis: If cells suffering severe PSII inhibition could reduce $P700^+$ with alternative reductant sourced through respiration, could this reductant be cycled around PSI, maintaining this photosystem in a functional state, and in effect 'recycling' the energy liberated through the oxidation of stored carbohydrates?

To answer this question, a technique for estimating rates of cyclic flux around PSI, established in angiosperms but unpublished in cyanobacteria, was adapted. It required the use of the NDH-1 mutant of 6803, and as such, the data was no longer generated in a thermophile. The results were not as clear as hoped, but do not discount the hypothesis.

Establishing the rational for 'recycling' respiratory reductant

Cyclic electron flux around PSI (CEF) is broadly defined as the reduction of the PQ pool with Fd, sourced from the oxidation of the P700* of PSI (Rumeau *et al.*, 2007). Pseudo cyclic flux (CEF_p) is the transfer of an electron from PSII through to a terminal oxidase downstream of PSI, described as the water-water cycle (Asada, 2000). Depending on the pathway, there can be a number of intermediate steps (in chloroplasts, this is the Mehler reaction (Badger *et al.*, 2000)), or a direct reduction of O_2 to H_2O (in cyanobacteria, the Flv1,3 proteins (Ermakova *et al.*, 2016)). Both of these pathways shift the ratio of NADPH to ATP, by pumping protons without the reduction of $NADP^+$. Whereas CEF can be considered a mechanism to ensure sufficient acceptor side is maintained for PSI, the pseudo cycle (CEF_p) is more of a regulatory 'safety valve'. Not only to shift the ratio of energetic molecules ATP and NADPH, but to modulate the redox potential and potentially remove excess reductant from the system. In both of these pathways, it is generally assumed that the donor to PSI is PSII: by Asada's definition, it is the 'water-water cycle'. However the progenitor to cyanobacetria, non-oxygenic bacteria such as the green sulphur bacteria, could source reductant from external donors like HS^-, H_2 or $FeSO_4$ (Widdel *et al.*, 1993, Falkowski *et al.*, 2008), and cycle this around their Type I bacterial photosystem to generate ATP. As such, a precedent exists in the evolutionary history of photosynthesis, that such a pathway can utilise reductant from a source other than PSII, to perform CEF.

The data in Chapter Four and Five support the idea that reductant from the respiratory chain was able to act as a surrogate for PSII, when this photosystem was inhibited by high temperature damage. It was hypothesised that reductant entering the PQ pool, via the SDH and NDH-1 complexes, preferentially reduced $P700^+$ over the terminal oxidases COX and Cyd. During illumination, it is well known that alternative and respiratory oxidases are poor competitors for reductant, compared to photosynthetic components including the cyt-b_6f complex, and the acceptor side of PSI (Bukhov and Carpentier, 2004, Nawrocki *et al.*, 2015). Once the PQ pool has been reduced, the source of the electron becomes unimportant, as far as the biochemistry is concerned. As such the question was posed, could respiratory reductant that reduces the PQ pool, poise the thylakoid membrane and allow for CEF to operate? If possible, does it mean that the oxidation of a single carbon compound could be used to drive PSI photochemistry, on multiple 'cycles' through the system? To clarify, this is not to say that a single molecule can be oxidised and its electron

be 're-cycled' indefinitely. However there seems to be no reason why reductant from respiration must follow the standard 'chlororespiratory' route to reduce O_2 (Rumeau *et al.*, 2007).

To avoid photodamage to PSI, cyanobacteria ensure a large acceptor side capacity is always available to keep the system in its oxidised form. Should PSII be inhibited, PSI is safe from photo-damage (Shimakawa *et al.*, 2016). However, in this 'safe' mode, it is not contributing to the cell's energy requirements. Light energy in its environment is not being translated into useful energy for the cell. However, 'bleeding' a slow stream of reductant into the PQ pool via respiration could provide the oxidised P700 system with an easy to manage rate of electron donation. This would keep the photosystem primarily in the 'safe' oxidised state, but would enable it to contribute to generating a proton gradient. To describe this idea, the term *'energy leveraging' w*as coined. This is a termed borrowed from finance, describing the use of borrowed money to generate more money, through investment. Similarly, cells could directly 'spend' the reductant released through respiration in cellular repair. However, using the reductant to enable PSI turnovers can be considered an investment, allowing the photosystem to function, 'leveraging' more energy from its environment.

To test this hypothesis, steady state fluxes of CEF were measured across a range of increasing incubation temperatures. The experimental aim was to observe how increasing incubation temperatures affected the estimated rate of steady state CEF, particularly at temperatures where PSII became severely inhibited through thermal damage. An established methodology for measuring steady state CEF had been published in the literature (Hu *et al.*, 2013, Kou *et al.*, 2015). However, it was designed for, and only ever used with angiosperms. No steady state estimations of CEF have been published from a cyanobacterium. Before the method could be applied to cyanobacterial samples however, it was first necessary to test that the hardware, software and user, were generating accurate data with the newly integrated MIMS/P700 system. As such, the first aim was to reproduce the published values with greenhouse grown spinach discs (Kou *et al.*, 2013). Once the system's performance was validated, it was then possible to attempt the CEF estimations with cyanobacterial samples. However, in order to calculate the flux of electron through P700, it was necessary to estimate the fraction of light partitioned to PSI. To do this, the equations demand that no CEF or back reactions within P700 can be occurring. The only

way to inhibit CEF in cyanobacterial cells is to inhibit the NDH-1 complex and this required the use of the M55 strain of 6803 (Ogawa, 1991), inhibited in CEF. Using the mesophilic strains for this experiment was an unfortunate step away from making a direct comparison with the BP.1 results. However, within the constraints of this project there was no other option.

6.1 Reproducing reported CEF values in Spinach leaf discs

In order to validate that the MIMS/P700 integrated system was operating correctly I attempted to measure CEF in an already published system, greenhouse grown spinach. Fred Chow has worked hard with numerous visitors to establish and publish the P700 CEF measurement in spinach. They used a Hansatech O_2 electrode and the light pulse method to derive accurate rates of gross O_2 evolution, which can be multiplied by four to estimate the flux of electrons entering the linear electron transport chain. This value is termed LEF_{O_2}, the linear Flux of Electrons based on O_2 evolution. Applying the MIMS to this measurement allowed for their assumptions regarding the accuracy of their determination for Gross O_2 measurements, to be tested - by ascertaining 'true values' for Gross O_2 evolution, instead of assuming that dark O_2 Uptake immediately post illumination was the same O_2 Uptake rate occurring during steady state illumination (Walker, 1987). The work conducted with spinach was beneficial for a number of reasons. Experimentally it provided a known system in which to:

- iron out a number of issues in the newly modified 'gas phase' MIMS cuvette
- establish and then rectify initial problems in the P700 LED illumination system
- compare my reconfigured MIMS data analysis spreadsheet, with an output in units of μmol(electron).m^{-2}.s^{-1}, necessary for CEF measurements, against well-established benchmarks.

The outcomes from this initial experimental validation was both confidence in the reliability of the integrated P700/MIMS system, and the data generated was used in a stand-alone figure, published in a special feature on current methodologies for measuring CEF, published in Photosynthesis Research (Fan *et al.*, 2016).

6.1.1 *Determining fi and $\Delta Flux$ in AA^+ & AA^- spinach discs*

The method to determine CEF was based upon the simple concept that:

$$CEF = \Delta Flux \text{ through the two photosystems}$$

As such, the method relied on determining the electron fluxes through the two photosystems, and the assumption of course being, that the difference = electrons cycling around PSI, as described by Kou et al. (2013).

Mathematically, this is described as

$$\Delta Flux = ETR1 - LEF_{O_2}$$

Where:

LEF_{O_2} = Flux of electrons generated at PSII (4 x Gross O_2 evolution rate)

and

$ETR1$ = Electron flux through PSI = $Y(I) \times A \times I \times f_i$

In which case:

$Y(I)$ = Photochemical Yield of PSI (determined via steady state P700 measurements, as described in section 5.2.2)

A = Absorptance (assumed to be 0.85 for leaves, (Evans and Poorter, 2001))

I = Irradiance (as set in experiment, measured between 400 and 700 nm)

f_i = the fraction of absorbed light partitioned to PSI

As a measure of the power of the integrated P700/MIMS system, all terms except for f_i can be simultaneously and directly measured. By rearranging the $ETR1$ equation, f_i can be solved for, if the flux of electrons through PSI is known.

$$f_i = \frac{ETR1}{Y(I) \times I \times A}$$

This counter-intuitive approach, that calculating the rate of electrons through PSI can only be conducted when the flux of electrons through PSI is known, makes sense when one considers that, under certain conditions in which CEF is absent:

$$ETR1 = LEF_{O_2}$$

Therefore, under conditions where CEF has been inhibited, $LEFO_2$ can be substituted into the equation for f_i, giving:

$$f_i = \frac{LEF_{O_2}}{Y(I) \times I \times A}$$

Once f_i has been determined for a set of conditions it is then possible to apply the original equation:

$$ETR1 = Y(I) \times A \times I \times f_i$$

to samples under conditions in which $ETR1 \neq LEF_{O_2}$, when CEF is active.

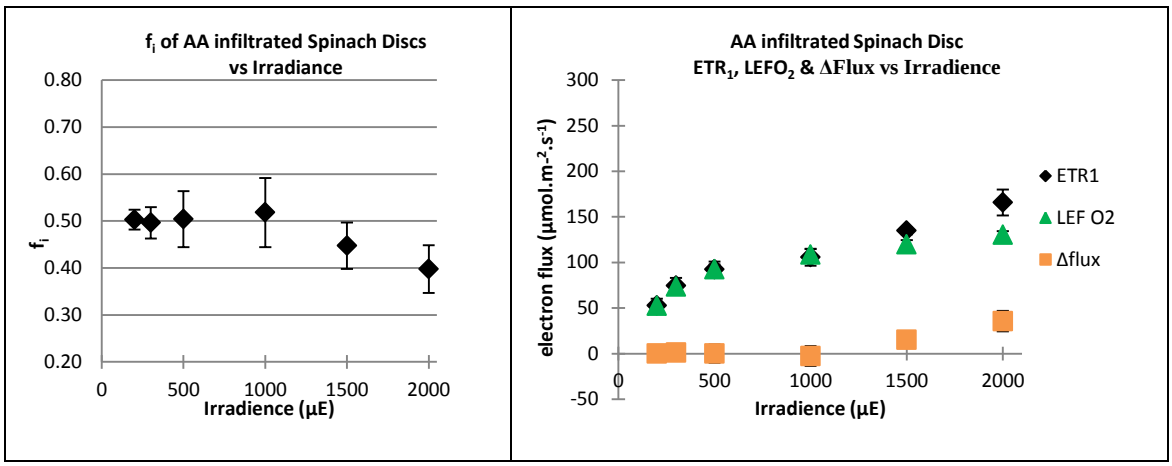

Fig. 6-1: Measuring fi and determining Δflux in cyclic electron flux inhibited spinach discs.
In the left panel, values for fi determined in spinach leaf discs inhibited in cyclic electron transport via vacuum infiltration with 200 µM antimycin A in 1% EtOH. The right panel presents $\mathbf{LEF_{O_2}}$, $ETR1$ and $\Delta Flux$ of antimycin A infiltrated spinach discs. The addition of AA inhibits the PGR-5 protein complex, inhibiting the transfer of electron between P700 and the NDH-1 complex, thus inhibiting cyclic electron transport. This condition is used to determine fi, the fraction of absorbed light portioned to PSI. It is necessary to determine fi under conditions of zero cyclic flux to create the conditions that $\mathbf{LEF_{O_2}}$ = Flux of electron through P700. Conditions: Temperature at 25 °C, CO_2 2 to 5 % maintained through 1M $NaHCO_3$ reservoir at pH 9.0 within cuvette. n = 3 ± SE

To inhibit CEF in spinach discs they were vacuum infiltrated with 200 µM Antimicin A (AA) (Kou *et al.*, 2013). AA targets the function of the PGR-5 protein, associated with the majority of CEF in higher plants (Tikkanen *et al.*, 2015). Steady state values for LEF_{O_2} and $Y(I)$ were measured across a range of irradiances from low (200 µE) to saturating (2000 µE), at 25 °C within a saturating [CO_2] atmosphere (≈5%), where µE is an abbreviation for µmol photons.m^{-2}.s^{-1}.

Under these conditions of impaired CEF, f_i was determined, with the results presented in the left panel of Fig. 6-1. The data clearly shows f_i remained stable at 0.5 – or a 50/50 split between the two photosystems, from 200 µE to 1000 µE. This value is both logical, and supported by the literature (Kou *et al.*, 2013). At high irradiances however,

>1000 µE, both $\boldsymbol{\Delta Flux}$ and $\boldsymbol{f_i}$ begin to shift away from the consistent value measured, for reasons relating to reduced $\boldsymbol{Y(I)}$ values, discussed below in section 6.1.3.

The established value for $\boldsymbol{f_i}$ of 0.5 was used to calculate the $\boldsymbol{ETR1}$ of AA infiltrated (AA^+) leaf discs, based on the equation described above. The $\boldsymbol{LEF_{O_2}}$, $\boldsymbol{ETR1}$ and calculated $\boldsymbol{\Delta Flux}$ of AA^+ spinach discs was then plotted as a function of irradiance, presented in the right panel of Fig. 6-1. Significantly, the data shows $\boldsymbol{\Delta Flux}$ remained at or near zero across all irradiances, until 1500 µE, the same irradiance at which $\boldsymbol{f_i}$ reduced below 0.5. This implied that rates of PSII based electron transport ($\boldsymbol{LEF_{O_2}}$) matched the electron flux through PSI. This was interpreted as no CEF around PSI (Kou *et al.*, 2013), and suggested that CEF was inhibited at up to 1000 µE. This validated that suitable conditions had been determined to inhibit CEF, and that the $\boldsymbol{f_i}$ value determined ≤ 1000 µE were therefore accurate.

The combined contributions of back reactions occurring in the P700 reaction centre driven by acceptor side limitation (Kou *et al.*, 2015), and elevated photon flux at irradiances > 1000 µE which presumably saturated the capacity of the system to maintain a 'forward momentum' (Rutherford *et al.*, 2012), likely led to a decrease in the $\boldsymbol{f_i}$ value determined from 0.5. This will be discussed further in 6.1.3.

6.1.2 *CEF in AA^- Spinach discs*

Having successfully inhibited CEF and determined $\boldsymbol{f_i}$ in 6.1.1, it became possible to determine steady state $\boldsymbol{ETR1}$ rates in fully functional, WT leaf discs. Measurements were conducted under identical conditions to those described above, with the results presented in Fig. 6-2. Significantly, the trends for $\boldsymbol{\Delta Flux}$ between the AA^+ (right panel of Fig. 6-1) and non-infiltrated (AA^-) discs (Fig. 6-2) were clearly different. Where a strong positive correlation was found in the AA^- discs to increasing irradiance, the AA^+ discs showed no correlation, until 1500 µE.

This suggests that between 200 and 1000 µE, $\boldsymbol{\Delta Flux}$ in AA^- discs was solely attributable to CEF, whilst at irradiance > 1000 µE, the majority of $\boldsymbol{\Delta Flux}$ in these discs was still a result of CEF, but back reactions within PSI may have contributed to the calculated value. Back reactions return electrons to the donor side of PSI, but these electrons have been transferred through PSI in the first place as part, counting as a component of $\boldsymbol{ETR1}$. Whilst increasing acceptor side limitation, $\boldsymbol{Y(NA)}$, discussed below in 6.1.3 may have driven the increased rate of back reactions in AA^+ discs, this trend was significantly lower in the

non-infiltrated discs. As such, the contribution of back reactions to $\boldsymbol{\Delta Flux}$ was likely to be much less significant in AA$^-$ discs. However, the extent of its possible contribution could not be measured here.

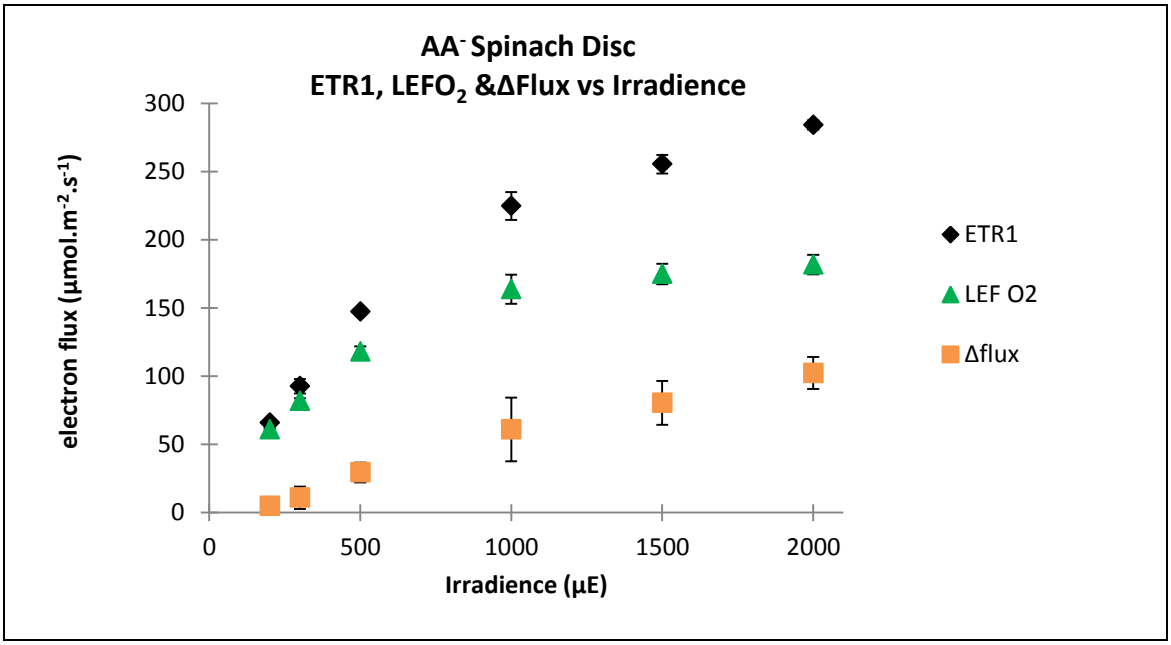

Fig. 6-2: $\boldsymbol{ETR1}$, $\boldsymbol{LEF_{O_2}}$ and $\boldsymbol{\Delta Flux}$ as a function of irradiance measured in non-infiltrated spinach discs. $ETR1$ calculated with fi value determined under conditions that exclude cyclic electron transport. $\Delta Flux$ = difference between linear electron flux measured through Gross O_2 evolution and flux through P700, determined as described in text = electrons cycled around P700. Conditions: Temperature at 25 °C, CO_2 2 – 5 % maintained through 1M $NaHCO_3$ reservoir at pH 9.0 within cuvette. n = 5 ± SE.

Beyond a comparison to the calculated $\boldsymbol{ETR1}$ rates in the right panel of Fig. 6-1, a key check that the data for AA$^-$ discs 'makes sense' is that the $\boldsymbol{\Delta Flux}$ at low irradiance (200 µE) was very low, as expected (Kou *et al.*, 2013), and increased with irradiance. The experiment closely resembles the results of previous work by Fred Chow, his students and collaborators (Kou *et al.*, 2013), and shows that the assumptions they have made when using the Hansatech O_2 electrode system were sufficiently accurate to measure CEF under steady state conditions. The data in Fig. 6-2 was published in (Fan *et al.*, 2016).

6.1.3 *Comparing $\boldsymbol{Y(I)}$, $\boldsymbol{Y(NA)}$ & $\boldsymbol{Y(ND)}$ in AA$^+$ and AA$^-$ Discs*

When undertaking P700 measurements to determine the photochemical yield of PSI ($\boldsymbol{Y(I)}$) as a function of irradiance during steady state photosynthesis, values for the non-photochemical yield of PSI, namely the Donor side limitation ($\boldsymbol{Y(ND)}$, due to oxidized P700) and Acceptor side limitation ($\boldsymbol{Y(NA)}$, due to reduction of electron acceptors), were also determined, as per the explanation in section 5.2.2. Plotting these values as a function of irradiance, from the data generated with AA$^+$ and AA$^-$ spinach discs, provided another layer of data with which to interpret the $\boldsymbol{\Delta Flux}$ results presented above. This analysis can be used

to interpret why calculated values for f_i shifted away from 0.5 at higher irradiances in AA$^+$ discs in Fig. 6-1. It can also illustrate the significant role played by CEF in higher plants for managing the energetic balance, on both the donor and acceptor sides of PSI.

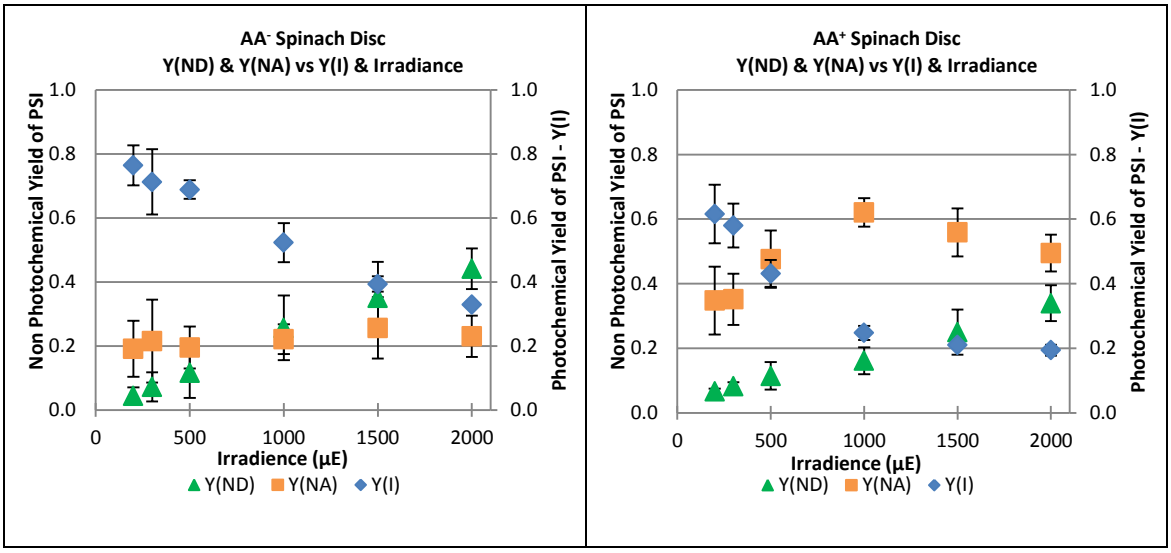

Fig. 6-3: $\boldsymbol{Y(I)}$, $\boldsymbol{Y(NA)}$ and $\boldsymbol{Y(ND)}$ of infilitrated vs non infiltrated spinach discs vs Irradience.
Comparison of the photochemical yield of PSI $Y(I)$ and the non photochemical yields, donor $Y(ND)$ and acceptor side $Y(NA)$ limitations, provides more information with which to interpret the electron fluxes through spinach discs inhibited in PGR-5 function by infiltration with 200 µM Antimycin A; to inhibit the majority of cyclic electron transport. Data was collected simultaneously with that displayed above in both Fig. 6-1 and Fig. 6-2, hence conditions were identical.

Interpretation of data in Panel A of Fig. 6-3 indicated that $\boldsymbol{Y(I)}$ of AA$^-$ discs was inversely correlated to irradiance, starting at a value of 0.76 at 200 µE and reducing very consistently across the entire range of irradiances to finish at 0.33 at 2000 µE. The $\boldsymbol{Y(NA)}$ in AA$^-$ discs remained very steady across the entire irradiance range, indicating that sufficient acceptors were available under steady state conditions, to oxidise P700* at all irradiances measured. This suggested that the loss of photochemical yield in non-infiltrated leaf discs was primarily caused by a steady increase in $\boldsymbol{Y(ND)}$. This term showed a strong positive correlation to irradiance across the entire range measured, a steady linear response mirroring that of $\boldsymbol{Y(I)}$. This was possibly driven by, and evidence for, the idea that the cyt b_6-f complex was a rate limiting, or regulatory, component in electron transport along the thylakoid membrane (Laisk and Oja, 1995). It became increasingly apparent as PSI began to turnover more rapidly than P700$^+$ could be re-reduced at high irradiance.

In the right panel of Fig. 6-3, data for AA$^+$ discs (in which CEF mediated through PGR-5 was essentially eliminated) shows a very different response to increasing irradiance. Not only is the overall $\boldsymbol{Y(I)}$ in these samples lower than the AA$^-$ samples, starting at a maximum of 0.6 at 200µE and finishing at 0.19 at 2000 µE, but in contrast to the AA$^-$ discs the decrease was not consistent against irradiance. It dropped very sharply between 200 µE

and 1000 µE (from 0.60 to 0.25), before reducing only slightly between 1000 and 2000 µE (0.25 to 0.19). The explanation for this loss in photochemical yield is not as straightforward as in the AA^- discs, and quite a lot of information about the role of cyclic mediated flux through PSI can be elucidated from a comparative analysis of the $Y(ND)$ and $Y(NA)$ curves in these samples.

The key driver of the reduction in $Y(I)$ in AA^+ discs across the initial range of irradiances (200 to 1000 µE) was the sharp increase in $Y(NA)$, which showed a very strong positive correlation across the initial irradiance range. The values climbed from 0.34 at 200 µE to a maximum value of 0.62 at 1000 µE. When compared to the AA^- discs, in which $Y(NA)$ remained steady throughout the measurement range, the impact of losing CEF became rapidly apparent. According to the data presented, the inhibition of CEF through PGR-5 amounted to a 25% loss of PSI photochemical yield at 200 µE, which climbed to a 48% reduction at 1000 µE when compared to the values for AA^- discs. This was driven primarily by a limitation of acceptor side capacity. The data also shows that $Y(ND)$ was also climbing with irradiance, in both the infiltrated and non-infiltrated discs. At up to 1000 µE irradiance however, the difference was not only marginal, the level of $Y(ND)$ was in fact lower in AA^+ samples. This was telling: a lower $Y(ND)$ can indicate that the acceptor side limitation of PGR-5 inhibited samples was high enough to physically slow the fluxes through PSI, to the extent that it reduced the amount of $P700^+$ being generated, and therefore the demand to be re-reduced had also diminished.

Further examination of the difference in $Y(ND)$ explains the other key trend in the $Y(I)$ and $Y(NA)$ data for AA^+ discs; $Y(I)$ levels stopped dropping rapidly and declined only minimally across the following 1000 µE (from 1000 µE to 2000 µE) whilst $Y(NA)$ values actually decrease across this range, in stark contrast to AA^- discs. Where PGR-5 was able to accept electrons from P700 (indirectly) and donate them back to the PQ pool or b_6-f complex, the data showed an increased capacity for PSI to be adequately serviced according to its redox needs – ie, each turnover of the photosystem was met by an available acceptor to oxidise P700*, and a donor to re-reduce $P700^+$, increasing the efficiency of the operations and resulting in a higher $Y(I)$, as already discussed. Above 1000 µE, $Y(NA)$ in AA^+ discs decreased because $Y(ND)$ had reached a level that was possibly driven by a limitation in either PSII activity, the transfer of electrons through the cyt-b_6f complex or a combination of both (Laisk and Oja, 1995). This is evidenced by the fact that LEF_{O_2} plateaued and turned

over (or gently peaked), at 1000 µE, and that AA^- samples also recorded a similar increase in $Y(ND)$. The data suggests that that the extra electrons injected to b_6-f via PGR-5, which may have served to reduce the level of $Y(ND)$ in AA^- samples, no longer made up any difference between the donor side capacities of AA^- and AA^+ samples, because the limitation in electron availability had reached a point of saturation for the b_6-f complex (and PSII as stated).

Once the level of irradiance driving PSI photochemistry reached this level it was clear that further decreases in $Y(I)$ were driven primarily by $Y(ND)$, as described above. The implications of this for $Y(NA)$ in AA^+ samples was a reduction in the rate of formation of P700*, with P700 spending more time as the cation awaiting reduction. The level of $Y(I)$ changed only slightly across this range, as the two limitations seemed to be cancelling each other out, instead of increasing each other.

The consequences of this for measurements of f_i were apparent in Fig. 6-1. At elevated irradiances (>1000 µE) the levels for f_i decreased from the otherwise steady value of 0.5, down to 0.4. The combined levels of $Y(ND)$ and $Y(NA)$, which were very high when compared to the AA^- discs, could be the explanation this.

There was a significant probability for the 'electron hole' on $P700^+$ to recombine with an electron residing on the acceptor side of PSI, due to the increased level of $Y(ND)$ at high irradiance, and the loss of electrons sourced through the cyclic pathway. This resulted in a significant increase in back reactions in the AA^+ discs at these high irradiances, which 'count' as an electron moving 'forwards' through the system.

Of course, there wasn't any net electron transfer. This overestimation of $ETR1$ disrupted the accounting used to calculatef_i, causing it to be underestimated. As this drop in f_i is an artefact, it was still considered accurate to use the f_i level of 0.5 when calculating $ETR1$ across all irradiances in AA^- discs (Kou *et al.*, 2013).

6.2 Cyanobacterial cyclic measurements

Using spinach to successfully reproduce published measurements of CEF was a valuable exercise: to iron out problems in the newly integrated P700 and MIMS set up, to validate the accuracy of the method in my system and an opportunity to learn about the interpretation

the data. Work discussed in Chapter 4, utilising the integrated P700 and MIMS measurements to simultaneously monitor the activity of PSI and PSII, as functions of temperature, had demonstrated the utility and accuracy of P700/gas flux measurements from cyanobacteria. These experiments had also driven me into the development of methods, namely the creation of 'cyano discs' (a surrogate for leaf discs) to enable the accurate measurement of P700 in cyanobacterial cells with our system, as discussed at length in section 3.3.3.

The final step was to create conditions under which no CEF was occurring in cyanobacterial cells, to enable the determination of f_i. Unfortunately, the CEF pathway in cyanobacteria differs substantially from that in higher plants, where PGR-5 is the primary intermediary complex involved, easily inhibited with Antimycin-A (Kou *et al.*, 2013). Cyanobacteria utilise a number of routes to cycle electrons back to the PQ pool – primarily, however, through the reduction of the NDH-$1_{1,2}$ complex (Battchikova *et al.*, 2011), by Fd (Peltier *et al.*, 2016), for which no known specific inhibitors exist.

As a result, it was necessary to utilise a well characterised respiratory mutant, the "M-55" NDH-1 Knock Out strain of S*ynechocystis PCC* 6803 (M55) (Ogawa, 1991), known to be impaired in CEF. The determination of f_i still required the addition of a low [AA] (50 μM) to inhibit a putative PGR-5 like component in the strain (Weimin Ma, personal communication); ensuring all CEF was supressed in this strain. Although the use of M55 and 6803 moved the specific relevance of the results away from BP.1 and thermophilic cyanobacteria generally, the possibility to measure CEF in a cyanobacterium, and to test a principle of the 'energy leveraging' hypothesis (See discussion in 7.5), was a worthwhile justification for conducting these experiments.

A large body of evidence in the literature suggests that the thermally weakest component of the mesophilic cyanobacterial strain, *Synechocystis* 6803, is PSII (Inoue *et al.*, 2001). Furthermore, the primary site of thermal lability is the 33 kDa extrinsic subunit (the manganese stabilising protein (MSP)) (Mamedov *et al.*, 1993, Pueyo *et al.*, 2002, Williamson *et al.*, 2007). As such, no work was conducted to reproduce the sort of data, generated with BP.1 cells, and presented in Chapter Four/Five. Instead, use was made of the multitude of published data available for 6803, especially from the comprehensive, *in-vivo* study of the impacts of transient thermal stress on 6803 written by Inoue et al., (2001).

With the integrated MIMS and P700 system successfully used to measure CEF in spinach and a method developed to utilise this system for cyanobacteria, it was almost possible to test the hypothesis that cyanobacteria utilise electrons sourced from respiration to perform CEF in the absence of PSII activity, brought about through severe thermal damage. Two final technical issues required solving, however: to optimise the growth conditions in my bubble lift cultivation system for the coccoid Synechocystis strains, and a simple yet accurate method to determine absorptance from 'cyano discs' needed development.

6.2.1 *Using 6803 and the M55 mutant – growth considerations*

Growing the *Synechocystis* strains in bubble lift cultivation, as had become the standard cultivation method during this project, was somewhat problematic. The coccoid cells were prone to clumping and forming a biofilm on the glass cultivation tubes. Out of concerns that this would lead to heterogeneity of samples, cultures were maintained at a low density (OD_{750} < 1.0) through daily dilution into heavily bleached (to remove organic residues from the glass), well rinsed and autoclaved growth tubes. This methodical approach successfully resulted in homogenous cell samples. In spite of this, as discussed in the following sections, something changed the photosynthetic rates being measured in the WT cells over the course of the CEF experiments.

The cause was unclear; nothing was altered throughout the course of the experimental period with respect to growth conditions or medium – whilst fresh samples were periodically inoculated from axenic plates, maintained by the wonderful technical assistant Lorraine Tucker of the Price Lab. Although it is possible that the WT culture may have suffered some form of heavy contamination, I am unable to provide the evidence to say it did or it did not conclusively because the use of contamination checks was not diligently applied. Although, based on the gas flux data, O_2 consumption rates are not consistent with a heavy contamination and every effort was taken to avoid this happening. At all times sterile techniques were used when taking samples or diluting cultures, in the laminar flow hood. It is very unfortunate that I only realised the O_2 rates were reducing once compiling all data sets for the thesis. Through the diligent use of controls in all experiments, however, it was still possible to ensure accurate conclusions can be drawn from the data.

6.2.2 *Measuring Absorptance of cyanobacterial cells on disc*

Absorptance was a critical component of the $ETR1$ calculation. It was used in conjunction with $Y(I)$, to determine the fraction of light that was driving PSI, from the total available irradiance (I) that had been partitioned to PSI (f_i). In spinach, it was reasonable to assume the absorptance to be approximately 0.85, based on the work by Evans and Poorter (2001), which showed most leaves fall into this absorptance range between 400 – 700nm. For cyano discs however, the absorptance was considered likely to be a function of the [Chl] on the disc, which could be highly variable from one disc to the next. It was therefore necessary to determine the correlation between disc absorptance and [Chl], to enable an absorptance value for each disc to be conveniently and accurately quantified through a basic spectrometric measurement of MeOH extracted discs, as shown in section 3.3.5.

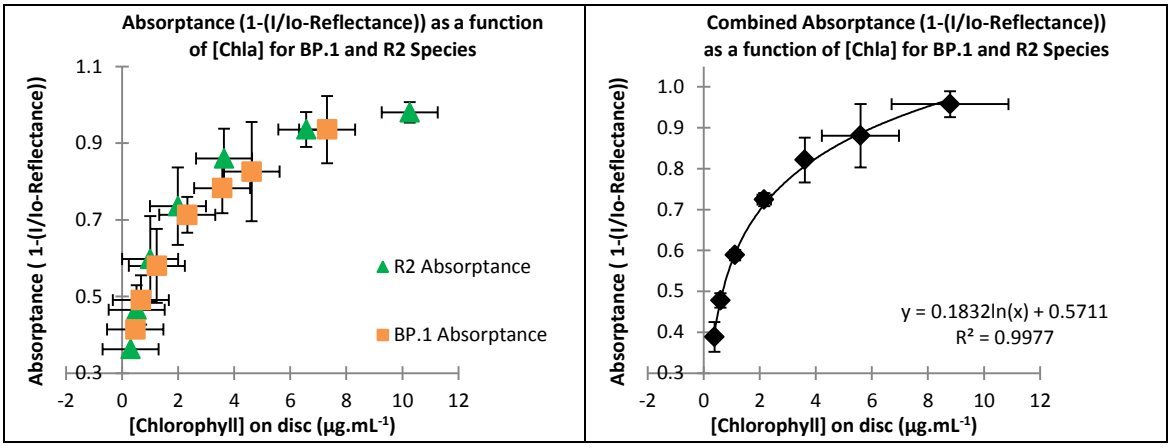

Fig. 6-4: Total absorptance of cyano discs as a function of [Chl].
Absorptance was calculated from measurements of transmission and reflectance between 400 and 700 nm using an integrating sphere and spectroradiometer, as discussed in materials and methods. The figure on the left presents absorptance of BP.1 and a mesophilic cyanobacterial species, R2 as a function of [Chl] on each disc. The similarity between two different species' absorptance as a function of [Chl] can be seen clearly in the right panel – showing the combined data from these two species. A dilution series of cell sample was used to create the range of [Chl] on the discs. Each 8 mm diameter disc was made in the same way and final [Chl] was determined through 1.0 mL MeOH extraction, quantified spectrometerically with the method of (Porra *et al.*, 1989). The equation of the logarithmic line of best fit, derived from the combined datasets in the right panel with an R^2 of 0.998, was used to calculate absorptance values for the 6803 and M55 strains used in cyclic electron flux measurements in the following sections. Error bars in left panel = SD of at least 3 samples per [Chl] range measured.

At the time that measurements of absorptance were being conducted I was cultivating and measuring the thermal response of the *Synechococcus* 7002 (R2) strain, to generate a comparative thermal response dataset for Chapter 4. Although I have not included this data in the thesis, I did use this strain in conjunction with the BP.1 strain for measurements of absorptance. Unfortunately, I did not anticipate the use of 6803 and M55 at the time of conducting the absorptance measurements. However, the result in the right panel of Fig. 6-4 shows that the strong correlation between absorptance and [Chl] held across species. As a result, the absorptance (A) values for M55 and WT 6803 cells used in

the CEF measurements was calculated based on the measured [Chl] of each cyano disc made, using the equation:

$$A = 0.1827 * \mathrm{Ln}([\mathrm{Chl}]) + 0.571$$

This equation represents the Logarithmic line of best fit through the combined absorptance data sets from measurements made with both BP.1 and R2, immobilised on 8 mm diameter glass fibre discs, from the data displayed on the right panel of Fig. 6-4. With an R^2 value of 0.998, the clear conclusion to be drawn was that the disc's [Chl] was an excellent surrogate for an actual, lengthy measurement, of the absorptance of each cyano disc individually. This was true across the entire range of [Chl] measured, but especially true around the range of the typical cyano discs, which averaged around 4 $\mu g.mL^{-1}$ and had a maximum of about 8$\mu g.mL^{-1}$, when extracted in 1.0 mL of 100 % MeOH.

6.2.3 *Determining f_i and Measuring the Rate of CEF as a Function of irradiance in Synechocystis 6803, and the NDH-1 mutant M55*

6.2.3.1 Methodological summary for CEF from 6803

Applying the MIMS/P700 set up to reproduce published results from a known system, glasshouse grown spinach, provided a control to demonstrate that both the instrumentation, and operator, were generating sensible data. It paved the way for trials of this technique to quantify steady state cyclic electron fluxes in cyanobacteria, by removing numerous unknowns. It follows that the first measurement made with cyanobacteria was a repeat of the successful experiments conducted with spinach discs. This allowed the spinach data to be used as a benchmark against which the new results could be assessed; as opposed to jumping into a more specific set of experiments in which the reliability of the data could remain speculative. As the primary CEF pathway in cyanobacteria is insensitive to known specific inhibitors, the M55 mutant (Ogawa, 1991), deficient in NDH-1 activity and known to be unable to perform CEF (Ohkawa *et al.*, 2000) was used to generate data for determining f_i, to create the case in which $ETR1 = LEFO_2$.

- All measurements in the following sections of this chapter were conducted using batch grown cells cultured in DTN medium, buffered at pH 8.0 with 20 mM Hepes at 30°C under ≈100 µE (or less) continuous fluorescent growth light in bubble lift reactors purged constantly with 2 % CO_2 enriched air. Cultures were diluted under

sterile conditions, into freshly washed and autoclaved tubes daily to be maintained at an OD_{750nm} < 1.0.

- 'Cyano-discs' were produced by concentrating a sample of freshly harvested cells into a high [Chl] pellet through centrifugation. The exact [Chl] of this concentrate was determined in MeOH, and an aliquot of known Chl mass, say 10 µg, was then injected into a large volume (say 5000 µL) of experimental buffer, containing 50 mM Hepes at pH 8.0 to resist pH changes as [TC] changed. The large volume of buffer was utilised to maintain sample homogeneity across the filter disc as the sample passed through. This procedure ensured each disc was made with the same available [Chl] and the same volume of filtrate passed through it, maximising the chances of reproducibility.
- In incubation experiments (to be discussed in the ensuing section i.e. not those looking at a range of irradiances), the same approach as described for thermal incubations of cells in 4.2.1 was used. The focus of the method was to ensure rapid equilibrium to the incubation temperature of the cell sample.
- After precisely 10 minutes of dark incubation (or in the case of irradiance measurements that did not require incubation, immediately) the total 5000 µL sample buffer/cells solution was gently filtered through a 10 mm glass fibre disc, under low vacuum in a custom built set-up. This returned the temperature of incubated samples rapidly, and consistently, back to room temp (25 °C) whilst also impregnating the filter disc with the cell sample.
- Significantly, a small volume of the buffer was always allowed to remain in the glass fibre disc, ensuring it and the embedded cells were saturated with buffer. To ensure the disc buffer [TC] was in constant equilibrium with the cuvette [CO_2], a small volume of Carbonic Anhydrase at 1 $mg.mL^{-1}$ (CA, Sigma bovine), was added to the disc. This ensured that accurate TC uptake rates were measured, and cells did not enter Ci limitation, as based on the data in Fig. 3-14. From the initial 10 mm disc, an 8 mm disc of homogenous cell covered glass fibre was cut with a leaf disc cutter (removing the masked edge) and loaded into the pre-equilibrated and calibrated to 30 °C, 1000 µL gas tight MIMS cuvette. This was all performed under very low green light illumination (essentially, darkness), to maximise sample homogeneity and maintain the 'dark' incubation status of samples.

- Disc samples were then equilibrated at 30 °C and left in the dark during a 5 min period preceding the measurements, during which time the MIMS cuvette was purged briefly with N_2 before 20 µL CO_2 gas and ≈30 µL $^{18}O_2$ was injected. After this 5 min period, the P700 system was re-zeroed (to balance the absorbance level between the measurement and reference wavelengths) and the P700max measurement, conducted under weak FR light, was performed. Following this, the $Y(I)$ measurement actinic light was activated, allowing the cells to reach a steady state of photosynthesis under the irradiance being measured, before the $Y(I)$ steady state measurement was conducted. This was the same sequence as is shown in the colour bar beneath gas fluxes in Fig 4-8. Each measurement was repeated three times to correct for instrument error (especially in the P700 system), on at least three samples.
- Following this, cells were allowed to settle in the dark again whilst the settings for the next level of illumination was set up and the procedure for P700max and $Y(I)$ were repeated. Or, in the case of thermal incubation experiments, a new sample was loaded. Extra CO_2 would be reinjected to the MIMS cuvette when levels became low, which was determined by multiplying the raw readouts from the Mass Spec. multiplied by the calibration factor for CO_2 for that day –a level of at least 1 % CO_2 was maintained.
- Total [Chl] was determined for each disc sample by adding the disc and 1.0 mL of MeOH into a 1.5 mL Eppy tube. The tubes were left in darkness, on ice, during the experimental time. Then overnight in the fridge to ensure all samples were equally extracted into the MeOH. They were loaded into a quartz cuvette for spectrophotometric analysis to determine [Chl] (Porra *et al.*, 1989).
- The range of irradiance used for measurements of cyano discs was reduced significantly from the range used with spinach. M55 was measured between 5 µE and 500 µE – with an emphasis placed on the lower irradiances where back reactions in PSI were less likely to affect the f_i value calculated, and from 20 µE to 1000 µE in the WT strain, to ensure a wide range of responses was measured.

6.2.4 *Validation of the steady state CEF measurement in cyanobacteria: results and comparison between the WT and Mutant.*

The results of this initial experiment presented in Fig. 6-5, show the clear difference between the M55 strain in the top right panel, and the WT in the top left panel. The former exhibited highly supressed $\boldsymbol{\Delta Flux}$ in comparison to the latter, which exhibited a strong increase in response to increasing irradiance. This was a good indication that the method was producing reasonable results. However, there were issues in the data relating to the value determined for $\boldsymbol{f_i}$ which confounded data analysis for a long time. This is clearly visible in the middle panel of Fig. 6-5, presenting $\boldsymbol{f_i}$ vs irradiance for M55 cells.

After calculation, the value did not approach 0.5 as had been obtained from spinach, and ought to be expected. Instead the value was low at only 0.4 and rapidly declined to < 0.3. This begged the question, why would a cell be diverting ≥ 60 % of absorbed photons to PSII, under conditions that are optimal for a 50/50 split in light energy partitioning?

A solution to the energy partitioning problem highlighted by the low $\boldsymbol{f_i}$ value was found through a literature search into the physiology of the M55 mutant suggesting the result is an artefact of the M55 mutant itself. By missing the electrons that would otherwise be cycled back into the PQ pool from CEF, and possibly respiration, relative oxidation state compared to the WT cells is increased in the mutant when measured under similar levels of illumination, and in the dark (Bolychevtseva *et al.*, 2015). The altered redox state of the PQ pool affects signal regulation for the State-Transitions of the light harvesting complex in 6803 (Ogawa *et al.*, 2013, Bolychevtseva *et al.*, 2015), leaving it 'stuck' in State-I (Olive *et al.*, 1997). This has the effect of reducing the partitioning of absorbed light to PSI and therefore reduces the $\boldsymbol{f_i}$ value.

Ogawa *et al.* (2013) demonstrated that this phenomenon has resulted in inaccurate interpretations of the photosynthetic yield of PSII and the overall photosynthetic efficiency of M55 samples based on fluorescence measurements. As such there is a precedent for this mutant to produce confounding results through light probe measurements. In section 6.2.6 some experimental evidence from this thesis work is presented to further support the literature explanation for inaccurate $\boldsymbol{f_i}$ values. It also provides evidence that the true value for $\boldsymbol{f_i}$ in the WT 6803 strain, capable of performing state transitionsought to be around 0.5.

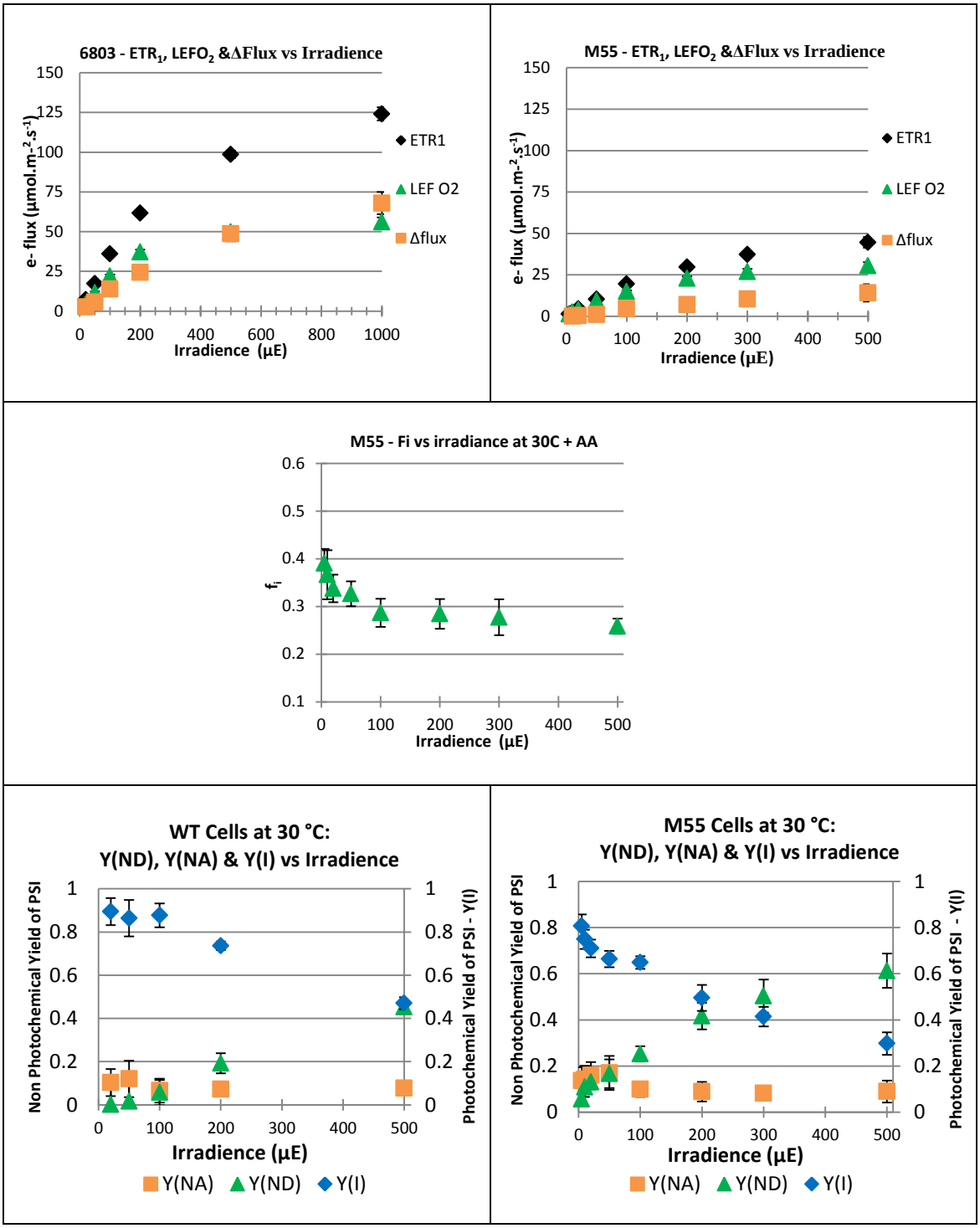

Fig. 6-5: $\boldsymbol{ETR1}$, $\boldsymbol{LEF_{O_2}}$ and $\boldsymbol{\Delta Flux}$ as a function of irradiance in M55 mutant and 6803 WT (top two panels). fi as determined with M55 mutant vs irradiance, middle panel. $ETR1$ rates determined in the WT cells were calculated using an fi value of 0.5, whilst M55 $ETR1$ rates were calculated using the fi of 0.4, for reasons discussed in the text. The downward trend in the fi with increasing irradiance is primarily driven by back-reactions in P700, for which the forward electron flow in the first place is counted as part of $ETR1$, as discussed in text. $Y(ND)$, $Y(I)$ and $Y(NA)$ data is presented in the bottom panels, determined from the same experiments used to determine $ETR1$, $\boldsymbol{LEF_{O_2}}$ and $\Delta Flux$ in the top panels, with WT cells on the left and M55 on the right. In contrast to higher plants, cyanobacteria tend suffer PSI donor side limitation. Samples were immobilised onto 8 mm glass fibre disc, standardised to [Chl] post measurement. Note the different range of irradiances used between the two samples, with M55 focusing at a lower range of irradiance to measure fi with more accuracy and WT across a broader range to observe the broad effect of irradiance on cyclic electron fluxes. Other experimental conditions: samples measured at 30 °C, 2% CO_2, n = 6 ±SE.

This data is presented in Fig. 6-7, and shows that after incubations that were likely to have irreversibly detached the phycobilisomes (as published by Inoue et al. (2001)) the fi value became 0.5. Further explanation is provided in section 6.2.5. As such, the $ETR1$ data presented in the top left panel of Fig. 6-5 for WT cells was calculated with the 0.5 value for f_i, whilst the top right panel for M55 cells uses the actual f_i measured, 0.4.

To interpret the rapid decline of f_i values shown in the middle panel of Fig. 6-5 it once again pays to interpret $Y(ND)$, $Y(NA)$ and $Y(I)$ values (presented in the lower left and right panels of Fig. 6-5) generated during the measurements of $LEFO_2, ETR1$ and $\Delta Flux$ (presented in the top panels). In contrast to the spinach data discussed earlier, in which a reduction of CEF led to a significant increase in acceptor side limitation, the $Y(NA)$ values remained stable and low (< 0.2) for both samples across the entire range of irradiances measured.

This could be the result of both the PSI/PSII ratio in cyanobacteria being the opposite to plants (Whitton and Potts, 2000) and also be a result of the large electron sinks present in cyanobacteria downstream of PSI, such as the Flv1-3 proteins capable of handling enormous electron fluxes to alternative acceptors like O_2, (Allahverdiyeva *et al.*, 2013, Yamamoto *et al.*, 2016). As such, a loss of CEF is less obvious when simply studying the $Y(NA)$ data from cyanobacterial samples such as this, meaning the primary driver of a loss in $Y(I)$ was a result of increasing levels of PSI donor side limitation ($Y(ND)$).

The $Y(ND)$ data is not straightforward to interpret, as when compared to higher plants, cyanobacteria tend to exhibit a much higher $Y(ND)$ for a given irradiance. Furthermore, the overall $Y(ND)$ trend between the WT and M55 mutant is quite similar. A large number of alternative electron sinks operating upstream of PSI, namely the plastoquinol terminal oxidase (PTOX), cytochrome oxidase, the alternative quinol oxidases (Hart *et al.*, 2005, Bailey *et al.*, 2008, Ermakova *et al.*, 2016) and possibly the flv2-4 pathway able to directly oxidise PSII (Bersanini *et al.*, 2014), are the primary drivers for donor side limitation at PSI in cyanobacteria (besides a loss of PSII function, as discussed in 5.2.2)

This is evidence of what is, in my opinion, the key survival strategy for cyanobacteria – underpinning some of their metabolic flexibility. It allows them to operate PSII at its maximal capacity regardless of conditions, whilst ensuring numerous safe pathways are available to quench any over-reduced electron carriers (obviously, and significantly for this chapter, State-transitions and some other strategies also play a role in managing over

excitation of PSII). This strategy allows for energy to be rapidly transferred between intercellular locations beyond the standard ETC, for tasks such as NO_3^{-1} reduction, carbon concentration or activities such as Na^+ pumping (Hart *et al.*, 2005). This could also be a result of the PSII to PSI ratios in cyanobacteria, which tends to be quite low in cyanobacetria compared to plants (Whitton and Potts, 2000).

Against the background of a generally high $Y(ND)$ value found in cyanboacteria, the data in the lower panels of Fig. 6-5 clearly shows a more rapid increase in this value for the M55 mutant at irradiances around the growth intensity of 100 µE, when compared to the WT. The trend of the $Y(ND)$ data from M55 closely mirrored the values for $Y(I)$, indicating that it was driving the rapid decline in photochemical yield of PSI. Whilst the $Y(I)$ in WT cells remains around 0.9 up to 100 µE, it has already dropped to 0.65 in the mutant – a strong indication that it was unable to provide sufficient electrons to re-reduce $P700^+$ efficiently. At these lower irradiances, this suggests the M55 cells were unsuccessfully balancing the electron fluxes between the photosystems.

In spite of the extra light energy directed to PSII in the M55 mutant by the State-I these cells are 'stuck in', M55 is known to suffer reduced rates of O_2 evolution compared to the 6803 WT (Ogawa *et al.*, 2013). A reduction in PSII function could go part way to explaining the reduced number of electrons available for re-reducing $P700^+$ that contributes to the elevated $Y(ND)$ measured in the mutant samples. However, when comparing the magnitudes of the data in Fig. 6-5, this does not go a long way to explaining the differences in $Y(ND)$ values.

At the growth irradiance of 100 µE, WT cells record an LEF_{O_2} of 22.2 µmol (electron).m^{-2}.s^{-1}, compared to the M55 rate of 14.9 µmol (electron).m^{-2}.s^{-1} – a difference of around 37 %. Meanwhile, the $Y(ND)$ value measured for WT cells at this irradiance was 0.07, compared the mutant's value of 0.25, a difference of around 76 %.

This was in addition to the fact that according to the f_i data, M55 cells were directing about 20 % less energy for a given irradiance to PSI – implying perhaps, that the system was undergoing fewer turnovers, reducing the amount of $Y(ND)$ being suffered.

In addition to the shortfall of electrons available from PSII, are those that would otherwise be supplied by CEF, and from respiration. According to Cooley and Vermaas (2001), the deficient NDH-1 complex of M55 has been shown to severely disrupt the tricarboxylic cycle, possibly due to the limited amount of available oxidised $NADP^+$ in these

cells, required as an electron acceptor by isocitrate dehydrogenase. Without this step, the cells are unable to produce succinate, leading to an inhibition of SDH activity. The SDH enzyme was found to be the most significant source of respiratory electrons for PQ reduction during dark respiration, at rates between 30 and 50 μmol (electron).mgChl^{-1}.hr^{-1} (Cooley and Vermaas, 2001). The significance of this electron source for re-reducing PQ in the light was not clear, although was probably low under conditions where the PQ pool was not highly oxidised (Cooley *et al.*, 2000).

At low irradiance, a high flux of electrons from SDH reducing PQ and reducing PSI would lead to an increase in $\boldsymbol{ETR1}$, and WT cells at 20 μE in top left of Fig. 6-5 presented a surprisingly large $\boldsymbol{ETR1}$ – almost 50 % higher than $\boldsymbol{LEF_{O_2}}$. In fact, this is consistent with the data in Cooley and Vermaas' (2001) paper on the impact of various complexes on the oxidation of the PQ pool. SDH deficient mutants had a rapidly oxidised PQ pool, as irradiance levels increased, compared to the WT (see table 1 of their publication).

As such, the values of $\boldsymbol{\Delta Flux}$ at low irradiances may not be an accurate estimation of electrons being cycled; if there was a large contribution in WT cells from respiratory electrons reducing PQ. The 100 μE growth irradiance favours the location of SDH and NDH-1 complexes to enable electrons to reduce P700^{+}, rather than terminal oxidases, as reported via confocal imaging of fluorescence tagged NDH-1/SDH mutants of *Synechococcus elongatus* PCC 7942 by Liu et al., (2012).

However, at an irradiance of around 100 μE, Cooley and Vermaas' (2001) data showed the difference between the WT and SDH deficient strain had reduced substantially, to be quite small. This is evidence that the rate of respiration through SDH was likely to be highly supressed at irradiances ≥100 μE. It suggests $\boldsymbol{\Delta Flux}$ rates presented in the lower left panel of Fig. 6-5 for WT discs were representative of CEF, and plus any contribution from back reactions (which ought to be quite low until $\boldsymbol{Y(I)}$ values drop significantly, at > 500 μE in the WT).

As the signal generated in the MIMS during this component of the project was aimed at the accurate calculation of $\boldsymbol{LEF_{O_2}}$, optimising the signal noise in the mass 44 (CO_2) signal was neglected. As such, the signal to noise ratio in the 44 signal was too high to perform accurate mass balance estimates, as was conducted in Chapter Four. As such, it was not possible to calculate an estimate of potential rates of respiration occurring during illumination, and the assumptions about SDH function could not be tested from this data set.

Once these factors were considered, the idea that a loss of CEF in M55 drove the increase in the measured $Y(ND)$, particularly at irradiances of > 100μE, was strongly supported. According to data in the top left of Fig. 6-5, at an irradiance of 100 μE, WT cells were cycling about 40 % of the electrons generated at PSII. This was calculated by a comparison of $LEFO_2$ and $ETR1$, 22.16 μmol(electron).m^{-2}.s^{-1} and 36.1 μmol (electron).m^{-2}.s^{-1} respectively. Again, this assumed that the rate of respiratory electrons reducing PQ (ie. SDH activity) was low. With $Y(I)$ at 0.9, it was fair to assume that very few, if any, back reactions led to an overestimation of the $ETR1$ value used. So by adding 40 % more electrons, the mutant would theoretically have a flux of 19.96 μmol(electron).m^{-2}.s^{-1} available from oxidation of the PQ pool (where both PSII and cycled electrons are available for reducing Plastocyanin/cyctochrome c-6).

As such, analysis of $Y(ND)$ and consideration for the cause of its rapid elevation in the mutant provided further evidence that CEF in M55 was severely disrupted, in contrast to the analysis of spinach, in which $Y(NA)$ was more obviously increased at high irradiance. Further, a comparison of calculated rates of $\Delta Flux$ between the WT and M55 also suggested that the mutant exhibited very little activity at PSI that was not directly correlated to the Linear electron flux from PSII. With such a low $Y(I)$ value recorded for the M55 samples, it is probable that the $\Delta Flux$ recorded is due primarily to back reactions within the P700 photosystem.

In summary, a repeat of the irradiance vs steady state CEF experiments performed initially with spinach, were repeated with cyanobacteria, in section 6.2, leading to the following conclusions:

- A cyano disc's [Chl] is an accurate predictor of the sample disc's absorptance
- By reproducing a set of steady state CEF measurements performed in plants, the results indicated that the methods initially developed for plants were successfully applied to cyanobacteria; however some assumptions must be carefully considered due to the sharing of the thylakoid between respiratory and photosynthetic processes
- Using the M55 mutant to determine f_i in cyanobacterial samples resulted in an underestimation of absorbed light being partitioned to PSI for WT samples. However, literature provided precedence for such artefacts and, as stated, data

presented below in section 6.2.6 provides justification that the WT ought to have a $f_i$value of 0.5 applied to it

- It was found that $Y(ND)$ was the primary cause of decreasing the $Y(I)$ in cyanobacterial samples, in contrast to spinach which clearly showed an increase in $Y(NA)$ drove decreases in $Y(I)$
- In the cyanobacterial samples, analysis of $Y(ND)$ data provided more information about the effect of inhibiting CEF on inter-chain redox states (and therefore the possible role of CEF in the sample), then the $Y(NA)$
- There does not seem to be a large input of electrons from SDH when WT samples are illuminated in spite of the significance of this source of reductants in darkness, based on the $\Delta flux$ rate at low irradiances.

The results provided confidence that an investigation into the thermal impacts on CEF rates in cyanobacteria was possible in the MIMS/P700 system.

6.2.5 $ETR1, LEFO_2$ and $\Delta Flux$, post thermal incubations at 500 µE

By reproducing published CEF values for spinach discs in 6.1 and then recreating the primary trends from these measurements with cyanobacteria (including the successful measurement of the completely opposite nature of PSI functional limitations that exist between higher plants and cyanobacteria with respect to $Y(ND)$ and $Y(NA)$) – I was satisfied that the MIMS/P700/cyano disc methodologies were working well and providing accurate data. It was now time to test the hypothesis that CEF not only increased in response to thermal stress of PSII, but could continue once PSII had ceased to function – an indication that electrons were being sourced from the oxidation of stored carbohydrates, and these may in fact be cycled in the absence of PSII function.

In contrast to previous measurements, testing the hypothesis required that $\Delta Flux$ be measured as a function of incubation temperature, and not irradiance. This required that a single set of standardised measurement conditions were used, in which only pre incubation temperature was altered. All conditions used in previous CEF measurements of cyanobacteria were maintained (ie. 30 °C, 2 % CO_2 with the addition of carbonic anhydrase to the cyano disc), but a single irradiance was selected. Initially a saturating irradiance of 500 µE was utilised, selected in the misguided thought that saturated rates of LEF_{O_2} were required to find the optimal $\Delta Flux$ signals. The results of these experiments simply showed

that the level of back reactions within PSI resulting from this high level of irradiance, as discussed above in 6.1.1, was such that any CEF signal was drowned out in the background.

This can be clearly seen in Fig. 6-6 which presents a comparison of $LEFO_2, ETR1$ and $\Delta Flux$ data from both M55 (right panel) and the WT (left panel) cells, following a ten minute dark across a range of temperatures, measured at an irradiance of 500 µE. No significant difference is observed between the WT and M55 strains with respect to the $\Delta Flux$ rate.

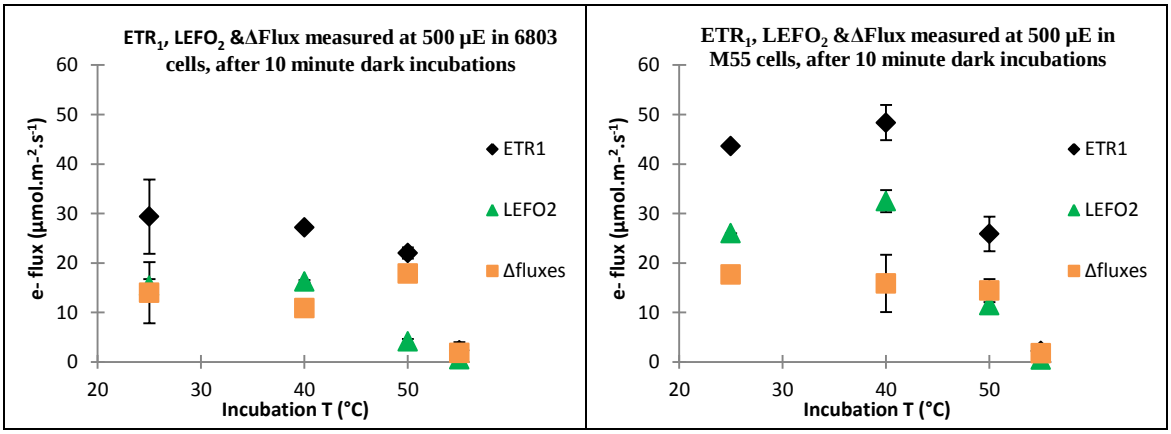

Fig. 6-6: Comparison of $ETR1$, LEF_{O_2} and $\Delta Flux$ as in WT and M55 at 500 µE irradiance after 10 minute dark incubations across a range of temperatures.
In order to measure the effect of high temperature incubations on rates of cyclic electron transport cells were incubated for 10 minutes in the dark, before being filtered onto glass fibre disc and measured in MIMS/P700 system. The irradiance of 500 µE was determined to be too high, and a large proportion of back reactions in P700 of each sample has resulted in no significant difference being observed between the WT and M55 samples. Cells were suspended on a glass fibre disc and measured at 500µE at 30 °C, 2 % CO_2. n = 3 ± SD.

This was originally considered very concerning, because it was expected that the M55 strain would not record much $\Delta Flux$ at all. Upon more careful inspection, and broader comparison of these data, it became clear that the rates for M55 cells at 500 µE in this experiment matched those from the previous experiment in the top right panel of Fig. 6-5.

In that earlier experiment, values for $LEFO_2, ETR1$ and $\Delta Flux$ rates were 30.5, 44.6 and 14.1 µmol (electron).$m^{-2}.s^{-1}$ respectively, whilst in this experiment after a 25 °C incubation they were 33.7, 47.1 and 13.4 µmol (electron).$m^{-2}.s^{-1}$, almost the same. Although the experiment did not work as expected, the data provided yet more confidence that the system was producing reproducible and sensible results. The difference in the scale between Fig. 6-6, being much lower along the y-axis compared to Fig. 6-5, increased the visibility of M55's $\Delta Flux$ compared to what I had noticed in that earlier experiment – a valuable lesson for the future.

Such a comparison for the WT cells, between this experiment and that presented in the top left panel of Fig. 6-5, show an unfortunate outcome in the work conducted during my experiments. In a failure to make careful analysis and comparisons of data sets throughout the experimental component of my PhD, specifically between completely different experimental phases (ie, data generated to validate the CEF measurement approach in Fig. 6-5 versus the data collected to really test the hypothesis in Fig. 6-6) I failed to notice that WT cells were not performing as well in these latter experiments. Rates of WT cells in top left panel of Fig. 6-5 for $\boldsymbol{LEFO_2, ETR1}$ and $\boldsymbol{\Delta Flux}$ were 50.0, 98.7 and 48.7 µmol (electron).$m^{-2}.s^{-1}$ respectively at 500 µE, whilst in the experimental data presented on the left in Fig. 6-6 after a 25 °C incubation they were only 15.4, 29.4 and 14.0 µmol (electron).$m^{-2}.s^{-1}$. This is just one third of the original rates and in fact puts the WT and M55 mutant on equal ground with respect to rates, in contrast to published data on photosynthetic rates in M55 vs WT (Ogawa *et al.*, 2013).

An experimental error such as this highlights the significance of running controls, and it was fortunate that in spite of the fact that I had devised value for $\boldsymbol{f_i}$, I remained curious enough to measure the difference between the WT and mutant samples under all conditions being investigated. As the following section will describe, this fact was highly significant, as it allowed for the observation to be made that the true value for $\boldsymbol{f_i}$ in the WT cells was likely to be 0.5 (see section 6.2.5). It also resulted in sufficient data being generated to support the conclusions, in spite of the error in checking the photosynthetic rates of the WT cells across the experimental period.

A repeat of the incubation experiment was conducted at 100 µE, an irradiance observed in Fig. 6-5 to result in sufficient $\boldsymbol{\Delta Flux}$ to enable accurate quantification, whilst avoiding significant back reactions, and under ideal conditions low rates of PQ pool reduction by SDH activity in the WT (Cooley and Vermaas, 2001).

6.2.6 $\boldsymbol{ETR1, LEFO_2}$ *and* $\boldsymbol{\Delta Flux}$ *at 100 µE, post thermal incubations*

The primary conclusion drawn from incubation comparisons of CEF at an irradiance of 500 µE, was to repeat the experiment at a lower irradiance to avoid back reactions at P700 which led to an overestimation of $\boldsymbol{\Delta Flux}$. In the top left panel of Fig. 6-5, an irradiance of 100 µE proved sufficient to initiate CEF in the WT cells at rates that were clearly distinguishable from the linear rate. It was therefore concluded that this would provide an optimal irradiance for

comparison of thermal incubations. The first component of the measurements to be considered were the derived values for f_i across the incubation range tested, as the results from this experiment had implications for all of the M55 derived values for f_i in this Chapter.

6.2.6.1 The value of f_i became variable at incubation > 50 °C.

As before, the M55 mutant was used to generate f_i values, to ensure the absence of any CEF, and as a control this was performed at each incubation temperature of interest. The result, presented top left in Fig. 6-7, included a surprise. Samples across the lower range of incubation temperature (25 – 40 °C) exhibited the already measured 60/40 split in absorbed light partitioning between PSII/PSI, an $f_i = 0.4$. However, after a ten minute dark incubation at 50 °C, the f_i value increased to a 50/50 split. The accuracy of this measurement immediately came into question. However, inaccurate results were quickly dismissed. (a) Data for the M55 cells remained consistent throughout the CEF experiments (unlike the WT cells). (b)The only change made between samples with respect to the protocol was the sample incubation temperature. (c)Each measurement was repeated at least three times. A clue to the cause of the increase in f_i came from an extensive investigation into the effects of temperature on photosynthesis performed on 6803 WT cells by Inoue *et al,* (2001). In this work they refer to an earlier paper (Inoue *et al.*, 2000) investigating the effects of high temperature treatments on the moderately thermophillic cyanobacterium *Thermosynechococcus vulcanus*, almost identical to the BP.1 strain.

They found that incubations at elevated temperatures resulted in the irreversible detachment of the phycobillisome from PSII, after incubation at 70 °C. The subsequent work with 6803 showed that this occurred at 50 °C, precisely the temperature at which f_i increased to 0.5 in my measurements. This provided evidence that the detachment of the phycobilisome, associated primarily with PSII under the 'stuck' State-I transition in M55, suddenly resulted in a rebalancing of the energy partitioning of absorbed light between the photosystems, resulting in a shift of f_i to 0.5. In response to this finding, all WT samples were reanalysed to utilise the f_i of 0.5 (i.e. all WT values presented throughout this chapter), as this seemed a more accurate value for cells able to properly manage their energy partitioning, under the ideal conditions being used in these experiments. An exception to this however, was for the incubation at 55 °C.

The apparent value for f_i, calculated with the M55 cells after the 55 °C incubation, dropped rapidly to only 0.07— a very low level. Was this value representative of the actual partitioning of light energy between PSI and PSII, or an artefact resulting from the damage caused to cells at high incubation temperature? The value coincided with the rate of $LEFO_2$, which essentially reached zero after 55 °C incubations in both WT (0.33 µmol.m-$^{-2}$.s^{-1}) and M55 (0.37 µmol.m-$^{-2}$.s^{-1}). This was problematic with respect to the assumptions made when calculating f_i, that $LEFO_2 = ETR1$:

$$f_i = \frac{LEF_{O_2}}{Y(I) \times I \times A}$$

According to data from Inoue *et al.* (2001), the phycobillisomes were still functional until 60 °C, in-spite of the fact they were irreversibly detached at around 50 °C. As such, it was expected that the total absorptance (I), did not change significantly. The photochemical yield of PSI, $Y(I)$, dropped to a mere 0.1 (see right panel Fig. 6-8), which would have acted as a slight offset for the very low $LEFO_2$ value. In total however, the denominator almost remained identical, whilst the numerator decreased significantly as $LEFO_2$ rates collapsed, resulting in an f_i value clearly approaching zero.

With O_2 evolution almost completely inhibited, very little energy was actually required by P680. Most likely the Manganese Stabilising Protein (MSP) had dissociated by this temperature, and the system had lost capacity to generate O_2, leaving the PSII complex most probably in a "Form C" (Inoue *et al.*, 2001). In spite of this, evidence from Mamedov *et al.*, (1993) supports the idea that the reaction centre itself was still able to function. Their work in isolated thylakoids required the addition of artificial donors and acceptors; however, could demonstrate that the system was still capable of photo-oxidising diphenolcarbazide (DPC) to reduce dichlorophenollindophenol (DCIP). As such, evidence supports the idea that P680 would have been capable of utilising some light energy, but certainly would not require 93 % of adsorbed irradiance. From this perspective, the value 0.07, determined for fi was considered a gross underestimate due to the break-down of assumptions used in the calculations to derive fi, as PSII failed. As such, it was possible to answer the question posed above, that the very low value for fi was no longer accurate, and likely a gross underestimate. It suggested that an accurate value for the partitioning of light between PSI and PSII could not be determined with this method under conditions that were not 'ideal', specifically, in the absence of sufficient PSII function. However, there was no way of speculating what the actual value was. As such, the rate of $ETR1$was calculated in both the

WT and M55 cells with the 0.07 value. The rates calculated for $ETR1$, and therefore $\Delta flux$, must therefore be considered as an underestimate.

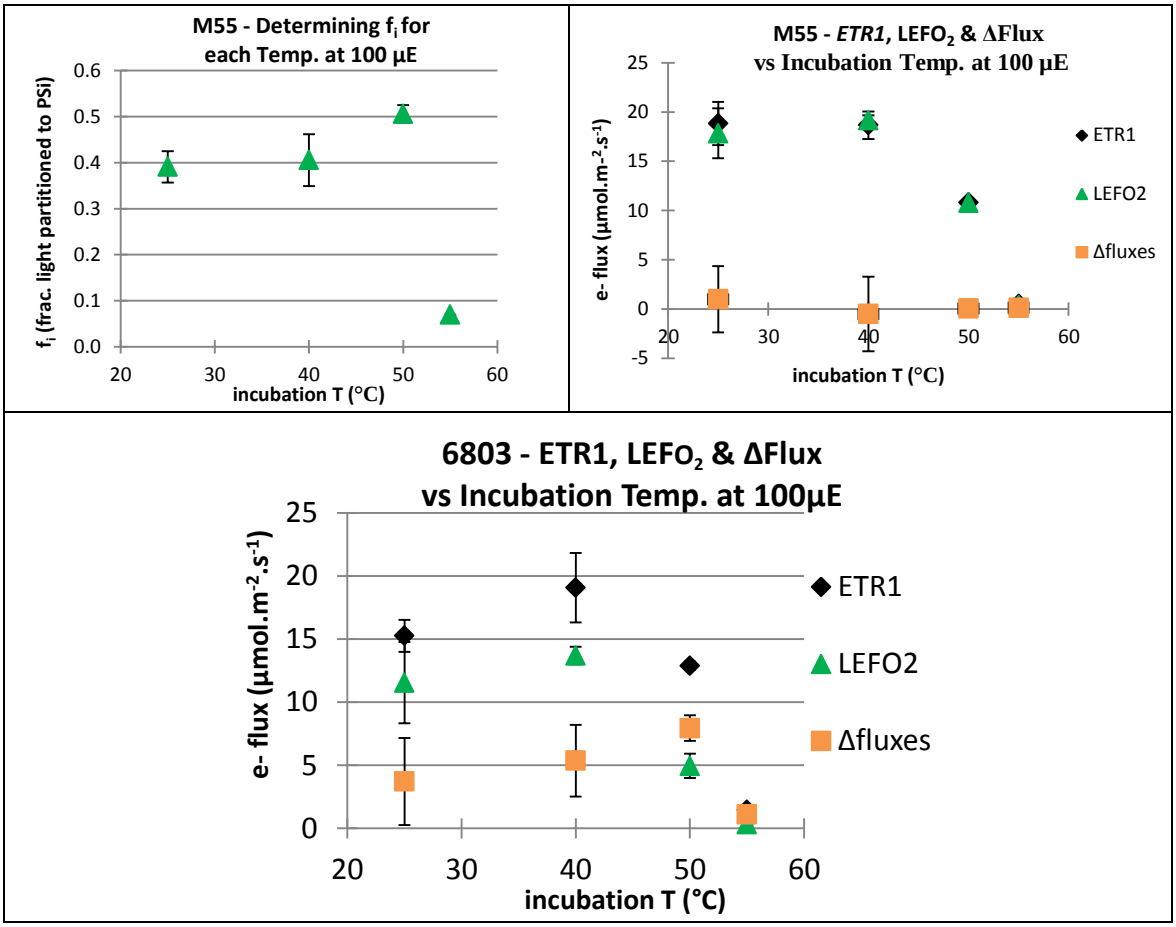

Fig. 6-7: fi determined in the M55 mutant and $ETR1$, LEF_{O_2} and $\Delta Flux$ determined in both M55 and the 6803 WT as a function of incubation temperature.

Cyanobacterial samples were incubated at the indicated temperatures for 10 minutes in the dark before being filtered through a 10 mm diameter glass fiber filter to produce a 'cyano disc', as discussed in Chapter 2. Discs were cut to 8 mm, a small addition of carbonic anhydrase at 1mg/mL was added and discs were then left in the dark for 5 mins at 30 °C in the 1000 µL gas tight MIMS cuvette. During this time a breif N_2 purge removed the standard atmosphere, a 20 µL injection of CO_2 and 30 µL $^{18}O_2$ was injected. P700 signals were zeroed after 5 minutes and measurmnets of P700max, $Y(I)$ under steady state conditions in addition to gas fluxes were recorded simultaneously. Values presented are the mean of at least three repeats and standard deviation.Cells were suspended on a glass fibre disc and measured at 100µE at 30 °C, 2 % CO_2. n = 3 ± SD.

6.2.6.2 Does the data show CEF can function without PSII?

Rates of $LEFO_2$, $ETR1$ and ultimately $\Delta flux$ from the WT and as a control, the M55 strain, are presented in the lower and top right panels of Fig. 6-7, respectively. As stated, both strains recorded very similar trends for $LEFO_2$ as a function of incubation temperature. As discussed in the preceding section (6.2.5), rates of $LEFO_2$ measured in the WT cells were lower than they had been in previous experiments. Although unfortunate, this fact did not disqualify the findings based on these data, due to the direct comparison possible between the WT and M55 control.

The $\Delta flux$ data presented for WT cells in the lower panel of Fig. 6-7 can be interpreted to show that the rates of CEF increased as a function of incubation temperature, essentially inverse to the rate of $LEFO_2$. In contrast to this, the M55 strain recorded no $\Delta flux$ at any of the incubation temperatures, providing strong evidence once again that the method being utilised was generating sensible data. The f_i value used to calculate $ETR1$ for each M55 sample were taken from those presented top left of Fig. 6-7, as measured with those samples. The WT data was calculated with the f_i value of 0.5, as discussed earlier, except for 0.07 at 55 °C. Significantly, even using this very low estimate of 0.07 to define the proportion of absorbed light driving PSI, the flux through PSI (1.46 µmol (electrons).$m^{-2}.s^{-1}$) was still larger than that measured for PSII (0.34 µmol (electrons).$m^{-2}.s^{-1}$). According to a two-tailed T-test, the difference was significant (P= 0.0048, n=4). The $LEFO_2$ rate had reduced to only 2.5 % of its maximal (13.7 0.34 µmol (electrons).$m^{-2}.s^{-1}$), to around the level of noise inherent in the measurements.

From a thorough search in the literature, this seems to be the first steady state estimation of cyclic electron fluxes conducted in cyanobacterial cells. It is certainly the first to estimate CEF directly from intact cells, cycling electrons through PSI, at temperatures that have eliminated almost all PSII activity. This result provided evidence that sufficient reducing equivalents were still able to enter the thylakoid electron transport chain, to maintain redox poising and allow for the cycling of electrons through b-$_6$f and PSI, in the absence of PSII function. The oxidised state of the PQ pool that was likely to result from thermally inhibited PSII in high temperature treated cells, was likely to keep the NDH and SDH complexes spatially separated throughout the thylakoid membrane, in orientations that will favour electron donation to $P700^+$, as opposed to terminal oxidases (Liu *et al.*, 2012). Furthermore, the low redox state would have been conducive to the to function of the SDH complex, to reduce the PQ pool (Cooley *et al.*, 2000).

Due to low value for f_i in the high temperature incubations, it is likely that the value presented was an underestimate of the true $\Delta flux$ rate, and therefore the rate of electrons passing through PSI. However, the contribution being made to this flux from complexes such as SDH, in the WT cells, is unknown. Due to the method for measuring gross O_2 evolution rates, reductant entering the PQ pool through the SDH complex, for example, would not necessarily be counted in the value for $LEFO_2$, unless it ended up reducing O_2. As such, the $\Delta flux$ may contain a contribution that was true 'cyclic' around PSI, but may also be

comprised partially of electrons from respiration that passed 'linearly'' through the complex to reduce $NADP^+$, for example. In any case, the data supports the hypothesis that the activity of PSI was greater than could have been supported by PSII, after incubations at damaging temperatures. Whether the reductant was being cycled, or driven linearly was not possible to ascertain.

6.2.7 *Can literature data support 'recycling' of respiratory reductant?*

The results in this experiment were not conclusive, it was not possible to state that the reductant reducing the PQ pool via what was most likely respiratory process along the thylakoid, were in fact being cycled around PSI. Data in the literature is able to provide evidence that sufficient thermal tolerance is exhibited by the systems required to perform CEF after these incubations. However, there is no work to differentiate the activity of PSI that has been driven by CEF, or potentially linear reduction of $P700^+$ with electrons sourced through respiration.

The following summary is evidence that the systems in 6803 should be able to perform CEF once PSII has been inhibited. According to Mamedov *et al.* (1993) PSI of various mesophilic phototrophs is still functional after between five, and up to 25 minute incubations at up to temperatures in the mid 50 °C range. In their comparative analysis of the impacts of high temperatures on electron transport and phosphorylation reactions in isolated chloroplasts of 6803, Mamedov *et al.* (1993) state that the thermal sensitivity of various reactions follows the order, from most sensitive to least sensitive: "evolution of oxygen > reactions of Photosystem II = synthesis of ATP > reaction involving cytochrome b6/f > reactions of Photosystem I". Photophosphorylation reactions, measured through luciferin/luciferase assays, had a $k_{0.5}$ of 48 °C after 25 minute incubation, although after 25 minutes at a 55 °C incubation, the reaction still maintained 25 % of maximal activity. This was the least sensitive of the reactions necessary for functional cyclic electron transport.

Supporting this data, *Balme et al.,* (2001) found that the reaction between $P700^+$ and plastocyanin in PSI fragments isolated from 6803, reached a maximum activity at 51 °C, before declining at higher temperatures. However, five minute incubation of the isolated plastocyanin at 55 °C resulted in the denaturing of 80 % of the sample, according to measurements of the sample fluorescence after excitation at 275 nm. Data on the thermal

stability of cyt-c_6 was not forthcoming from a literature search. In spite of this, however, the results of *Mamadov et al's.,* (1993) work strongly support that cyclic electron transport activity could still be conducted after 25 minute incubation at 55 °C between PQ and PSI, as their assay using duroquinol (DQH_2) oxidation to methyl vialogen (MV) reduction, which occurs via PSI and requires a step between b_6f and PSI (either plastocyanin or cyt c6), yielded a $k_{0.5}$ of 56 °C.

A recent paper, based on measurements of brown macros algae inhibited in PSII function by osmotic stress concluded that respiratory reductant was indeed poising the thylakoid for CEF. It was the title of their paper. However, it my opinion that the authors have not considered the 'linear' pathway through PSI of respiratory reductant. This is considered in more detail in section 7.5.

This data supports the physical capacity of cells to perform electron transport around PSI, at temperatures that had inhibited PSII. It was not possible to state whether the reductant was indeed cycling, or simply passing through linearly. Nonetheless, the data provides very good evidence that an alternative source to PSII was able to drive PSI photochemistry. As such, the data strongly supports the energy leveraging hypothesis, as a cyanobacterial response to thermal stress.

6.3 Comparing $Y(I)$, $Y(NA)$ & $Y(ND)$ at 100µE from incubated samples of M55 and 6803

The photochemical yield of PSI ($Y(I)$) and its donor ($Y(ND)$) and acceptor side limitations ($Y(NA)$) from the incubation experiments were generated from data used to calculate rates of $ETR1$, for both M55 and WT samples. This data provided another lens through which electron fluxes could be viewed and interpreted and is presented in Fig. 6-8. Values for WT samples are presented on the left, and M55 on the right. Due to the nature of the data, direct comparisons can be made between this data, and the results presented in Fig. 6-7.

Significantly, a high level of consistency was found between experiments for the M55 sample data between these and earlier experiments. This was clear from a comparison with previously measured values for $Y(I)$, $Y(ND)$ and $Y(NA)$ at an irradiance of 100 µE, presented in the bottom right panel of Fig. 6-5, when compared to those presented here

after incubation at 25 °C. However, this same comparison for WT cells suggested that the samples used in these incubation experiments were suffering donor side limitation.

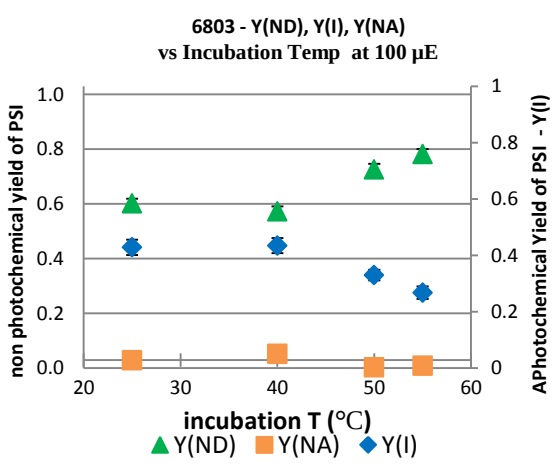

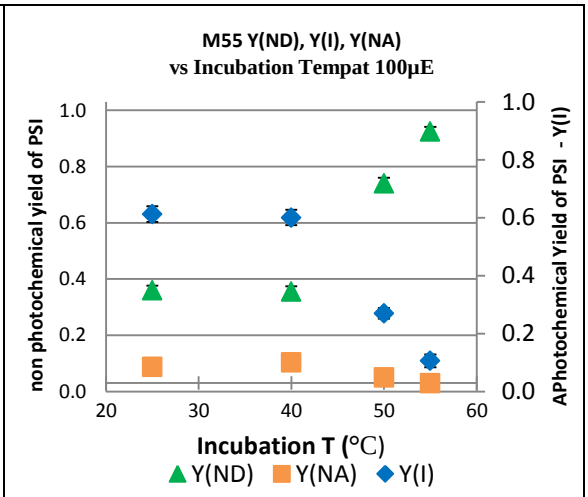

	Raw Values			
Incubation	LEF_{O_2} (µmol(electron).m^{-2}.s^{-})		$Y(ND)$	
Temp (°C)	WT	M55	WT	M55
40	13.7	19.2	0.54	0.32
50	4.9	10.8	0.69	0.71
55	0.34	0.38	0.75	0.89

	Proportional Values			
Incubation	% decrease LEF_{O_2}		% increase $Y(ND)$	
Temp (°C)	WT	M55	WT	M55
40	0	0	0	0
50	64	44	22	55
55	98	98	28	64

Fig. 6-8: $Y(ND)$, $Y(I)$, $Y(NA)$ vs Incubation Temperature at 100 µE. Comparison of WT cells on the left and M55 on the right.
Data was captured during measurements to ascertain rates of $ETR1$ presented in Fig 7 and as such the same conditions were used. Cyanobacterial samples were incubated at the indicated temperatures for 10 minutes in the dark before being filtered through a 10 mm diameter glass fibre filter to produce a 'cyano disc', as discussed in Chapter 2. Discs were cut to 8 mm, a small addition of carbonic anhydrase at 1mg/mL was added and discs were then left in the dark for 5 mins at 30 °C in the 1000 µL gas tight MIMS cuvette. During this time a brief N_2 purge removed the standard atmosphere, before 20 µL CO_2 and 30 µL $^{18}O_2$ was injected. P700 signals were zeroed after 5 minutes and measurements of $P700_{max}$, $Y(I)$ under steady state conditions in addition to gas fluxes were recorded simultaneously. Values presented are the mean of at least three repeats and standard deviation.

In the earlier measurements in the bottom left of Fig. 6-5 at 100 µE, WT cells recorded a $Y(ND)$ of only 0.07. In contrast, after the 25 °C incubation (i.e. no damage), WT samples in top left panel of Fig. 6-8 recorded a $Y(ND)$ of 0.57. Although the primary causes of donor side limitation in cyanobacteria stemming from alternative electron sinks upstream of PSI have been discussed, the likely cause of this change was probably attributable to the very low $LEFO_2$ values recorded in the incubation experimental data. In comparison to the

earlier data presented in Fig. 6-5, the rates of $LEFO_2$ in WT samples incubated at 25 °C were approximately 50 % lower. This unfortunately suggests that the activity of PSII itself was somehow affected in WT samples used for incubation experiments.

Through observing the data in Fig. 6-8 for M55 cells in the upper right panel, there seems to be a very slight increase in the value of $Y(NA)$ in the M55 cells when compared to WT cells at temperatures where PSII was still delivering electrons (25 °C and 40 °C). This was consistent with the finding of AA^+ spinach discs, lacking the capacity to perform CEF in Fig. 6-3. However, the value in M55 was relatively insignificant when directly compared to the spinach discs, which could be the result of the high acceptor side capacity maintained by the FLV1-3 complexes in 6803, able to directly reduce O_2 to H_2O with excess reductant in a 'pseudo cyclic' pathway (Allen, 2003, Allahverdiyeva *et al.*, 2013) to generate a proton gradient.

It is evidence that suggests the M55 cells were lacking sufficient acceptors, compared to the WT samples, which exhibited literally zero acceptor side limitation. However, in the earlier $Y(NA)$ comparisons between WT and M55 in Fig. 6-5, it could be seen that the mutant was not suffering an appreciably larger acceptor side limitation. As such, the difference in this case may be due to the lower rate of reductant generated by the relatively low functionality of PSII in the WT cells.

At the lower range of incubation temperatures (25 – 40 °C) the values of $Y(NA)$, $Y(ND)$ and $Y(I)$ for both WT and M55 remain stable, indicating that the 40 °C incubation resulted in no damage to either sample. This result was broadly in line with electron flux data presented in Fig. 6-7, and 6803's response to elevated temperatures presented by Inoue *et al.,* (2001). If the 40 °C data points were therefore taken as a baseline, then interesting differences in the responses between the mutant and WT can be observed. Such a comparison has been presented in the table presented within Fig. 6-8.

After 10 minutes at 50 °C, both the WT and the mutant suffered large increases in $Y(ND)$, and a consequent decreases in $Y(I)$. This all correlated highly with significant decreases in $LEFO_2$, (from Fig. 6-7). It is the relative magnitude of these changes that are interesting to consider.

When compared to data after a 40 °C incubation, the increase in $Y(ND)$ for WT cells, incubated at 55 °C for ten minutes, was 22 %; however, it suffered a 64 % reduction in the $LEFO_2$ flux. In the same comparison, M55 samples recorded a 55 % increase in $Y(ND)$

after losing a proportionally smaller, 44 % $LEFO_2$ electron flux. One point that must be made is the WT cells already suffered a very high $Y(ND)$ compared to expectations, and as a result the smaller increase in $Y(ND)$ at this stage is possibly less important than it ought to be (in other words, if the cells had been more healthy there could have been a similarly big reduction for WT samples).

Data from Inoue *et al.,* (2001), shows that a 55 °C incubation for 5 minutes of WT cells grown at 25 °C and 35°C resulted in declined photosynthetic rates of 45 % and 25 % respectively (Inoue *et al.*, 2001) . Therefore, a 10 minute incubation of cells grown at 30 °C reducing by 64 % is quite high, although not unreasonable, considering the length of exposure to damaging temperatures was doubled in comparison to this published work. The relative resistance to damage exhibited by M55 in this context is quite interesting, although it will not be investigated here further.

The very large change in $Y(ND)$ data for the M55 sample could indicate that detachment of phycobilisomes from PSII in the otherwise 'stuck' State-I of these cells, discussed earlier, may have resulted in proportionally less energy being diverted to the PSII complex. This would result in fewer electrons being delivered from PSII to PSI. In addition to this, there are many more PSI than PSII centres in 6803 (Cooley and Vermaas, 2001), which results in a more rapid oxidation of PQ when fewer alternative electron sources are available to re-reduce the samples. As such, the larger increase in $Y(ND)$ for M55 cells can both support the idea that $f_i$value shifts to 0.5 due to the detachment of phycobilisomes, whilst also providing evidence that WT cells, suffering a proportionally smaller increase in $Y(ND)$, were able to heavily supplement the lost PSII activity with electrons sourced through perhaps respiration, also perhaps the cycling of electrons around PSI. Comparing the following incubation temperature step at 55 °C against the 40 °C benchmark in the table of Fig. 6-8, the difference in response between WT and M55 cells became stark. The total increase in $Y(ND)$ for WT cells was 28 % compared to 64 % in M55, although the WT started at a higher value. So to exclude this factor it is pertinent to simply compare the increase in $Y(ND)$ from 50 °C to 55 °C: from 0.69 to 0.75 in WT and from 0.71 to 0.89 in M55. This represented an 8 % and 20 % (to almost 90% impairment of function in the case of M55) increase, respectively.

The reduction of $LEFO_2$ electron fluxes became irrelevant at this point, as it reached almost zero in both samples. The fact that under this condition the WT cells still exhibited

the capacity to utilise PSI, and maintained a $Y(I)$ of 0.26 compared to the M55 sample's 0.10, suggested that a source of electrons were available in WT cells, that was not available in the M55 sample. With no electrons entering the system from PSII, the only likely source was from respiratory electrons, reducing the PQ pool via complexes such as the SDH and NDH-1 (Berry *et al.*, 2002).

Interestingly, in the earlier experiment comparing the response of cells to varying irradiance, a very low level of $\Delta Flux$ was recorded at the lowest irradiance in WT cells (20 µE, top left panel of Fig. 6-5), which suggested that NDH-1/SDH complexes were not pumping a very large electron flux into the thylakoid for the reduction of $P700^{+}$. This supported the idea that electrons sourced through respiratory sources may have reduced the PQ pool, poising the thylakoid membrane for CEF (Alric, 2015). Hence, after severe thermal damage that preferentially inhibited PSII, there is clear evidence that can be interpreted to mean cells were cycling electrons through PSI. With the capacity of the intersystem electron transport components to still function after this thermal incubation already established in section 6.2.6, it is possible that these electrons are also being cycled around PSI. However, the data cannot conclusively show this was true, although there is no reason to say it is not possible. The data is consistent with the energy leveraging hypothesis, regardless of whether or not the reductant was truly being cycled around PSI, or simply passing through it.

6.4 Key Findings from Chapter 6.

The results in chapter six have shown that (1) it was possible to successfully utilise the integrated MIMS/P700 system to measure cyclic electron transport in a spinach leaf disc. (2) It was also possible to estimate the flux of CEF in cyanobacteria. However, (3) the measurement's assumptions did not work once PSII suffered severe damage. (4) Thermal damage to PSII resulted in increased $\Delta Flux$ rates in in the 6803 strain, consistent with the interpretation of increased CEF. However, (5) it was not possible to separate true 'cyclic' flux, from the potential for linear flux of alternative reductant passing linearly through PSI. A repeat of this experiment with a comparison of WT, the M55 (lacking NDH_1 and SDH activity) and an SDH mutant, would enable the fluxes be 'teased apart' more thoroughly. (6) there may be many cases in the literature where phototrophs have suffered damage to PSII, and

the authors have hypothesised increased CEF, when in fact the source of reductant was from 'chlororespiratory like' pathways.

Chapter 7.

Results discussion & conclusions

Summarising the data & extending the findings

Chapter Overview: Testing and extending the four hypotheses

Four primary hypotheses underpin the work conducted in this thesis. Their evolution reflects the progress, and to some extent the circumstances, of this PhD. In this Chapter, each will be discussed separately in sections 7.1, 7.2, 7.3 and 7.4, with respect to the data presented in Chapters Four, Five and Six: together with further literature support. In section 7.5, the scope of the key findings is extended.

> *It is argued that in response to a loss of PSII function, an alternative donor is used to supplement reductant required by the thylakoid membrane during illumination, sourced through "chlororespiratory like electron transport" (Havaux, 1996).*

It is suggested that although the concept of 'illuminated chlororespiration' is not new: it seems to be rarely considered as a stress response, or this response becomes subsumed into what can be simplistically interpreted as cyclic flux around PSI. Data and its interpretation in this thesis were compared to an example from the literature, to support the criticism of authors who state that changes to P700 redox kinetics are solely the result of elevated CEF rates.

Two ideas are then suggested, to further the commonly considered benefits provided by illuminated chlororespiratory responses, as were originally summarised by Bukhov and Carpentier (2004). They are based on the principles of maximising both the energy potential from stored reductant, and the still functional cellular systems, in response to environmental stress. These ideas are displayed figuratively in panel C of Fig 7-1.

The first idea relates to the 'recycling' (in a cyclic path around PSI) of the finite stored chemical potential energy supplies of phototrophs, namely the energy stored in glycogen bonds in cyanobacteria (Gründel *et al.*, 2012), to help maintain a proton gradient (for multiple physiological benefits) during times where PSII is severely inhibited. This is illustrated with the 'blue/yellow striped', and pure blue arrows, in panel C of Fig 7-1. Significantly, this pathway would provide the cells with the ability to utilise the energy harvesting capability of undamaged PSI, and associated thylakoid complexes, in the case of PSII specific inhibition. Their alternative is to allow this secondary energy harvesting system to sit in the 'safe' but 'useless' oxidised state, until the damaged PSII complexes are repaired: presumably with

finite supplies of energy released through the oxidation of carbohydrate reserves (represented by the purple arrow in panel C of Fig 7-1).

As the energy being used to drive PSI is not directly being 'spent' but rather 'invested, this concept is considered as the 'leveraging' of stored energy, against that potentially available from the environment. It represents the idea that energy must be made available to the thylakoid, in order that the thylakoid be able to function in its task of translating energy into a form suitable for use by the organism. Parallels are therefore drawn between this concept, and some simple ideas of the financial system.

The second idea draws on concepts relating back to heterocysts of N-fixing cyanobacteria. These cells utilise PSI activity to drive 'low energy potential' NADH, generated by some steps in the TCA cycle (significantly, including the function of the SDH complex in cyanobacteria), into the high energy potential NADPH required for the majority of anabolic processes. This linear pathway, able to elevate the reducing potential of respiratory sourced reductant, presented as 'green/yellow striped' and solid green arrows in panel C of Fig 7-1.

I also propose that a clear name should be ascribed to the 'illuminated chlororespiration' stress response. The first reason is that by definition 'chlororespiration' implies the reduction of O2 to H2O at a terminal oxidase, whereas this pathway, in its 'purist' sense, is trying to avoid this energetically wasteful step. The second reason is to enhance the ability of photosynthetic physiologists to clearly state when this pathway, or response, may have been observed. This is based on the observation that trying to find examples of this response in the literature was surprisingly difficult: given that aspects of 'illuminated chlororespiration' are more frequently reported than was immediately obvious. Below are four examples of the different terms found, that all describe aspects of the same process:

- *"chlororespiratory like electron transport"* – Related to potatoes leaves under heat stress (Havaux, 1996).
- "*NADPH from the oxidative pentose phosphate pathway drives the operation of cyclic electron flow around photosystem I"* – Brown macro algae suffering salinity/osmotic stress inhibition of PSII (Lu *et al.*, 2016)
- "*suppression of photosynthetic electron transport by respiration due to heat stress"* – Heat stress response found in cyanobacteria, algae and plants (Lajkó *et al.*, 1997)
- "*Oxidation of stromal reductant*" – Heat stress in algae (Bukhov *et al.*, 2002)

There are more examples, from different stresses, but the range of descriptions provided here exemplify the issue, that 'illuminated chlororespiration' is a broadly observed, variably described, response.

It may be possible that, with such a large collection of descriptions currently permeating the literature to describe it, its significance as a phenomenon has been overlooked. Part of the reason for this is that the response possibly applies to so many scenarios where PSII has been preferentially inhibited. As such, there is a potential opportunity to unify a component of stress recovery, relating to (for example) stresses of high irradiance, heat, osmotic potential, chemicals and nutrient deficiencies. This provides a good reason to promote the idea more clearly within the stress research/plant energetics community.

A consequence of the fact it has been poorly defined, in my opinion, is that authors may not consider that it is functioning, when they make conclusions based solely on $P700^+$ re-reduction kinetics, for example. So, the conclusion that elevated rates of $P700^+$ re-reduction rates implies an elevated rate of CEF around PSI, is a conclusion often made in the absence of steady state measurements (i.e., are based on single flash kinetics of P700). Furthermore, this is often lacking any gas flux data to discount possible components of a respiratory source of alternative reductant to $P700^+$ (which 'appears' as cyclic electron transport around PSI with flash spectroscopy of P700). By introducing a clear terminology, more attention may be given to possibility of this response to stress.

The significant potential impacts of the energy saving aspects of illuminated chlororespiration at an ecosystem scale are considered briefly. Then the significance that thylakoid components between PSII and Rubisco are consistently found to exhibit greater resilience to stress, than the primary source and sink reductant, is also given some consideration.

7.1 Integrated MIMS/P700 measurements provided sufficient information, and resolving power for the *in vivo* deconvolution of complex cellular physiology

Investigating cellular physiology *in vivo* is exceedingly complicated. Ruuska *et al.* (2000) stated that determining an accurate *in vivo* value for the photosynthetic electron flux

to O_2 in leaves, in spite of the authors' utilisation of simultaneous MIMS based gas fluxes, chlorophyll fluorescence and a number of well characterised mutants for comparison, "remains difficult". That was an investigation of C_3 leaves, however, which requires an extra level of consideration due, for example, to the high potential for photorespiration, possible shifts in stomatal conductance or possible artefacts, such as the alkalinisation of the stroma that may lead to erroneous CO_2 uptake fluxes (Havaux, 1996).

In relatively simple cyanobacteria, a number of the possible variables are already substantially reduced, such as minimised rates of photorespiration being expected due to activity of CO_2 concentrating mechanisms around Rubisco (Price *et al.*, 2008). Nonetheless, the average cyanobacterium comprises over 1000 protein families (Mulkidjanian *et al.*, 2006). The expression of these proteins, their activity, and their impacts on physiological processes are regulated by numerous complex and delicate feedbacks, and signalling systems. Cyanobacterial electron transport chains and metabolism is also highly flexible, and able to rapidly shift, thanks in part to the sharing of key electron transport components between the photosynthetic and respiratory chains (Mullineaux, 2014b).

In spite of the complexity, and difficulty, associated with *in vivo* measurements, there is an absolute requirement for accurate physiological assessments to be undertaken of *in vivo* systems. This could be to validate predictions made with genetic models (You *et al.*, 2015) or to confirm the functionality of components assayed *in vitro (Koike and Katoh, 1980),* discussed in section 7.2. Through combinations of modern investigatory tools, including molecular biology and the various 'omics (genome, phenome, metabolome, transcriptome, etc) and modelling (*in silico* studies), the functional regulation and damage of entire cellular systems, not simply individual proteins, are slowly being elucidated.

In this thesis, the integration of MIMS based gas fluxes (incorporating isotopic differentiation for O_2 evolving and consuming reactions, along with CO_2 fluxes), were found in their own right, to provide significant levels of information pertaining to the responses of moderately thermophilic cyanobacterial cells to temperature stress. This was to both low temperatures, in section 4.1.2, and to high temperatures in 4.2. The former observations will require more independent verification. The conclusions drawn, that elevated rates of O_2 uptake at suboptimal temperatures were driven by a limitation in the rates of the Calvin Benson Bassham cycle, were purely speculative (although based on sound literature).

The latter point, however, was explored through an in-depth analysis of the gas fluxes: utilising a mass balance estimation framework (Radmer and Kok, 1976). This analysis hinged on the fact that two of the gas fluxes measured, O_2 evolution and uptake, were *gross* rates. From this it was possible to test assumptions about the net gas flux rates, to explore the feedbacks that make up whole cell measurements. It was the addition of simultaneous P700 measurements, however, that allowed for strong conclusions to be made in support of the gas flux findings: especially the hypothesis that reductant from respiration, found to function in the light, was able to reduce $P700^+$.

As such, this thesis has provided more support to the expanding area of integrated gas flux/light probe measurements. In recent years the use of MIMS and P700 has become a significant method for the elucidation of electron fluxes to various in-vivo components: such as Ermakova *et al.* (2016), who used the technique to help determine the fate of reductant within the thylakoid, to understand functional roles of various alternative oxidases in cyanobacteria. Or Yamamoto *et al.* (2016), who used these combined techniques to understand the function of transgenically expressed Flv1-3 proteins within *Arabidopsis* plants. In this paper, the authors were able to examine the relationships between the photochemical yield of PSI, its donor/acceptor side limitations and the rates of photosynthesis, CO_2 fixation and O_2 uptake: to help make their conclusions about the activity of the Flv1-3's, their source of reductant, and how they interacted with native proteins in the system.

Where this thesis stands apart, however, is that no attempt was made to investigate the specific activity of a single cellular component, such as Ndh-1, the FLv1-3 or SDH complexes. The application of these integrated systems was an attempt to deconvolute complex gas flux signals from native cyanobacteria, to observe and elucidate their responses to suffering heat stress: without a reliance on mutants or chemical inhibitors. In some respects, the approach taken is therefore more of a hybrid approach. It combined the methodological approach of Zhang and Sharkey (2009), in the manner that the gas flux and spectroscopic systems were integrated, with that of Inoue *et al.* (2001), in the way they made comparisons between damaged and control organisms to make conclusions about the step-wise protein damage occurring within PSII.

However, the techniques used in this thesis were more robust than the data generated by those authors, thanks to the high resolving power and simultaneous isotopic

measurements, provided by the MIMS. With just a single set of data from the integrated system, the MIMS/P700 instrument provided more detail on the activity of cells after thermal incubation than the three separate measurements undertaken by Zhang and Liu (2016), in their investigation of heat stress on the cyanobacterium *Arthrospira sp*. Their result essentially shows that as PSII failed the rate of CEF around PSI increased: as did respiration. However, without conclusive gas flux data (only having access to net O_2 fluxes), the authors could not really provide much evidence for some of their interpretations. For example, they arrive at the same conclusion as work in this thesis, that the supply of reductant from PSII limited photosynthesis, and not CO_2 fixation. However there is no data presented on CO_2 fixation rates.

The MIMS/P700 integrated system also proved itself whilst undertaking measurements for the estimation of steady state CEF around PSI, initially in spinach discs, then with the cyano discs of 6803 and the Ndh-1 mutant, M55. By determining gross O_2 evolution rates for the calculation of $\boldsymbol{LEFO_2}$, it was possible to validate previous methods used by Kou *et al.* (2013) who relied on an O_2 electrode and the flash O_2 evolution method.

The other significant aspect of utilising the MIMS to make this measurement was that it made it possible to monitor the actual [CO_2] around the leaf disc. This data is not shown in the thesis, but early measurements suffered from low rates, and this turned out to be a result of CO_2 limitation in the sealed system. This led to the addition of 1.0 M $NaHCO_3$ at pH 9.0 on a filter disc within the cuvette, to maintain a saturating CO_2 atmosphere, as discussed by Walker (1987). The data presented in Fig. 6-2 and published (Fan *et al.*, 2016) was an excellent validation of the earlier published methods.

7.1.1 *The future for MIMS measurements*

Future investigations using a similar set-up would benefit greatly from incorporating the second stable isotope, $^{13}CO_2$, as was demonstrated by Haupt-Herting and Fock (2002). This could provide gross values for all primary respiratory gas fluxes involving O_2, CO_2, and provide a significant increase in the confidence of conclusions made at damaging temperatures.

Another future application of this methodological set-up will be to undertake analysis of cyanobacterial/algal mutants, designed to generate gaseous products such as H_2 or isoprene (Wilhelm and Jakob, 2011). Using cyano discs, with which precise sample

absorptance can be measured (See section 6.2.2), a modern mass spectrometer with the capacity to rapidly switch detectors and magnet settings to precisely measure both standard gases, such as CO_2 and O_2, their relevant isotopes, and the process gas as a function of calibrated irradiance. This will enable much more sophisticated energy balance and cellular responses, to determine potentially useful mutants, and analyse/tailor their production costs and efficiencies.

7.2 Hypothesis: PSII exhibits lower thermal tolerance than other key metabolic components of the moderate thermophile BP.1

Previous work investigating the thermal tolerance of *Thermosynechococcus elongatus* BP.1 (BP.1) has provided evidence of a strong correlation between net O_2 evolution rates, growth rates and temperature: following a tight bell curve around the optimal temperature, 57 ° C (Yamaoka *et al.*, 1978). The narrow optimal range defined for growth, and contiguous relationship between optimal growth and lethal temperatures, fit the general observations regarding thermophilic photosynthesis made by Berry and Björkman (1980) (see Fig. 2).

However, one experimental finding made with gross O_2 evolution measurements, discussed in section 4.1, suggests that activity of PSII was not as inhibited by low temperature, as a comparison of net O_2 evolution rates versus temperature would suggest. At suboptimal temperatures, the high rates of PSII function was offset by an equally high 'regulatory' O_2 consumption (50% of all O_2 produced was consumed, see panel A,C in Fig 4-2), possibly through Flv1-3 proteins (Allahverdiyeva *et al.*, 2013). This suggested that components downstream of PSII involved in linear electron transport, likely relating to CO_2 fixation, were responsible for impaired growth at lower temperatures (Yamaoka *et al.*, 1978). No further investigation of low temperature stress was conducted in this thesis. Its scope was refined to advance the understanding of the BP.1's cellular responses to transient exposure to damaging high temperatures.

In previous work on this topic, conducted by numerous authors to elucidate the tolerance to temperature of individual components of the BP.1 cells, various complexes have been biochemically isolated and assayed *in vitro*. This includes the PSI reaction centre, FeS clusters F_A, F_B and F_x, ferredoxin-NADP oxidoreductase (FNR_L – I believe this activity was being tested, based on the method), Cyt-C_6 and Fd. All showed activity at temperatures

greater than those found to damage PSII severely (Hirano *et al.*, 1980, Koike and Katoh, 1980, Sonoike *et al.*, 1990).

However, no *in vivo* work has been conducted to confirm the functionality of significant components, such as PSI, the Calvin-Benson-Bassham cycle or even respiration, after thermal damage. No work has been published on the stability or activity of the ATP synthase in BP.1 either, and it has been assumed in this thesis that the complex exhibits a similar thermal tolerance to the other primary thylakoid based proteins, downstream of PSII, described here. This is a significant assumption, as a primary rationalisation for the hypothesis discussed in section 7.5 involves the generation of ATP after high temperature damage to PSII.

To investigate hypothesis 7.1, the approach was taken to find active cellular components after PSII had been severely inhibited, by super-optimal temperatures. As such, the first component of the thesis was to identify the activity of PSII, and then monitor its performance as a function of temperature. Three different measurements of PSII activity were corroborated in this thesis work. The primary measurement was the gross O_2 evolution of PSII, measured through isotopic differentiation of oxygen evolving and consuming activities of cells (Radmer and Kok, 1976), made possible through the utilisation of MIMS and the enrichment of the $^{18}O_2$ isotope in samples.

Normalising these values to the maximum, rates of Gross O_2 evolution were found to correlate strongly with the similarly normalised values of F_v/F_m, the well accepted fluorescence measurement for photochemical capacity of PSII (Maxwell and Johnson, 2000), presented in Panel B, Fig.4-3. Further, gross O_2 evolution, normalised to maximal values, was found to very closely trend the measurement of PSII kinetic area, an estimation of relative PSII activity (Jia *et al.*, 2014), presented in Fig 5-4. However, a possible over-estimation of the kinetic area's size, driven by an alternative source of reductant once PSII was inhibited by high temperatures (discussed in section 5.5.1), meant the values did not correlate as well as literature data suggests they ought (Hu *et al.*, 2013).

As opposed to showing problems with the method, this latter point was considered evidence to support the hypothesis, as will be discussed below with reference to the second hypothesis (7.2). In conclusion therefore, the measurements of gross O_2 evolution from BP.1 cells in the MIMS cuvette were considered an accurate proxy measurement for PSII activity in the samples.

7.2.1 *Examining cellular activity, once PSII had failed*

Gas flux measurements performed at a single, optimal temperature (55 °C), after a ten minute dark incubation of cells at a range of damaging temperatures, was found to be a more reproducible, accurate, and allowed for higher resolution data (see 4.2) of thermal damage than assaying cellular photosynthetic performance at the temperatures of interest (see section 4.1). The results from the incubation method indicated that PSII suffered catastrophic damage somewhere between 63 °C and 65 °C (see Panel B, Fig 4-5). This was based on a 'step change' (as opposed to a gradual reduction) in gross O_2 evolution rates of ~ 95 %, occurring between the ten minute incubation temperatures of 62 °C and 65 °C. This result is strongly supported by the results of thylakoid activity, isolated from BP.1 cells, measured by (Kaurov Yu *et al.*, 1990) after five minute incubations.

In support of the hypothesis, at temperatures ≥ 65 °C where PSII was severely inhibited, the following measurements support that a number of significant cellular activities were still able to function:

1. Oxygen uptake fluxes, in the light and the dark, shown in panel A & B of Fig 4-5, indicated that cellular respiration was not only functional in the dark, *it was no longer inhibited by illumination at photosynthetically saturating irradiances.*
2. Results of a gas flux mass balance estimation, performed on gas flux measurements of cells incubated at 65 °C, discussed in Section 4.4, were strongly consistent with the tested assumption that CO_2 fixation was still active at rates = 100 % of the remaining PSII activity. This was further corroborated by consideration of gas flux dynamics between light and dark, observed in raw data in the 65 °C panel of Fig 4-8. This analysis also supported the O_2 data, from the first point, with respect to respiration rates.
3. Analysis of P700 data collected simultaneously with gas fluxes, post thermal incubations (discussed in section 5.4), indicated that the photochemical Yield of PSI declined at a slower rate than the rapid loss of PSII could account for – as illustrated by the normalised to maximum comparison of gross O_2 evolution rates and $\boldsymbol{Y(I)}$ data (presented in Fig 5-3). Investigating what drove the redox dynamics of P700, after PSII was severely inhibited, became the foundation for the second hypothesis (7.2), discussed below.

These results suggested that three primary cellular components were still functional at temperatures where the activity of PSII had been severely inhibited (to < 5% maximal rates). This finding brings the understanding of BP.1 cellular physiology firmly into line with the physiology of other phototrophs, in which the elevated thermal tolerance of respiration is well documented (Gifford, 2003, O'Sullivan *et al.*, 2013).

It shows that the ΔT of PSII function and the tolerance of other photosynthetic and respiratory processes, is maintained in moderately thermophilic cells, as it has been shown to exist consistently in mesophiles (Zhang and Liu, 2016). The result also provides further evidence that the physiology of true 'thermophiles', growing optimally at temperatures ~ 15 °C higher than the BP.1 cells (i.e., *Synechococcus lividus* H-fX) seems markedly different, where CO_2 fixation seemed to fail before the activity of PSII (Meeks and Castenholz, 1978).

7.2.2 *Discussion of results, PSII failed before other components*

The finding that CO_2 fixation was still occurring after incubations at 65 °C (where PSII had been substantially inhibited) was consistent with the idea that significant cellular components, including thylakoid membrane based complexes, systems downstream of PSI, and those utilised by the Calvin Benson Bassham cycle, were still functional (i.e., all components, excluding PSII, in Fig 7-1). Furthermore, this *in vivo* set of measurements provided some support, and some constraints, to the published results of *in vitro* measurements, performed on biochemically isolated components of BP.1. Published values show that the $K_{0.5}$ of thermal protein degradation of Cyt C_{553} (commonly referred to as Cyt C_6) was 85 °C , the $K_{0.5}$ for ferredoxin (Fd) functionality was determined at 75 °C (Koike and Katoh, 1979), the functional $K_{0.5}$ of NADPH-ferredoxin-oxidoreductase ($FNR_{(L?)}$) was 76 °C (Koike and Katoh, 1980) whilst the activity of P700 and its primary acceptor, P430, possessed functional $K_{0.5}$ of 93 °C and 75 °C respectively (Sonoike *et al.*, 1990). Even a cursory comparison of results from *in vitro* measurements with *in vivo* data, suggests that the $K_{0.5}$ of *in vitro* systems is a poor indicator of *in vivo* cellular function. However, this does not discount the value of *in vitro* measurements of this nature. The majority of the published *in vitro* data sets show similar trends to temperature as the *in vivo* system. The reality is that the source of energy for driving many cellular reactions is likely to be a greater limitation to *in vivo* function (as was suggested in this thesis, with respect to *in vitro* measurements of Rubisco activity (section 4.14, Fig 4.4)), than necessarily the stability of individual complexes once cells suffer severe stress (where a single component in a chain fails, the function of all suffers). This exemplifies the need for steady state, *in vivo* measurements, to validate the biological applicability of such data-sets.

The results presented in Panels A,C of Fig 4-2, and panel A of Fig 4-5, discussed throughout Chapter Four, strongly support those published by Yamaoka *et al.* (1978) and Inoue *et al.* (2000); who both found that the activity of the cells was highly temperature

dependant, and correlated strongly with the function of PSII. However, neither paper investigated the relative remaining function of supplemental processes, like respiration, once PSII was inhibited. A thorough literature search suggests no measurements of the thermal stability of respiration exist for this model organism, except for some basal rates at a single temperature. These were found to support the rates measured in this thesis for undamaged cells (see section 4.1.2.5). Disappointingly, even papers investigating the structure/function of key thylakoid based components of respiration, Ndh -1L (Wulfhorst *et al.*, 2014), do not perform gas flux measurements of the BP.1 mutants generated, to investigate the functional activity of the enzyme they are working to understand and how genetic/structural changes affect activity.

7.2.2.1 The type of damage suffered by PSII at ~ 65 °C

A comparison between data in this thesis and conclusions drawn from Inoue *et al.* (2001), regarding the denaturing of PSII's extrinsic subunits in cyanobacteria, suggests that the most thermally sensitive component of the BP.1 cells was the instability of a specific component: likely the manganese stabilising protein (MSP), or perhaps the reaction centre (Inoue *et al.*, 2000). Applying Inoue *et al's.* (2001) model of PSII thermal inhibition (developed with *Synechocystis* 6803) to data in this thesis, suggests that the MSP dissociated, leading to damage of the manganese calcium cluster – producing a large proportion of "Form C" , or possibly "Form D" PSII structures (see Fig 9, Inoue *et al.* (2001)). The difference between them is the reaction centre chlorophyll's activity, (determined with fluoresence) – although neither form generates O_2. Conclusions from Inoue *et al's.*, (2000) work on *Thermosynechoccocus vulvanus* (the almost identical species to BP.1, at the nucleotide level, (Katoh *et al.*, 2001)), suggests that the reaction centre of PSII, and that of the oxygen evolving complex, were equally labile. This supports the formation of Form D, i.e., damage occurred to the reaction centre as well as dissociating the MSP.

The stark contrast between catastrophic PSII inactivation, between 62 °C and 65 °C, and the initial increase, followed by a slow yet steady decline in rates of respiration, observed in Panels A and B of Fig 4-5, supports the idea of a rapid dissociation: as opposed to a slow denaturing/loss of activity. Yamaoka *et al's.*, (1978) finding, that BP.1 cells incubated for 5 mins at 65 °C could no longer be recovered, suggests that the damage accrued by PSII occured very rapidly, further evidence of a single weak point in the system at these elevated temperatures. That the cells are very difficult to cultivate at 60 °C (Yamaoka

et al., 1978) suggests perhaps that rates of damage at this temperature may be similar to rates of repair. Respiration itself, however, showed robust activity at higher temperatures, being still functional after a 67 °C incubation. This indicates that, in spite of the relatively tight tolerance between optimal and lethal temperatures exhibited by thermophilic phototrophs: Berry and Björkman's (1980) idea about the reversible thermal stress of 'starvation' still applies. However, compared to mesophiles, this is to a very confined thermal window.

The conditions used during recovery likely impact the capacity to survive thermal incubations, as Inoue *et al's.* (2000) work with *S. vulcanus* showed it was able to survive a 70 °C incubation for 5 mins in darkness, which according to the authors' data inhibited a large proportion of PSII function. Whether provided with standard actinic light, a low recovery light, or kept in darkness during recovery was unfortunately not stated, or compared in their paper. Such an experiment was not performed during this thesis either, as the initial aims of the PhD work did not extend to stress response/recovery mechanisms. However, I now hypothesise that providing some light to enable PSI turnover may have had an impact on the capacity of cells to recover from sever PSII inhibition, for reasons discussed below (in section 7.5).

7.2.3 *Key cellular components were more tolerant than PSII to transiently high temperatures*

Which component of PSII was damaged was less significant to this study, than the fact that PSII (as the primary source of reductant for the thylakoid membrane), was inhibited by a 10 minute incubation at 65 °C. In spite of this damage, other primary cellular systems investigated in this thesis continued to function at rates which seemed to be determined more by limitations set by the lack of available reductant, than any damage they suffered, per se.

For example, a large increase in the PSI donor side limitation ($Y(ND)$), the associated loss of the PSI photochemical Yield ($Y(I)$) (Fig 5-3) and the significant suppression of carbon fixation, was correlated strongly to the loss of PSII function after a 65 °C incubation. However, *in vitro* measurements of Rubisco function in Chapter 4, still showed 20 % of maximal rates after a 70 °C incubation (Fig 4-4), suggesting that at least this enzyme's function would unlikely to have been the driver of the cessation of CO_2 fixation *in vivo*. In fact, the Calvin Benson Bassham cycle was still found to be functioning at 100 % of

the remaining PSII function (see discussion in 4.4.3) after the 65 °C incubation. This suggests the remaining proportion of Rubisco found to be functional *in vitro* after elevated thermal incubations was able to utilise the remaining reductant generated by the few remaining functional PSII centres, to continue CO_2 fixation *in vivo*.

Significantly, the P700 data and gas fluxes strongly supported the conclusion that PSI was still functionally intact, and participating in photochemistry: most probably with reductant sourced through the elevated rates of respiration that were no longer suppressed in the light. In conclusion, the data in this thesis clearly supports the hypothesis that post PSII inhibition, other key cellular processes were able to maintain function.

7.3 Hypothesis: At temperatures that inhibit PSII, reductant sourced from respiration can drive the activity of PSI.

- PSI became a component of the respiratory chain

The generation of this second hypothesis came directly from the evidence used to support the first hypothesis. Specifically, the observations that after incubations at 65 °C, the activity of PSII was reduced to < 5% of its maximal activity:

- Yet PSI was still turning over with 15 % of maximal efficiency (Fig 5-3)
- Cellular respiration rates became significantly higher than non-damaged temperatures, in spite of the measurement temperature being constant (Panel B, Fig 4-5), see Student's T test as discussed in section on Dark O_2 and CO_2 gas fluxes on page 118.
- Respiration in the dark was not suppressed in the light (See discussion in section 4.4.1)
- Comparison of the PSII Kinetic area data in Fig 5-4 with PSII activity determined through gross O_2 evolution rates, and examination of the raw $P700_{max}$ data in Fig 5-5, indicated that PSII Kinetic area had been overestimated due to impaired post saturating pulse rates of re-oxidation.

Data in Fig 5-3 showed that the donor side limitation of P700 ($Y(ND)$) was driven by the loss of PSII activity, illustrating the large influence that reductants from PSII had on the functional activity of PSI. To account for the disparity between the PSI and PSII turnovers observed, once PSII was inhibited, an elevated cyclic electron flux was considered (and is often cited as a response to high temperature exposure (Yamori and Shikanai, 2016)).

However, the conclusion discussed in section 4.4.1, based on mass balance estimates of the measured gas fluxes, in combination with observations from the raw gas fluxes in the 65 °C panel of Fig 4-8, suggested that CO_2 fixation was functioning at rates equal to remaining PSII activity.

This ruled out that remaining PSII activity alone was poising the thylakoid membrane for cyclic flux around PSI (Alric, 2015), as the fixation of CO_2 would 'bleed' the system of reductant, leading to heavily oxidised Fd: the likely donor for cyclic electron flux (Peltier *et al.*, 2016). Therefore, to enable the continued redox dynamics of PSI, another source of reductant was required, as determined through measurements of P700 and discussed in section 5.3. The obvious clue to the alternative source of reductant came from the significantly elevated fluxes of respiratory gases, measured in darkness after a 65 °C incubation (Panel B, Fig 4-2), which after the application of mass balance estimations, in section 4.4.1, was shown to be no longer suppressed in the light.

To explain these observations the following hypothesis was formed: as PSII became inhibited, the oxidation of sugars supplemented this photosystem as a source of reductant. Another way of thinking about this was that PSI became a component of the respiratory chain: because it played a functional role in the oxidation of sugars, and as will be discussed in 7.5.2, helped to increase the energy potential of a proportion of reductant sourced from respiration (at least the component oxidised by the SDH complex).

7.3.1 *Literature examples of alternative $P700^+$ reduction*

The observation that respiration was no longer suppressed in the light is an old one; however, has been referred to as the 'down-regulation' of photosynthesis by respiration (Lajkó *et al.*, 1997). This is in fact, the opposite way of interpreting the results found in this thesis. The idea that the oxidation of sugars can reduce the PQ pool is also old: In fact, Hirano *et al.* (1980) wrote the paper "Plastoquinone as a common link between photosynthesis and respiration in a blue-green alga" based on measurements performed with BP.1.

There are precedents that cyanobacterial thylakoids, and algal/plant chloroplasts, can utilise an alternative source of reductant to PSII, sourced through the oxidation of an organic substrate for use in photosynthetic processes. Although this seems to describe the idea of chlororespiration, as will be discussed below (section 7.5.2), there are differences

between the definition of chlororespiration and the illuminated energisation of the thylakoid membrane with respiratory reductant, that warrant these two concepts be considered independently

Picoplankton in oligotrophic oceans, unable to access sufficient nitrogen to synthesise PSII, utilise PSI to cycle reductant sourced from external organic compounds, to help fix N_2 (Grossman *et al.*, 2010). This is an idea confirmed further through recent lab based experiments (Saroussi *et al.*, 2016). The mutant of 6803 lacking PSII and respiratory oxidases, described by Howitt *et al.* (2001), also sourced external reductant and organic compounds for growth. Based on redox measurements of the PQ pool and elevated growth rates in the light, it was deemed able to cycle this reductant around PSI, for energetic gains. Also in 6803 cells, Liu *et al.* (2012) blocked donation of electrons from PSII into the thylakoid with the addition of DCMU, to investigate the physical movement of key thylakoid based enzymes involved in CEF (NDH-1) and the injection of respiratory reductant into the thylakoid membrane (SDH). The addition of the herbicide did not stop the cycling of electrons. In green algae like *Chlamydomonas*, the pathway has been well studied (Johnson and Alric, 2013), in macro algae it is hypothesised that stromal reductants poise PSI for cyclic when PSII is inhibited by desiccation (Gao and Wang, 2012) and in plants, too, evidence suggests that an alternative donor to PSI under stress conditions is sourced through the oxidation of respiratory reductant (Havaux, 1996), or 'stromal reductant' (Bukhov *et al.*, 2002).

In spite of the large body of evidence that alternative donors to PSI can rapidly help to balance the energetic requirements of illuminated thylakoids lacking sufficient PSII activity (across cyanobacteria, plants and algae), it seems that few authors clearly state this was, or was not, occurring in their reporting on measurements of stress responses. Even the relatively recent review of "High temperature effects on electron and proton circuits of photosynthesis" by Sharkey and Zhang (2010), acknowledges that *"the relationship between increased redox status of PS I and more oxidized PS II centres has not yet been explored"*: yet in their review no clear reference was made to the possible involvement of 'chlororespiratory like' activity contributing to this cellular status in plants.

It is generally accepted that high temperature stress, for example, leads to an elevation of cyclic electron flux around PSI. This is often determined through hastened $P700^+$ re-reduction, or decreased P700 oxidation rates, measured in a non-steady state

system (Aihara *et al.*, 2016, Li *et al.*, 2016). However this fails to account for the fact that (a) an alternative donor to the PQ pool may be required to poise the thylakoid for cyclic electron transport, if PSII is inhibited or (b) that 'illuminated chlororespiration' will lead to an increase in reductant passing through PSI, as $P700^+$ has a greater affinity for reductant than terminal oxidases (Bukhov and Carpentier, 2004) (as demonstrated by the inhibition of 'dark chlororespiration' by a saturating pulse).

Nonetheless, a number of recent examples of physiological studies in macro algae, investigating desiccation (Gao and Wang, 2012) and osmotic stress (Lu *et al.*, 2016) that preferentially inhibited PSII function, concluded that respiratory reductant was driving $P700^+$ re-reduction in the light. However, Lu *et al.* (2016) did not include any gas flux data to really support their hypothesis that the oxidative pentose phosphate pathway (OPPP) was providing the NADPH used by the cells to re-reduce $P700^+$. Instead the authors relied primarily on the action of chemical inhibitors, measurements of cellular NADPH/NADH concentrations and light probe measurements under varying levels of salinity, to support their hypothesis. As will be discussed in 7.5.2, an increased ratio of NADPH to NADH could in fact be evidence of elevated 'illuminated chlororespitory' like pathways, driving a linear electron transport route through PSI (Green arrow, Fig 7-1).

7.3.2 *Thesis data supports $P700^+$ was reduced by respiration*

During actinic illumination at 500 µE following incubations at 65 °C that severely inhibited PSII in BP.1 cells, it is probable that the PQ pool tended towards being highly oxidised (discussed in 4.2). The lack of reductant entering the thylakoid membrane, combined with the high excitation pressure experienced by PSI, led to a severe donor side limitation ($\boldsymbol{Y(ND)}$) of P700 (Fig. 5-2). Under these conditions, Cooley *et al.* (2000) predict the up-regulation of SDH activity, as this complex is able to donate electrons directly to a strongly oxidised PQ pool (based on a comparison of redox potentials between the different redox species involved).

Evidence for reduction of $P700^+$ by alternative donors was found and discussed throughout Chapter Five. In section 5.5.2 the observation was made that weak FR light, designed to preferentially and substantially oxidise PSI, became less effective at oxidising P700, as was determined through a number of observations. The steady state $P700^+$ signal, measured under weak FR illumination during $\boldsymbol{P700_{max}}$ measurements, declined in proportion with the peak obtained when adding a saturating pulse. This data was displayed

in Panel A of Fig 5-6. As respiration rates declined, determined through dark gas fluxes in panel B of Fig 4-5, the oxidation state of steady state weak FR light increased again, in proportion to the saturating pulse peak: suggesting a correlation. In section 5.5.3 the rates of $P700^+$ re-reduction in the dark, at the cessation of actinic illumination during $\boldsymbol{Y(I)}$ measurements, were compared in panel B of Fig 5-6. This also suggested a correlation between large declines in respiration rates, and the rate of re-reduction of $P700^+$ in the final 50 ms of the dark period: at temperatures that had severely inhibited PSII function. This exact conclusion was also drawn by Havaux (1996), in measurements conducted on potato leaves subject to inhibitory thermal damage. Finally, as noted, the decline of the PSII kinetic area with temperature trended PSII function very closely, but the magnitude of change was significantly less (discussed in section 5.5.1). Comparison of raw $\boldsymbol{P700_{max}}$ curves with increasing temperature showed that the re-oxidationof P700 by FR light, post saturating flash, became steadily delayed: leading to over-estimation of the area of the curve, and was hypothesised to be a result of alternative reduction of $P700^+$.

These two data sets were taken as mutually supportive, although somewhat anecdotal, evidence for a role in respiratory processes reducing $P700^+$. A more objective observation to support the hypothesis was made through comparison of the raw data generated during the $\boldsymbol{P700_{max}}$ and $\boldsymbol{Y(I)}$ measurements (presented in Fig 5-5 and discussed in section 5.5.4). Through this comparison, the extent to which *weak* FR light was 'under oxidising' the total pool of P700 became apparent. Whereas the data in panel A of Fig 5-6 suggested that the total level of steady state oxidation during weak FR illumination declined by only a few percent, (compared to the saturating pulse oxidation peak (as discussed in 5.5.2), a comparison between the two curves showed that the entire $\boldsymbol{P700_{max}}$ curve had been severely depressed at temperatures where PSII suffered and respiration had increased. Samples lacking PSII activity, exposed to 500 µE actinic illumination, became much more oxidised than the $\boldsymbol{P700_{max}}$ peaks. This was considered strong support to the idea that an alternative source of reductant was able to re-reduce $P700^+$, at rates much greater than could be re-oxidised in the weak FR light. Significantly, the irradiance of the weak FR light was determined, through comparative measurements in undamaged samples, to be adequate for the oxidation of approximately 90 % of P700 in the samples, as can be seen in the top panel of Fig 5.6.

7.3.3 *Anoxygenic, aerobic respiration? The competition for O_2*

The title of this section is trying to highlight the idea that the hypothesised 'linear path' of reductant through PSI, to $NADP^+$ and then potentially into some form of anabolic cellular metabolism, could upset the stoichiometric assumptions about respiration. Under the conditions used in these experiments, respiratory pathways would have been aerobic. However, the mass balance estimation analysis of gas fluxes after incubations at 67 °C and 70 °C (section 4.4.4) provided the final piece of data that PSI became a 'participant in respiration', when cells suffered thermal damage from transient exposure to super-optimal temperatures.

All gas fluxes analysed after incubations < 67 °C were balanced within the 5 % margin of error (see Fig 4-7, although note that the 65 °C incubation did balance with the application of Eqn. 3), deemed acceptable in this thesis, through application of one of the two mass balance equations discussed in 4.3.1. However, the fluxes at 67 °C and 70 °C, regardless of the assumptions used to test the results, would not balance after incubations. Consistently, the rate of CO_2 efflux, and the uptake of O_2, could not be matched. The former flux was always greater than the latter, but significantly this was only found to occur during illumination (Panel A, B Fig 4-5).

At these very high incubation temperatures, nearly 100 % of the gas fluxes measured during illumination were considered a product of respiration: both net O_2 and net CO_2 fluxes were negative (implying uptake) and the activity of PSII had declined to only ~ 2% of its maximal rate (Fig 5-3). Although the data after high incubation temperatures was noisy, a comparison between the experimental blank (used to confirm that background consumption offsets for MIMS gas flux calculations were accurate) in Fig 4-9, and the data in the 67 °C and 70 °C panels of Fig 4-8, clearly shows the addition of cells to the cuvette drove the gas fluxes measured. In other words, the signals were not so noisy as to be meaningless: it was a consistent level of noise, around a mean. The data was deemed useful, replicated three times, and warranted consideration.

As such, where assumptions about aerobic respiration in cyanobacteria support a respiratory quotient of around 1.0 (Fogg, 1973) between O_2 uptake and CO_2 efflux, this dropped to about 0.7 at 67 °C and to only 0.3 at 70 °C. This supported the hypothesis that oxygen was in competition as a terminal acceptor. Significantly, this was only found to occur when samples were illuminated. In the dark, rates of CO_2 efflux remained essentially

unchanged from the illuminated rates (well within the margin of measured error), whilst the uptake of O_2 increased, to return to a quotient of 1.0 (Panel A,B Fig 4-5).

Significantly, NO_3^- was specifically excluded from the measurement buffer and cells were rinsed in NO_3^- free buffer before measurements, to exclude nitrate reduction as an alternative acceptor. Yet a readily available, non-oxygen terminal acceptor, available only in the light, could have been $NADP^+$ on the acceptor side of PSI. This is especially if it was then used in anabolic metabolism. This possible pathway is presented in panel C, Fig 7-1 as the "green arrow", representing linear transport of respiratory reductant, via NADPH, to be reduced through some anabolic cellular processes.

That $P700^+$ was in competition with O_2 for reductant, is exactly as Lajkó *et al.* (1997) described with respect to the B_6-f complex of cyanobacteria, algae and plant thylakoids, after thermal incubations that increased rates of 'chlororespiration'. In that paper, the authors describe a competition between thylakoid based terminal oxidases, and the primary pathway for photosynthesis: observed through KCN inhibition of the oxidases leading to increased flux through b_6-f. However, the authors considered the upregulation of respiration as down regulating photosynthetic rates after high temperature exposure. This interpretation is disputed in this thesis: the opposite explanation is considered more likely.

7.4 Hypothesis: Reductant sourced through respiration may poise the redox balance of the thylakoid membrane, enabling the cycling of electrons around PSI if PSII is inhibited

The reduction of the PQ pool through the oxidation of photo-assimilate was shown to be sufficient for the maintenance of active PSI turnover after BP.1 cells had suffered severe heat induced PSII inhibition (see section 5.7 & discussion of Hypothesis 7.2). This led to the further hypothesis, that the reductant sourced from respiration could possibly poise the thylakoid membrane for cyclic electron flux (CEF) around PSI (Alric, 2015), possibly resulting in the 'recycling' of respiratory reductant to pump protons and generate ATP.

In the light, terminal oxidases are outcompeted by the photosynthetic complexes for reductant (Bukhov and Carpentier, 2004). Reductant sourced through respiration that reduces the PQ pool will therefore not necessarily find O_2 as a terminal acceptor, being

instead elevated to reduce Fd by the activity of PSI. This is represented by the green and blue striped arrow, running through the thylakoid membrane in panel C of Fig 7-1. Assuming that these electrons were not utilised to reduce a respiratory oxidase (as in traditional chlororespiration (Rumeau *et al.*, 2007)), an alternative oxidase (Ermakova *et al.*, 2016), or reduce $NADP^+$ (Bothe *et al.*, 2010), it would be possible theoretically for reduced Fd to re-reduce PQ, or possibly through the cyt-b_6/f directly, thus 'recycling' the reductant sourced through respiration.

The following literature based findings provided evidence that these assumptions were at least plausible:

- Schuurmans *et al.* (2014) concluded that cyanobacterial cells prefer to maintain the PQ pool's redox state, than necessarily the production of energetic molecules. This provides a precedent that cells could down regulate the production of NADPH, to favour re-reduction of the PQ pool, if PSII was inhibited.
- In the light, alternative and respiratory oxidases are poor competitors for reductant, compared to photosynthetic components such as the acceptor side of PSI (Bukhov and Carpentier, 2004, Nawrocki *et al.*, 2015).
- The physical location of the Ndh-1/SDH complexes changes in the light to optimise the probability of reducing $P700^+$ over terminal respiratory oxidases (Liu *et al.*, 2012).

Furthermore:

- This entire process was recently suggested by Lu *et al.* (2016), with respect to PSII inhibition by salinity stress in brown algae, in extension to their earlier work indicating a similar response to desiccation (Gao and Wang, 2012).

Therefore, a number of elements of cell physiology align with the idea that respiratory sourced reductant can be recycled around PSI, under conditions where cellular respiration has not been down regulated in the light. Data in Chapter Four (see section 4.2) suggested that this was the case when PSII activity has been inhibited by exposure to high temperatures.

The idea is consistent with some photosynthetic pathways demonstrated by ancient, anoxgenic photosynthetic systems. These systems rely on the oxidation of substrates such as HS^-, H_2 or $FeSO_4$ (Widdel *et al.*, 1993, Falkowski *et al.*, 2008). In the case of green sulphur bacteria, this is around a Type I bacterial photosystem. However, anoxygenic photosynthetic bacteria can also utilise organic compounds, such as acetate or succinate. In the case of the purple bacteria *Rhodobacter sphaeroides*, electrons released through the oxidation of

succinate, by an SDH complex, are cycled around the reaction centre to generate a proton gradient (Jenney *et al.*, 1996).

Three papers, already mentioned, support this pathway existing in photooxytrophs as well: The first is Grossman *et al.'s* (2010) finding that picoplankton in oligotrophic oceans cycle reductant, sourced through heterotrophic activity, around PSI to survive. The second relates to the 6803 mutant inhibited in PSII and all respiratory oxidases (Howitt *et al.*, 2001) able to utilise the same strategy. The third is Lu *et al.* (2016), who state that respiratory NADPH can be cycled around PSI in brown macro algae inhibited in PSII function.

7.4.1 *Thesis data supporting recycling of respiratory reductant*

To investigate the possibility of this occurring in cyanobacterial cells suffering severe thermal inhibition of PSII, measurements of CEF were undertaken under steady state conditions of photosynthesis. Such a measurement has not been published in cyanobacteria. Measurements of CEF are very difficult to make, particularly under steady state conditions, as no products are generated or reactant consumed (Fan *et al.*, 2016). Most attempts to investigate CEF in cyanobacteria are made via P700 re-reduction kinetics, post illumination. Often the pre-illumination is not steady-state (Howitt *et al.*, 2001), or even actinic light (Aihara *et al.*, 2016). However, a method published by Kou *et al.* (2013), developed with C_3 plants was considered an interesting technique to apply to cyanobacteria. This method relied on finding the difference between fluxes of steady state linear electron transport (through gross O_2 evolution measurements), and the calculated turnovers of PSI: considered an estimate of cyclic electron transport (see section 6.1.1). The use of this technique was the driver for development of the 'cyano leaf' method, discussed in section 3.3.3. These were then utilised in various measurements discussed in Chapters Four, Five and Six.

Before applying the method directly to an untried cyanobacterial system, this method was initially conducted with glasshouse grown spinach discs, to test the accuracy of the integrated P700/MIMS system. By successfully reproducing the published results from Kou *et al.* (2013), the data in Fig 6-3 demonstrated that both the system was working well, and the assumptions used by the original authors to estimate gross O_2 evolution rates (with pulsed actinic light) were accurate. This result was reported in Fan *et al.* (2016).

The method was then applied to cyanobacteria. Unfortunately, the work had to depart from investigating the moderate thermophile BP.1, due to the need to inhibit 100%

of CEF when determining the partitioning of light between the two photosystems. In spinach this could be achieved by the addition of Antimycin A (AA) and exposing the discs to low irradiances. However, in cyanobacteria the majority of the CEF pathway is AA insensitive, as it does not rely on the (proton gradient regulator) PGR-5 route (Shikanai, 2016), and instead utilises Fd reduction of the PQ pool via the Ndh-$1_{1,2}$ complex (Peltier *et al.*, 2016). As such, the Ndh-1 deficient strain of 6803, designated M55 (Ogawa, 1991) needed to be utilised.

To test the hypothesis, steady state estimations of the relative rates of cyclic electron flux around PSI were calculated, in cyano discs of 6803, and the Ndh-1 mutant M55, after cells were incubated for 10 minutes in the dark at a range of temperatures. The results, presented in Fig 6-7 and discussed in section (6.2.5) were strongly consistent with the hypothesis, but also unclear (with some of the issues discussed in the following section). However, the clear data was that $\boldsymbol{\Delta Flux}$ increased with increasing temperatures in the WT cells, until gross O_2 evolution dropped significantly after a 55 °C. In-spite of this drop, there was still a statistically significant $\boldsymbol{\Delta Flux}$ between the flux through PSII and PSI. The 55 °C incubation inhibited ~ 100 % of the activity of PSII, in both the WT and M55 cells, consistent with the studies of thermal acclimation conducted with 6803 cultures by Inoue *et al.* (2001). The gross O_2 evolution rate of WT cells illuminated at 100 µE, expressed as a flux of electrons per square metre (as $\boldsymbol{LEFO_2}$), dropped from a maximum rate of 13.7 to 0.3 µmol(e^-).m^{-2}.s^{-1} between incubations at 40 °C and 55 °C respectively. M55 cells dropped from a maximum of 19.2 to 0.3 µmol(e^-).m^{-2}.s^{-1} between the same incubation temperatures. As the activity of PSII was most probably close to completely inhibited and the flux through PSI was still found to be statistically significantly higher through PSI, the result strongly supports the hypothesis that an alternative source of reductant, such as respiration, was able to drive PSI. As no difference between the flux of electrons generated at PSII and PSI was recorded in the M55 cells, it could be concluded that no CEF was functional in the mutant. This was expected, and significantly, ruled out back reactions in PSI from contributing to the $\boldsymbol{\Delta Flux}$ value in the WT cells. As such, this result supported the hypothesis.

This supports the conclusions of Lu *et al.* (2016) that NADPH sourced through the OPPP could drive operation of cyclic flux around PSI. It also supports the idea that respiratory reductant can be 'recycled' around PSI (represented by the blue, and blue/green striped arrows in Panel C of Fig 7-1), in a similar way perhaps, to anoxygenic, single photosystem bacteria.

7.4.2 *Potential issues with the result, and how they manifest in the literature*

It was mentioned that the result strongly supported the hypothesis, but was also unclear. That the rates determined for fluxes through PSII and PSI matched each other in the M55 strain was an excellent validation that the method worked, as this result was expected. A second validation was the finding that rates of $\boldsymbol{\Delta Flux}$ increased in the WT samples, with increasing thermal stress, including as rates of linear electron transport ($\boldsymbol{LEFO_2}$) decreased at 50 °C, as would be expected (Yamori *et al.*, 2016). As such, the result that CEF continued once PSII was severely inhibited by incubation at 55 °C (Fig. 6-7, also see Inoue *et al.* (2001) for response of 6803 WT cells to this range of incubation temperatures) is considered robust. There is plenty of evidence, already discussed in this Chapter, that the alternative source of reductant could have derived through respiratory processes.

Yet, in spite of a relatively clear result that CEF seemed to be functional as PSII was completely inhibited, a couple of considerations must be made when interpreting the data: which don't seem to be made in the literature. The first is that according to Cooley *et al.* (2000), the functionality of SDH in M55 cells is also inhibited, likely due to a lack of substrate from various feedbacks into the respiratory system. This is considered the explanation for impaired rates of dark respiration, reported for this strain (Ogawa, 1991). The M55 mutant therefore consists of too many individual changes to make strong comparative conclusions. If the SDH complex was a primary pathway for reductant to reduce the PQ pool from respiration, then there is no way to clearly differentiate CEF through PSI in the WT, from a potential linear path from SDH (or any other stromal reduction of the PQ pool) through PSI.

This is the problem I see in the simple interpretation of increased $P700^+$ re-reduction rates being used to imply increased rates of CEF around PSI, by authors such as Li *et al.* (2016). In their paper investigating the role of the NDH complex in mitigating heat stress experienced by WT, and an NdhJK mutant of tobacco, the authors conclude that cyclic fluxes in the light, but dark reduction of PQ with stromally sourced reductant, were roles played by the complex to minimise thermal damage. This conclusion was based on comparisons between the WT and mutant of fluorescence measurements of PSII, P700 measurements (purely oxidation/re-reduction kinetics using low intensity FR light and a flash of saturating light), an inhibitor of PTOX, net rates of CO_2 fixation and a western blot of primary proteins being studied: under heat stress and a control. How were the authors able to separate

purely cyclic flux around PSI, from the possible linear flux of reductant from stromal reductant through to NADPH, or to the terminal acceptor via Fd, in the light?

Another issue this paper raised for me was that the term 'chlororespiration' seemed to be applied simply to refer to the activity of PTOX, and/or NDH, as they are components of the chlororespiratory chain. However, it was not clear that chlororespiration, or CEF around PSI, which both utilise these complexes, was driving the observed response. This is evidence of the need for a more specific term, to differentiate 'chlororespiration' from the illuminated variant, where reduction of $P700^+$ through stromal/respiratory sources of reductant takes place.

7.4.3 *How to address this problem?*

In the steady state estimations of $\Delta Flux$, conducted in Chapter six, the mass balance estimation approach to the gas fluxes could have provided evidence for the likelihood that SDH function was contributing to the level of $\Delta Flux$. However, this was very difficult, because the raw data in these measurements became too noisy to perform precision mass balance estimations (as was performed with the BP.1 cells). Signal noise is a part of life when using MIMS. Each Teflon membrane is different, and they degrade over time. At the time of performing the $\Delta Flux$ experiments, the concept of performing a mass balance estimation was not being considered, and as such, although the data was sufficiently clear to determine $\Delta Flux$, it was not for an accurate mass balance estimation.

In future, it is hoped to be able to compare M55, WT and an SDH impaired mutant (Cooley and Vermaas, 2001). It is hypothesised that if the $\Delta Flux$ of M55 = zero, then the difference between the SDH (where $\Delta Flux$ = CEF – SDH activity) and WT (where $\Delta Flux$ = CEF + SDH activity) could be a more accurate estimation of the respiratory reductant actually being cycled around PSI. During the repeat of this experiment, consideration will be given to minimise the Teflon membrane signal noise, to ensure a mass balance can also be conducted with the data. Furthermore, as will be discussed below, $^{13}CO_2$ will be added to provide a thorough data set.

Nevertheless, the data in this thesis, in combination with evidence from the literature that PSII inhibition in other phototrophs led to the 'potential' cycling of alternative reductant (Lu *et al.*, 2016), strongly supports hypothesis 7.3, that respiratory sourced reductant can be cycled around PSI, as PSII is inhibited.

7.5 Extending the findings of this thesis

The idea that respiratory sourced reductant can function to supplement the activity of inhibited PSII, under stress, is by no means new. It is discussed by many authors, referred to throughout this Chapter already, as a response to numerous PSII specific stresses. However, it is this author's opinion that the possible role played by illuminated 'chlororespiratorty like' electron transport, is not considered frequently enough under stress conditions that would seem likely to support such a cellular response. Instead, a component of this is frequently cited: cyclic electron flux around PSI, without sufficient consideration given to how the thylakoid membrane has been poised to enable this flux.

The data in this thesis focused on the physiological response of cyanobacterial cells to damaging high temperatures. In this case, high temperature was found to impact upon PSII more than other systems within the cells: in line with literature discussed in the introduction. However, numerous environmental stresses preferentially inhibit PSII in other phototrophs too: including cyanobacteria, algae and plants. Of primary environmental relevance is photo-damage (Li *et al.*, 2016), and inhibition by factors such as nutrient deficiency (Saroussi *et al.*, 2016), poisoning such as heavy metals (Cuchiara *et al.*, 2015), or toxicity (Patzelt *et al.*, 2016) and osmotic pressure/salinity (Lu *et al.*, 2016).

In response to a loss of reductant sourced from PSII, evidence in this thesis suggested that the cells examined were supplementing the thylakoid membrane's requirement for reductant with electrons sourced through respiration during illumination. Two energetically expedient rationales are suggested to support this stress response mechanism:

The first is to maximise the utility of functional cellular components. When only one system has been impacted by an environmental stress, it makes sense that still useable systems are kept functional as much as possible. This may not only help in generating the required energetic molecules used in anabolic repair processes, but as Sharkey and Zhang (2010) suggest, maintaining a proton gradient can minimise damage to thylakoid based protein complexes.

The second idea relates to the finite nature of these alternative electrons. If two identical organisms suffered identical stress, but one could harness radiant energy through the function of PSI with reductant from respiration (say, the function of the SDH complex), whilst

the other could only generate energetic molecules (specifically NADPH) via the Oxidative Pentose Phosphate pathway (OPPP) or the Tricarboxylic Acid (TCA) cycle, with no energetic input from the environment via functional PSI, it is conceivable that the second organism would succumb to stress earlier through starvation (illustrated with the purple arrow in panel C of Fig 7-1). This is especially true in response to repeated stress events (such as daily photodamage events), and especially if a number of stresses occurred simultaneously. The conclusion from Lu *et al.* (2016), that NADPH from the OPPP reduced PSI in a macro algae growing in the intertidal zone, suffering daily osmotic inhibition of PSII, fits this perfectly. However, the authors do not enter into any assessment of the data, except to report the likelihood that this response was observed; as such, they do not consider this sort of possible advantage.

7.5.1 *The illumination of chlororespiration*

"The energy leveraging hypothesis"

In their review of alternative donors to PSI, Bukhov and Carpentier (2004) define three benefits of the processes associated with driving PSI activity with alternative reductant:

- *"adjustment of ATP/NADPH ratio required for CO_2 fixation*
- *generation of the proton gradient for the down-regulation of PSII and for ATP supply*
- *the active transport of inorganic carbon in algal cells"*

In this thesis I wish to propose a fourth potential benefit, related to managing the levels of ATP/NADPH, but more specifically related to maximising the energy utilisation/efficiency of the system, especially when PSII is subject to severe inhibition. It centres on maximising the useful energy that can be extracted from PSI, and its associated protein complexes (which were found to be resilient to heat stress in this thesis), and minimising the use of finite energy reserves being stored in the cells (ie, glycogen).

Whether electrons are simply arriving from PSII and being elevated in reducing potential by PSI to fix CO_2 (yellow arrow in panel A, Fig 7-1), or are cycled around this photosystem (red arrows, Panel A Fig 7-1): some source of reductant is required to allow PSI to perform its work of fixing light energy into chemical potential energy. In some ways therefore, PSI needs to 'have energy' to 'make energy', or else it simply sits in the oxidised

form (Shimakawa *et al.*, 2016) which, although not damaging, doesn't provide useful input to the system.

In this work, and in the conclusions of Lu *et al.* (2016), samples suffering inhibition of PSII were hypothesised to utilise alternative donors to maintain PSI function. In both cases, this source was considered likely to be reductant generated through respiratory pathways. Therefore, cells were tapping into a finite resource (glycogen) to increase the amount of available energy, by allowing for PSI to function. As mentioned in the Chapter introduction, this reductant could have been used directly to perform work (purple arrow in panel C, Fig 7-1): it was instead 'invested', by allowing PSI function to harvest more light energy.

In finance, the concept of leveraging is to use borrowed capital for an investment, expecting the profits made to be greater than the interest payable. It follows that you "have to have money, to make money".

Likewise in a thylakoid membrane lacking PSII function, organisms have to 'spend reductant' to be able to capture and convert light energy for use by the cell with PSI:

They 'leverage' the energy available in their stores, against that available in their environment, by enabling PSI to use light and cycle electrons derived from the respiratory reductant poising the thylakoid.

Two energetically favourable outcomes of driving PSI with reductant sourced through respiration are discussed in greater detail below in sections 7.5.2 and 7.5.3. The first is the possibility that a linear electron pathway through PSI could elevate lower energy potential NADH, produced through some respiratory steps such as the oxidation of succinate to fumarate, to high energy potential NADPH, required for many cellular processes (whilst decreasing the need to diminish the proton gradient to drive a transhydrogenase system and in fact, contributing to the formation of this gradient). The second involves the 'recycling of reductant' around PSI, to maintain proton motive force for the numerous advantages this can provide phototrophs.

7.5.2 *'Linear' energy leveraging, rationale and evidence*

Cooley *et al.* (2000) consider the conditions of a highly oxidised PQ pool to favour the function of the SDH complex, and Cooley and Vermaas (2001) consider this pathway to be a significant alternative donor to the PQ pool, an idea that is still supported (Mullineaux, 2014a). The SDH complex is a component of the tricarboxylic cycle (TCA), which according

to Zhang and Bryant (2011) is modified in cyanobacteria to promote NADPH production, the reductant preferred by cyanobacterial metabolism over NADH (Spaans *et al.*, 2015). However, the acceptor utilised by SDH is not $NADP^+$, and as such direct activity of this complex fails to generate NADPH. One mechanism used to overcome the issue of metabolic steps such as SDH that generate NADH, is the function of transhydrogenase complexes that phosphorylate NADH to NADPH. However, this process comes at the energetic cost of diminishing the electrochemical trans-membrane gradient of the thylakoid (Kämäräinen *et al.*, 2016). It makes sense in this scenario, that the reductant generated through SDH activity ought be 'converted' to the higher energy potential NADPH, and not simply lost to O_2 reduction in the fashion of standard chlororespiration, as illustrated by the green/yellow striped and green arrows in panel C of Fig 7-1.

The reduction of the PQ pool by SDH, or NDH can support the generation of NADPH via linear electron transport through PSI which instead of costing the cells potential electrochemical energy (as in the transhydrogenase function), this process can add to it. In algae, the presence of the NDH-2 complex, which can utilise NADH generated through the TCA cycle directly, makes this an obvious pathway. Its relevance may be less clearly relevant for higher plants, however, with no clear route for NADH reduction of the PQ pool currently described (Peltier *et al.*, 2016).

Results discussed in this thesis provided some evidence that cyanobacterial cells attempted to maximise the electron flux of respiration through the thylakoid, in spite of respiration rates declining, which supports the idea that cells were attempting to maximise the production of useful energy, over simply driving respiratory/alternative oxidases. In section 5.5.3, it was hypothesised that the flux of respiratory reductant entering the thylakoid membrane was only a proportion of the total respiratory flux measured for the cell. However, as the total flux of measured respiration declined at 67 °C, the rates of P700 re-reduction did not decline, consistent with a constant flux of respiratory sourced PQ pool reductant.

The hypothesis used to explain this observation was that cells prioritised the use of thylakoid based respiration, and one reason for this could be to maximise the generation of NADPH. This supports the logic of such a system, and provides a rational for why PSI may become a component in the respiratory chain: for the conversion of 'low energy potential' NADH into higher energy potential NADPH. It was shown by Lu *et al.* (2016) that the

amount of NADH decreased, whilst NADPH increased in the brown algae found to be reducing $P700^+$ with NADPH from the OPPP. The authors hypothesised that glycometabolites from TCA cycle were directed into the OPPP when samples suffered PSII inhibition through salt stress. They argue more NADPH was produced to support CEF around PSI: however, never considered that the function of PSI may have performed the energetic translation that increased the amount of NADPH in the samples. In their recent paper, Kämäräinen *et al.* (2016) demonstrated the significance of NADPH for cells relying on respiration, by knocking out the activity of a membrane bound transhydrogenase, able to reduce $NADP^+$ with NADH and proton motive force. This comes at the cost of ATP, by diminishing the proton gradient across the thylakoid membrane. The linear respiratory pathway through PSI would add to the thylakoid's proton gradient and generate NADPH using solar energy.

Evidence of such a pathway also exists in specialised cyanobacterial cells, capable of nitrogen fixation, called heterocysts. The environment within these cells is maintained strictly anoxic, to protect the oxygen sensitive nitro/hydro -genase enzymes (Bothe *et al.*, 2010). These specialised cyanobacterial cells still possess a functional thylakoid membrane, however, PSII is mostly absent. The oxidation of translocated sugars from vegetative cells (those neighbouring and physically linked to heterocysts, containing active PSII) has been hypothesised as a component of the reductant used to reduce the PQ pool of the PSII lacking heterocysts (Milligan *et al.*, 2007). An active PSI can then utilise this reductant for two primary purposes:

The first is to drive Mehler type reactions, likely through a subset of heterocyst specific Flv1-3 proteins, to reduce any excess O_2 within the cell to H_2O (Ermakova *et al.*, 2014).

The second relates to the respiratory pathways functional in heterocysts, where the oxidation of some sugars (such as Malate and Glyceraldehyde-3-P), produces NADH, and not NADPH. Whereas the NADH can reduce the PQ pool, it must have the higher potential

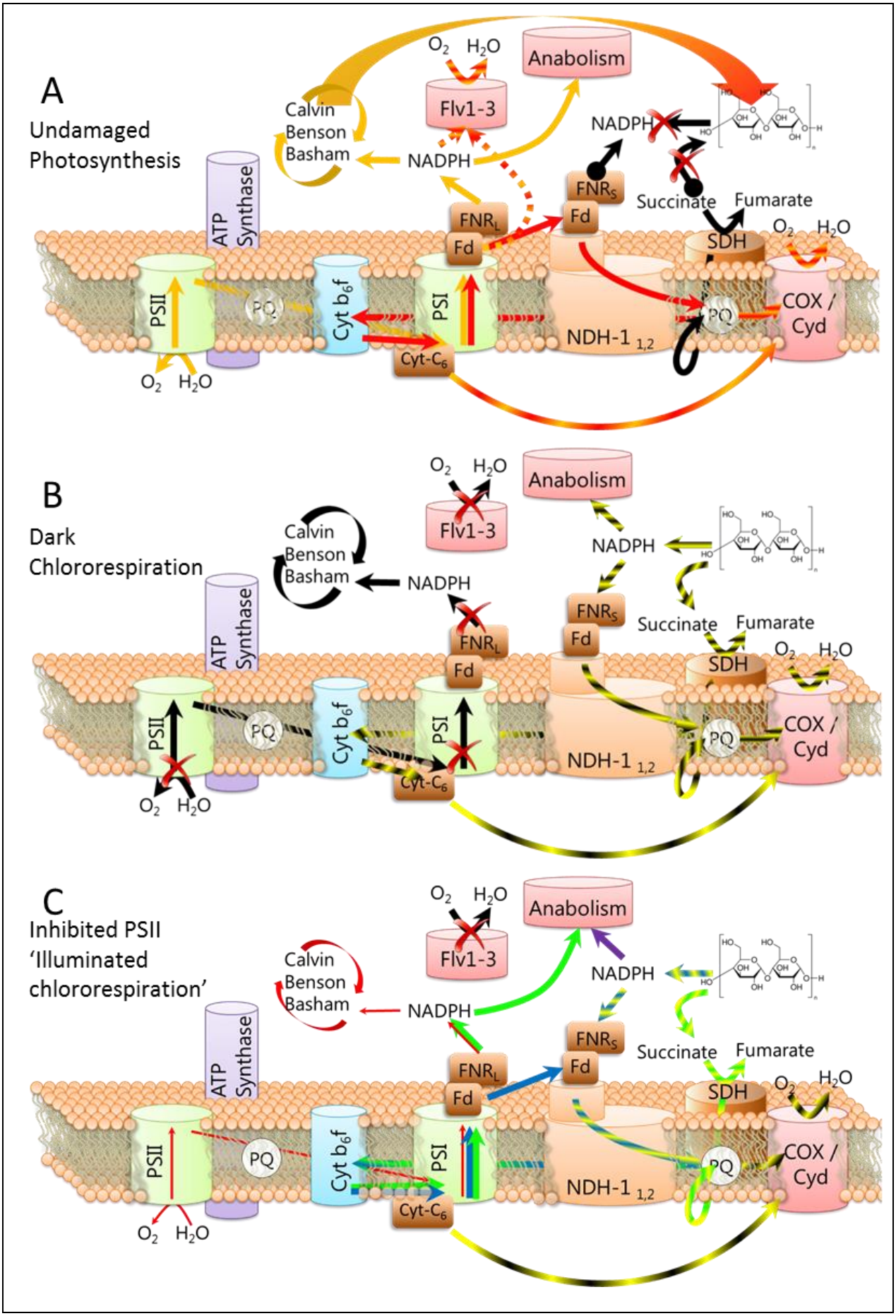

Fig. 7-1: Schematic of electron transport routes through thylakoid membranes of cyanobacterial cells: Comparison of undamaged cells in light and darkness, with illuminated samples suffering PSII inhibition (ie. incubations ≥ 65 °C in this thesis work with BP.1 cells)

Complexes are purely representative and no attempt to account for flux proportions has been made. The translocation of protons and the phycobilisomes/their movement through predicted state transitions under the different scenarios examined here have been omitted for clarity. Note the arrows denoting the PQ pool's diffusion through the membrane, behind complexes to cyt-b_6f, can be difficult to see. Figure modified from Peltier *et al.* (2016), panel C, Fig 2. The top surface of each thylakoid represents the stromal face, the bottom is the lumen.

A: **Undamaged, illuminated thylakoids, performing standard Linear (yellow arrows) and Cyclic (red arrows) electron transport**. Yellow/red striped arrows represent examples of 'regulatory O_2 consumption' at various oxidases, the dashed arrows indicate literature uncertainty of the electron donor. LARGE yellow to red fading arrow across the top represents glycogen synthesis: with yellow side representing linear electron sink, the red side representative of idea that stored carbohydrate becomes an electron source during illuminated chlororespiration when PSII is inhibited (discussed in C), conceptually considered a form of 'delayed' cyclic electron flux. Black arrows show down-regulation of glycogen oxidation/respiratory pathways through redox feedbacks. Protons and ATP not shown, but water oxidation at PSII, activity at the cyt-b_6f, and the NDH-$1_{1,2}$ complexes, contribute to the generation of proton motive force (PMF) for ATP generation at the ATP synthase.

B: Standard chlororespiratory pathways operating in darkness. Black arrows represent down regulation of pathways due to a lack of photosystem activity: including CO_2 fixation or function of Mehler type regulatory O_2 uptake. Yellow/black striped arrows represent linear chlororespiratory pathways, branching at PQ pool. The oxidation of PQ pool by terminal oxidases shifts the redox balance to up-regulate oxidation of carbohydrates, via pathways such as the oxidative pentose phosphate pathway or tricarboxylic cycle (TCA), generating NAD(P)H. Reduction of PQ pool via the SDH complex, or through the NDH-$1_{1,2}$, (contributing to PMF) with reduced Fd, produced by FNR_S through the oxidation of NADPH. Reduced PQ can be oxidised directly through respiratory terminal oxidases, or diffuses through the membrane to the Cyt-b_6f, further contributing to PMF, before cyt-c_6 reduces O_2 at COX. Note, NADPH can also drive anabolic processes directly: ATP is still generated by the activity of ATP synthase, but only via a single pass of reductant, as no cyclic is available due to a lack of photosystem function in darkness. As such, reductant must follow a linear pathway to reduce O_2.

C: Illuminated chlororespiration: Leveraging the energy in stored carbohydrates against that available in the environment by driving PSI with reductant sourced through illuminated respiration. Chlororespiration is no longer confined to a linear pathway back to O_2, allowing for the cycling around PSI to generate PMF, and also to increase the energy potential of NADH, produced through function of some respiratory components, to NADPH for anabolic processes. Evidence for these processes is provided in Chapters Four, Five and Six. Panel C is based primarily on data generated in BP.1 cells after incubations ≥ 65 °C, where PSII was inhibited and respiration was functional.

The red linear arrows represent PSII function at severely diminished rates. Data in chapter Four indicated carbon fixation rates = 100% of PSII function, represented by the fact that this is also red coloured. No regulatory O_2 consumption was detected. Limited PSII activity in actinic light likely resulted in PQ pool being oxidised, upregulating respiratory pathways (as shown in Chapter Four, by negative values for both net O_2 and CO_2 fluxes in the light at rates = dark). Function of SDH, where succinate oxidation produces fumarate and 'directly' reduces PQ pool, generates lower reducing power than NADPH. Instead of simply driving standard chlororespiratory pathway directly to respiratory terminal oxidase (black/yellow striped arrow), PQ diffusion to Cyt-b_6f would provide cells with capacity to pump protons and then reduce Cyt-C_6, which preferentially reduces $P700^+$ over terminal oxidases. At PSI, this low energy reductant can be leveraged against the energy in the environment (light) to generate high energy potential NADPH, for use in anabolic processes: this conversion is represented by the green arrows. As such, SDH based respiratory reductant is represented by the yellow/green arrows, where it could be chlororespiratory, or be used for energy leveraging. Such a pathway would result in 'anoxygenic' respiration, and evidence was found for this, where the respiratory quotient reduced from 1.0 down to 0.7 after a 67 °C incubation, in Chapter Four, during illumination only. Blue and Yellow striped arrows represent reductant generated through various respiratory pathways, which already maximise their amount of NADPH generated. This can be used directly for anabolic processes, as shown by the purple arrow. However, the yellow/blue striped arrows represent the possible flux of a proportion of this through FNR_S to reduce Fd, which can then reduce the PQ pool via NDH-$1_{1,2}$. This step contributes to proton motive force. Once reduced, the branched pathway of PQ diffusion can see it reduce a respiratory terminal oxidase (yellow/black striped arrows) or can reduce Cyt b_6f. As this source of reductant potentially includes that from SDH, a Green/Blue striped arrow represents this diffusion. Via Cyt-c_6 this reductant will also preferentially reduce $P700^+$ over terminal acceptors. At PSI, reduction of Fd allows for either the reduction of $NADP^+$, and regeneration of NADPH, or else the repeating of NDH$1_{1,2}$ reduction of PQ, again adding to the PMF across the thylakoid, represented by the blue arrows. Hence the blue/yellow striped arrows from the oxidation of stored carbohydrates, representing that the reductant can participate in traditional chlororespiration, or be leveraged against the energy in the environment to maximise the utility of cell's energy stores and of functional components and systems through 'recycling' around PSI.

Abbreviations: PSII, Photosystem II; PQ, Plastoquinone; cyt b_6f, Cytochrome b_6f complex; Cyt-C_6, Cytochrome C_6; PSI, Photosystem I; Fd, Ferredoxin; FNR, Ferredoxin-NADP reductase; FNR_L, Large FNR isoform; FNR_S, Small FNR isoform; SDH, Succinate dehydrogenase; COX, Cytochrome aa3 oxidase; Cyd, Cytochrome bd quinol oxidase; Flv1-3; Flavodiiron proteins 1/3; NADH-$1_{1,2}$ NAD(P)H PQ oxidoreductases – containing either D_1 or D_2 subunit.

of NADPH to reduce N_2. As such, PSI is used to increase the reducing potential of this reductant (see fig 5 Bothe *et al.* (2010)), generating NADPH from NADH for use by the nitrogenase enzyme.

With respect to data in this thesis, activity of the 'Mehler like' reactions would result in O_2 reduction and as such, the stoichiometry of the respiratory chain would be maintained with a quotient of around 1.0. However, should NADPH instead be used for the reduction of N_2, any O_2 uptake from that respiratory processes would be absent. As such, this becomes an "anoxygenic pathway" for "aerobic respiration". Similarly, in results of gas flux measurements in 4.2, if the source of CO_2 efflux during experiments was due to respiratory processes reducing the PQ pool (discussed in 4.4.4), any NADPH generated by the activity of PSI, then utilised for anabolic processes, no longer utilised O_2 as the terminal acceptor.

This was consistent with the decreasing respiratory quotients, observed only during illumination, discussed in section 4.4.4.

7.5.3 *Cyclic energy leveraging of respiratory products - Recycling reductant to generate ATP & PMF*

The second subtle take on chlororespiration being considered in this thesis is that the reduction of the PQ pool by respiration can poise the thylakoid for cyclic electron transport around PSI. In section 7.4 above, the analysis and discussion of results from Chapter Six provided evidence that the 6803 cells seemed capable of performing cyclic electron flux in the absence of PSII activity. This idea is supported by Bukhov and Carpentier (2004) in their review of alternative donors to PSI, and has been shown in multiple examples from the literature, such as the role for CEF in picoplankton of oligotrophic oceans (Grossman *et al.*, 2010), discussed above.

The most striking example may be Howitt *et al's.*, (2001) PSII and terminal oxidase mutant of 6803, however. The cells were able to grow heterotrophically, but when illuminated were able to utilise respiratory reductant to drive cyclic electrons: which was found to increase the rate of growth. The source of reductant in these cases was not limited by that stored internally, but it served the same purpose: to leverage energy from the environment by maintaining the functionality of PSI. However, in this case it is hypothesised that the process can help to minimise the amount of stored reductant required, since electrons from the stored reductant are cycled with the help of light energy.

In response to environmental stress that specifically inhibited PSII, results in both this thesis, and underpinning Lu *et al's.* (2016) work, showed that measurements of $Y(I)$ seemed too high after PSII had been inhibited: to be solely a result of cyclic electron flux from any remaining PSII activity. The conclusions from both sets of experiments support the idea that reductant sourced through respiration could be cycled around PSI. However, the reasons provided by Lu *et al.* (2016) keep to well defined and oft cited rationales for cyclic electron transport: maintenance of PMF across the thylakoid to help induce non-photochemical quenching (in the algae). They do not consider possible energetic advantages.

The paper lacks gas flux data, relying on chlorophyll *a* fluorescence and P700 measurements, with the addition of inhibitors. As such, the conclusions drawn by the authors are not far reaching: they can confirm the probable re-reduction of $P700^+$ by respiratory sourced reductant, but that this is truly being cycled is a problematic statement for exactly the reason it is difficult to make this conclusion in Chapter Six. Even the re-reduction of $P700^+$ by alternative reductant from the stroma, being driven linearly to generate NADPH, would be interpreted as being a 'cyclic' flux in the author's interpretation, and would require that the thylakoid complexes be oriented in a manner reminiscent of standard cyclic fluxes.

7.5.4 *Evidence it could apply to a broad range of phototrophs*

Numerous stresses faced on a daily basis by oxygenic phototrophs have the potential to impact more severely on PSII than either PSI or the other primary components of the photosynthetic electron transport chain. There is evidence that some of these stresses, such as heat stress, can improve the rate of PSII repair (Ueno *et al.*, 2016). Many of these stresses, such as heat, drought and excessive irradiance, can impact upon phototrophs simultaneously, on a frequent (daily) basis. There are considerable possible advantages available to organisms that can conserve their stores of energy, or can minimise their use of stored energy to maintain/repair damaged systems: whilst maximising the input from the environment through the use of functional energy harvesting PSI, and its related complexes.

Although PSI can be safely protected from photodamage by ensuring adequate donor side capacity maintains it in an oxidised sate, there is good reason to provide it with reductant: to harvest energy from the environment and make it available for metabolism. This includes the generation/maintenance of PMF, the elevation of low energy potential NADH to high energy potential NADPH, or to increase the amount of available ATP, without 'burning up' the stored energy supplies in one pass. A plethora of evidence supports the

idea that illuminated chlororespiration has been found to be functional in cyanobacteria, algae and plants. The concept of chlororespiration was essentially defined in green algae, (Bennoun, 1982) and the illuminated form is now studied as a matter of course (Saroussi *et al.*, 2016). There is evidence in higher plants and algal chloroplasts of functional respiratory pathways that could supply the required stromal reductant (Singh *et al.*, 1993).

Bukhov and Carpentier (2004) suggest that illuminated chlororespiration may be able to 'cycle' the reductant around PSI. Havaux (1996) concluded that electron donation to $P700^+$ from stromal reductant in leaves of C_3 plants, subjected to elevated temperatures which inhibited in PSII function, was much greater compared to untreated leaves. One of the expected advantages of such a system functioning would be enhanced recovery of PSII damaged samples in light, compared to darkness, which was a conclusion Kreslavski *et al's.* (2008) investigation of thermal/photoinhibition and recovery of PSII, in wheat seedlings.

Although the authors claim an increased rate of CEF facilitated the accelerated recovery: once again they would have been unable to differentiate 'standard CEF' from potential 'chlororespiratory CEF', through the *in vitro* measurements they performed to determine rates of phosphorylation and cyclic fluxes on isolated thylakoids from the various treated and control plants. However, had they considered the latter concept, they could have possibly also tested for this, through the addition of extra NADPH to a set of the samples as well.

Thus, an assortment of evidence in the literature supports the hypothesis that the rapid response to transient high temperature stress examined in this thesis could potentially be applied to numerous PSII specific stresses, across a range of photosynthetic organisms. This includes both the linear and cyclic concepts of 'illuminated chlororespiration'.

7.5.5 *Eco-physiological relevance of proposed 'energy leveraging' ideas: evolutionary advantage of minimising energy use*

A striking example of the need for phototrophs to conserve energy is the prediction that "carbon starvation" will be one of the primary drivers of a predicted 100 % forest mortality across the Southwestern United States by 2050 (McDowell *et al.*, 2016). A single hot, sunny day on a droughted tree can destroy their photosynthetic apparatus (Sevanto *et al.*, 2014). Trees possessing the capacity to maximise the utilisation of functioning systems to continue harvesting energy available from the environment under these conditions would

likely hold an evolutionary advantage, over those that could only utilise their stored carbon in a 'single pass' (in other words, relying solely on the 'purple arrow' in Panel C or Fig 7-1). This is a purely speculative extension of the hypothesis, designed to illustrate the idea that evolutionarily, there is a sound rationale to support the feasibility of such a process. This would also apply, as mentioned earlier, to the daily osmotic/desiccation stress of brown algae growing in the intertidal zone found to reduce PSI with NADPH (Lu *et al.*, 2016).

An area where the results in this thesis, and the 'energy leveraging hypothesis' may be explored in the future, is a further investigation into the ΔT tolerance between the primary photosystem and other thylakoid components of 'highly thermophilic phototrophs'. Where the work in this thesis confirmed that the moderate thermophile BP.1 exhibits a similar difference in thermal tolerance between PSII and other cellular components as exhibited by mesophiles, no such work has been conducted in very high temperature phototrophs growing at the upper thermal range (~ 70 °C to 73 °C). As discussed in the introduction, the overall limit to the thermal evolution of photosynthetic prokaryotes is not entirely understood. Debate still remains, as to whether it is the primary electron source (PSII), or sink (carbon fixation) that has relegated oxyphototrophs to a relatively cool existence (in comparison to non-photosynthetic bacteria and archaea) (Cox *et al.*, 2011).

The results in this thesis spike this author's curiosity: is the ΔT between photosystems maintained in highly thermophilic phototrophs? Hypothesising that the difference is not as pronounced, and PSI activity is as thermally sensitive as the PSII system, does this remove the cell's capacity to manage a loss of PSII caused by transient thermal stress? Could this perhaps have contributed to the lack of further thermal evolution? Defining the stress response and clarifying its benefits

7.5.6 *Providing a name to clarify the difference between chlororespiration, and illuminated chlororespiration.*

The interaction between respiration and the thylakoid membrane is often referred to as chlororespiration. This is defined as: the reduction of the PQ pool by stromal sourced reductant (generally in darkness), that can generate a proton gradient and reduces O_2 to H_2O at a terminal oxidase such as PTOX (Peltier and Cournac, 2002, Quiles, 2006). This pathway is presented in Panel B or Fig 7-1. In eukaryotes, the term differentiates thylakoid based respiration, from mitochondrial respiration (Li *et al.*, 2016). In cyanobacteria it would

seem more accurate to use this term to differentiate thylakoid respiration from that occurring along the plasma membrane, although this does not seem to be the way the term is used (Mullineaux, 2014a). In all cases where chlororespiration is discussed, the common ideas include the reduction of O_2 at a terminal oxidase and the impacts on the redox state of the PQ pool in darkness. The most significant component defining this pathway is the sink for reductant.

I suggest formalising a new definition for 'illuminated chlororepiratory like PQ pool reduction', driven by alternative sources of reductant to PSII, that occurs in the light under conditions that have inhibited PSII (see panel C of Fig 7-1). The focus of this pathway is the source of reductant, and what happens to it. Although it involves reduction of the PQ pool through respiration, from that point on the reductant can be utilised for linear and/or cyclic electron transport: which may or may not reduce O_2. It certainly should produce an H^+ gradient across the thylakoid, and can generate NADPH, depending on which process is being driven. In the case of reducing NADPH, the illuminated chlororespiratory system is operating in a linear mode (Green and green/yellow striped arrows in panel C, Fig 7-1). Data in Chapter Four suggests that such a pathway does not necessarily involve the reduction of O_2 as a terminal acceptor. As such, it is not strictly chlororespiration.

In spite of the number of stresses that preferentially inhibit PSII, where illuminated chlororespiration could provide organisms with potential advantages, the substitution of PSII sourced reductant with that generated through respiration (or otherwise from the stroma), is not often considered in the literature. Where it is, however, the descriptions are very broad (as mentioned in the introduction to this chapter, where four different examples were provided).

It is proposed, therefore, that a new term should be considered to describe 'illuminated chlororespiration': to properly differentiate it from the idea of 'textbook' chlororespiration, that assumes an O_2 terminal acceptor and does not give consideration to some of the potential energetic benefits afforded by this 'new' stress response mechanism. I do not propose 'energy leveraging' as a term, this is a hypothesised energetic benefit of the process, which in my opinion is currently not considered in the literature. Furthermore, in this thesis the term 'respiration' has been used quite loosely: in reality strict 'respiration' is not the only potential source of stromal reductant (including the malate shunt etc., in eukayrotes). As such, I propose the term:

delayed cyclic electron flux, or transport

Which can be shortened to CEF_d, to easily differentiate it from traditional CEF.

It pays homage to fact that its function will likely prove difficult to separate from standard CEF with common P700 measurements. Furthermore, the term is technically accurate, as the stromal reductant will more than likely have had to pass through PSI at some point already, on the journey from PSII to the Calvin-Benson-Bassham cycle (represented by the large yellow to red fading arrow in panel A of Fig 7-1).

In usage, under conditions where PSII activity has been impaired and rates of P700 kinetics indicate CEF is up regulated, authors without access to further tools to differentiate the two alternative PSI donors (the cycling of PSII reductant and/or the injection of stromal/respiratory reductant) could simply state that "the increased re-reduction rates of $P700^+$ observed could be due to CEF and/or CEF_d. In the case where authors work to unpick the two potential sources of flux, they can add "analysis x and y supports that it was a combination of both pathways" or else "no evidence of stromal/respiratory reductant was found as determined through the measurements conducted".

I believe that the clarification of this pathway with a specific term, whatever that may be, will increase the amount of attention paid to its potential energetic benefits, and its significance in stress responses, by photosynthetic physiologists.

7.5.7 *Concluding remarks on 'illuminated chlororespiration'*

To conclude this section, the extension of the combined results presented in this thesis suggests that a previously described, but poorly defined stress response was activated when cyanobacterial cells were incubated at a range of increasing temperatures. The pathway:

- is rapidly activated (in comparison to transcriptional or retrograde signalling systems) in response to a decrease in the redox status of the thylakoid membrane caused by PSII specific inhibition, and could therefore apply to a number of stresses;
- is potentially exhibited across a broad range of phototrophs;
- has been previously identified, but seems to be poorly distinguished from other, more commonly discussed, energetic responses to stress, which are more related to balancing energetic demands;
- could hark back to an ancestral anoxygenic phototrophic system; and

- may provide phototrophs with extra resilience in environments where they face repeated, discrete stress events: especially in response to multiple combined stresses, through a specific increase in the 'energy efficiency' of providing cellular maintenance requirements.

It is hypothesised that providing a clear name to this response may help the physiology community more readily identify if it is occurring.

7.6 Thesis Novelty

In comparison to what has been found, through a significant literature search, this thesis:

- presents the most comprehensive physiological data set on the response of the moderately thermophilic, model cyanobacterium *Thermosynechococcus elongatus* BP.1 to be produced;
- contains the first use of MIMS techniques conducted at thermophilic temperatures (up to 65 °C);
- is the first attempt to estimate steady state fluxes of CEF around PSI in a cyanobacterium;
- has independently (i.e. without setting out to find anything of this nature), found evidence for a cellular response to PSII inhibition, that has been referred to in a number of literature examples;
    - However in this work the rationale for reducing the PQ pool with alternative donors has been extended to include a number of potential energetic advantages that may improve the resilience of photosynthetic organisms to repetitive, PSII specific stresses; and
    - has identified a potential issue in the literature, that this potential stress response has not been differentiated from another, similar response, CEF of PSII sourced reductant.

7.7 Future Directions

The main hypotheses and ideas presented in this thesis were developed in the later stages of the PhD project, coming together as the full picture of the data emerged. As such, many of the simple experiments that could have been conducted to test the physiological

significance of the proposed thermal damage responses could not be performed. These include:

- *Comparing the recovery of cells that have been incubated at 65 °C*, shown in Chapter Four to be inhibit > 95 % of PSII function, under different conditions. For example darkness, a range of actinic irradiances and a PSI specific wavelength. Within this general experimental set-up, conducting supplementary measurements to determine the level of stored carbohydrates before and after recovery, in order to test the hypothesis that enabling PSI to function with respiratory reductant can provide an overall energetic advantage to cells. A second test would be to compare the overall resilience of samples being repeatedly stressed and allowed to recover under the different conditions.
- *Repeating the estimation of steady state cyclic electron fluxes*, conducted in Chapter Six, to compare the WT, M55 and the SDH mutants, as described in 7.3.3. This could provide a clearer distinction between the level of flux passing through PSI directly through an NDH-1 cyclic pathway, or possibly linearly through from the SDH complex. It could be an estimate of the difference between true CEF and potentially CEF_d.
- *Comparing the capacity of these mutants to recover from exposure the PSII inhibiting temperatures*. To test the capacity of cells unable to continue 'driving PSI' with respiratory sourced reductant, when PSII has been inhibited.
- *Separating the measured responses of increased $P700^+$ re-reduction kinetics between standard CEF and the proposed CEF_d, without mutants.* This may be possible by comparing 'dark starved' samples, already lacking readily available carbohydrate stores to oxidise, against a control following heat stress. This could be further compared with the addition of an exogenous source of sugars.
- *Further investigate the source of the NADPH production reported by* Lu *et al.* (2016) would provide a significant insight into the possible involvement of the proposed linear pathway from 'illuminated chlororespiratory like' reduction of the PQ pool to NADPH. Was this pathway at least partially responsible for the large increase in the NADPH:NADH ratio reported during PSII inhibition?
- *Investigating the potential role of 'illuminated chlororespiratory like' pathways in plants*. Model systems such as *Arabidopsis* could be used for experiments similar to those proposed for the cyanobacterial mutants. However PGR-5 and NDH-1

responses could be distinguished further. The various mutants are already available, including some of chloroplast localised enzymes, such as malate dehydrogenase, could be investigated for their role in the proposed stress response.

- *Further the understanding of thermophilic phototrophs*, to examine the hypothesis that greater thermal tolerance downstream of PSII plays an active role in providing recovery from PSII specific stress/damage. To do this, a range of experiments, similar to those described in Chapters Four and Five, would be conducted with a high temperature thermophilic cyanobacterium. The incorporation of the second stable isotope, $^{13}CO_2$ to MIMS measurements, would provide values of Gross CO_2 fluxes, in addition to the gross oxygen rates. The tolerance to temperature of key components and processes would be examined and compared. Do these organisms growing on the edge exhibit the same ΔT as mesophiles, as has been shown in the moderate thermophile? If not, could this partial loss of metabolic flexibility help explain the inability of phototrophs to adapt to a higher temperature environment?

Literature Cited

AIHARA, Y., TAKAHASHI, S. & MINAGAWA, J. 2016. Heat induction of cyclic electron flow around photosystem i in the symbiotic dinoflagellate Symbiodinium. *Plant Physiology,* 171**,** 522-529.

ALLAHVERDIYEVA, Y., MUSTILA, H., ERMAKOVA, M., BERSANINI, L., RICHAUD, P., AJLANI, G., BATTCHIKOVA, N., COURNAC, L. & ARO, E. M. 2013. Flavodiiron proteins Flv1 and Flv3 enable cyanobacterial growth and photosynthesis under fluctuating light. *Proceedings of the National Academy of Sciences of the United States of America,* 110**,** 4111-4116.

ALLAHVERDIYEVA, Y., SUORSA, M., TIKKANEN, M. & ARO, E.-M. 2014. Photoprotection of photosystems in fluctuating light intensities. *Journal of Experimental Botany*.

ALLAKHVERDIEV, S. I., KRESLAVSKI, V. D., KLIMOV, V. V., LOS, D. A., CARPENTIER, R. & MOHANTY, P. 2008. Heat stress: An overview of molecular responses in photosynthesis. *Photosynthesis Research,* 98**,** 541-550.

ALLEN, J. F. 2003. Cyclic, pseudocyclic and noncyclic photophosphorylation: new links in the chain. *Trends in Plant Science,* 8**,** 15-19.

ALLEN, J. P. & WILLIAMS, J. C. 1998. Photosynthetic reaction centers. *FEBS Lett,* 438**,** 5-9.

ALRIC, J. 2015. The plastoquinone pool, poised for cyclic electron flow? *Frontiers in Plant Science,* 6.

AMINAKA, R., TAIRA, Y., KASHINO, Y., KOIKE, H. & SATOH, K. 2006. Acclimation to the Growth Temperature and Thermosensitivity of Photosystem II in a Mesophilic Cyanobacterium, Synechocystis sp. PCC6803. *Plant and Cell Physiology,* 47**,** 1612-1621.

ASADA, K. 2000. The water-water cycle as alternative photon and electron sinks. *Philosophical Transactions of the Royal Society B: Biological Sciences,* 355**,** 1419-1431.

ATKIN, O. K., BRUHN, D., HURRY, V. M. & TJOELKER, M. G. 2005. Evans Review No. 2: The hot and the cold: unravelling the variable response of plant respiration to temperature. *Functional Plant Biology,* 32**,** 87-105.

ATKIN, O. K., SCHEURWATER, I. & PONS, T. L. 2006. High thermal acclimation potential of both photosynthesis and respiration in two lowland Plantago species in contrast to an alpine congeneric. *Global Change Biology,* 12**,** 500-515.

ATKIN, O. K. & TJOELKER, M. G. 2003. Thermal acclimation and the dynamic response of plant respiration to temperature. *Trends in Plant Science,* 8**,** 343-351.

BADGER, M. R., PALMQVIST, K. & YU, J.-W. 1994. Measurement of CO2 and HCO3− fluxes in cyanobacteria and microalgae during steady-state photosynthesis. *Physiologia Plantarum,* 90**,** 529-536.

BADGER, M. R. & PRICE, G. D. 2003. CO2 concentrating mechanisms in cyanobacteria: molecular components, their diversity and evolution. *Journal of Experimental Botany,* 54**,** 609-622.

BADGER, M. R., VON CAEMMERER, S., RUUSKA, S. & NAKANO, H. 2000. Electron flow to oxygen in higher plants and algae: rates and control of direct photoreduction (Mehler reaction) and rubisco oxygenase. *Philos Trans R Soc Lond B Biol Sci,* 355**,** 1433-46.

BAILEY, S., MELIS, A., MACKEY, K. R. M., CARDOL, P., FINAZZI, G., VAN DIJKEN, G., BERG, G. M., ARRIGO, K., SHRAGER, J. & GROSSMAN, A. 2008. Alternative photosynthetic electron flow to oxygen in marine Synechococcus. *Biochimica et Biophysica Acta (BBA) - Bioenergetics,* 1777**,** 269-276.

BALME, A., HERVÁS, M., CAMPOS, L. A., SANCHO, J., DE LA ROSA, M. A. & NAVARRO, J. A. 2001. A comparative study of the thermal stability of plastocyanin, cytochrome c6 and Photosystem I in thermophilic and mesophilic cyanobacteria. *Photosynthesis Research,* 70**,** 281-289.

BARBER, J. 2008. Photosynthetic generation of oxygen. *Philosophical Transactions of the Royal Society B: Biological Sciences,* 363**,** 2665-2674.

BATTCHIKOVA, N., WEI, L., DU, L., BERSANINI, L., ARO, E. M. & MA, W. 2011. Identification of novel Ssl0352 protein (NdhS), essential for efficient operation of cyclic electron transport around photosystem I, in NADPH:plastoquinone oxidoreductase (NDH-1) complexes of Synechocystis sp. PCC 6803. *J Biol Chem,* 286**,** 36992-7001.

BAUERLE, W. L., WESTON, D. J., BOWDEN, J. D., DUDLEY, J. B. & TOLER, J. E. 2004. Leaf absorptance of photosynthetically active radiation in relation to chlorophyll meter estimates among woody plant species. *Scientia Horticulturae,* 101**,** 169-178.

BECK, C., KNOOP, H., AXMANN, I. M. & STEUER, R. 2012. The diversity of cyanobacterial metabolism: genome analysis of multiple phototrophic microorganisms. *BMC Genomics,* 13**,** 56.

BECKMANN, K., MESSINGER, J., BADGER, M., WYDRZYNSKI, T. & HILLIER, W. 2009. On-line mass spectrometry: membrane inlet sampling. *Photosynthesis Research,* 102**,** 511-522.

BENNOUN, P. 1982. Evidence for a respiratory chain in the chloroplast. *Proc Natl Acad Sci U S A,* 79**,** 4352-6.

BERNÁT, G., APPEL, J., OGAWA, T. & RÖGNER, M. 2011. Distinct Roles of Multiple NDH-1 Complexes in the Cyanobacterial Electron Transport Network as Revealed by Kinetic Analysis of P700(+) Reduction in Various ndh-Deficient Mutants of Synechocystis sp. Strain PCC6803. *Journal of Bacteriology,* 193**,** 292-295.

BERRY, J. & BJÖRKMAN, O. 1980. Photosynthetic Response and Adaptation to Temperature in Higher-Plants. *Annual Review of Plant Physiology and Plant Molecular Biology,* 31**,** 491-543.

BERRY, S., SCHNEIDER, D., VERMAAS, W. F. & ROGNER, M. 2002. Electron transport routes in whole cells of Synechocystis sp. strain PCC 6803: the role of the cytochrome bd-type oxidase. *Biochemistry,* 41**,** 3422-9.

BERSANINI, L., BATTCHIKOVA, N., JOKEL, M., REHMAN, A., VASS, I., ALLAHVERDIYEVA, Y. & ARO, E.-M. 2014. Flavodiiron Protein Flv2/Flv4-Related Photoprotective Mechanism Dissipates Excitation Pressure of PSII in

Cooperation with Phycobilisomes in Cyanobacteria. *Plant Physiology,* 164**,** 805-818.

BLANKENSHIP, R. E. 2010. Early Evolution of Photosynthesis. *Plant Physiology,* 154**,** 434-438.

BOLYCHEVTSEVA, Y. V., KUZMINOV, F. I., ELANSKAYA, I. V., GORBUNOV, M. Y. & KARAPETYAN, N. V. 2015. Photosystem activity and state transitions of the photosynthetic apparatus in cyanobacterium Synechocystis PCC 6803 mutants with different redox state of the plastoquinone pool. *Biochemistry (Mosc),* 80**,** 50-60.

BOTHE, H., SCHMITZ, O., YATES, M. G. & NEWTON, W. E. 2010. Nitrogen fixation and hydrogen metabolism in cyanobacteria. *Microbiol Mol Biol Rev,* 74**,** 529-51.

BOUSSAC, A., VERBAVATZ, J.-M. & SUGIURA, M. 2008. Isotopic labelling of photosystem II in Thermosynechococcus elongatus. Netherlands, Dordrecht: Springer Science & Business Media.

BROCK, T. D. 1970. High Temperature Systems. *Annual Review of Ecology and Systematics,* 1**,** 191-220.

BRYANT, D. A. 1995. *The Molecular Biology of Cyanobacteria*, Springer.

BUKHOV, N. & CARPENTIER, R. 2004. Alternative Photosystem I-Driven Electron Transport Routes: Mechanisms and Functions. *Photosynthesis Research,* 82**,** 17-33.

BUKHOV, N., EGOROVA, E. & CARPENTIER, R. 2002. Electron flow to photosystem I from stromal reductants in vivo: the size of the pool of stromal reductants controls the rate of electron donation to both rapidly and slowly reducing photosystem I units. *Planta,* 215**,** 812-20.

CAPLOW, M. 1968. Kinetics of Carbamate Formation and Breakdown. *Journal of the American Chemical Society,* 90**,** 6795-&.

CARPENTIER, R. 1999. Effect of High-Temperature Stress on the Photosynthetic Apparatus. *Handbook of Plant and Crop Stress, Second Edition.* CRC Press.

CASTENHOLZ, R. W. 1969. Thermophilic blue-green algae and the thermal environment. *Bacteriological Reviews,* 33**,** 476-504.

ČERVENÝ, J., SINETOVA, M., ZAVŘEL, T. & LOS, D. 2015. Mechanisms of High Temperature Resistance of Synechocystis sp. PCC 6803: An Impact of Histidine Kinase 34. *Life,* 5**,** 676.

COOLEY, J. W., HOWITT, C. A. & VERMAAS, W. F. J. 2000. Succinate:Quinol Oxidoreductases in the Cyanobacterium Synechocystis sp. Strain PCC 6803: Presence and Function in Metabolism and Electron Transport. *Journal of Bacteriology,* 182**,** 714-722.

COOLEY, J. W. & VERMAAS, W. F. 2001. Succinate dehydrogenase and other respiratory pathways in thylakoid membranes of Synechocystis sp. strain PCC 6803: capacity comparisons and physiological function. *Journal of Bacteriology,* 183**,** 4251-4258.

COX, A., SHOCK, E. L. & HAVIG, J. R. 2011. The transition to microbial photosynthesis in hot spring ecosystems. *Chemical Geology,* 280**,** 344-351.

CUCHIARA, C. C., SILVA, I. M. C., DALBERTO, D. S., BACARIN, M. A. & PETERS, J. A. 2015. Chlorophyll a fluorescence in sweet potatoes under

different copper concentrations. *Journal of soil science and plant nutrition,* 15**,** 179-189.

ENAMI, I., KITAMURA, M., TOMO, T., ISOKAWA, Y., OHTA, H. & KATOH, S. 1994. Is the primary cause of thermal inactivation of oxygen evolution in spinach PS II membranes release of the extrinsic 33 kDa protein or of Mn? *Biochimica et Biophysica Acta (BBA) - Bioenergetics,* 1186**,** 52-58.

ERMAKOVA, M., BATTCHIKOVA, N., RICHAUD, P., LEINO, H., KOSOUROV, S., ISOJARVI, J., PELTIER, G., FLORES, E., COURNAC, L., ALLAHVERDIYEVA, Y. & ARO, E. M. 2014. Heterocyst-specific flavodiiron protein Flv3B enables oxic diazotrophic growth of the filamentous cyanobacterium Anabaena sp. PCC 7120. *Proc Natl Acad Sci U S A,* 111**,** 11205-10.

ERMAKOVA, M., HUOKKO, T., RICHAUD, P., BERSANINI, L., HOWE, C. J., LEA-SMITH, D., PELTIER, G. & ALLAHVERDIYEVA, Y. 2016. Distinguishing the roles of thylakoid respiratory terminal oxidases in the cyanobacterium Synechocystis sp. PCC 6803. *Plant Physiology*.

EVANS, J. R. & POORTER, H. 2001. Photosynthetic acclimation of plants to growth irradiance: the relative importance of specific leaf area and nitrogen partitioning in maximizing carbon gain. *Plant, Cell & Environment,* 24**,** 755-767.

FALKOWSKI, P. G., FENCHEL, T. & DELONG, E. F. 2008. The microbial engines that drive Earth's biogeochemical cycles. *Science,* 320**,** 1034-9.

FAN, D.-Y., FITZPATRICK, D., OGUCHI, R., MA, W., KOU, J. & CHOW, W. S. 2016. Obstacles in the quantification of the cyclic electron flux around Photosystem I in leaves of C3 plants. *Photosynthesis Research***,** 1-13.

FELLER, U., CRAFTS-BRANDNER, S. J. & SALVUCCI, M. E. 1998. Moderately High Temperatures Inhibit Ribulose-1,5-Bisphosphate Carboxylase/Oxygenase (Rubisco) Activase-Mediated Activation of Rubisco. *Plant Physiology,* 116**,** 539-546.

FLORES, E., FRIAS, J. E., RUBIO, L. M. & HERRERO, A. 2005. Photosynthetic nitrate assimilation in cyanobacteria. *Photosynth Res,* 83**,** 117-33.

FOGG, G. E. 1973. *The Blue-green algae,* London, New York,, Academic Press.

GAO, S. & WANG, G. 2012. The enhancement of cyclic electron flow around photosystem I improves the recovery of severely desiccated Porphyra yezoensis (Bangiales, Rhodophyta). *Journal of Experimental Botany*.

GIFFORD, R. M. 2003. Plant respiration in productivity models: conceptualisation, representation and issues for global terrestrial carbon-cycle research. *Functional Plant Biology,* 30**,** 171-186.

GROSSMAN, A. R., MACKEY, K. R. M. & BAILEY, S. 2010. A perspective on photosynthesis in the oligotropic oceans: Hypotheses concerning alternative routes of electron flow. *Journal of Phycology,* 46**,** 629-634.

GRÜNDEL, M., SCHEUNEMANN, R., LOCKAU, W. & ZILLIGES, Y. 2012. Impaired glycogen synthesis causes metabolic overflow reactions and affects stress responses in the cyanobacterium Synechocystis sp. PCC 6803. *Microbiology,* 158**,** 3032-3043.

HART, S. E., SCHLARB-RIDLEY, B. G., BENDALL, D. S. & HOWE, C. J. 2005. Terminal oxidases of cyanobacteria. *Biochem Soc Trans,* 33**,** 832-5.

HAUPT-HERTING, S. & FOCK, H. P. 2002. Oxygen exchange in relation to carbon assimilation in water-stressed leaves during photosynthesis. *Ann Bot,* 89 Spec No, 851-9.

HAVAUX, M. 1996. Short-term responses of Photosystem I to heat stress : Induction of a PS II-independent electron transport through PS I fed by stromal components. *Photosynth Res,* 47, 85-97.

HAVAUX, M. & TARDY, F. 1996. Temperature-dependent adjustment of the thermal stability of photosystem II in vivo: possible involvement of xanthophyll-cycle pigments. *Planta,* 198, 324-333.

HAVAUX, M., TARDY, F., RAVENEL, J., CHANU, D. & PAROT, P. 1996. Thylakoid membrane stability to heat stress studied by flash spectroscopic measurements of the electrochromic shift in intact potato leaves: influence of the xanthophyll content. *Plant, Cell & Environment,* 19, 1359-1368.

HERVÁS, M., NAVARRO, J. A., DÍAZ, A. & DE LA ROSA, M. A. 1996. A Comparative Thermodynamic Analysis by Laser-Flash Absorption Spectroscopy of Photosystem I Reduction by Plastocyanin and Cytochrome c6 in Anabaena PCC 7119, Synechocystis PCC 6803, and Spinach. *Biochemistry,* 35, 2693-2698.

HESKEL, M. A., O'SULLIVAN, O. S., REICH, P. B., TJOELKER, M. G., WEERASINGHE, L. K., PENILLARD, A., EGERTON, J. J. G., CREEK, D., BLOOMFIELD, K. J., XIANG, J., SINCA, F., STANGL, Z. R., MARTINEZ-DE LA TORRE, A., GRIFFIN, K. L., HUNTINGFORD, C., HURRY, V., MEIR, P., TURNBULL, M. H. & ATKIN, O. K. 2016. Convergence in the temperature response of leaf respiration across biomes and plant functional types. *Proceedings of the National Academy of Sciences,* 113, 3832-3837.

HIRANO, M., SATOH, K. & KATOH, S. 1980. Plastoquinone as a common link between photosynthesis and respiration in a blue-green alga. *Photosynthesis Research,* 1, 149-162.

HIRANO, M., SATOH, K. & KATOH, S. 1981. The effect on photosynthetic electron transport of temperature-dependent changes in the fluidity of the thylakoid membrane in a thermophilic blue-green alga. *Biochimica Et Biophysica Acta,* 635, 476-87.

HOCH, G. & KOK, B. 1963. A mass spectrometer inlet system for sampling gases dissolved in liquid phases. *Archives of Biochemistry and Biophysics,* 101, 160-170.

HOHMANN-MARRIOTT, M. F. & BLANKENSHIP, R. E. 2011. Evolution of photosynthesis. *Annu Rev Plant Biol,* 62, 515-48.

HOICZYK, E. & HANSEL, A. 2000. Cyanobacterial Cell Walls: News from an Unusual Prokaryotic Envelope. *Journal of Bacteriology,* 182, 1191-1199.

HOWITT, C. A., COOLEY, J. W., WISKICH, J. T. & VERMAAS, W. F. 2001. A strain of Synechocystis sp. PCC 6803 without photosynthetic oxygen evolution and respiratory oxygen consumption: implications for the study of cyclic photosynthetic electron transport. *Planta,* 214, 46-56.

HU, Y. Y., FAN, D. Y., LOSCIALE, P., CHOW, W. S. & ZHANG, W. F. 2013. Whole-tissue determination of the rate coefficients of photoinactivation and repair of photosystem II in cotton leaf discs based on flash-induced P700 redox kinetics. *Photosynth Res,* 117, 517-28.

INOUE, N., EMI, T., YAMANE, Y., KASHINO, Y., KOIKE, H. & SATOH, K. 2000. Effects of High-Temperature Treatments on a Thermophilic Cyanobacterium Synechococcus vulcanus. *Plant and Cell Physiology,* 41**,** 515-522.

INOUE, N., TAIRA, Y., EMI, T., YAMANE, Y., KASHINO, Y., KOIKE, H. & SATOH, K. 2001. Acclimation to the Growth Temperature and the High-Temperature Effects on Photosystem II and Plasma Membranes in a Mesophilic Cyanobacterium, Synechocystis sp. PCC6803. *Plant and Cell Physiology,* 42**,** 1140-1148.

JENNEY, F. E., PRINCE, R. C. & DALDAL, F. 1996. The membrane-bound cytochrome cy of Rhodobacter capsulatus can serve as an electron donor to the photosynthetic reaction center of Rhodobacter sphaeroides. *Biochimica et Biophysica Acta (BBA) - Bioenergetics,* 1273**,** 159-164.

JIA, H., DWYER, S. A., FAN, D. Y., HAN, Y., BADGER, M. R., VON CAEMMERER, S. & CHOW, W. S. 2014. A novel P700 redox kinetics probe for rapid, non-intrusive and whole-tissue determination of photosystem II functionality, and the stoichiometry of the two photosystems in vivo. *Physiol Plant,* 152**,** 403-13.

JOHNSON, X. & ALRIC, J. 2013. Central Carbon Metabolism and Electron Transport in Chlamydomonas reinhardtii: Metabolic Constraints for Carbon Partitioning between Oil and Starch. *Eukaryotic Cell,* 12**,** 776-793.

JORDAN, P., FROMME, P., WITT, H. T., KLUKAS, O., SAENGER, W. & KRAUSS, N. 2001. Three-dimensional structure of cyanobacterial photosystem I at 2.5 A resolution. *Nature,* 411**,** 909-17.

KÄMÄRÄINEN, J., HUOKKO, T., KREULA, S., JONES, P. R., ARO, E.-M. & KALLIO, P. 2016. Pyridine nucleotide transhydrogenase PntAB is essential for optimal growth and photosynthetic integrity under low-light mixotrophic conditions in Synechocystis sp. PCC 6803. *New Phytologist***,** n/a-n/a.

KANA, T. M. 1992. Oxygen Cycling in Cyanobacteria, with Specific Reference to Oxygen Protection in Trichodesmium spp. *In:* CARPENTER, E. J., CAPONE, D. G. & RUETER, J. G. (eds.) *Marine Pelagic Cyanobacteria: Trichodesmium and other Diazotrophs.* Dordrecht: Springer Netherlands.

KATOH, H., ITOH, S., SHEN, J.-R. & IKEUCHI, M. 2001. Functional Analysis of psbV and a Novel c-type Cytochrome Gene psbV2 of the Thermophilic Cyanobacterium Thermosynechococcus elongatus Strain BP-1. *Plant and Cell Physiology,* 42**,** 599-607.

KATOH, S. 1988. Photosystem-I and Photosystem-Ii Preparations from Thermophilic Synechococcus. *Methods in Enzymology,* 167**,** 263-269.

KAUROV YU, N., BELYANSKAYA, G. K., IVANOV, II & RUBIN, A. B. 1990. Thermal stability of electron transport in PS II membranes and particles from the thermophilic cyanobacteria. *Gen Physiol Biophys,* 9**,** 189-202.

KLUGHAMMER, C. & SCHREIBER, U. 2008. Saturation Pulse method for assessment of energy conversion in PS I. *In:* HEINZ WALZ GMBH, E., GERMANY (ed.) *PAM Application Notes (2008)* Germany.

KOIKE, H. & KATOH, S. 1979. Heat-stabilities of cytochromes and ferredoxin isolated from a thermophilic blue-green alga. *Plant and Cell Physiology,* 20**,** 1157-1161.

KOIKE, H. & KATOH, S. 1980. Thermal properties of NADP:ferredoxin oxidoreductase and ferredoxin isolated from a thermophilic blue-green alga. *Photosynthesis Research,* 1**,** 163-170.

KOIKE, H., SATOH, K. & KATOH, S. 1982. Heat-stabilities of Electron Transport Related to Photosystem I in a Thermophilic Blue-green Alga, Synechococcus sp. *Plant and Cell Physiology,* 23**,** 293-299.

KOK, B. 1949. On the interrelation of respiration and photosynthesis in green plants. *Biochimica Et Biophysica Acta,* 3**,** 625-631.

KOU, J., TAKAHASHI, S., FAN, D.-Y., BADGER, M. R. & CHOW, W. S. 2015. Partially dissecting the steady-state electron fluxes in Photosystem I in wild-type and pgr5 and ndh mutants of Arabidopsis. *Frontiers in Plant Science,* 6**,** 758.

KOU, J. C., TAKAHASHI, S., OGUCHI, R., FAN, D. Y., BADGER, M. R. & CHOW, W. S. 2013. Estimation of the steady-state cyclic electron flux around PSI in spinach leaf discs in white light, CO2-enriched air and other varied conditions. *Functional Plant Biology,* 40**,** 1018-1028.

KRESLAVSKI, V., TATARINZEV, N., SHABNOVA, N., SEMENOVA, G. & KOSOBRYUKHOV, A. 2008. Characterization of the nature of photosynthetic recovery of wheat seedlings from short-term dark heat exposures and analysis of the mode of acclimation to different light intensities. *J Plant Physiol,* 165**,** 1592-600.

KRUSE, J., ALFARRAJ, S., RENNENBERG, H. & ADAMS, M. 2016. A novel mechanistic interpretation of instantaneous temperature responses of leaf net photosynthesis. *Photosynth Res,* 129**,** 43-58.

LAISK, A. & OJA, V. 1995. Coregulation of electron transport through PS I by Cyt b 6 f, excitation capture by P700 and acceptor side reduction. Time kinetics and electron transport requirement. *Photosynthesis Research,* 45**,** 11-19.

LAJKÓ, F., KADIOGLU, A., BORBÉLY, G. & GARAB, G. 1997. Competition between the photosynthetic and the (chloro)respiratory electron transport chains in cyanobacteria, green algae and higher plants. Effect of heat stress. *Photosynthetica,* 33**,** 217-226.

LEA-SMITH, D. J., BOMBELLI, P., VASUDEVAN, R. & HOWE, C. J. 2016. Photosynthetic, respiratory and extracellular electron transport pathways in cyanobacteria. *Biochimica Et Biophysica Acta,* 1857**,** 247-55.

LEVITT, J. 1980. *Responses of plants to environmental stresses. Volume I. Responses of Plants to Environmental Stresses,* New York, Academic Press.

LI, Q., YAO, Z. & MI, H. 2016. Alleviation of photoinhibition by coordination of chlororespiration and cyclic electron flow mediated by NDH under heat stressed condition in tobacco. *Frontiers in Plant Science,* 7.

LIBERTON, M., PAGE, L. E., O'DELL, W. B., O'NEILL, H., MAMONTOV, E., URBAN, V. S. & PAKRASI, H. B. 2013. Organization and Flexibility of Cyanobacterial Thylakoid Membranes Examined by Neutron Scattering. *The Journal of Biological Chemistry,* 288**,** 3632-3640.

LIU, L.-N. 2016. Distribution and dynamics of electron transport complexes in cyanobacterial thylakoid membranes. *Biochimica et Biophysica Acta (BBA) - Bioenergetics,* 1857**,** 256-265.

LIU, L.-N., BRYAN, S. J., HUANG, F., YU, J., NIXON, P. J., RICH, P. R. & MULLINEAUX, C. W. 2012. Control of electron transport routes through

redox-regulated redistribution of respiratory complexes. *Proceedings of the National Academy of Sciences,* 109**,** 11431-11436.

LONG, B. M., PRICE, G. D. & BADGER, M. R. 2005. Proteomic assessment of an established technique for carboxysome enrichment from Synechococcus PCC7942. *Canadian Journal of Botany,* 83**,** 746-757.

LU, X., HUAN, L., GAO, S., HE, L. & WANG, G. 2016. NADPH from the oxidative pentose phosphate pathway drives the operation of cyclic electron flow around photosystem I in high-intertidal macroalgae under severe salt stress. *Physiologia Plantarum,* 156**,** 397-406.

MA, W. M., MI, H. L. & SHEN, Y. G. 2010. Influence of the redox state of Q(A) on phycobilisome mobility in the cyanobacterium Synechocystis sp strain PCC 6803. *Journal of Luminescence,* 130**,** 1169-1173.

MAMEDOV, M., HAYASHI, H. & MURATA, N. 1993. Effects of glycinebetaine and unsaturation of membrane lipids on heat stability of photosynthetic electron-transport and phosphorylation reactions in Synechocystis PCC6803. *Biochimica et Biophysica Acta (BBA) - Bioenergetics,* 1142**,** 1-5.

MAXWELL, K. & JOHNSON, G. N. 2000. Chlorophyll fluorescence—a practical guide. *Journal of Experimental Botany,* 51**,** 659-668.

MAXWELL, P. C. & BIGGINS, J. 1976. Role of cyclic electron transport in photosynthesis as measured by the photoinduced turnover of P700 in vivo. *Biochemistry,* 15**,** 3975-81.

MCDOWELL, N. G., WILLIAMS, A. P., XU, C., POCKMAN, W. T., DICKMAN, L. T., SEVANTO, S., PANGLE, R., LIMOUSIN, J., PLAUT, J., MACKAY, D. S., OGEE, J., DOMEC, J. C., ALLEN, C. D., FISHER, R. A., JIANG, X., MUSS, J. D., BRESHEARS, D. D., RAUSCHER, S. A. & KOVEN, C. 2016. Multi-scale predictions of massive conifer mortality due to chronic temperature rise. *Nature Clim. Change,* 6**,** 295-300.

MEEKS, J. C. & CASTENHOLZ, R. W. 1971. Growth and photosynthesis in an extreme thermophile, Synechococcus lividus (Cyanophyta). *Archiv für Mikrobiologie,* 78**,** 25-41.

MEEKS, J. C. & CASTENHOLZ, R. W. 1978. Photosynthetic properties of the extreme thermophile synechococcus lividus—II. Stoichiometry between oxygen evolution and CO2 assimilation. *Journal of Thermal Biology,* 3**,** 19-24.

MILLIGAN, A. J., BERMAN-FRANK, I., GERCHMAN, Y., DISMUKES, G. C. & FALKOWSKI, P. G. 2007. Light-dependent oxygen consumption in nitrogen-fixing cyanobacteria plays a key role in nitrogenase protection1. *Journal of Phycology,* 43**,** 845-852.

MUHLENHOFF, U. & CHAUVAT, F. 1996. Gene transfer and manipulation in the thermophilic cyanobacterium Synechococcus elongatus. *Molecular & General Genetics,* 252**,** 93-100.

MULKIDJANIAN, A. Y., KOONIN, E. V., MAKAROVA, K. S., MEKHEDOV, S. L., SOROKIN, A., WOLF, Y. I., DUFRESNE, A., PARTENSKY, F., BURD, H., KAZNADZEY, D., HASELKORN, R. & GALPERIN, M. Y. 2006. The cyanobacterial genome core and the origin of photosynthesis. *Proceedings of the National Academy of Sciences of the United States of America,* 103**,** 13126-13131.

MULLINEAUX, C. W. 2014a. Co-existence of photosynthetic and respiratory activities in cyanobacterial thylakoid membranes. *Biochimica Et Biophysica Acta-Bioenergetics,* 1837**,** 503-511.

MULLINEAUX, C. W. 2014b. Electron transport and light-harvesting switches in cyanobacteria. *Frontiers in Plant Science,* 5**,** 7.

NAKAMURA, Y., KANEKO, T., SATO, S., IKEUCHI, M., KATOH, H., SASAMOTO, S., WATANABE, A., IRIGUCHI, M., KAWASHIMA, K., KIMURA, T., KISHIDA, Y., KIYOKAWA, C., KOHARA, M., MATSUMOTO, M., MATSUNO, A., NAKAZAKI, N., SHIMPO, S., SUGIMOTO, M., TAKEUCHI, C., YAMADA, M. & TABATA, S. 2002. Complete Genome Structure of the Thermophilic Cyanobacterium Thermosynechococcus elongatus BP-1. *DNA Research,* 9**,** 123-130.

NAWROCKI, W. J., TOURASSE, N. J., TALY, A., RAPPAPORT, F. & WOLLMAN, F.-A. 2015. The Plastid Terminal Oxidase: Its Elusive Function Points to Multiple Contributions to Plastid Physiology. *Annual Review of Plant Biology,* 66**,** 49-74.

NEDWELL, D. B. 1999. Effect of low temperature on microbial growth: lowered affinity for substrates limits growth at low temperature. *FEMS Microbiology Ecology,* 30**,** 101-111.

O'SULLIVAN, O. S., WEERASINGHE, K. W. L. K., EVANS, J. R., EGERTON, J. J. G., TJOELKER, M. G. & ATKIN, O. K. 2013. High-resolution temperature responses of leaf respiration in snow gum (Eucalyptus pauciflora) reveal high-temperature limits to respiratory function. *Plant, Cell & Environment,* 36**,** 1268-1284.

OGAWA, T. 1991. A gene homologous to the subunit-2 gene of NADH dehydrogenase is essential to inorganic carbon transport of Synechocystis PCC6803. *Proc Natl Acad Sci U S A,* 88**,** 4275-9.

OGAWA, T., HARADA, T., OZAKI, H. & SONOIKE, K. 2013. Disruption of the ndhF1 Gene Affects Chl Fluorescence through State Transition in the Cyanobacterium Synechocystis sp. PCC 6803, Resulting in Apparent High Efficiency of Photosynthesis. *Plant and Cell Physiology,* 54**,** 1164-1171.

OHKAWA, H., PAKRASI, H. B. & OGAWA, T. 2000. Two Types of Functionally Distinct NAD(P)H Dehydrogenases inSynechocystis sp. Strain PCC6803. *Journal of Biological Chemistry,* 275**,** 31630-31634.

OLIVE, J., AJLANI, G., ASTIER, C., RECOUVREUR, M. & VERNOTTE, C. 1997. Ultrastructure and light adaptation of phycobilisome mutants of Synechocystis PCC 6803. *Biochimica et Biophysica Acta (BBA) - Bioenergetics,* 1319**,** 275-282.

PATZELT, D. J., HINDERSIN, S., KERNER, M. & HANELT, D. 2016. Responses of photosystems I and II of Acutodesmus obliquus to chemical stress caused by the use of recycled nutrients. *Applied Microbiology and Biotechnology,* 100**,** 361-370.

PELTIER, G., ARO, E.-M. & SHIKANAI, T. 2016. NDH-1 and NDH-2 Plastoquinone Reductases in Oxygenic Photosynthesis. *Annual Review of Plant Biology,* 67**,** 55-80.

PELTIER, G. & COURNAC, L. 2002. Chlororespiration. *Annu Rev Plant Biol,* 53**,** 523-50.

PELTIER, G. & SARREY, F. 1988. The Kok effect and the light-inhibition of chlororespiration in Chlamydomonas reinhardtii. *FEBS Letters,* 228**,** 259-262.

PORRA, R. J., THOMPSON, W. A. & KRIEDEMANN, P. E. 1989. Determination of accurate extinction coefficients and simultaneous equations for assaying chlorophylls a and b extracted with four different solvents: verification of the concentration of chlorophyll standards by atomic absorption spectroscopy. *Biochimica et Biophysica Acta (BBA) - Bioenergetics,* 975**,** 384-394.

PRICE, G. D., BADGER, M. R., WOODGER, F. J. & LONG, B. M. 2008. Advances in understanding the cyanobacterial CO(2)-concentrating-mechanism (CCM): functional components, Ci transporters, diversity, genetic regulation and prospects for engineering into plants. *Journal of Experimental Botany,* 59**,** 1441-1461.

PUEYO, J. J., ALFONSO, M., ANDRES, C. & PICOREL, R. 2002. Increased tolerance to thermal inactivation of oxygen evolution in spinach Photosystem II membranes by substitution of the extrinsic 33-kDa protein by its homologue from a thermophilic cyanobacterium. *Biochimica Et Biophysica Acta,* 1554**,** 29-35.

QUILES, M. J. 2006. Stimulation of chlororespiration by heat and high light intensity in oat plants. *Plant, Cell & Environment,* 29**,** 1463-1470.

RADMER, R. J. & KOK, B. 1976. Photoreduction of O(2) Primes and Replaces CO(2) Assimilation. *Plant Physiol,* 58**,** 336-40.

RAE, B. D., FORSTER, B., BADGER, M. R. & PRICE, G. D. 2011. The CO2-concentrating mechanism of Synechococcus WH5701 is composed of native and horizontally-acquired components. *Photosynth Res,* 109**,** 59-72.

ROWLAND, J. G., PANG, X., SUZUKI, I., MURATA, N., SIMON, W. J. & SLABAS, A. R. 2010. Identification of components associated with thermal acclimation of photosystem II in Synechocystis sp. PCC6803. *PLoS One,* 5.

RUMEAU, D., PELTIER, G. & COURNAC, L. 2007. Chlororespiration and cyclic electron flow around PSI during photosynthesis and plant stress response. *Plant, Cell & Environment,* 30**,** 1041-1051.

RUTHERFORD, A. W., OSYCZKA, A. & RAPPAPORT, F. 2012. Back-reactions, short-circuits, leaks and other energy wasteful reactions in biological electron transfer: Redox tuning to survive life in O 2. *FEBS Letters,* 586**,** 603-616.

RUUSKA, S. A., BADGER, M. R., ANDREWS, T. J. & VON CAEMMERER, S. 2000. Photosynthetic electron sinks in transgenic tobacco with reduced amounts of Rubisco: little evidence for significant Mehler reaction. *J Exp Bot,* 51 Spec No**,** 357-68.

SAGE, R. F. & KUBIEN, D. S. 2007. The temperature response of C3 and C4 photosynthesis. *Plant, Cell & Environment,* 30**,** 1086-1106.

SALVUCCI, M. E., PORTIS, A. R. & OGREN, W. L. 1986. Light and CO(2) Response of Ribulose-1,5-Bisphosphate Carboxylase/Oxygenase Activation in Arabidopsis Leaves. *Plant Physiology,* 80**,** 655-659.

SAMBORSKA, B. & KIMBER, MATTHEW S. 2012. A Dodecameric CcmK2 Structure Suggests β-Carboxysomal Shell Facets Have a Double-Layered Organization. *Structure,* 20**,** 1353-1362.

SAROUSSI, S. I., WITTKOPP, T. M. & GROSSMAN, A. R. 2016. The Type II NADPH Dehydrogenase Facilitates Cyclic Electron Flow, Energy-Dependent Quenching, and Chlororespiratory Metabolism during Acclimation of Chlamydomonas reinhardtii to Nitrogen Deprivation. *Plant Physiology,* 170**,** 1975-1988.

SCHUURMANS, R. M., SCHUURMANS, J. M., BEKKER, M., KROMKAMP, J. C., MATTHIJS, H. C. P. & HELLINGWERF, K. J. 2014. The Redox Potential of the Plastoquinone Pool of the Cyanobacterium Synechocystis Species Strain PCC 6803 Is under Strict Homeostatic Control. *Plant Physiology,* 165**,** 463-475.

SCHUURMANS, R. M., VAN ALPHEN, P., SCHUURMANS, J. M., MATTHIJS, H. C. P. & HELLINGWERF, K. J. 2015. Comparison of the Photosynthetic Yield of Cyanobacteria and Green Algae: Different Methods Give Different Answers. *PLoS One,* 10**,** e0139061.

SESSIONS, A. L., DOUGHTY, D. M., WELANDER, P. V., SUMMONS, R. E. & NEWMAN, D. K. 2009. The continuing puzzle of the great oxidation event. *Curr Biol,* 19**,** R567-74.

SEVANTO, S., MCDOWELL, N. G., DICKMAN, L. T., PANGLE, R. & POCKMAN, W. T. 2014. How do trees die? A test of the hydraulic failure and carbon starvation hypotheses. *Plant, Cell & Environment,* 37**,** 153-161.

SHARKEY, T. D. 2005. Effects of moderate heat stress on photosynthesis: importance of thylakoid reactions, rubisco deactivation, reactive oxygen species, and thermotolerance provided by isoprene. *Plant, Cell & Environment,* 28**,** 269-277.

SHARKEY, T. D., BADGER, M. R., VON CAEMMERER, S. & ANDREWS, T. J. 2001. Increased heat sensitivity of photosynthesis in tobacco plants with reduced Rubisco activase. *Photosynthesis Research,* 67**,** 147-156.

SHARKEY, T. D. & ZHANG, R. 2010. High Temperature Effects on Electron and Proton Circuits of Photosynthesis. *Journal of Integrative Plant Biology,* 52**,** 712-722.

SHIKANAI, T. 2014. Central role of cyclic electron transport around photosystem I in the regulation of photosynthesis. *Curr Opin Biotechnol,* 26**,** 25-30.

SHIKANAI, T. 2016. Chloroplast NDH: A different enzyme with a structure similar to that of respiratory NADH dehydrogenase. *Biochimica et Biophysica Acta (BBA) - Bioenergetics,* 1857**,** 1015-1022.

SHIMAKAWA, G., SHAKU, K. & MIYAKE, C. 2016. Oxidation of P700 in photosystem I is essential for the growth of cyanobacteria. *Plant Physiology*.

SINGH, K. K., CHEN, C. G., EPSTEIN, D. K. & GIBBS, M. 1993. Respiration of sugars in spinach (*Spinacia-oleracea*), Maize (*Zea-mays*), and *Chlamydomonas-reinhardtii* F-60 with emphasis on the hexose kinases. *Plant Physiology,* 102**,** 587-593.

SONOIKE, K., HATANAKA, H., KATOH, S. & ITOH, S. 1990. Heat-Stability of Iron-Sulfur Centers and P-700 in Photosystem I Reaction Center Complexes Isolated from the Thermophilic Cyanobacterium Synechococcus elongatus. *Plant and Cell Physiology,* 31**,** 865-870.

SPAANS, S. K., WEUSTHUIS, R. A., VAN DER OOST, J. & KENGEN, S. W. M. 2015. NADPH-generating systems in bacteria and archaea. *Frontiers in Microbiology,* 6**,** 742.

SUORSA, M. 2015. Cyclic electron flow provides acclimatory plasticity for the photosynthetic machinery under various environmental conditions and developmental stages. *Frontiers in Plant Science,* 6.

TAGAWA, K., TSUJIMOTO, H. Y. & ARNON, D. I. 1963. ROLE OF CHLOROPLAST FERREDOXIN IN THE ENERGY CONVERSION

PROCESS OF PHOTOSYNTHESIS. *Proceedings of the National Academy of Sciences of the United States of America,* 49**,** 567-572.

THOMAS, J. C., UGHY, B., LAGOUTTE, B. & AJLANI, G. 2006. A second isoform of the ferredoxin:NADP oxidoreductase generated by an in-frame initiation of translation. *Proc Natl Acad Sci U S A,* 103**,** 18368-73.

TIKKANEN, M., RANTALA, S. & ARO, E.-M. 2015. Electron flow from PSII to PSI under high light is controlled by PGR5 but not by PSBS. *Frontiers in Plant Science,* 6.

UENO, M., SAE-TANG, P., KUSAMA, Y., HIHARA, Y., MATSUDA, M., HASUNUMA, T. & NISHIYAMA, Y. 2016. Moderate Heat Stress Stimulates Repair of Photosystem II During Photoinhibition in Synechocystis sp. PCC 6803. *Plant and Cell Physiology*.

UMENA, Y., KAWAKAMI, K., SHEN, J.-R. & KAMIYA, N. 2011. Crystal structure of oxygen-evolving photosystem II at a resolution of 1.9 Å. *Nature,* 473**,** 55-60.

VERMAAS, W. F. J. 2001. Photosynthesis and Respiration in Cyanobacteria. *eLS.* John Wiley & Sons, Ltd.

WALKER, D. 1987. *The use of the oxygen electrode and fluorescence probes in simple measurements of photosynthesis,* Sheffield, Research Institute for Photosynthesis, University of Sheffield.

WHITMARSH, J. 2000. Electron transport and energy transduction. *In:* RAGHAVENDRA, A. S. (ed.) *Photosynthesis: A Comprehensive Treatise.* Cambridge University Press.

WHITTON, B. & POTTS, M. 2000. Introduction to the Cyanobacteria. *In:* WHITTON, B. P., . M (ed.) *The Ecology of Cyanobacteria.* New York: Kluwer Academic Publishers.

WIDDEL, F., SCHNELL, S., HEISING, S., EHRENREICH, A., ASSMUS, B. & SCHINK, B. 1993. Ferrous iron oxidation by anoxygenic phototrophic bacteria. *Nature,* 362**,** 834-836.

WILHELM, C. & JAKOB, T. 2011. From photons to biomass and biofuels: evaluation of different strategies for the improvement of algal biotechnology based on comparative energy balances. *Applied Microbiology and Biotechnology,* 92**,** 909-919.

WILLIAMSON, A., CONLAN, B., HILLIER, W. & WYDRZYNSKI, T. 2011. The evolution of Photosystem II: insights into the past and future. *Photosynthesis Research,* 107**,** 71-86.

WILLIAMSON, A. K., LIGGINS, J. R., HILLIER, W. & WYDRZYNSKI, T. 2007. The importance of protein–protein interactions for optimising oxygen activity in photosystem II: reconstitution with a recombinant thioredoxin—manganese stabilising protein. *Photosynthesis Research,* 92**,** 305-314.

WULFHORST, H., FRANKEN, L. E., WESSINGHAGE, T., BOEKEMA, E. J. & NOWACZYK, M. M. 2014. The 5 kDa Protein NdhP Is Essential for Stable NDH-1L Assembly in Thermosynechococcus elongatus. *PLoS One,* 9**,** e103584.

XU, M., LV, J., FU, P. & MI, H. 2016. Oscillation kinetics of post-illumination increase in Chl fluorescence in Cyanobacterium Synechocystis PCC 6803. *Frontiers in Plant Science,* 7.

YAMAMOTO, H., TAKAHASHI, S., BADGER, M. R. & SHIKANAI, T. 2016. Artificial remodelling of alternative electron flow by flavodiiron proteins in Arabidopsis. *Nature Plants,* 2**,** 16012.

YAMAOKA, T., SATOH, K. & KATOH, S. 1978. Photosynthetic activities of a thermophilic blue-green alga. *Plant and Cell Physiology,* 19**,** 943-954.

YAMORI, W., MAKINO, A. & SHIKANAI, T. 2016. A physiological role of cyclic electron transport around photosystem I in sustaining photosynthesis under fluctuating light in rice. *Scientific Reports,* 6**,** 20147.

YAMORI, W. & SHIKANAI, T. 2016. Physiological Functions of Cyclic Electron Transport Around Photosystem i in Sustaining Photosynthesis and Plant Growth. *Annual Review of Plant Biology.*

YOU, L., HE, L. & TANG, Y. J. 2015. Photoheterotrophic fluxome in Synechocystis sp. strain PCC 6803 and its implications for cyanobacterial bioenergetics. *Journal of Bacteriology,* 197**,** 943-950.

ZHANG, L. & LIU, J. 2016. Effects of heat stress on photosynthetic electron transport in a marine cyanobacterium Arthrospira sp. *Journal of Applied Phycology,* 28**,** 757-763.

ZHANG, R. & SHARKEY, T. D. 2009. Photosynthetic electron transport and proton flux under moderate heat stress. *Photosynth Res,* 100**,** 29-43.

ZHANG, S. & BRYANT, D. A. 2011. The Tricarboxylic Acid Cycle in Cyanobacteria. *Science,* 334**,** 1551-1553.

ZILLIGES, Y. & DAU, H. 2016. Unexpected capacity for organic carbon assimilation by Thermosynechococcus elongatus, a crucial photosynthetic model organism. *FEBS Letters,* 590**,** 962-970.